A 2′-ALKYNYLNUCLEOTIDE STRATEGY FOR SITE-DIRECTED SPIN LABELLING OF DNA

A THESIS SUBMITTED TO THE
BOARD OF THE FACULTY OF PHYSICAL SCIENCES
IN PARTIAL FULFILMENT OF THE REQUIREMENTS FOR THE DEGREE OF

DOCTOR OF PHILOSOPHY

MARIUS MYRENG HAUGLAND

ST PETER'S COLLEGE
UNIVERSITY OF OXFORD

TRINITY TERM 2016



A 2′-alkynylnucleotide strategy for site-directed spin labelling of DNA

Marius Myreng Haugland, St Peter's College
Doctor of Philosophy, Trinity Term 2016

This thesis describes the synthesis of derivatives of 2′-ethynyl-2′-deoxynucleosides **I–III** (Figure I), and their conversion into phosphoramidite building blocks for DNA synthesis. Herein is also outlined the preparation of azide-bearing nitroxyl radicals **IV–VII**.

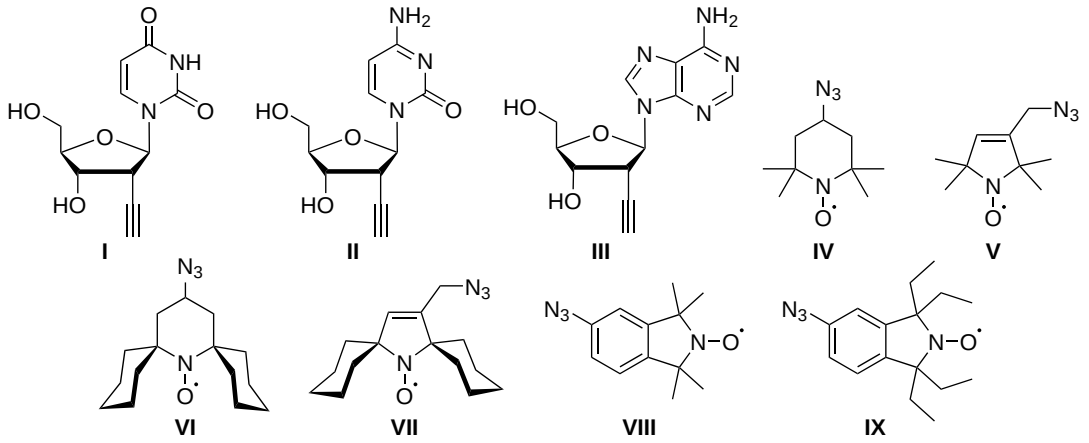
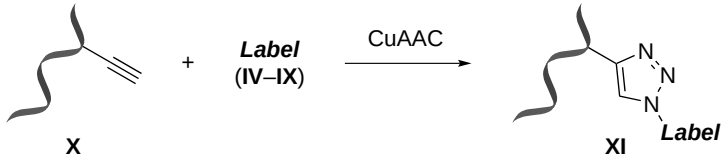


Figure I: Target compounds described in this thesis.

After site-selective incorporation of 2′-alkynylnucleosides **I–III** into DNA using a standard solid-supported phosphoramidite protocol, the modified oligonucleotides **X** (Scheme I) were spin labelled with the azide-bearing nitroxyl spin labels *via* the Cu(I)-catalysed azide-alkyne $[3+2]$ Huisgen cycloaddition (CuAAC or 'click' reaction). For this purpose, azides **VIII** and **IX** were also explored, albeit their synthesis is described elsewhere. The destabilising effect of the spin labelling was determined by UV denaturation studies and circular dichroism, and the spin labelled DNA was investigated by EPR spectroscopy. It was found that this novel site-directed spin labelling strategy afforded conformationally restricted systems, and that the structure of the spin label exerts a significant influence on the results.



Scheme I: Site-specifically alkynylated DNA strands were subjected to site-directed spin labelling with azide nitroxyl spin labels.

Acknowledgements

I would like to extend my gratitude to the following people, without whom this enterprise would never have been completed, or indeed even begun.

Firstly, to Prof. Ed Anderson, for giving me the chance to work in his research group for the past four years. For all his support, generosity, unlimited enthusiasm, and for teaching me so much. Also, to our collaborators, Dr Janet Lovett, Prof. Tom Brown and Dr Afaf El-Sagheer, for all their patience and time, and for lending their invaluable expertise.

Thanks also to the Norwegian State Educational Loan Fund for loans and grants to enable this undertaking, and to the Middle Common Room of St Peter's College for funding to attend a conference.

To Rachel, Javi and Robert, for keeping me company in the strange world on the boundary between organic chemistry, biochemistry and spectroscopy.

To the technical staff in the Department of Chemistry, especially Dr Will Myers at the Centre for Advanced Electron Spin Resonance and Dr Barbara Odell at the NMR spectroscopy facility.

To my proofreaders: Ed, Janet, Afaf, Guilhem, Carlos, Bryony, Rob, Christian, Yao, and Mujji.

To the past and present members of the Anderson group, for all their advice, help and friendship. Thank you for all the laughs, both inside and outside the lab. Especially to Haraldur and Rob, my DPhil mates, for walking the long road with me. To the Brown group, for welcoming me into their lab and beyond.

To Ebba, to my college friends, Jasper, Hazel, Meredith, Joanna and Josh, and to the Choir of St Peter's College. Thank you for reminding me that chemistry is not all.

To my cariad Huw, for keeping me sane, and for brightening up even the darkest days.

To my family, for their unconditional love and support, and for enabling me to make my dream come true.

Oxford, September 2016

Marius Myreng Haugland

List of symbols and abbreviations

A Adenosine

a The hyperfine splitting constant

$\mathbf{A_{260}}$ UV absorption at 260 nm

$\mathbf{A_{504}}$ UV absorption at 504 nm

Anal. Combustion elemental analysis

Atm. Atmosphere

$\mathbf{B_0}$ Magnetic field strength

Bn Benzyl

bs Broad singlet

Bz Benzoyl

C Cytosine

c Concentration (specific optical rotation)

CD Circular dichroism

COSY Homonuclear correlation spectroscopy

CPG Controlled pore glass

CuAAC The Cu(I)-catalysed azide-alkyne $[3+2]$ Huisgen cycloaddition

CW Continuous wave

D Dihydrouridine

d Doublet

dA 2′-Deoxyadenosine

dC 2′-Deoxycytidine

dd Doublet of doublets

$\boldsymbol{D_{\mathrm{dip}}}$ Dipolar coupling constant

DEER Double electron-electron resonance

dG 2′-Deoxyguanosine

DIBAL Diisobutylaluminium hydride

DIC *N,N*′-Diisopropylcarbodiimide

DIPEA Diisopropylethylamine, Hünig's base

DMAP 4-Dimethylaminopyridine

DMF *N,N*-Dimethylformamide

DMSO Dimethylsulfoxide

DMTr 4,4′-Dimethoxytriphenylmethyl, 4,4′-dimethoxytrityl

DNA Deoxyribonucleic acid

DPEPhos Bis[(2-diphenylphosphino)-phenyl] ether

dppf 1,1′-Ferrocenediyl-bis(diphenyl-phosphine)

dq Doublet of quartets

dRib 2′-Deoxyribosyl

dsDNA Double-stranded DNA

dsept Doublet of septets

dT 2′-Deoxythymidine

dt Doublet of triplets

dU 2′-Deoxyuridine

EDTA Ethylenediaminetetraacetic acid

EI+ Positive electron impact ionisation

EPR Electron paramagnetic resonance

equiv. Equivalents

ES+ Positive electrospray ionisation

ES− Negative electrospray ionisation

ESI Electrospray ionisation

FI+ Positive field ionisation

FRET Förster resonance energy transfer

G Guanosine

g The electron g-value

GCMS Gas chromatography-mass spectrometry

$\boldsymbol{h}$ Planck's constant

HCV Hepatitis C virus

hex Hexane

HMBC Heteronuclear multiple-bond correlation spectroscopy

HOBT Hydroxybenzotriazole

HPLC High-performance liquid chromatography

HRMS High resolution mass spectrometry

HSQC Heteronuclear single-quantum correlation spectroscopy

hwhh Half-width at half-height

$\boldsymbol{I}$ Spin

IMes 1,3-Bis(2,4,6-trimethylphenyl)-imidazol-2-ylidene

IR Infrared

$\boldsymbol{J}$ Exchange coupling constant

$\boldsymbol{K_{eq}}$ Equilibrium constant

L Resin loading, in µmol/g

LC-HRMS Liquid chromatography-high resolution mass spectrometry

LRMS Low resolution mass spectrometry

$\vec{\mathbf{M}}$ Net magnetisation vector of spins in a magnetic field

m Multiplet

***m*-CPBA** *m*-Chloroperbenzoic acid

miRNA MicroRNA

MMTr 4-Monomethoxytriphenylmethyl, 4-monomethoxytrityl

m.p. Melting point

$\mathbf{m_{resin}}$ Mass of resin

mRNA Messenger RNA

Ms Methylsulfonyl, mesyl

$\boldsymbol{m_s}$ The spin quantum number

$\vec{\boldsymbol{M}}_{\mathbf{x,y}}$ The net magnetisation in the x,y observer plane of a rotating frame model

$\vec{\boldsymbol{M}}_{\mathbf{z}}$ The net magnetisation along the z-axis of a rotating frame model

N North (3′-endo) furanose pucker

***n*-BuLi** *n*-Butyllithium

n/d Not determined

NHC N-Heterocyclic carbene

NMR Nuclear magnetic resonance

$\mathbf{OD_{260}}$ Optical density at 260 nm

$\boldsymbol{P}$ Pseudorotation phase angle

PELDOR Pulsed electron-electron double resonance

q Quartet

qt Quartet of triplets

quant. Quantitative

$\boldsymbol{R}$ Interspin distance

Red-Al Sodium bis(methoxyethoxy)-aluminium hydride

$\mathbf{R}_f$ Retardation factor

Rib Ribosyl

RNA Ribonucleic acid

RNAi RNA interference

ROS Reactive oxygen species

RP-HPLC Reversed phase high-performance liquid chromatography

rRNA Ribosomal RNA

rt Room temperature

S South (2′-endo) furanose pucker

s Singlet

SDSL Site-directed spin labelling

siRNA Small interfering RNA

ssDNA Single-stranded DNA

ssRNA Single-stranded RNA

T Thymidine

t Triplet

t Delay time before pump pulse in the DEER experiment

$\mathbf{T_1}$ Longitudinal relaxation time

$\mathbf{T_1^{-1}}$ Longitudinal relaxation rate

$\mathbf{T_2}$ Transverse relaxation time

$\mathbf{T_2^{-1}}$ Transverse relaxation rate

TBAF Tetra-*n*-butylammonium fluoride

TBS *tert*-Butyldimethylsilyl

TBTA Tris(benzyltriazolylmethyl)amine

td Triplet of doublets

TEAA Triethylammonium acetate

TEAB Triethylammonium bicarbonate

TEMPO 2,2,6,6-Tetramethylpiperidine 1-oxyl

TEMPONE 4-Oxo-2,2,6,6-tetramethyl-piperidine 1-oxyl

Tf Trifluoromethylsulfonyl, triflyl

TFA Trifluoroacetic acid

TFE 2,2,2-Trifluoroethanol

THF Tetrahydrofuran

THPTA Tris(hydroxypropyltriazolyl-methyl)amine

TIPDS 1,1,3,3-Tetraisopropyldisiloxane-1,3-yl

TLC Thin layer chromatography

$\mathbf{T_m}$ Phase memory time

$\mathbf{T_m^{-1}}$ Echo dephasing rate

$\mathbf{T_m^{260}}$ UV melting temperature

TMS Trimethylsilyl

tq Triplet of quartets

tRNA Transfer RNA

Ts *p*-Toluylsulfonyl, tosyl

tt Triplet of triplets

U Uridine

UDG Uracil-DNA glycosylase

UV Ultraviolet

V Hahn echo intensity

$\mathbf{[\alpha]_D}$ Specific optical rotation

$\boldsymbol{\beta}$ Flip angle of a microwave pulse

$\boldsymbol{\Delta}$ Heat

$\boldsymbol{\delta}$ Chemical shift

$\boldsymbol{\Delta E}$ Energy difference of Zeeman splitting

$\boldsymbol{\Delta\varepsilon}$ Molar circular dichroism

$\boldsymbol{\varepsilon}$ Molar extinction coefficient

$\boldsymbol{\theta}$ The angle between the magnetic field and the axis defined by two spins

$\boldsymbol{\lambda}$ Wavelength

$\boldsymbol{\mu_B}$ The Bohr magneton

$\boldsymbol{\nu}$ Frequency

$\boldsymbol{\tau}$ Evolution time

$\boldsymbol{\tau_m}$ Pseudorotational degree of puckering

$\boldsymbol{\chi}$ Molar fraction

$\boldsymbol{\Psi}$ Pseudouridine

$\boldsymbol{\Omega}$ Resonant excitation frequency

$\boldsymbol{\omega_A}$ Observe or probe frequency

$\boldsymbol{\omega_B}$ Pump frequency

$\boldsymbol{\omega_{dip}}$ Dipolar coupling frequency

Contents

Abstract i

Acknowledgements ii

List of symbols and abbreviations iii

Contents vi

1 Introduction **1**

1.1 A brief introduction to EPR spectroscopy 1

1.2 Nitroxyl spin labels 9

1.3 Nucleic acids 13

1.4 Studying nucleic acids with EPR spectroscopy 21

1.5 Aims of the proposed work 26

2 Synthesis of 2′-ethynyl-2′-deoxynucleosides **29**

2.1 2′-Ethynyl-2′-deoxyuridine 29

2.2 2′-Ethynyl-2′-deoxycytidine 36

2.3 2′-Ethynyl-2′-deoxyadenosine 37

3 Synthesis of nitroxyl spin labels **49**

3.1 Synthesis of tetramethylpiperidinyl nitroxyl **40** 51

3.2 Synthesis of tetramethylpyrrolinyl nitroxyl **106** 53

3.3 Synthesis of bis(spirocyclohexyl)piperidinyl nitroxyl **107** 56

3.4 Synthesis of bis(spirocyclohexyl)pyrrolinyl nitroxyl **108** 61

3.5 Isoindolinyl spin labels 63

4 Site-directed spin labelling of oligodeoxynucleotides **65**

4.1 Functionalisation of DNA at dT residues 65

4.2 Functionalisation of DNA at dC and dA residues 83

4.3 Circular dichroism studies 87
4.4 The effect of sugar puckering 90
4.5 2′-Ethynyl-2′-deoxyuridine 5′-triphosphate 93

5 EPR analysis of spin labelled DNA **96**
5.1 CW EPR of 2′-triazolyl spin labelled DNA 96
5.2 Determination of relaxation rates 102
5.3 Pulsed EPR of 2′-triazolyl spin labelled DNA 104
5.4 Measuring short interspin distances 113

6 Conclusions and future work **117**

7 Experimental **120**
7.1 General considerations 120
7.2 Synthesis of reagents 122
7.3 Synthesis of 2′-ethynyl-2′-deoxyuridine derivatives 125
7.4 Synthesis of 2′-ethynyl-2′-deoxycytidine derivatives 138
7.5 Synthesis of 2′-ethynyl-2′-deoxyadenosine derivatives 143
7.6 Synthesis of spin labels 158
7.7 DNA synthesis, characterisation and spin labelling 175

References **179**

1 Introduction

Over the past decade, electron paramagnetic resonance (EPR) spectroscopy has become established as a powerful tool for investigating the structure of biomolecules.[1–8] This highly versatile method enables not only the measurement of distances and angles, but also provides information on the dynamic behaviour of complex biological systems. As this method relies on the presence of unpaired electron spins (which are not necessarily naturally present in the biological system under study), significant effort has been directed toward the development of increasingly sophisticated methods for the site-specific modification of biopolymers, with the aim of introducing unpaired spins. This concept, generally termed site-directed spin labelling (SDSL), continues to drive research in biological applications of EPR spectroscopy.

This introductory chapter will give a brief explanation of the theory and fundamentals of EPR spectroscopy, with an emphasis on the theory relevant to applications in biological systems. Spin labels based on nitroxyl radicals (also known as aminoxyl radicals), and the factors governing their properties, are then discussed. Following a short summary of the structure and function of nucleic acids, an overview of common strategies developed for SDSL will be presented. The chapter concludes with an outline of the aims of this project.

1.1 A brief introduction to EPR spectroscopy

When an electron is placed in a magnetic field B_0, interaction between the field and the electron's magnetic dipole moment causes the energy levels of the system to be split (known as the Zeeman effect). Since the electron has a spin $I = \frac{1}{2}$, there are two possible energy states corresponding to $m_s = +\frac{1}{2}$ and $m_s = -\frac{1}{2}$, where m_s is the electron spin quantum number. The splitting of the energy states (ΔE) is dependent on the field strength B_0, as shown in Equation 1.1:

$$\Delta E = g\mu_B B_0 \Delta m_s = g\mu_B B_0 \tag{1.1}$$

where g is the g-value (discussed below) and μ_B is the Bohr magneton (a constant).[9] Since $\Delta E = h\nu$, where h is Planck's constant and ν is the frequency of irradiation causing a transition between the two energy states, Equation 1.1 transforms into Equation 1.2:

$$h\nu = g\mu_B B_0 \tag{1.2}$$

In continuous wave (CW) EPR spectroscopy, a sample is irradiated at a constant microwave frequency ν, while the strength of the magnetic field B_0 is varied. Consequently, the unit of the horizontal axis of CW EPR spectra is field strength (measured in Gauss, G).* The CW EPR spectra in this thesis have been recorded at X-band frequencies ($\sim$9.7 GHz).

The g-value, given by rearrangement of Equation 1.2 as

$$g = \frac{h\nu}{\mu_B B_0} \tag{1.3}$$

is characteristic of a given radical. The g-value can, in simplified terms, be viewed as a proportionality constant accounting for differences in the angular momentum of an electron associated with a nucleus, as compared to a free electron.† Nitroxyl radicals typically have g-values in the range of 2.0055–2.0065, close to the free electron value of 2.0023.[10] By contrast, the g-values of transition metals may vary widely due to the effect of spin-orbit coupling; for example, Cu^{2+} may have g-values up to 2.3, depending on the coordination geometry.[9]

In the presence of a nucleus with a magnetic moment (i.e. spin $I \neq 0$), the electron will experience the additional local magnetic field around the nucleus. The interaction between the nucleus and the electron, called the hyperfine interaction, causes a splitting of the EPR signal. If the electron is equally coupled to n nuclei of spin I, there will be $2nI + 1$ lines. The distance between the lines is given as the hyperfine splitting constant, a.

*Cf. other spectroscopic techniques, where ν is varied at constant B_0 and so give spectra where frequency ν is the unit of the x-axis.

†More generally, the g-value is a tensor whose anisotropy (dependence on orientation with respect to B_0) may be observed in immobilised samples.

A CW EPR spectrum of the nitroxyl radical TEMPO (**1**) is shown in Figure 1.1. The EPR signal of the nitroxyl radical is split into a triplet by interaction with the abundant ^{14}N nucleus ($I = 1$), giving rise to three lines separated by the hyperfine splitting constant a_N. Note that the spectrum is displayed as the first derivative of the absorption signal, owing to a technique known as field modulation with phase sensitive detection, which is used to enhance the sensitivity of CW EPR.

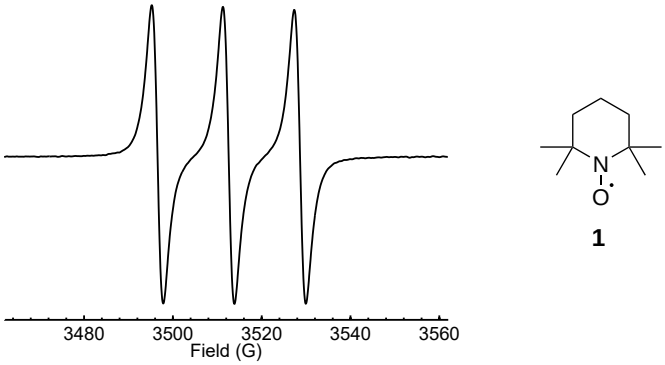


Figure 1.1: CW EPR spectrum of TEMPO (**1**, 100 μM in $CHCl_3$) recorded at X-band (9.86 GHz) at room temperature.

When more than one radical is present in a system, the distance R between the radicals can be calculated from the measurable magnetic dipole-dipole interaction between the two electron spins. In cases where the g-values are only weakly anisotropic, and the dipolar coupling is small compared to the energy level splitting (ΔE in Equation 1.1), the dependence of distance R on the dipolar coupling frequency ω_{dip} is given by

$$\omega_{dip} = \frac{D_{dip}}{R^3}(1 - \cos^2\theta) \tag{1.4}$$

where D_{dip} is the dipolar coupling constant and θ is the angle between the magnetic field B_0 and the axis defined by the two spins.[1] Note therefore that $R \propto \omega_{dip}^{-1/3}$.

Equation 1.4 has an important consequence: Because the dipolar coupling is dependent on the angle θ, the dipolar interaction of a rapidly rotating molecule is averaged to zero. Thus, only immobilised samples can be used to measure distances. This is usually achieved by dissolving the analyte in a solvent mixture that forms a glass (an amorphous solid) at

low temperatures, such as a water/glycerol mixture, and performing measurements on the frozen sample.

In CW EPR of organic radicals, the dipolar coupling can be observed directly as a broadening of the spectral lines, and be measured by lineshape analysis of the CW EPR lines.[10,11] However, it can be difficult or even impossible to distinguish the dipolar contribution from other factors causing line broadening. For distances shorter than 1 nm in particular, the contribution from exchange coupling (J-coupling) must also be considered.[1] For distances above 2 nm, the line broadening contribution from dipolar coupling is overshadowed by other line broadening mechanisms.[12] In particular, the line width of inhomogeneous samples at low temperature is dominated by the anisotropy of the g-tensor, as well as unresolved hyperfine interactions with small splitting constants.[1] This is one amongst several reasons that pulsed EPR methods have become the most important tool for distance determination with EPR spectroscopy.

1.1.1 Pulsed EPR methods

Where CW EPR is based on irradiation at a constant microwave frequency while sweeping the magnetic field, pulsed EPR techniques employ a static magnetic field and a pulse of microwave frequencies perpendicular to the magnetic field direction, reminiscent of the pulsed techniques used in modern NMR spectroscopy.[12]

A bulk of spins in a magnetic field carries a net, macroscopic magnetisation vector $\vec{\mathbf{M}}$, whose components are precessing about the magnetic field axis. By convention we choose a coordinate system with the z-axis parallel to the direction of the magnetic field B_0, and rotating about this axis at a frequency Ω equal to the resonant excitation frequency. In the ideal, fully homogeneous ensemble of spins, all the spins will have the same Larmor frequency. Applying a microwave pulse along the x-axis flips the magnetisation vector around this axis, most often with a flip angle $\beta = \frac{\pi}{2}$. Thus, immediately after the microwave pulse, $\vec{\mathbf{M}}$ is precessing around the y-axis. The net magnetisation in the xy-plane (the $\vec{M}_x$ and $\vec{M}_y$ components of $\vec{\mathbf{M}}$) is the *transverse magnetisation*, which is measured as the

output signal in pulsed EPR. The *longitudinal magnetisation* along the z-axis, $\vec{M}_z$, is for the moment zero.

The excited state of $\vec{\mathbf{M}}$ starts to relax back to the thermal equilibrium as soon as the microwave pulse is switched off. This first-order (exponential) relaxation process can be considered as two coinciding processes, where the longitudinal component $\vec{M}_z$ is relaxing back to the ground state magnetisation with the rate T_1^{-1} given as the inverse longitudinal relaxation time T_1. Simultaneously, through transverse relaxation the x,y-component $\vec{M}_{x,y}$ decays with rate T_2^{-1}, where T_2 is the transverse relaxation time.

Most modern pulsed EPR experiments are based on multiple pulse sequences, recording an electron spin echo (also known as a Hahn echo). After the initial $\frac{\pi}{2}$ pulse flips $\vec{\mathbf{M}}$ to precess around the y-axis, the spin magnetisation vectors of each spin packet start precessing around the z-axis at their individual Larmor frequencies. In a real and inhomogeneous system, where the spin packet Larmor frequencies are not identical, this is seen as a fanning out (defocusing) of $\vec{M}_{x,y}$ in the rotating frame picture. If, after an evolution time τ a π pulse is applied along the x-axis, the defocusing $\vec{M}_{x,y}$ is inverted on the y-axis. The π pulse does not change the direction of the precessing spins, so over a second time interval τ the transverse magnetisation $\vec{M}_{x,y}$ is refocused by realignment of all the individual spin magnetisation vectors. Importantly, the refocusing restores the narrow, homogeneous linewidth even in inhomogeneous frozen samples, thereby greatly enhancing the resolution of pulsed EPR spectra. The refocusing is detected as an electron spin echo, the intensity of which is a function of τ. The decrease of the echo intensity with increasing τ is described by the phase memory time T_m, which accounts for decay due to transverse relaxation (T_2) as well as other relaxation mechanisms which are beyond the scope of this text.

The double electron-electron resonance (DEER) experiment, also known as PELDOR (pulsed electron-electron double resonance), has proven particularly valuable for the measurement of distances in biopolymers. This experiment is one of only a few methods suitable for distance measurements in the 2–10 nm range, and takes advantage of the dipolar coupling ω_{dip} between two spins A and B as described in Equation 1.4.

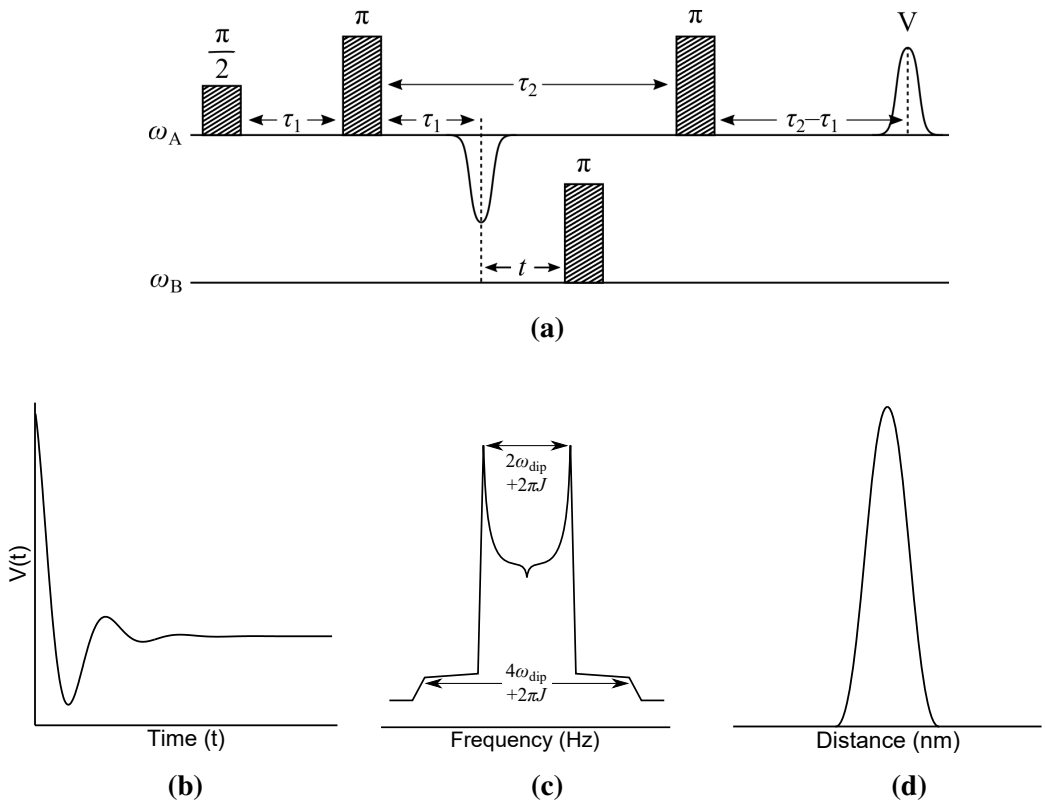


Figure 1.2: **(a)** Pulse sequence for the four-pulse DEER experiment. **(b)** A time-domain DEER spectrum shows the echo intensity V as an exponentially decaying sinusoidal function of t. **(c)** The time-domain spectrum can be Fourier transformed into the frequency domain, displaying a Pake pattern. **(d)** By Tikhonov regularisation, the time-domain data may alternatively be transformed into a distance distribution.

The pulse sequence of the 4-pulse DEER experiment is shown in Figure 1.2a. The experiment uses a refocused Hahn echo pulse sequence employing a $\frac{\pi}{2}$ pulse, two π pulses and two evolution times τ_1 and τ_2 in analogy to the above discussion. These pulses are selective for only spin A of the AB spin pair, at the so-called *observe* or *probe frequency* ω_A. An additional π pulse at a different *pump frequency* ω_B at time t causes the B-spin to flip. Because the AB spin pair is coupled, this changes the Larmor frequency of spin A by $\pm\omega_{dip}$. Consequently, the refocused $\vec{M}_{x,y}$ at the Hahn echo is offset from the y-axis, decreasing the echo intensity. By repeating the pulse sequence many times, varying the time $0 < t < \tau_2 - \tau_1$, a sinusoidal modulation of the echo intensity V given by

$$V(t) = V_0 \cos(\omega_{dip} t) \tag{1.5}$$

is observed, where V_0 is the echo intensity at $t = 0$. In theory, by fitting the experimental DEER data to Equation 1.5 the dipolar coupling frequency ω_{dip} can be measured, and thus the interspin distance R can be calculated (Equation 1.4).

In principle, a time-domain DEER spectrum (Figure 1.2b) can be Fourier transformed into a frequency-domain spectrum (Figure 1.2c). In the *Pake pattern* displayed in this spectrum, the distance between the singularities is given as $2\omega_{dip} + 2\pi J$. If the interspin distance is large (≥ 2 nm) and the spins are only spatially coupled, the exchange coupling contribution (J) is negligible. When the spectrum is of sufficient quality, and the edges of the Pake pattern can be observed, the dipolar and exchange couplings can be separated, as the distance between the edges is given by $4\omega_{dip} + 2\pi J$.

In practice, however, the time-domain DEER spectrum is usually transformed into a distance distribution (Figure 1.2d) through a numerical algorithm known as *Tikhonov regularisation*. Although this approach does not distinguish the contribution of exchange coupling, and so is only suitable for interspin distances ≥ 2 nm, it presents the DEER data in an intuitively approachable format where the global maximum on the vertical axis (of arbitrary units) represents the highest probability for the interspin distance R. Tikhonov regularisation is a particularly powerful method for situations where several conformations of different R contribute to the overall ω_{dip}, as it can even provide information about the distribution of the various distances.

Relaxation is one of the limiting factors on the measuring time of pulsed EPR, and thus also limits the resolution and the maximum distance measurable in these experiments. The longer the evolution time τ_2 in the DEER experiment, the greater the maximum distance that can be accurately measured. Thus, there is a considerable interest in the field of EPR spectroscopy for methods to extend T_m relaxation times of spin labels. Furthermore, the development of spin labels with long T_m even at room temperature would permit pulsed EPR experiments to be performed on samples at physiologically relevant temperatures, thereby greatly enhancing the applicability of EPR spectroscopy to the study of biological systems.

1.1.2 EPR vs. FRET

Förster resonance energy transfer (FRET) spectroscopy is a well-established method for studying distances and dynamics in biological systems, with a distance range similar to that of pulsed EPR spectroscopy.[13] Where EPR distance studies are based on the interaction of spin labels, FRET studies consider the non-radiative transfer of energy between chromophores. The fluorescent donors and acceptors used for FRET are usually non-identical, which complicates the labelling strategies. In contrast, EPR measurements can be performed on pairs of identical spin labels. Moreover, the fluorescent tags used for FRET are often much larger than the typical EPR spin label, making them potentially more disruptive to the structure and activity of the modified biopolymer. To avoid this, FRET labels are usually conformationally less restricted than spin labels, and are often conjoined to the biopolymer with a long, flexible linker.[13] A consequence of this is that FRET is usually not able to provide information about angles, whereas this information is available from a rigid, well-defined spin labelled system. The well-defined nature of spin labelled systems also makes it easier to correlate the measured distances with the molecular structure of the labelled biopolymer.

It is also technically easier to calculate a distance distribution from dipolar couplings, than it is to measure it with fluorescence intensities. In the case of FRET, care must be taken to deconvolute the FRET interaction from other fluorescence quenching mechanisms.[13] To this end, it may be necessary to perform several fluorescence measurements with standard samples with or without modifications. This is normally not necessary for most pulsed EPR methods.

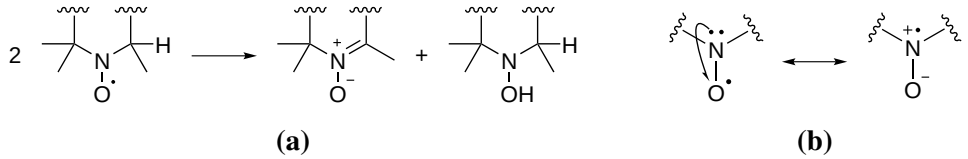
The primary advantages of FRET over EPR is its higher concentration sensitivity, and that it can be applied to liquid solutions at physiological temperatures, thus allowing the real-time monitoring of biological processes.[13] Pulsed EPR suffers from the need to use cryogenic temperatures with the most widely available spin labels, making the method unable to provide direct dynamic information. This reiterates the potential for improved spin labels with extended T_m at ambient temperature.

1.2 Nitroxyl spin labels

EPR spectroscopy requires the presence of a spin-active entity, i.e. a molecule containing an unpaired electron. In biomolecules, certain protein-complexed transition metals are examples of naturally occurring spin-active sites. However, the majority of biomolecules are diamagnetic, and thus require the introduction of a spin label – a small molecule containing an unpaired spin – through SDSL, as discussed below. It is well known that the method of label attachment is crucial to the success of an SDSL strategy; however, the structure of the spin label itself also plays an important role to this end. This section provides an introduction to nitroxyl-based spin labels and the factors that govern their properties.

Many chemical entities, such as chelated metal ions (e.g. Gd(III), Cu(II) or Mn(II))[14–16] or tetraarylmethyl-derived radicals,[15,17–19] can be used as spin labels. The most commonly used class, however, is the α,α′-tetrasubstituted nitroxyl radicals (also known as nitroxides or aminoxyl radicals), presumably due to their high stability and relative ease of synthesis. In addition to preventing disproportionation by α-H abstraction, yielding equimolar amounts of hydroxylamine and nitrone (Figure 1.3a), these alkyl substituents provide kinetic stabilisation of the radical by steric shielding. Additional electronic stabilisation is provided by delocalisation of the unpaired electron over the N–O bond (Figure 1.3b), where around 70% of the spin density is localised on oxygen and the remaining 30% resides on nitrogen.[20] Because the theory behind experiments such as DEER approximates the spin to a point, the localised nature of nitroxyl radicals makes them attractive for use as spin labels.

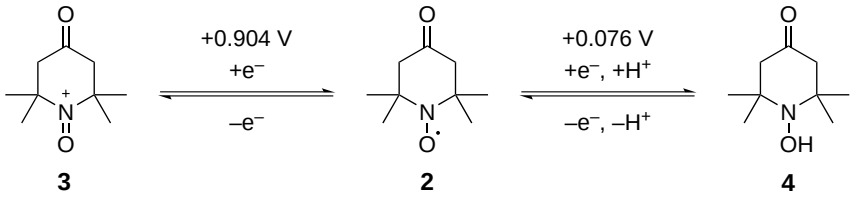
Nitroxyl radicals (e.g. TEMPONE, **2**) are susceptible to reduction as well as oxidation



(a) **(b)**

Figure 1.3: **(a)** α-Substituents prevent the disproportionation of nitroxyls into nitrones and hydroxylamines. **(b)** The radical is further stabilised by delocalisation.

(Scheme 1.1). This carries significance for the use of nitroxyls as spin labels in biological systems, which are often reducing environments. Single-electron oxidation generates oxoammonium salt **3**, itself a strong oxidising agent. Alternatively, single-electron reduction of the nitroxyl by relatively mild reducing agents, such as the biologically important glutathione or ascorbic acid, generates hydroxylamine **4**. Stronger reducing agents, such as aluminium hydrides, may fully reduce the nitroxyl to a secondary amine (not shown). The presence of inductive electron-withdrawing groups on or in the nitroxyl-containing ring[21] or on the α-substituents[22] destabilise the oxoammonium salt and thus disfavour the oxidation of nitroxyls, while simultaneously making reduction to a hydroxylamine more feasible. Conversely, inductive electron-donating groups increase the propensity for oxidation, and decrease the susceptibility of nitroxyl radicals towards reduction.



3 **2** **4**

Scheme 1.1: Nitroxyl radicals are susceptible to reduction to hydroxylamines or oxidation to oxoammonium salts. Literature reduction potentials were determined by cyclic voltammetry in aqueous buffer (pH 7.4).[22]

The size and nature of the nitroxyl-containing ring is of major importance to the redox stability of nitroxyls (Figure 1.4a). For example, it has been shown that ascorbic acid reduces 6-membered piperidine-derived nitroxyls (**1**) more rapidly than 5-membered unsaturated 3-pyrroline-derived nitroxyls (**5**). Saturated 5-membered pyrrolidine-derived nitroxyls (**6**) are the most stable towards reduction.[23,24]

The rate of reduction is also influenced by the steric protection of the nitroxyl radical provided by the α,α′-substituents (Figure 1.4b).[25–28] Compared to a tetramethyl-substituted spin label (**7**), the rate of reduction by excess ascorbic acid is halved in a bis(spirocyclohexyl)-substituted piperidine nitroxyl radical (**8**).[25] Tetraethyl-substitution (**9**) further reduces the reduction rate by a factor of up to 70; crystal structures[25] show

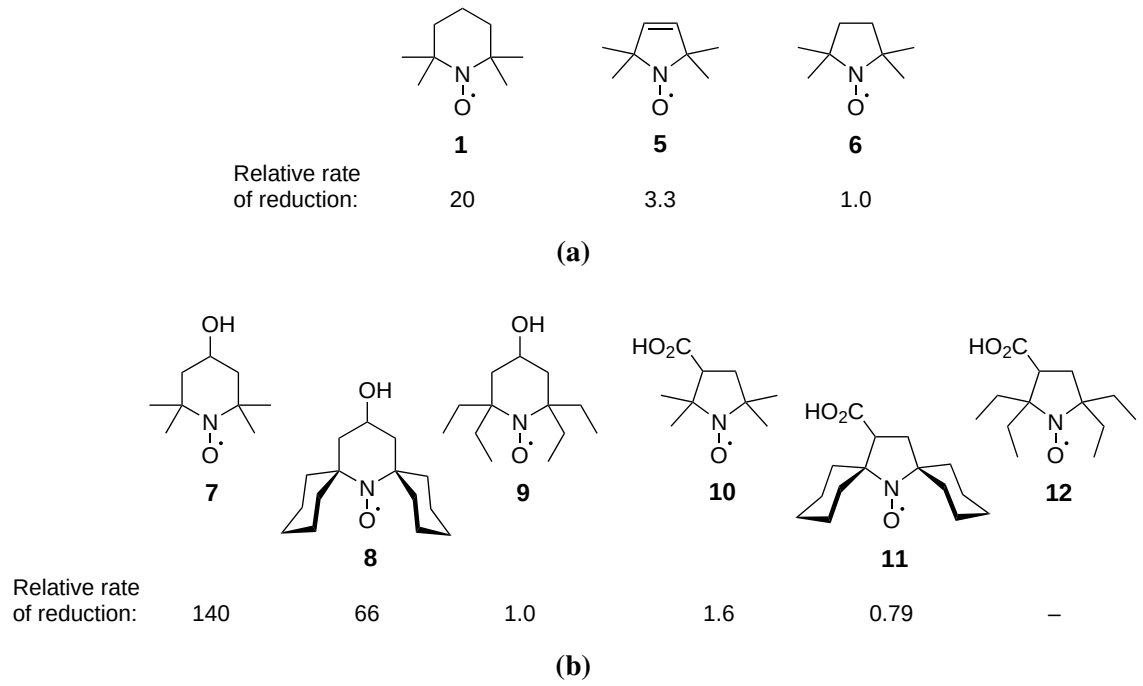


Figure 1.4: Reduction rates of nitroxyls by ascorbic acid in aqueous buffer (pH 7.4) are dependent on **(a)** the size and nature of the nitroxyl-bearing ring,[24] and **(b)** the steric protection provided by the α-substituents.[25]

that the ethyl substituents offer more effective steric crowding around the nitroxyl because they are not confined to a chair conformation as the spirocyclohexyl substituents are. A similar trend is also observed in a series of carboxylic acid pyrrolidine nitroxyl radicals (**10** vs. **11**).[‡] Remarkably, tetraethyl-substituted pyrrolidine nitroxyl **12** was shown to be very stable towards reduction, with 98% of the radical still present after incubation with 100 equivalents of ascorbic acid in a buffered solution for 5.5 hours.[25]

As mentioned in Section 1.1.1, the phase memory time T_m of a spin label limits the resolution and the maximum distance measurable in pulsed EPR experiments such as DEER. For this reason there is considerable interest in the development of new spin labels displaying extended relaxation times. It has been shown[29,30] that rotation of methyl groups at temperatures above 60 K occurs at a frequency comparable to that of the hyperfine anisotropy between the nitroxyl radical and the $I = \frac{1}{2}$ protons of the α-methyl groups.

[‡]Note that rates for the piperidine and pyrrolidine series in Figure 1.4b should not be compared directly. In a buffered system, electrostatic repulsion between the carboxylates of pyrrolidines **10**–**12** and ascorbate, as well as the inductive electron-donating ability of the carboxylate, are thought to contribute to lowering of the reduction rate.

The anisotropy of this interaction provides a mechanism for relaxation of the excited spin. Eaton and co-workers[31,32] showed that this mechanism is removed in the more rigid bis(spirocyclohexyl)-substituted nitroxyls (e.g. **8** and **11**), whose relaxation rates remain low enough to allow DEER measurements to be performed up to 125 K. Higher temperatures were not attempted, because relaxation rates increased rapidly as the water/glycerol glass matrix began to soften. These temperatures are, however, still achievable using liquid N_2 as the cryogen, thus considerably reducing the cost of the experiment compared to the liquid He used for measurements at 50 K. Moreover, the authors suggested that using a matrix that remains rigid at even higher temperatures could further extend the upper temperature limit.

Bis(spirocyclohexyl)-substituted spin labels have so far seen limited use in the SDSL of nucleic acids. Bagryanskaya and co-workers recently used the activated ester **13** (Figure 1.5) to spin label the 3′-terminus of an RNA duplex *via* an amide bond (**14**) in an interesting RNA-templated alkylation strategy.[33] Due to the long and flexible nature of the linker between the RNA backbone and the amide, this system yielded wide DEER distance distributions. Nevertheless, the strategy was recently applied to labelling a long segment of hepatitis C virus (HCV) genomic RNA.[34] The same group also used the same activated ester **13** in a different labelling strategy using a shorter and more conformationally restricted linker (**15**).[35] After successfully measuring interspin distances by DEER in DNA duplexes

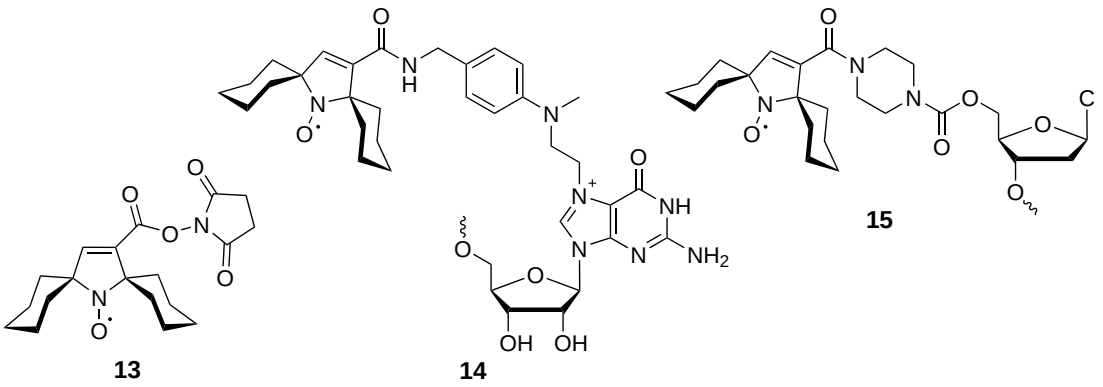


Figure 1.5: Bis(spirocyclohexyl)-substituted nitroxyl spin labels previously incorporated into nucleic acids.

immobilised in dehydrated trehalose at 298 K, the authors found that bis(spirocyclohexyl)-substituted spin labels only displayed extended relaxation times compared to a tetramethyl-substituted label when incorporated into an oligonucleotide, suggesting that the improved relaxation properties of spirocyclic spin labels may be due more to the interaction between the label and biomolecule, and the length and nature of the linker, than the intrinsic relaxation properties of the label.

1.3 Nucleic acids

Following the elucidation of the structure of deoxyribonucleic acid (DNA) in 1953,[36–38] much progress in the area of nucleic acid research was made throughout the latter part of the 20th century. The identification of new functions for oligonucleotides has renewed attention to the field in recent years. One notable advance is the discovery of catalytically active nucleic acids, DNAzymes and ribozymes, which catalyse biotransformations such as amide bond formation by rRNA in protein synthesis or ligation or cleavage of RNA or DNA strands (e.g. in self-splicing introns).[39–42] Another example is the discovery of aptamers, nucleic acids which selectively bind other biomolecules or small molecules with high affinity. Aptamers have emerged as a powerful tool in biotechnology; they have been used as biosensors, in bioimaging applications, and even as therapeutics or drug vectors.[43–46] In Nature, aptamers occur as riboswitches, segments of mRNA involved in translational autoregulation.[42,47–49] A final but significant example of novel applications for nucleic acids is RNA interference (RNAi),[50] which is based on hybridisation of endogenous micro-RNAs (miRNAs) or exogenous small interfering RNAs (siRNAs) with cellular mRNA to inhibit translation into a protein and cause degradation of the mRNA, thus effectively silencing a gene.[51] Beyond its utility as a tool for molecular biology, RNAi technologies show great promise in therapeutic applications, and a number of siRNA drug candidates are currently undergoing clinical trials.[52,53]

Common to these examples is that a detailed understanding of nucleic acid structure proved crucial to the discovery and development of novel applications. This section aims to

provide a brief summary of the structures of DNA and RNA, in the context of understanding their functions.

The primary structure of nucleic acids is well understood.[51] Deoxyribonucleic acid (DNA) is a polymer of 2′-deoxyribonucleotides (Figure 1.6a), while ribonucleic acid (RNA) consists of the corresponding ribonucleotides. Each nucleic acid (DNA or RNA) primarily contain four out of the five nucleosides, adenosine (A), cytidine (C), guanosine (G), and thymidine (T, in DNA) or uridine (U, in RNA), and the order of these in the polymer (Figure 1.6b) encodes the genetic information. It is thought that the predominance of T rather than U in DNA can be explained by the relative chemical instability of C; spontaneous hydrolytic deamination of C transforms this nucleobase into U, thereby altering the genetic code. However, enzymes known as uracil-DNA glycosylases (UDGs) recognise and excise U nucleobases in DNA, thereby triggering the enzymatic base excision repair pathway correcting the mutation.[51] As 'genuine' T residues are distinguished by the enzymes, UDGs

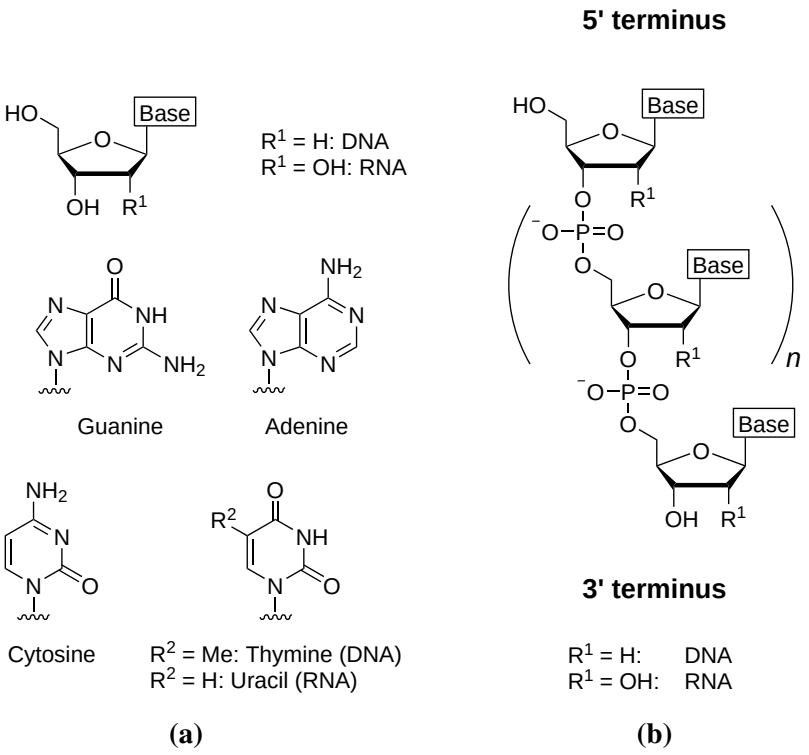
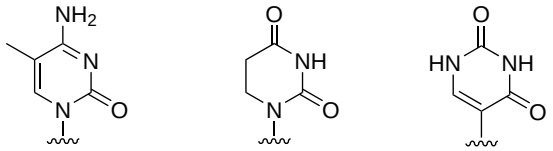


Figure 1.6: Primary structure of nucleic acids. **(a)** Nucleosides consist of ribose or 2′-deoxyribose condensed with one out of five nucleobases. **(b)** Through phosphodiester bonds, nucleotides form oligomers and polymers.

are able to correctly restore the genetic sequence.

Structural modifications of the canonical nucleotide framework are thought to play an important role in the biochemistry of nucleic acids. For example, 5-methylation of cytidine (**16**, Figure 1.7) has been shown to act as an epigenetic marker associated with downregulation of gene transcription in eukaryotes.[54] Postsynthetic modifications are particularly abundant in mature RNA; prominent examples include dihydrouridine (D, **17**) and pseudouridine (Ψ, **18**) present in tRNA.[51]



16 **17** **18**

Figure 1.7: Postsynthetically modified nucleobases such as 5-methylcytidine, dihydrouridine and pseudouridine are ubiquitous in nucleic acids.

The conformations adopted by the (deoxy)ribofuranosyl moiety has important consequences for the secondary structures of nucleic acids (see below). The concept of pseudorotation has been used to describe the continuum of conformations available to five-membered rings in terms of the phase angle P and degree of puckering τ_m.[55] P, which can be considered the angular coordinate on the pseudorotation wheel (Figure 1.8a), indicates which atoms in the sugar ring deviate from the plane defined by the remaining atoms, whereas τ_m (the radial coordinate) indicates how far away from the plane the atoms lie. In (deoxy)ribonucleosides a complex interplay of sterics, torsional strain, stereoelectronic effects and intramolecular hydrogen bonding contribute to the relative stability of conformers.[56,57] It is known from a large body of X-ray crystallographic data[58] that the sugar ring generally prefers 3′-endo puckered conformations, also called *north* conformations (N, $-10° \leq P \leq +40°$), or 2′-endo (*south*, S, $140° \leq P \leq 185°$) conformations. τ_m typically has a value of 25–45°.[59]

In solution at room temperature, the various conformers of nucleosides are rapidly interconverting. NMR studies have shown that the conformational distribution of nucleosides

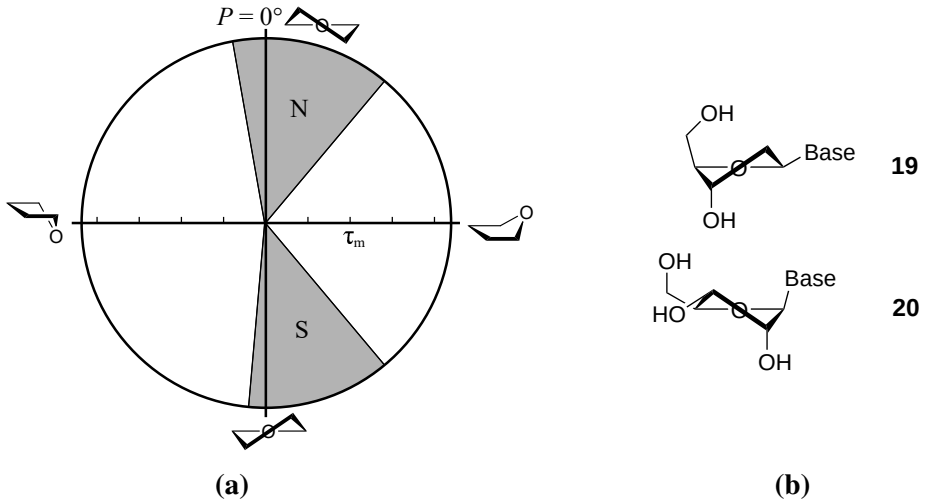


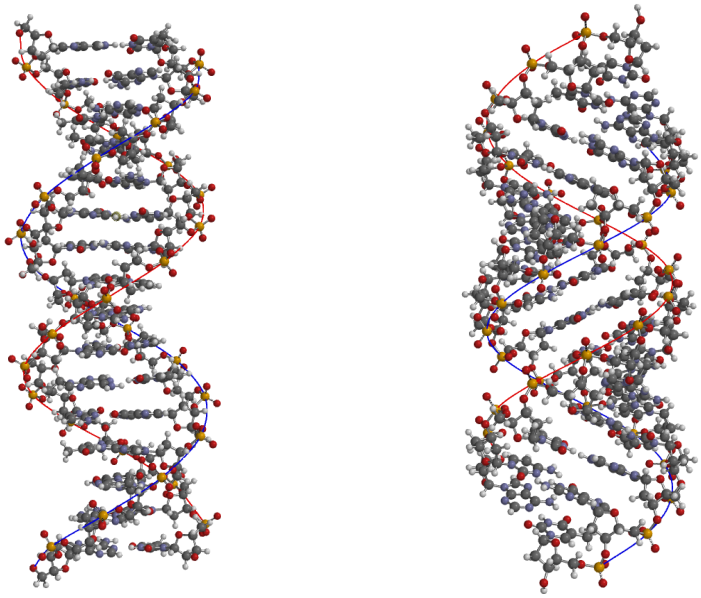
Figure 1.8: (a) A pseudorotation wheel describes all conformations available to the ribofuranosyl moiety of nucleosides; conformations in the N or S regions are preferred. **(b)** Deoxyribonucleosides prefer S-type conformations (**19**), while ribonucleosides often have N-type conformations (**20**).

can be simplified to an N⇌S two-point equilibrium, with an energy barrier of interconversion of 2–5 kcal/mol.[60–62] A majority of deoxyribonucleosides show a preference for S-type conformations (**19**, Figure 1.8b), driven by a stabilising O3′-O4′ gauche effect.[56] The presence of an additional 2′-hydroxyl group in ribonucleosides largely cancels out this effect through a corresponding O2′-O4′ gauche stabilisation in the N conformations, leading to a more even distribution between N- and S-type conformers. An N1′-O4′ anomeric effect can however only be present in N conformations, where the nucleobase occupies a pseudoaxial position (**20**), driving the conformational equilibrium towards N-puckering.[56] This effect is more pronounced for pyrimidines than for purines, owing to the relative electron deficiency of the former. Moreover, the larger steric bulk of purines drives the conformational equilibrium towards S-type conformers, in which the nucleobase occupies a pseudoequatorial position.[56,61]

In aqueous solutions, nucleic acids tend to form well-defined secondary structural motifs. A driving force for this is the hydrophobicity of the aromatic nucleobases, which aggregate in the interior of the structure, leaving the hydrophilic ribose and phosphodiester backbone exposed to the aqueous solution.[63] This arrangement further minimises electrostatic phosphate repulsion. The structures are often stabilised by π-stacking interactions

between the aromatic nucleobases.[64] In many motifs, further stability is imparted by base pairing; by complementary alignment of the hydrogen bond donor and acceptor functional groups in the nucleobases, inter-base hydrogen bonding contributes to aligning the bases in a well-defined manner.[51] Depending on conditions such as water content, the base sequence, or presence of modifications (e.g. modified nucleobases, see Figure 1.7), a variety of secondary structural motifs may be available to the nucleic acid.

The iconic B-form double helix is perhaps the most common secondary structural motif of double-stranded DNA (dsDNA, Figure 1.9a).[59] Canonical AT and GC Watson-Crick base pairing ensures a high degree of uniformity in this classical structure, which is the predominant form of dsDNA under aqueous, physiological conditions.[51] At low relative humidity, or for certain sequences, A-form DNA becomes the favoured secondary structure of dsDNA (Figure 1.9b).[59] However, for RNA and mixed RNA-DNA duplexes (of biological relevance e.g. during transcription or for nucleic acid therapeutics), the A-form is the predominant type of double helix under common physiological conditions.[59] Though both of these structures are right-handed double helices, there are notable geometrical



(a) **(b)**

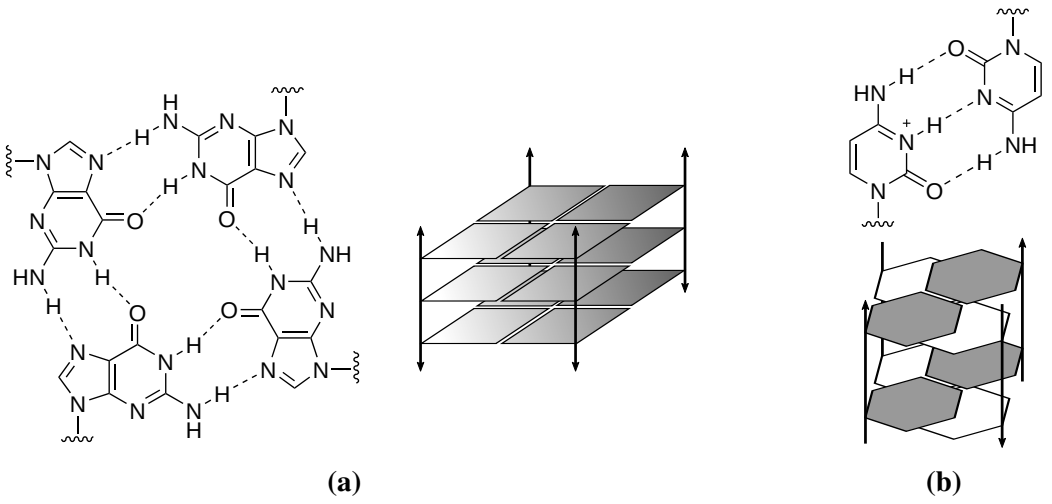
Figure 1.9: Secondary structure of DNA. **(a)** B-form DNA. **(b)** A-form DNA. Idealised models built in Spartan 14.

Table 1.1: Geometrical differences between B-form and A-form DNA.[51]

	B-form	**A-form**
Diameter	20 Å	26 Å
Base pair per helical turn	10.5	11
Helix rise per base pair	3.4 Å	2.6 Å
Base tilt	6°	20°
Sugar pucker	2′-endo (S)	3′-endo (N)

differences (summarised in Table 1.1) making A-form DNA shorter and wider than B-form DNA.[51] Notably, nucleotides occur in S conformations in B-DNA, while in A-DNA the deoxyribose has an N-type pucker. The preference for A-RNA may thus be rationalised by the shift of ribonucleoside conformational equilibria towards N conformations (see above).

Many other secondary structural motifs besides the double helices are known. G-quadruplexes are a prominent example in DNA, consisting of stacked tetrads of Hoogsteen-base paired guanosines (Figure 1.10a).[59] Many topological forms of G-quadruplexes are possible, depending on the relative alignment of their constituent DNA strand(s). G-quadruplexes are thought to occur *inter alia* in G-rich telomeric sequences at the 3′-termini of eukaryotic genomic DNA, and several biological regulatory functions have recently



(a) **(b)**

Figure 1.10: Examples of secondary structural motifs in nucleic acids. **(a)** G-quadruplexes in DNA consist of stacked tetrads of Hoogsteen-base paired guanosines. Several combinations of parallel and antiparallel arrangements are possible. **(b)** The i-motif consists of four intercalating strands, where two and two strands are held together by base pairs between C and 3-*N*-protonated C.

been proposed.[65] The i-motif (Figure 1.10b), another secondary structural element, has been identified in C-rich sequences (such as the complementary strand to the G-quadruplex forming telomeric sequences) crystallised at low pH.[59]

Compared to DNA, RNA is thought to possess a far greater plethora of structural variation. This may perhaps be seen in connection with the relatively exclusive role of DNA as the repository of hereditary information, and its general confinement to the cellular nucleus in eukaryotic organisms. Unlike DNA, RNA in nature is often found as single stranded RNA (ssRNA), which is able to adopt a large number of secondary structural motifs beyond the duplex, many of which are implied to be significant for any functional properties of the nucleic acid. Through non-Watson-Crick hydrogen bonding (e.g. between G and U, or any nucleobase and the 2′-hydroxyl functionality, accessible in the minor groove) RNA (as well as DNA) can also form triplexes or quadruplexes.[51,59] Other common secondary structural motifs include loops, bulges, hairpins and pseudoknots (Figure 1.11); although these motifs are more commonly encountered in RNA, they can in principle be adopted by any nucleic acid.[51,59]

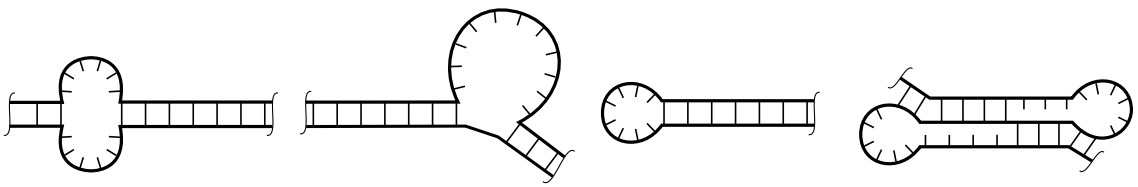


Figure 1.11: Other common secondary structural motifs in nucleic acids include (left to right) loops, bulges, hairpins and pseudoknots.

The tertiary structures of many biologically interesting nucleic acids have been characterised, and a number of computer algorithms for tertiary structure prediction have been developed based on these.[66] An important example of the relationship between secondary and tertiary structure is provided by yeast phenylalanine tRNA,[67] the secondary structure of which exhibits all the highly conserved tRNA secondary structural motifs (Figure 1.12a). The crystal structure (Figure 1.12b), however, reveals that the classical ‘cloverleaf’ representation is not an accurate description of the tertiary structure of tRNAs. The tertiary structure features many interactions which cannot be easily illustrated in a two-dimensional

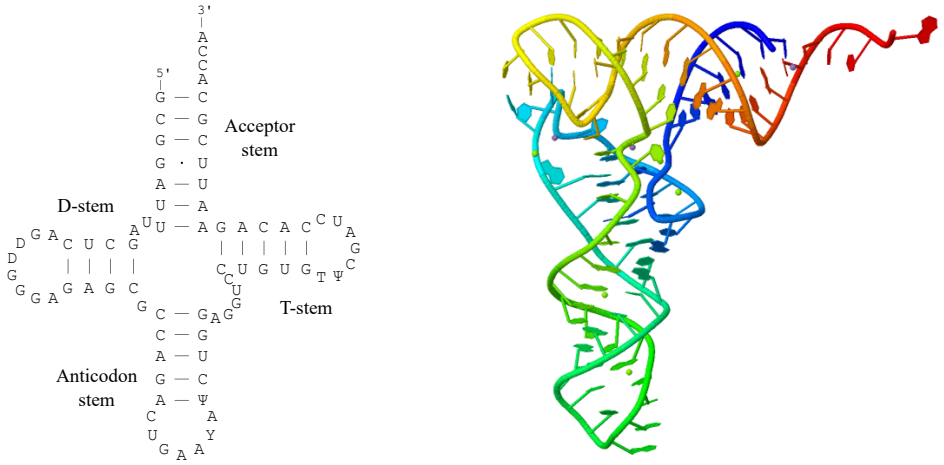


Figure 1.12: Yeast phenylalanine tRNA **(a)** secondary and **(b)** tertiary structures (PDB ID 1EHZ).[67] Methylation of nucleotides in the secondary structure is omitted for clarity.

representation; it is stabilised by a number of interactions beyond the obvious base pairing and π-stacking, such as non-canonical base pairs, helix stacking between the anticodon and D-stems and between the acceptor and T-stems, and 11 coordinated divalent cations.[67]

Although there are many examples of known tertiary structures of nucleic acids, they are generally less well-understood than secondary or primary structural elements. This may in part be ascribed to the technical difficulties of crystallising large nucleic acids (in particular flexible, disordered RNA strands), thus preventing them from being studied by X-ray crystallography.[59] Conditions used for crystallisation may also potentially affect the structural arrangement, such as favouring non-Watson-Crick base-paired helical arrangements over extrahelical loops in some RNAs.[59,68] Nevertheless, thousands of crystal structures of relatively short nucleic acids are known, albeit most of them complexed with a protein or a ligand. NMR studies are also proven to be a useful and complementary solution-state method for investigating the tertiary structure of nucleic acids.[59] In general, good agreement is observed between NMR- and crystallography-derived tertiary structures. However, NMR investigation of nucleic acids longer than 50–60 nucleotides is very challenging.[69] Complementary and highly sensitive spectroscopic techniques such as FRET and EPR (see Section 1.1) are thus proving increasingly valuable tools for the study of the structure and even motions of large nucleic acids which are not prone to crystallisation.[34,70,71]

1.4 Studying nucleic acids with EPR spectroscopy

Developing improved methods for the characterisation of biopolymers is crucial to furthering our understanding of their structure and function. EPR spectroscopy, the fundamentals of which were introduced in Section 1.1, is an increasingly popular technique to this end. Much previous attention has been given to SDSL of proteins, and studying them by means of EPR spectroscopy. After the solid-phase synthesis of oligonucleotides became an automated and widespread technique in the 1980s, SDSL of nucleic acids has also been gaining momentum. This section will provide an overview of previous approaches to covalent SDSL of nucleic acids, for the purpose of studying them with EPR spectroscopy.

Two primary approaches are employed towards covalent SDSL of nucleic acids: Labelling during the solid-phase synthesis of the oligonucleotide, or labelling after the biopolymer has been synthesised. The former method has been popular, as it ensures site-selective and highly efficient labelling. However, nitroxyl radicals, the core functionality of most spin labels, can be degraded by the standard conditions used in the phosphoramidite solid-phase synthesis of oligonucleotides.[72] In particular, nitroxyls have been shown to be incompatible with iodine[73–76] and relatively strong acids such as trichloroacetic acid.[73,74,77,78] Thus, this approach usually requires expertise in optimisation of the oligonucleotide synthesis, or some degree of laborious manual oligonucleotide synthesis. Nevertheless, there are many successful examples of this SDSL approach, a selection of whom are shown in Figure 1.13.

The first example of SDSL using the phosphoramidite method for oligonucleotide synthesis was reported in 1988, using the 5-ethynyl-dU linked spin label **21**.[79–81] The authors claim that the nitroxyl label is compatible with the phosphoramidite chemistry, but no yields are reported. This modification, and a variation using a 6-membered nitroxyl moiety where the spin density (N–O bond) lies on the axis of the rotatable acetylene linker, has also later been used by others,[75,82–85] as well as the same modification on a dC residue.[86] Another approach has been to attach the spin label to exocyclic amine groups (**22**, **23**), thus also offering access to spin labelled purine bases.[87–89] Extremely rigid systems are obtained using the fused quinolone-derived non-natural base **24**.[90–93] However,

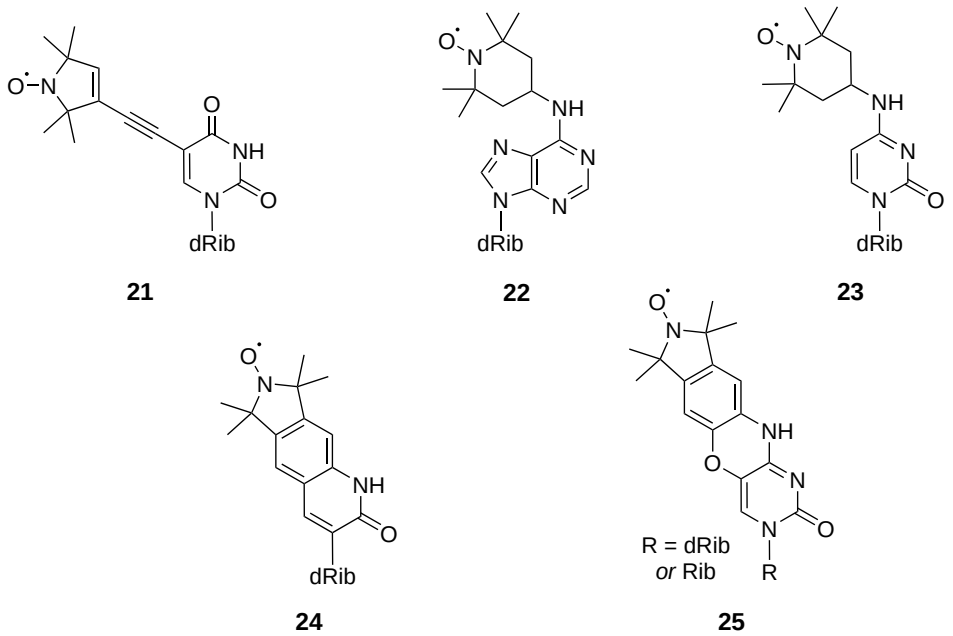


Figure 1.13: Selected examples of previous SDSL approaches where the spin label was incorporated during the synthesis of the oligonucleotide. Rib = ribosyl, dRib = 2′-deoxyribosyl.

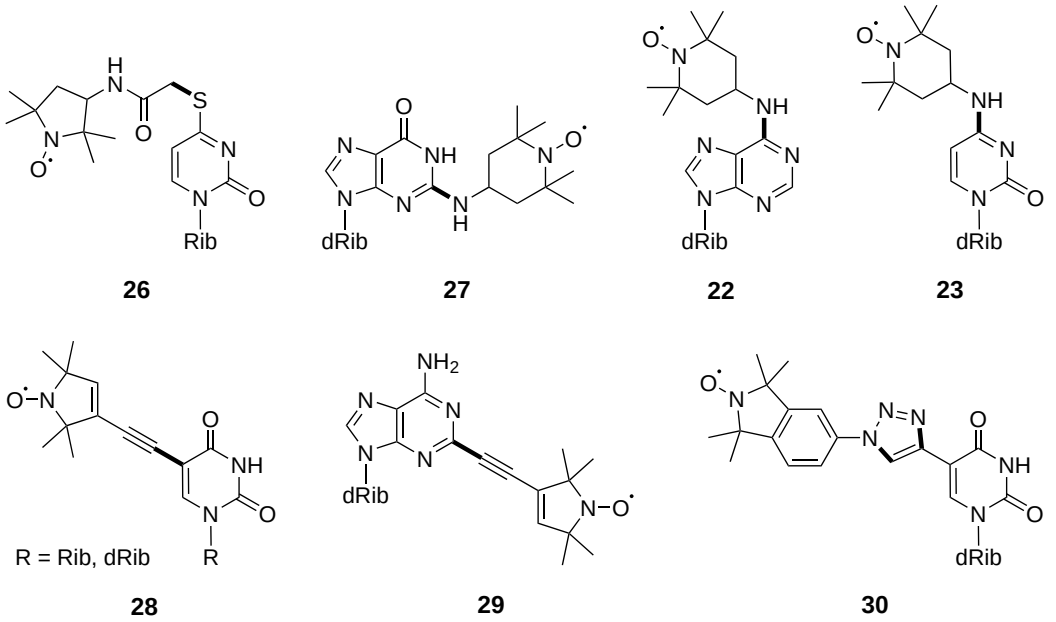
this base suffers from limited aqueous solubility, and furthermore requires a non-natural hybridisation partner, 2-aminopurine, on the complementary strand. These issues were resolved by Sigurdsson *et al.* with the C analogue **25** (in the literature often represented as **Ç**, "C-spin").[94] This spin label has been highly successful, and seen widespread application both in the study of biological systems and the development of EPR techniques.[72,89,95–102]

It is notable that, to date, all examples of SDSL during the oligonucleotide synthesis incorporate the spin label on the nucleobase moiety of the nucleotides. This may come down to the synthetic convenience of introducing a modification at this unit. In particular, functionalisation of the 5-position of pyrimidine nucleosides U/T and C has been popular, presumably because the phosphoramidite building blocks of 5-iodouridine and 5-iodocytidine are commercially available. One strength of this strategy, including all the examples in Figure 1.13, is that the label is projected into the major groove of the oligonucleotide duplex, thus avoiding large structural perturbations. One drawback, however, is that modification of the nucleobase limits the applicability of the SDSL strategy to only one (or, in some cases of pyrimidine modification, two) out of the four possible nucleotides in a given nucleic acid sequence.

For the second main approach to covalent SDSL, where the spin label is installed after the oligonucleotide has been assembled (*post-synthetically*), chemical incompatibility of the nitroxyl radical is not an issue. By reacting the spin label with a site-selectively pre-installed functional group, the SDSL can be performed without the need to change the standard conditions for automated oligonucleotide synthesis. Although the resulting linker groups are, in some cases, more flexible, the post-synthetic labelling strategy benefits from a high degree of divergence in that different spin labels (or indeed fluorescent or radiolabels) can be installed at the very last synthetic step. Figure 1.14 shows a selection of previous approaches to post-synthetic SDSL.

The nucleobase has been the most frequent point of modification for post-synthetic SDSL (Figure 1.14a). One of several strategies to this end has been the formal alkylation of exocyclic functional groups. This has been achieved by treatment of 4-thiouridine with electrophiles such as α-iodoacetamides to give the relatively flexible thioether **26**.[103–105] Notably, this strategy alters the hydrogen bonding properties of the nucleobase. This is avoided in a second approach, where nucleophilic displacement of pre-installed leaving groups such as fluoride (**27**) or electron deficient phenolates (**22**, **23**) by amine spin labels affords more rigid systems.[101,106–110] Alternatively, spin labels have been introduced by functionalisation of the nucleobase by Sonogashira coupling (**28**, **29**)[76,111–116] or Cu(I)-catalysed azide-alkyne $[3+2]$ Huisgen cycloaddition (CuAAC or the 'click' reaction, **30**).[117–119] All of the examples in Figure 1.14a allow the spin label to reside in the major groove of the duplex, except for the modifications of the 2-position of purines (**27**, **29**) which project into the minor groove.

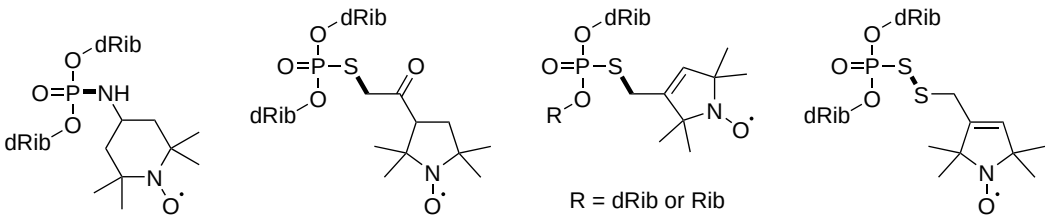
The phosphodiester bond of the nucleic acid backbone can also be spin labelled (Figure 1.14b). This has previously been achieved by oxidation of an H-phosphonate in the presence of an amine spin label (**31**),[120–122] or by alkylation of phosphorothioates by electrophiles such as α-iodoacetamides (**32**),[123–126] allylic iodides (**33**)[127–134] or methanethiosulfonates (**34**).[135] The prime appeal of phosphodiester labelling is that it is entirely independent of the nucleobase, making this SDSL strategy independent of the oligonuc-



26 **27** **22** **23**

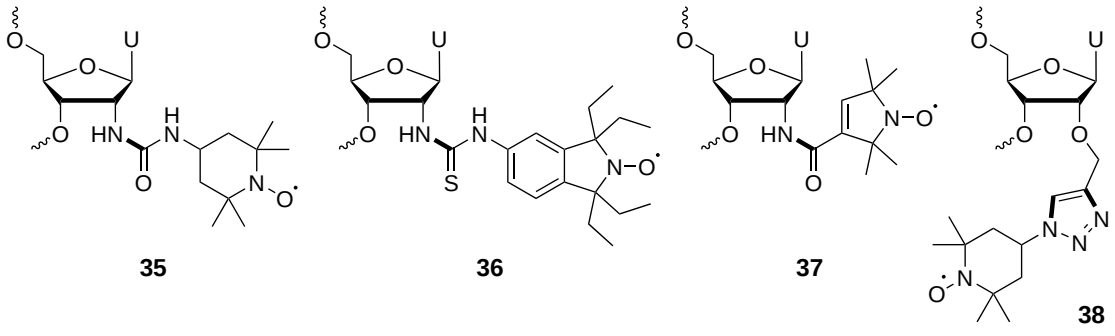
28 **29** **30**

(a)



31 **32** **33** **34**

(b)



35 **36** **37** **38**

(c)

Figure 1.14: Examples of previous SDSL approaches where the spin label was incorporated post-synthetically **(a)** on the nucleobase, **(b)** on the phosphodiester bond, or **(c)** on the ribose moiety. Bonds formed in the labelling step are bold. Rib = ribosyl, dRib = 2′-deoxyribosyl.

leotide sequence. Furthermore, labelling at the phosphodiester situates the label on the edge of a double helix, making structural disruption less likely.[6] However, a more exposed label may be more mobile, as it is not confined to a well-defined environment such as a groove. This strategy is moreover complicated by the formation of diastereomers at the phosphorus atom.[132,136] Furthermore, phosphodiester labelling normally requires a deoxyribose or 2′-methoxyribose on the 5′-side of the modification, as phosphorothioates are susceptible to intramolecular strand cleavage by nucleophilic attack of the 2′-alcohol.[137]

Labelling of the ribose skeleton has seen relatively few applications in SDSL (Figure 1.14c). Nevertheless, labelling 2′-aminouridine residues with isocyanate spin labels to provide semi-rigid 2′-ureido-linked spin labels (**35**) has proven popular, likely due to the commercial availability of 2′-amino-2′-deoxyuridine and -cytidine phosphoramidites and a spin label precursor.[138–150] It is however notable that this strategy has not yet been applied to labelling A and G residues. A recent improved protocol for this SDSL strategy made use of more hydrolytically resistant aromatic isothiocyanates, giving thioureido-linked spin labels (**36**) with enhanced rigidity.[28] This is, so far, the only example of tetraethyl-substituted spin labels in nucleic acids; as detailed in Section 1.2, such nitroxyl spin labels are particularly stable towards bioreducing conditions. Interestingly, attempts at spin labelling through amide bond formation at the same position (**37**) resulted in significant destabilisation of the duplex structure.[151] Triazole **38** is the only example[§] of the employment of 'click' chemistry for general SDSL of the ribose moiety.[153] Although the 2′-*O*-propargyl ether modification is commercially available as a phosphoramidite building block for all the nucleotides, SDSL with this long and flexible linker was found to give low precision EPR data with wide DEER distance distributions.

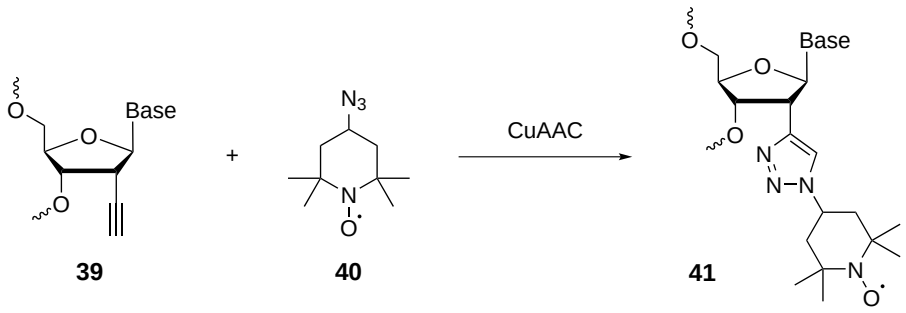
[§] A recent study incorporated pre-labelled guanosine residues *via* a 2′,5′-phosphodiester bond (resulting in a 2′-branched oligonucleotide) using a DNAzyme.[152] As the labelling efficiency is strongly sequence-dependent, this approach is not applicable to general SDSL.

1.5 Aims of the proposed work

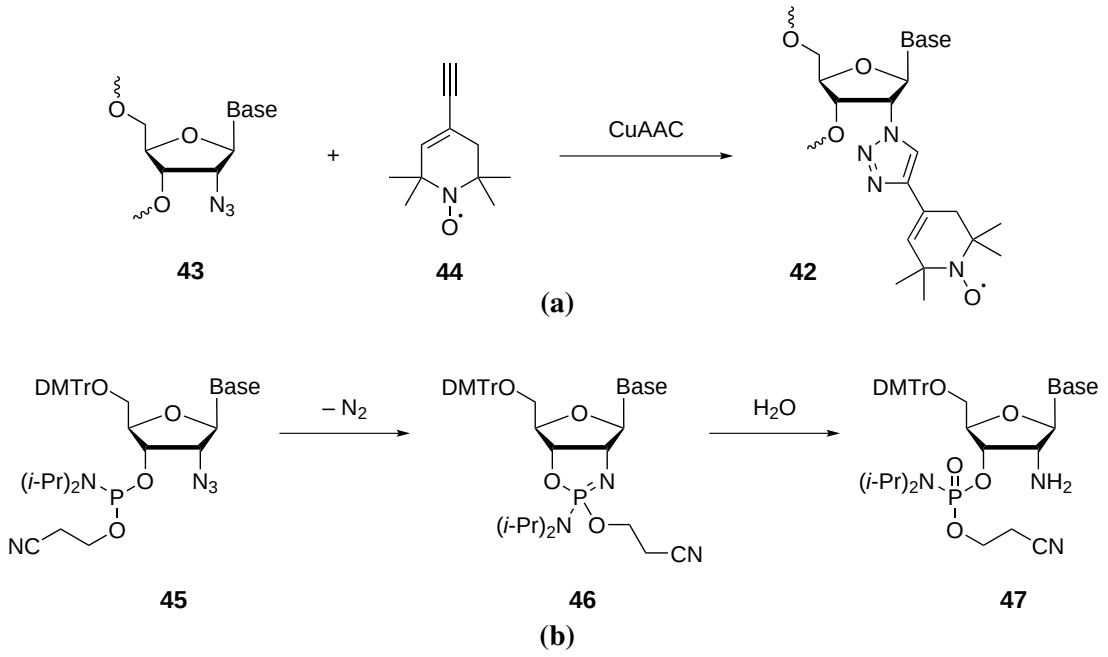
As has been shown in this chapter, SDSL of nucleic acids is a thriving and active area of research. Current challenges within the field remain to achieve rigid but non-perturbing labelling, in a positionally flexible manner that is independent of the identity of the nucleobase at the desired residue of labelling. The 2′-position of the (deoxy)ribose moiety is interesting in this context, as labelling at this position may allow the spin label to nest in the minor groove of an oligonucleotide double helix. By finely tuning the properties of the spin label, a balance may be struck between the seemingly conflicting requirements for rigidity and low structural disruption. The very few past strategies to achieve SDSL at the 2′-position (see Figure 1.14c) are ascribed to the synthetic challenge of nucleotide modification. It is, however, encouraging that techniques which achieve both rigidity and structural compatibility (e.g. **35**, **36**) have in general proven very successful.

In light of this, a new strategy for the site-directed spin labelling of oligonucleotides through functionalisation of the 2′-position of nucleotides is proposed (Scheme 1.2). After incorporation of a 2′-ethynylnucleoside into an oligo(deoxy)nucleotide (**39**), SDSL may be achieved by the highly efficient and orthogonal Cu(I)-catalysed 'click' reaction with an azide-functionalised spin label (e.g. **40**). The resulting 2′-triazole-linked spin label (**41**) features only two rotatable bonds between the spin label and the DNA backbone, and should thus provide a rigid system.

Previous work in the Anderson group explored a similar 'click' SDSL strategy yielding triazole **42** *via* 2′-azidonucleotide **43** and alkyne-functionalised spin label **44** (Scheme 1.3a),



Scheme 1.2: Proposed new strategy for SDSL at the 2′-position of nucleic acids.



Scheme 1.3: Previous work in the Anderson group **(a)** towards a new strategy for SDSL at the 2′-position of nucleic acids, **(b)** resulting in an intramolecular Staudinger reduction preventing incorporation of 2′-azidonucleotides into internal positions of nucleic acids.

i.e. with the 'click' coupling partners inverted relative to the present strategy.[154] The benefit of this approach was that 2′-azidonucleosides are easy to synthesise from the corresponding 2′-*O*-arabinofuranoside derivatives. However, a serious limitation of this strategy was the incompatibility of azides towards the phosphoramidite chemistry employed for standard automated solid-phase DNA synthesis. To functionalise internal sequence positions, 3′-phosphoramidite nucleoside building block **45** (Scheme 1.3b) is required. The proximity between this functionality and the 2′-azide results in a facile intramolecular Staudinger reduction in these intermediates, producing cyclic phosphoramidimidate **46** which upon hydrolysis becomes an unreactive 2′-amino-3′-phosphoramidate nucleoside (**47**). Although 2′-azidonucleosides could be mounted on a resin, and incorporated at the 3′-terminus of DNA oligomers, this approach only provides access to SDSL at the 3′-terminus of the DNA oligomers.[¶] By inverting the 'click' coupling partners, all functionalities are stable to the automated oligonucleotide synthesis conditions. Coupled with a post-DNA synthesis SDSL

[¶]2′-Azidonucleotides have since been incorporated into internal positions of RNA by interruption of the automated oligonucleotide cycle and manual installation of the azidonucleotide by the phosphodiester method.[155,156] The modification was not used for spin labelling.

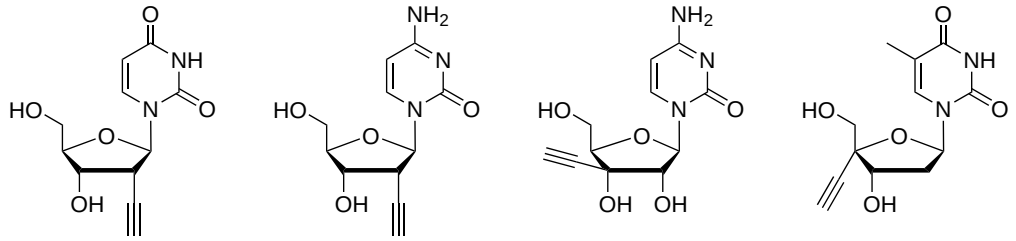
strategy, the proposed approach additionally avoids exposure of the nitroxyl functionality to potentially degrading reagents used in the oligonucleotide synthesis.

A final advantage of this strategy is its late-stage divergence. After site-specific incorporation, the alkyne can be functionalised with a wide range of spin labels, or indeed other groups such as radiolabels or fluorescent labels. This flexibility affords the opportunity to explore and finely tune the properties of the spin labelled system by varying the structure of the spin label as discussed above. In particular, it enables the exploration of spin labels with enhanced relaxation properties[33–35] or stability;[28] such labels have only very recently been incorporated into nucleic acids.

2 Synthesis of 2′-ethynyl-2′-deoxynucleosides

2′-Alkynylnucleosides were first reported in 2002 by Shuto and co-workers,[157,158] with the preparation of 2′-ethynyl-2′-deoxyuridine and -cytidine (**48** and **49**, respectively, Figure 2.1) motivated by the antiviral and/or antitumor properties displayed by a number of alkyne-functionalised nucleoside derivatives (e.g. **50** and **51**, Figure 2.1). However, no subsequent report of the biological activity of these compounds was published, and these nucleosides were not incorporated into oligonucleotides.

This chapter describes efforts to optimise the synthesis of derivatives of 2′-ethynyl-2′-deoxyuridine (**48**) and -cytidine (**49**), the development of the equivalent alkyne-bearing deoxyadenosine derivative, and the conversion of these 2′-alkynylnucleosides into building blocks for automated solid-phase DNA synthesis.



48 **49** **50** **51**

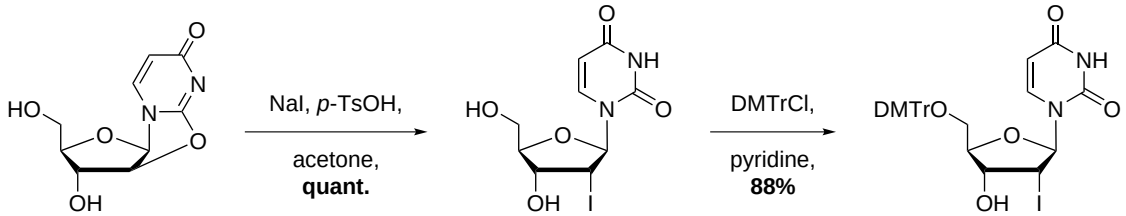
Figure 2.1: 2′-Ethynyl-2′-deoxyuridine and -cytidine, and alkynylnucleosides exhibiting antiviral and antitumor properties.

2.1 2′-Ethynyl-2′-deoxyuridine

Inspired by the work of Shuto,[157,158] a similar route towards 2′-ethynyl-2′-deoxyuridine was embarked upon (Scheme 2.1); preliminary work on this chemistry[159] was performed by visiting PhD student Javier Peña.* Treatment of inexpensive, commercially available 2,2′-*O*-cyclouridine (**52**) with sodium iodide under acidic conditions afforded 2′-iodouridine (**53**) in quantitative yield. The next step was the installation of a protecting group at

*Peña successfully completed the synthesis up to compound **65**, although most synthetic steps required further optimisation as described herein.

the 5′-alcohol; this is a prerequisite for the automated oligonucleotide synthesis protocol. Whereas Shuto's original route employed a monomethoxytrityl (MMTr) ether, modern oligonucleotide synthesis relies on the more electron rich dimethoxytrityl (DMTr) ether (which is therefore more easily cleaved using milder acids). The DMTr group was installed (**54**) by treatment of the iodonucleoside with a small excess (1.2 equiv.) of DMTrCl in pyridine. Small amounts of the 3′,5′-diprotected product were observed; however, a lower excess of reagent led to incomplete conversion.

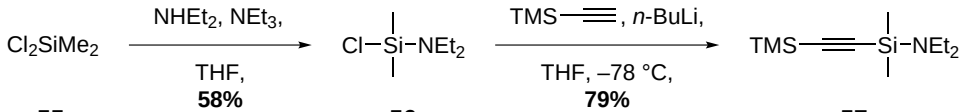


52 **53** **54**

Scheme 2.1: The synthesis of the alkynyluridine building block started with preparation and protection of a 2′-iodonucleoside.

To prepare iodonucleoside **54** for an intramolecular radical atom transfer reaction, a siloxane-tethered alkyne was needed. To this end, dichlorodimethylsilane (**55**, Scheme 2.2) was reacted with diethylamine to prepare a moisture sensitive chloroaminosilane (**56**), which was in turn subjected to monoaddition of lithium TMS-acetylide to form the alkyne-bearing silylating reagent **57**.

The reaction between nucleoside **54** and aminosilane **57** to form alkynylsiloxane **58** required significant re-optimisation from the Shuto literature procedure (Table 2.1), as reproducing the reported conditions[157,158] (Entry 1) resulted in low conversion. Furthermore, elimination of HI to form cyclouridine derivative **59** was observed,[†] particularly at higher



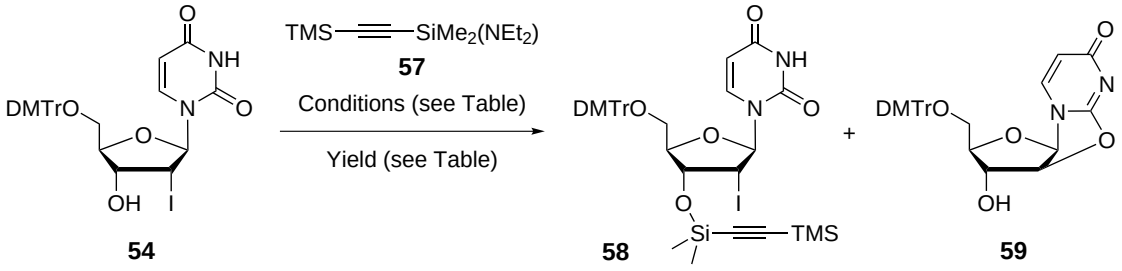
55 **56** **57**

Scheme 2.2: Preparation of a reagent to generate a siloxane-tethered alkyne.

[†] Although this compound was not isolated and characterised, its presence in the crude product (alongside the detritylated analogue **52**) was verified by comparison of ^{1}H NMR data with literature values.[160]

temperatures (Entry 2), as well as loss of the acid-labile DMTr group, while lower temperature (Entry 3) did not significantly improve the yield. Pleasingly, however, pretreatment of aminosilane **57** with methyl iodide greatly improved the conversion and isolated yield (Entry 4), although conversion deteriorated when the reaction was scaled up. It was found that addition of imidazole (Entry 5) to the reaction led to high conversion independent of scale, and furthermore completely prevented detritylation. When the reaction was revisited using conditions developed for the corresponding adenosine substrate (Entry 6, see also Table 2.3), siloxane **58** could be obtained in almost quantitative yield.

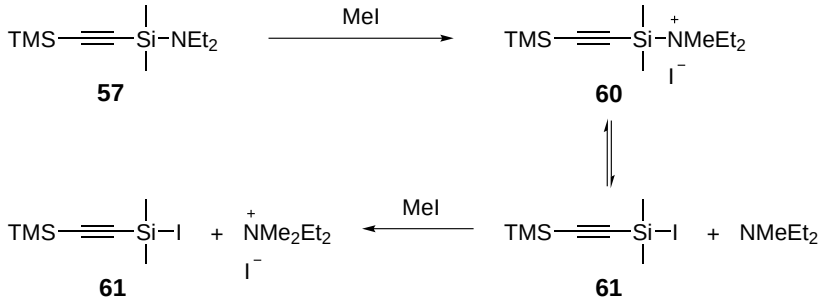
Table 2.1: Optimisation of the 3′-*O*-silylation of nucleoside **54**.



54 **58** **59**

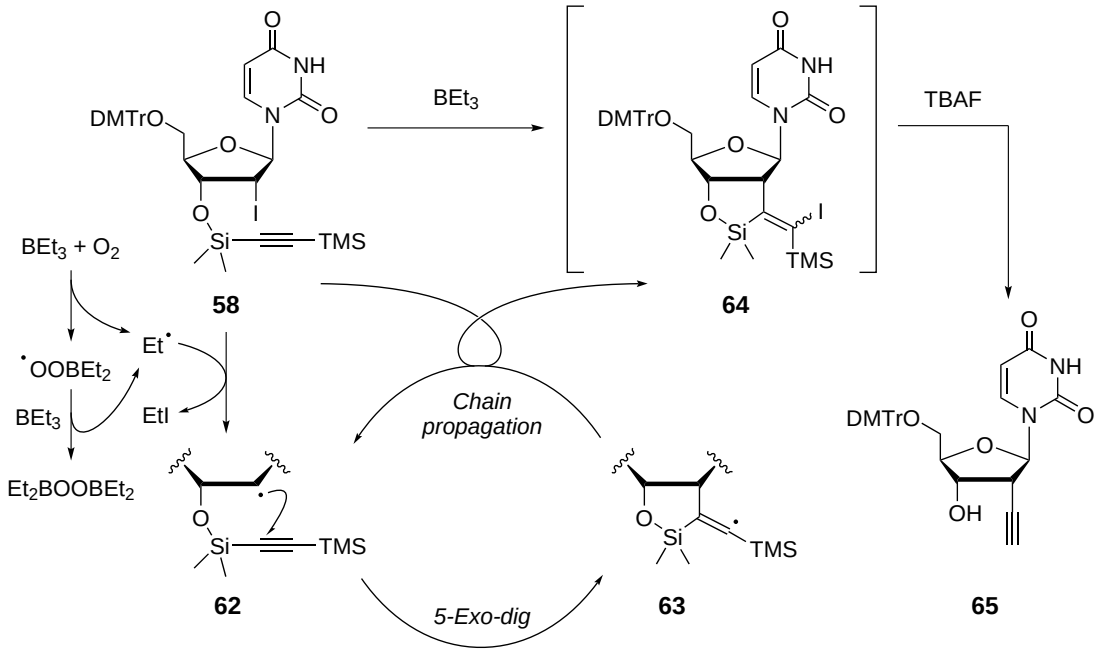
Entry	Ratio MeI:57	Additive	Solvent	T	Time [h]	Yield 58 [%]
1	—	—	THF	rt	4.5	31
2	—	—	THF	35 °C	3	19
3	—	—	THF	0 °C	4.5	36
4	1:1	—	THF	rt	3	70
5	1:1	Imidazole (0.5 equiv.)	THF	rt	3	71
6	**2:1**	**Imidazole (2.5 equiv.), DMAP (0.2 equiv.)**	**CH_2Cl_2**	**rt**	**1.5**	**96**

Although unprecedented for alkynylsilazanes, preactivation of aminosilanes with methyl iodide has been sporadically described, and used to effect transformations such as formation of silylated iodohydrins from epoxides,[161] preparation of bis(trimethylsilyl)amines,[162] and ring-opening iodosilylation of cyclic ethers.[163] The activation presumably takes place through *N*-alkylation of aminosilane **57** (Scheme 2.3), with the resultant equilibrium between silylammonium salt **60** and iodosilane **61** driven towards the latter by consumption of a second equivalent of methyl iodide.[162,163]



Scheme 2.3: Activation of aminosilane **57** leads to *in situ* formation of a silyl iodide.

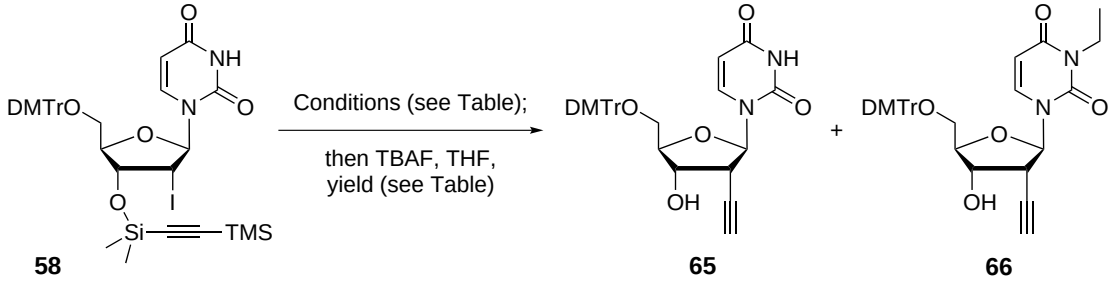
Alkynylsiloxane **58** is set up for the key radical atom transfer reaction. This reaction is initiated by triethylborane, which in the presence of atmospheric oxygen produces ethyl radicals (Scheme 2.4). Shuto *et al.*[157] proposed a mechanism for the reaction in which 2′-iodine abstraction from **58** produces a 2′-radical **62**, which through 5-*exo-dig*-cyclisation generates the unusual vinylic radical **63**, stabilised by two silicon atoms *via* hyperconjugation. This intermediate would then propagate the chain reaction *via* iodine abstraction from **58**, affording vinyl iodide **64**. In the reported procedure, rather than isolating this intermediate, a solution of TBAF was added to the reaction mixture upon complete consumption of iodide **58**, thereby effecting a desilylation-elimination reaction to generate 2′-alkyne **65**.



Scheme 2.4: Proposed mechanism of the radical atom transfer reaction.

When iodonucleoside **58** was submitted to the conditions optimised by Peña[159] (Entry 1, Table 2.2), using 1 equivalent of triethylborane in a THF solution as the initiator, the unexpected ethylated product **66** was obtained in moderate yield, presumably through nucleophilic attack on ethyl iodide generated in the reaction. Lowering the amount of initiator (Entry 2) allowed the desired alkyne **65** to be isolated from the complex reaction mixture, albeit in low yields and after extensive reaction times. Attempting to reproduce the conditions used by Shuto *et al.*[157] (Entry 3) did not lead to any reaction; the published procedure was performed "under argon", which was taken to mean a fully degassed system. This result is unsurprising given that some oxygen (e.g. dissolved in the solvent) is needed for the initiation of the radical chain reaction (Scheme 2.4); it was therefore concluded that Shuto's procedure must have been performed under inert gas, but without degassing the

Table 2.2: Optimisation of the radical atom transfer reaction to prepare **65**.



58 **65** **66**

Entry	Solvent	Atm.	Initiator	Equiv. initiator	Equiv. 2,6-lutidine	Time [h]	Yields [%]	
							65	**66**
1	PhMe	Air	BEt_3/THF	1.0	0	6.5	0	49
2	PhMe	Air	BEt_3/THF	0.3	0	27.5	24	7
3	PhMe	N_2	BEt_3/THF	0.3	0	5	0	n/d
4	PhH	N_2	$(Bu_3Sn)_2$, hν	0.5	0	3.5	61	—
5	PhH	Air	BEt_3/hex	0.3	0	2	9	n/d
6	PhH	Air	BEt_3/hex	0.3	0.3	2	71	n/d
7	PhH	Ar	BEt_3/hex	0.3	0.3	0.75	64	n/d
8	PhH	Ar	BEt_3/hex	0.3	0	2.5	25	8
9	PhMe	Air	BEt_3/hex	0.3	0.3	9	0	0
10	PhH	Air	BEt_3/THF	0.3	0.3	2	0	0
11	PhF	Air	BEt_3/hex	0.3	0.3	2	71	n/d
12	PhCl	Air	BEt_3/hex	0.3	0.3	2	64	n/d
13	**PhH**	**N_2**	**BEt_3/hex**	**0.1**	**0.1**	**0.5**	**98**	**n/d**

solvent.

At this stage, departing from the previously reported methodology, the reaction was attempted using different radical initiators (Entry 4). Initiation with $(Bu_3Sn)_2$ and UV irradiation, using benzene as the solvent, pleasingly gave a much cleaner reaction profile, and provided alkyne **65** in good yield. However, in light of the toxicity of organostannanes, triethylborane remained the initiator of choice. With the realisation that the reaction solvent would likely play a critical role, triethylborane in hexane solution (as used in the original procedure[157]) was attempted, with benzene as the solvent (Entry 5). Although the isolated yield was low, the reaction proceeded more cleanly and rapidly than previous BEt_3-initiated reactions. However, loss of the DMTr group from **58** and **65** appeared to occur to a large extent, presumably due to enhanced Lewis acidity of triethylborane in this ether-free solvent. The reaction mixture was thus buffered with 2,6-lutidine (Entry 6), selected so as to not coordinate with the borane and thereby prevent oxygen coordination and initiation, which gave alkyne **65** in high yields. Intriguingly, performing the reaction under inert atmosphere (but without degassing the solvent) enhanced the rate of the radical reaction (Entry 7); however, addition of 2,6-lutidine still proved necessary (Entry 8). Control experiments (Entries 9 and 10, cf. Entry 6) confirmed that toluene is unsuitable as a reaction solvent, and that triethylborane in THF is an unsuitable reagent.

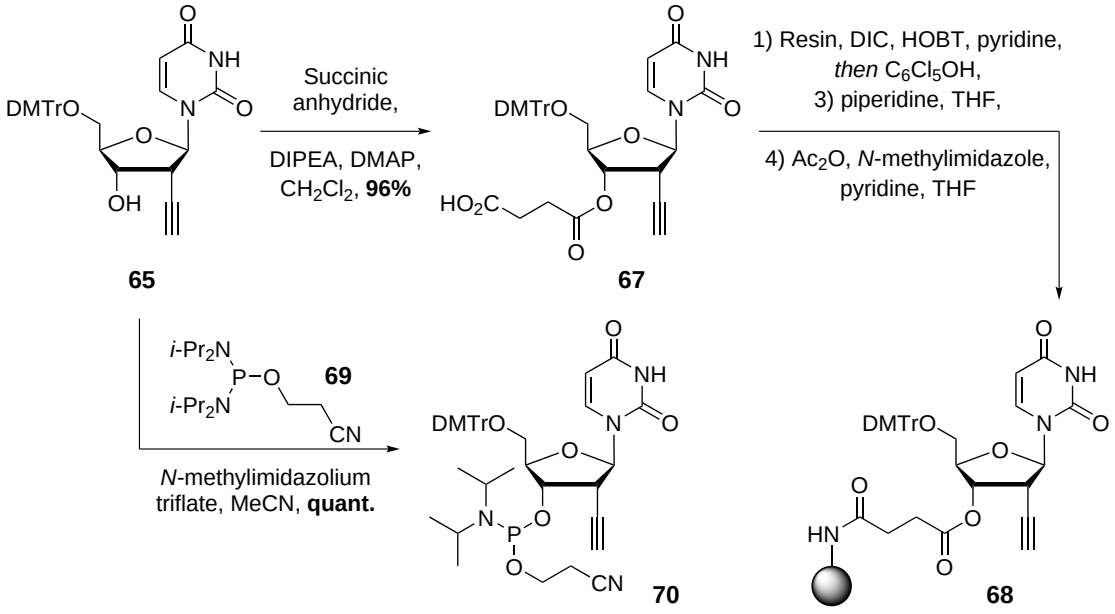
Further efforts to optimise the reaction included evaluation of less toxic solvents (Entries 11 and 12); although fluorobenzene showed promising results, reaction yields deteriorated with increasing scale. When scaling up the conditions of Entry 7, it was found that increasing amounts (21%) of ethyl adduct **66** was formed; however, reducing the loading of triethylborane and 2,6-lutidine to 0.1 equivalents (Entry 13) minimised side product formation, and provided alkyne **65** in excellent yields, including on multigram scales.

Alkynylnucleoside **65** required further derivatisation to allow it to be incorporated into oligonucleotides. To enable labelling of 3′-terminal positions, nucleoside **65** was 3′-*O*-succinylated (**67**, Scheme 2.5) and subsequently immobilised on a controlled pore

glass (CPG) resin (**68**) using an *N,N′*-diisopropylcarbodiimide (DIC) mediated peptide coupling catalysed by hydroxybenzotriazole (HOBT) and pentachlorophenol. The coupling was followed by quenching residual acid **67** with piperidine, and subsequent capping of unreacted amine groups on the resin with acetic anhydride. The nucleoside loading on resin **68** was measured to 37 μmol/g by the standard DMTr assay method.[164]

To enable labelling of internal sequence positions, the 3′-alcohol required conversion into a 3′-(cyanoethyl)phosphoramidite. Reaction with the phosphordiamidite reagent **69** in the presence of a mildly acidic, nucleophilic activator has been reported to provide a milder procedure for 3′-*O*-phosphitylation of nucleosides than the commonly used (cyanoethyl)chlorophosphoramidite.[165] Tetrazole is a commonly used activator in this process, but its availability is restricted due to its explosive nature. 4,5-Dicyanoimidazole has been reported as a safe replacement,[166] but only moderate conversion into phosphoramidite **70** was achieved with this reagent. Pleasingly, however, an excess of *N*-methylimidazolium triflate[167] was found to effect phosphitylation in quantitative yields.

In summary, 2′-ethynyl-2′-deoxyuridine derivative **65** was synthesised from 2,2′-*O*-cyclouridine (**52**) in a total yield of 83% over four steps. In comparison, Shuto *et al.* prepared the deprotected analogue **48** in 35% over the same number of steps, using a similar

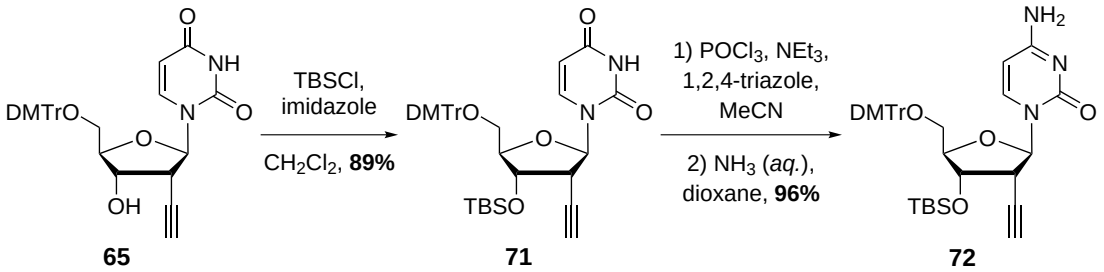


Scheme 2.5: Derivatisation of **65** into building blocks for oligonucleotide synthesis.

route.[157] Nucleoside **65** was further derivatised in high yields into building blocks for automated solid-phase oligonucleotide synthesis.

2.2 2′-Ethynyl-2′-deoxycytidine

Uridine derivative **65** can conveniently be converted to the corresponding cytidine derivative by exploiting the reactivity of the nucleobase.[168] The 3′-alcohol was protected as a silyl ether (**71**, Scheme 2.6), which was subsequently exposed to an excess mixture of phosphorus oxychloride and 1,2,4-triazole, thereby producing an intermediate 4-(1,2,4-triazolyl-1-yl)-uridine derivative which was not isolated. Upon full conversion and workup of the intermediate, the crude material was treated with an excess of ammonia solution, which led to aminolysis of the triazole to produce cytidine derivative **72** in excellent yield.

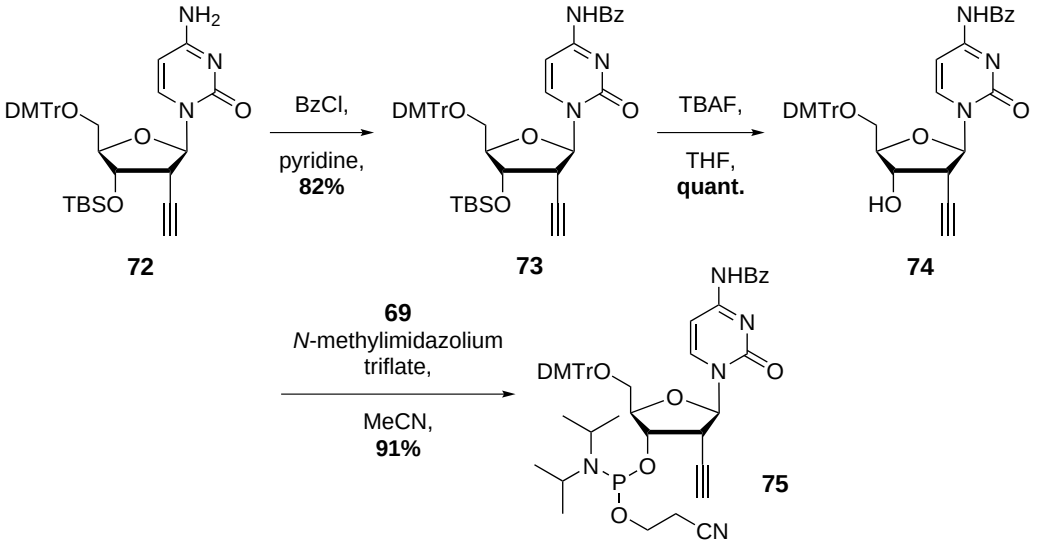


65 **71** **72**

Scheme 2.6: Conversion of uridine derivatives to cytidine derivatives.

Alkynylcytidine derivative **72** was further derivatised into a phosphoramidite building block for incorporation into oligonucleotides. After protection of the exocyclic amine functionality as a benzamide (**73**, Scheme 2.7), as required for the oligonucleotide synthesis, the 3′-*O*-siloxane was cleaved to alcohol **74**. The alcohol was further derivatised into the (cyanoethyl)phosphoramidite **75** using the method optimised for the analogous uridine derivative (see Scheme 2.5).

In conclusion, 2′-ethynyl-2′-deoxycytidine building block **75** was prepared from alkynyluridine derivative **65** in a total yield of 64% over five steps. Shuto *et al.* did not attempt to prepare this building block; rather, they converted a derivative of alkynyluridine **48** into deprotected alkynylcytidine (**49**) in 88% yield over one step.[158]

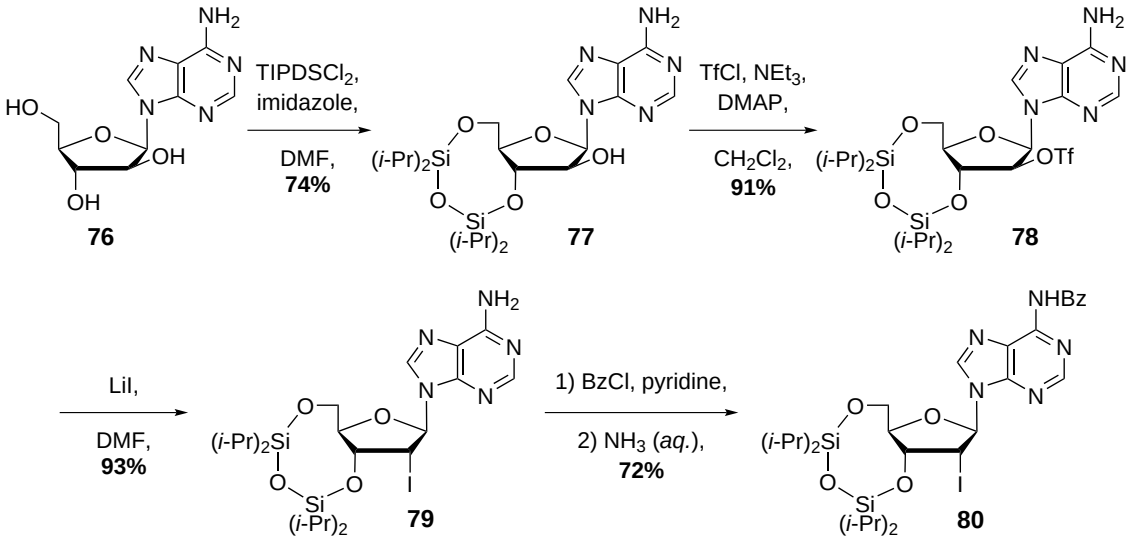


Scheme 2.7: Functionalisation of the alkynylcytidine nucleoside into a phosphoramidite oligonucleotide building block.

2.3 2′-Ethynyl-2′-deoxyadenosine

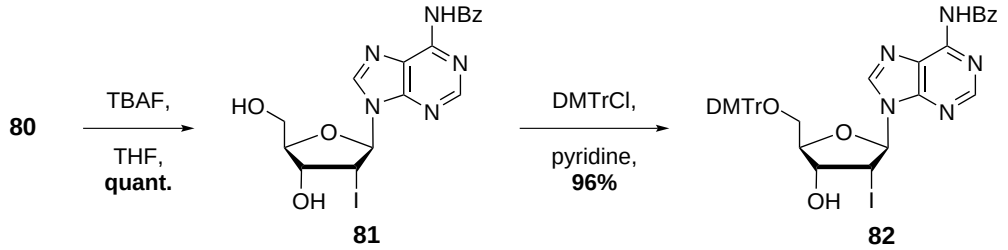
As 2′-ethynyl-2′-deoxyuridine derivative **65** cannot be conveniently converted directly to the corresponding adenosine, a *"de novo"* synthetic route towards an alkynyladenosine derivative is required. Furthermore, because no adenosine analogue of cyclouridine (**52**, Scheme 2.1) is available as the starting material, a longer synthetic sequence is needed to install the crucial 2′-iodide. Building on a previously published route to 2′-iodoadenosine derivatives,[169] the commercially available arabinoadenosine (**76**, Scheme 2.8) was selected as the starting material.[‡] Following protection of the 3′,5′-diol as disiloxane **77**, the 2′-alcohol was converted into a leaving group (**78**) by chemoselective triflylation in the presence of the nucleobase amine by treatment with triflyl chloride. The triflate was subsequently subjected to an S_N2 reaction with lithium iodide, producing 2′-iodoadenosine derivative **79** in excellent yields on multigram scales. Following iodination, the adenyl amine was protected by benzoylation (as required for the oligonucleotide solid-phase synthesis); unexpectedly, the dibenzoyl imide was initially formed, even with a single equivalent of benzoyl chloride. However, double benzoylation followed by mono-aminolysis afforded the desired benzamide **80** in good yields.

[‡]Preliminary work by Peña led to the successful synthesis of **80**, albeit under non-optimised conditions.[159]



Scheme 2.8: Synthetic route for the installation of a 2′-iodide on an adenosine derivative.

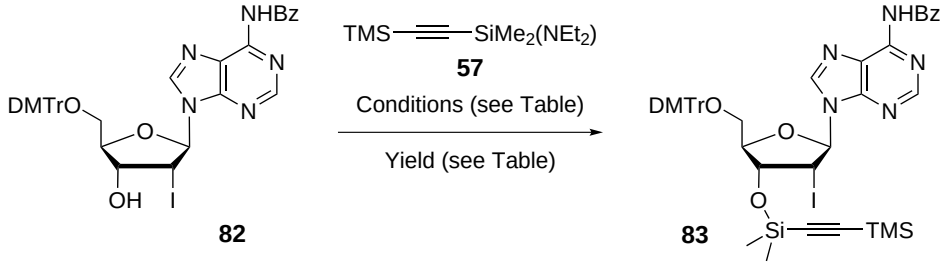
With the required 2′-iodide in place, the disiloxane protecting group of nucleoside **80** was cleaved to the 3′,5′-diol (**81**, Scheme 2.9) by treatment with TBAF, and the 5′-*O*-dimethoxytrityl group was installed (**82**). At this point, introduction of the siloxane-tethered alkyne to the 3′-alcohol was necessary, and alcohol **82** was subjected to the conditions that had been optimised for the corresponding uridine derivative **54** (Table 2.3, Entry 1). Surprisingly, however, no reaction was observed. As DMF has been shown to be an excellent solvent for silylations, and imidazole an efficient catalyst,[170] these conditions were screened (without activation of the aminosilane with methyl iodide, Entry 2), along with the catalytic effect of DMAP (Entry 3). Pleasingly, some siloxane product (**83**) was isolated under these conditions, albeit in modest yields. However, removal of DMF required the product to be exposed to elevated temperatures, which caused some decomposition; to avoid this, CH_2Cl_2 was evaluated as the reaction solvent and found to give improved yields



Scheme 2.9: Deprotection and reprotection of the iodoadenosine derivative.

(Entry 4). Combining the catalytic effects of imidazole and DMAP with preactivation of the aminosilane, now with a 2 : 1 ratio of methyl iodide to aminosilane **57** as suggested by the proposed mechanism of activation (see Scheme 2.3), provided complete conversion after short reaction times (Entry 5). However, the isolated yields were surprisingly low, and at this stage it was realised that alkynylsiloxane **83** was unstable to purification by column chromatography. It was however found that siloxane **83** could be subjected to a mildly basic aqueous workup, and submitted to the subsequent step without any further purification.

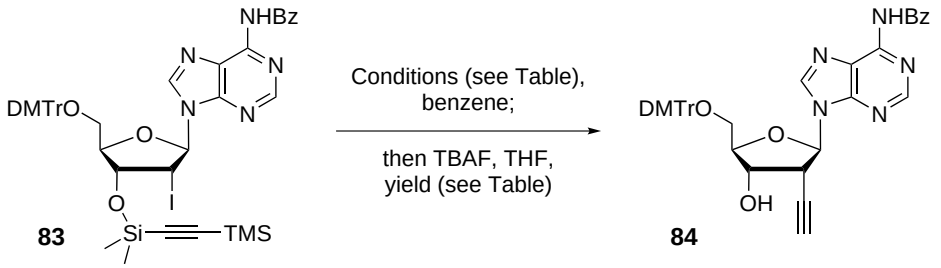
Table 2.3: Optimisation of the 3′-*O*-silylation of nucleoside **82**.



Entry	Ratio MeI:57	Additive	Solvent	T	Time [h]	Isolated yield [%]
1	1:1	Imidazole (0.5 equiv.)	THF	rt	5.5	0
2	—	Imidazole (2 equiv.)	DMF	rt	49	23
3	—	DMAP (0.5 equiv.)	DMF	rt	72	25
4	—	Imidazole (2 equiv.)	CH_2Cl_2	rt	43	37
5	**2:1**	**Imidazole (2.5 equiv.), DMAP (0.2 equiv.)**	**CH_2Cl_2**	**rt**	**2**	**10**

Substrate **83** is set up for the key radical atom transfer reaction to form alkyne **84** (Table 2.4). When the material was submitted to the conditions optimised for the corresponding uridine substrate **58** on a similarly small scale (Entry 1; see also Table 2.2, Entries 6 and 7), the reaction unexpectedly produced a number of unidentified products and gave only moderate conversion, resulting in a low yield. Increasing the amount of initiator and 2,6-lutidine (Entry 2) led to an increase in the isolated yield of alkyne **84**, although unknown side products and unreacted starting material were still observed. A further increase of the amount of initiator and base (Entry 3) led to the formation of a

Table 2.4: Optimisation of the radical atom transfer reaction to prepare **84**.



Entry	Atm.	Equiv. BEt_3/hex	Equiv. 2,6-lutidine	Time [h]	Yield [%]
1	N_2	0.3	0.3	6.5	23[a]
2	N_2	1	1	7	39[b]
3	N_2	2	2	1.5	0
4	Air	0.1	0.1	95	0
5	Air	0.3	0.3	95	0
6	**N_2**	**0.4**[c]	**0.4**[c]	**4.5**[c]	**51**[b]

[a] Over one step (using pure **83**). [b] Over two steps (using crude **83**).
[c] Initial conditions: 0.1 equiv. BEt_3/hex and 0.1 equiv. 2,6-lutidine. Reinitiation with both reagents (0.1 equiv.) at 0.5 h, and 2.5 h (0.2 equiv.).

complex mixture, from which no desired product was isolated. Performing the reaction with lower amounts of initiator under air (Entries 4 and 5) led to no conversion, even after extended reaction times. Performing the reaction on a larger scale, under the high-yielding conditions used for uridine substrate **58** (Entry 6), led to initiation of the radical chain reaction and initially clean conversion. However, after some time, the reaction appeared to stall and no further conversion was observed. Addition of more triethylborane (as well as 2,6-lutidine) appeared to reinitiate the reaction; this was performed twice. Disconcertingly, a number of side products started to appear with increasing reaction time, and therefore the reaction was terminated even though full conversion was not achieved. The reaction was not further optimised as sufficient quantities (∼200 mg) of 2′-alkynyladenosine derivative **84** had been produced, and the final isolated yield of 51% over two steps was deemed acceptable.

The reason for the lower reactivity of adenosine derivative **83** compared to its uridine counterpart **58** is not clear. It may be hypothesised that the lower reactivity (but also lower

stability) of this substrate could be explained by a different conformational preference of the furanose ring. Although a systematic high-field NMR investigation of the coupling constants was not performed, characterisation-quality ^{1}H NMR data (400 MHz) can be used to establish a crude estimate of the equilibrium populations of an assumed two-state, rapidly interconverting equilibrium between an N-type and an S-type nucleoside conformation. It has been shown[171] that the equilibrium constant K_{eq} for the N $\rightleftharpoons$ S equilibrium can be estimated by the ratio

$$K_{eq} = \frac{\chi_S}{\chi_N} \approx \frac{^3J_{1'2'}}{^3J_{3'4'}} \tag{2.1}$$

where χ_S and χ_N are the molar fractions of nucleoside in the S and N conformation, respectively, and $^3J_{1'2'}$ and $^3J_{3'4'}$ are the H1′-H2′ and H3′-H4′ coupling constants, respectively. Equation 2.1 can be rewritten into Equation 2.2:

$$\chi_N = \frac{^3J_{3'4'}}{^3J_{1'2'} + ^3J_{3'4'}} \tag{2.2}$$

Using Equation 2.2, the conformational distribution of the radical atom transfer substrates for uridine (**58**, Figure 2.2a) and adenosine (**83**) were estimated (Table 2.5). As expected for 2′-deoxynucleoside derivatives, an S-conformation (**85**, Figure 2.2b) is favoured over the N-conformation **86** for both compounds, although to a much larger extent (84% S) for the adenosine derivative.

An altered conformational preference of substrate **83** may lead to a reduction in the rate of the desired iodide abstraction and/or 5-*exo-trig*-cyclisation in the radical atom transfer

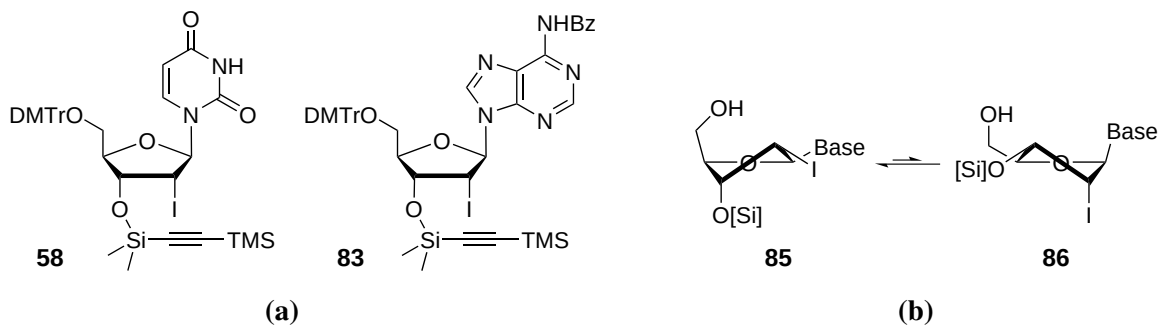


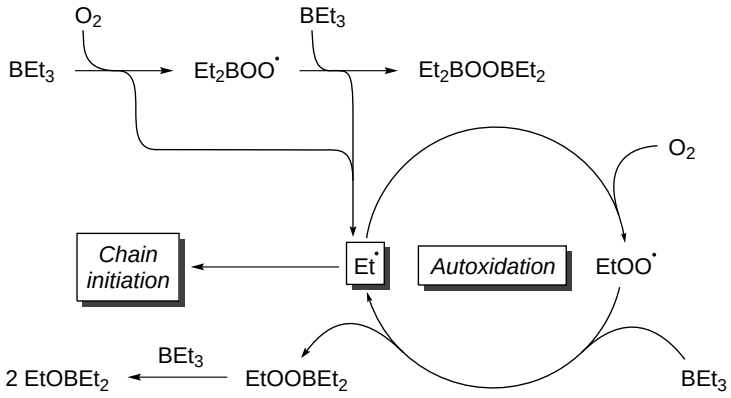
Figure 2.2: (a) Structure of the iodosiloxane nucleosides. **(b)** The iodosiloxane nucleosides prefer an S-type conformation . [Si] = –Si(CH$_3$)$_2$CCSi(CH$_3$)$_3$.

Table 2.5: Estimation of conformer populations for the radical atom transfer reaction substrates **58** and **83** using ^{1}H NMR coupling constants (400 MHz, $CDCl_3$) at ambient temperature.

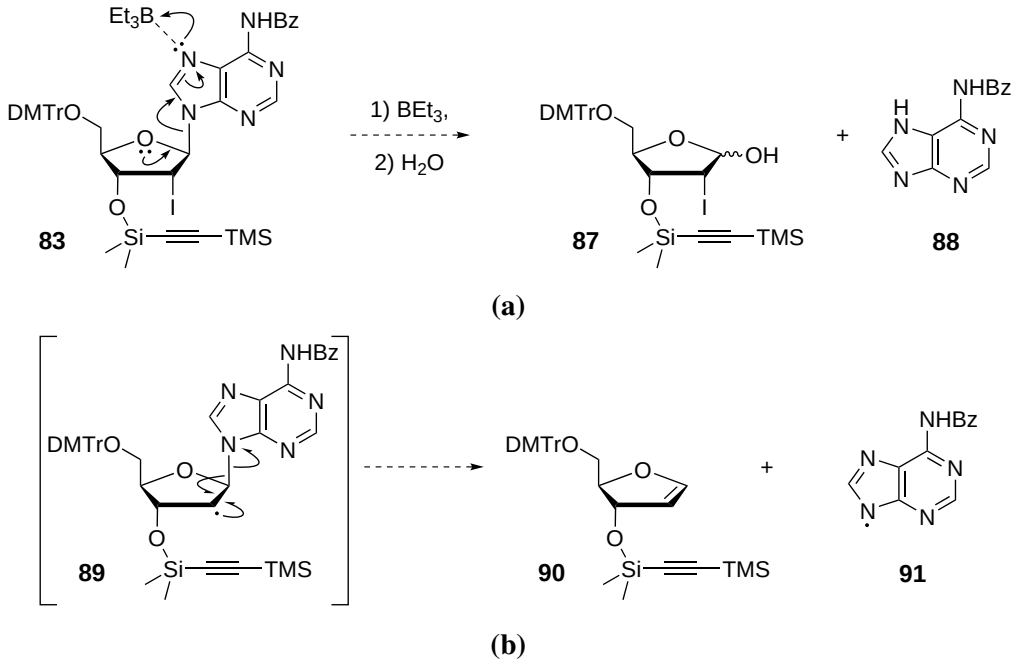
Compound	^3J [Hz]		χ_N
	H1′-H2′	H3′-H4′	
58	5.8	4.1	0.41
83	8.1	1.5	0.16

reaction with triethylborane (see the mechanism in Scheme 2.4), for example as a result of the siloxane-tethered alkyne being further away from the 2′-radical in S-conformation **85**. If the desired chain reaction becomes too slow, competing autoxidation of the initiator may become the dominant radical path, leading to cannibalisation of triethylborane and depletion of oxygen from the system (Scheme 2.10).[172] This may explain the low conversion of iodosiloxane **83**, as well as the need to reinitiate the radical reaction (Table 2.4, Entry 6). It may also explain the seemingly contradictory observation that the radical reaction of uridine iodosiloxane **58** is faster at lower concentrations of oxygen (see Table 2.2, Entries 6 and 7); increased concentration of O_2 leads to an increasing amount of autoxidation, reducing the concentration of initiator and lowering the rate of the desired radical chain reaction.

Another possible explanation for the low yields and abundance of side products, is that purine nucleotides are known to be susceptible to degradation by glycosidic cleavage to a much larger extent than pyrimidine nucleotides; the rate of depurination in DNA is



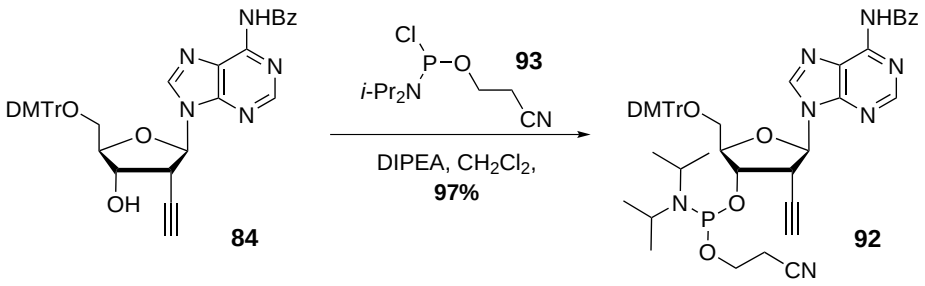
Scheme 2.10: Competing autoxidation of triethylborane can lead to reaction termination, low rates and low yields, in particular for slow/inefficient chains and at high concentrations of oxygen.



Scheme 2.11: Potential degradation pathways of adenosine derivatives such as **83** *via* **(a)** ionic, and **(b)** radical pathways, rendering adenosine derivatives poorer substrates for a radical atom transfer method to install a 2′-ethynyl group.

∼20 times that of depyrimidination.[173] The rate difference in these acid-catalysed processes is ascribed to the higher basicity of purines (at N7) than pyrimidines, leading to more facile protonation to form a glycosidic leaving group in the former case. Although the numerous side products observed in the reaction of iodosiloxane adenosine derivative **83** were not isolated and characterised, it can be hypothesised that the Lewis acidity of triethylborane can contribute to degradation of **83** (and/or even the product, **84**) to furanose derivative **87** (Scheme 2.11a) and 6-*N*-benzoyladenine (**88**) *via* a depurination-like side reaction. Moreover, 2′-radicals such as **89** (Scheme 2.11b), which are indeed desired intermediates in the radical atom transfer chain reaction, can be envisaged to degrade by β-scission, resulting in the formation of furanose glycal **90** and resonance-stabilised free radical nucleobase **91**.

With sufficient quantities of 2′-alkynyladenosine derivative **84** in hand, this material could be transformed into the corresponding 3′-(cyanoethyl)phosphoramidite **92** (Scheme 2.12). Surprisingly, the previously optimised reaction with phosphordiamidite reagent **69** and *N*-methylimidazolium triflate afforded no conversion. However, treatment with the more reactive chlorophosphoramidite (**93**) and base led to formation of phosphoramidite **92**



Scheme 2.12: Phosphitylation of 2′-ethynyl-2′-deoxyadenosine derivative **84**.

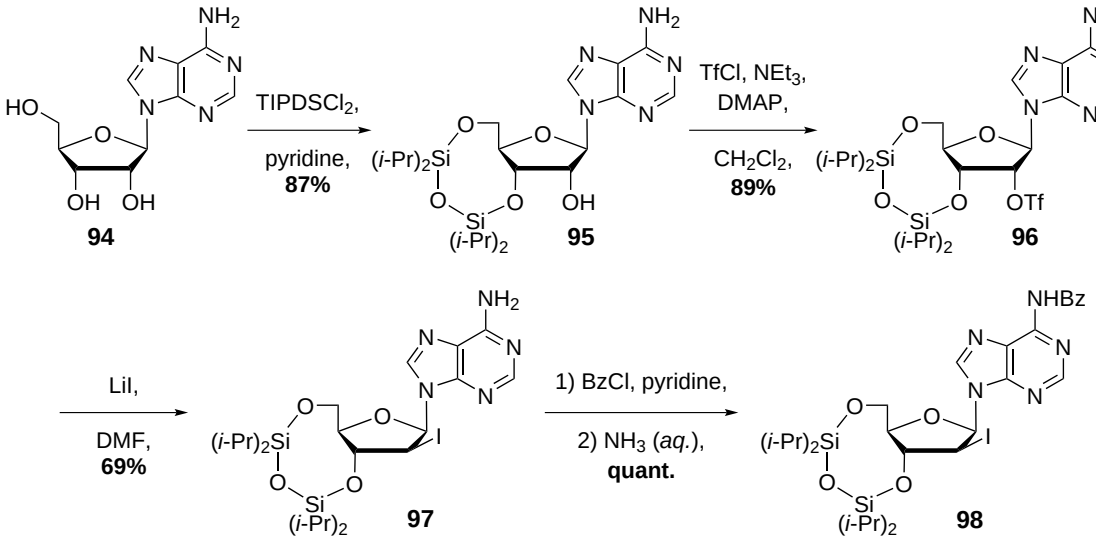
in excellent yields. Adenosine phosphoramidite **92** was found to be very unstable and prone to oxidation compared to uridine and cytidine phosphoramidites **70** and **75**, and required careful handling under inert atmosphere.

In summary, the novel 2′-ethynyl-2′-deoxyadenosine phosphoramidite building block **92** was synthesised in a total yield of 21% over nine steps from arabinoadenosine (**76**).

2.3.1 Epimer synthesis

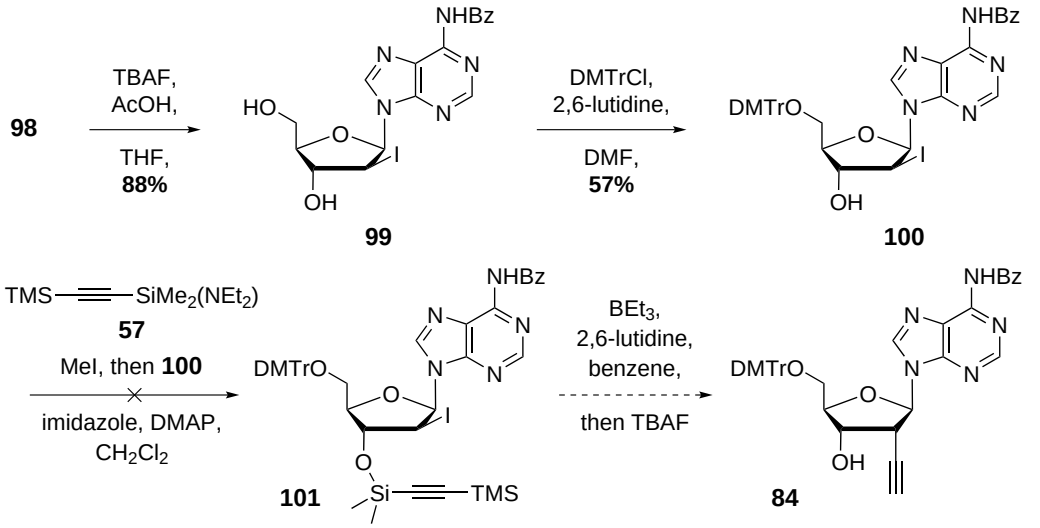
Due to the unforeseen difficulties in the synthesis of 2′-alkynylated adenosine derivatives described above, alternative routes were considered. It was reasoned that an epimeric 2′-iodonucleoside with the iodide in an arabino-configuration might prove to be more reactive in the radical atom transfer reaction. As the derived radical may readily and rapidly invert, an arabinoiodide precursor should nonetheless allow a C–C bond forming radical addition to take place on the opposite side of the furanose ring, leading to an alkyne with the desired ribo-configuration. To this end, an equivalent synthetic route to the one previously used (Schemes 2.8 and 2.9 and Tables 2.3 and 2.4) was initiated, starting with adenosine (**94**, Scheme 2.13). Straightforward 3′,5′-*O*-disiloxane protection (**95**) was followed by conversion of the 2′-alcohol into a triflate (**96**) and subsequent nucleophilic installation of the 2′-arabino-iodide (**97**), before the adenyl amine was protected as a benzamide (**98**).

Although this epimeric synthetic route was high-yielding and reliable to this point, deprotection to reveal the 3′,5′-diol proved problematic. Whereas treatment of disiloxane **98** with commercially available TBAF-solution provided diol **99** (Scheme 2.14) in 65% yield, it was found that buffering the reaction mixture with an equimolar amount of acetic acid



Scheme 2.13: Preparation of a 2′-arabino-iodonucleoside.

increased the yield (88%) by reducing the formation of a 2′,3′-epoxide from the revealed *trans*-iodohydrin. Epoxide formation,[174] as well as 1′,2′-elimination of HI,[175] was also an issue in the subsequent trityl protection of the 5′-alcohol, where using a stoichiometric amount of base (rather than pyridine as the solvent, as in previous tritylation reactions) provided trityl ether **100** in acceptable yields. This product was, however, found to be very unstable; upon submission to the penultimate step, installation of the siloxane-tethered alkyne (**101**), only decomposition was observed. At this stage, this route was abandoned to



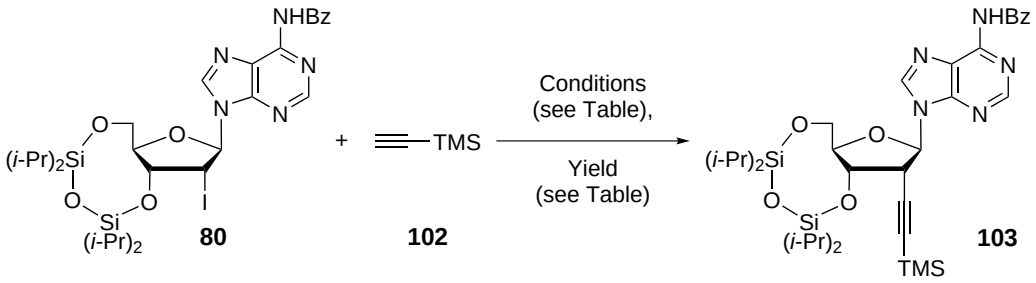
Scheme 2.14: Efforts to prepare the epimeric adenosine substrate for the key radical atom transfer reaction, which failed at the penultimate step.

focus on other aspects of the project.

2.3.2 Alternative strategies for nucleoside alkynylation

In parallel with the optimisation of the radical methodologies described above, other methods to incorporate an alkyne at the 2′-position were also considered. Although a number of methods for C(sp^3)–C(sp) cross-couplings have recently been developed,[176–180] these have not been demonstrated on highly sterically encumbered systems such as nucleoside derivatives, and furthermore do not address the requirement for diastereocontrol at the 2′-position. Moreover, the iodonucleoside substrates were expected to be susceptible to 1′-β-hydride elimination, even if the challenging oxidative addition could take place. Nevertheless, a few attempts were made at submitting *N*-benzoylated iodonucleoside **80** (Table 2.6) to

Table 2.6: Attempts at employing a Sonogashira cross-coupling to install a 2′-alkyne in adenosine derivative **80**.

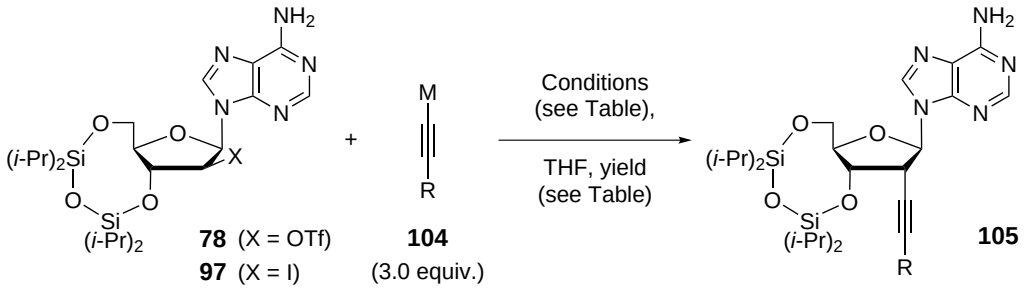


Entry	Equiv. 102	Conditions	T	Time [h]	Yield [%]
1	1.2	$Pd(PPh_3)$ (10 mol%), CuI (10 mol%), THF/NEt_3 (1:1)	rt	24	0
2	1.2	$Pd(OAc)_2$ (10 mol%), IMes·HCl, CuI (20 mol%), THF/NEt_3 (1:1)	rt	4	0
3	2.0	$PdCl_2$(dppf) (10 mol%), CuI (20 mol%), THF/NEt_3 (1:1)	rt	6.5	0
4	2.0	$PdCl_2$(DPEPhos) (10 mol%), CuI (20 mol%), THF/NEt_3 (1:1)	rt	6.5	0
5	2.0	$PdCl_2$(dppf) (10 mol%), CuI (20 mol%), THF/NEt_3 (1:1)	60 °C	19	0
6	2.0	$PdCl_2$(DPEPhos) (10 mol%), CuI (20 mol%), THF/NEt_3 (1:1)	60 °C	19	0

Sonogashira coupling conditions with trimethylsilylacetylene (**102**), aiming to produce 2′-alkynylnucleoside **103**. Standard Sonogashira conditions (Entry 1) did not lead to any change of the reaction mixture, and the reaction was abandoned. NHC ligands such as IMes have been reported in Pd-catalysed alkynylations of sp^3 bromides;[176] although partial conversion of the starting material was achieved using this system (Entry 2), no products could be identified in the resulting complex mixture. Bidentate ligands such as dppf and DPEPhos have also been shown to promote reductive elimination[181] and were screened (Entries 3 and 4), but did not lead to conversion of iodonucleoside **80**, even at elevated temperature for extended reaction times (Entries 5 and 6). As no sign of promise was shown by these preliminary attempts, this ambitious cross-coupling strategy was abandoned.

Attempts at subjecting triflate **78** and iodide **97** to an S_N2 reaction by various metal acetylides (**104**) are summarised in Table 2.7. Exposure of triflate **78** to a threefold excess

Table 2.7: Attempts at 2′-alkynylation of adenosine derivatives *via* nucleophilic substitution.



Entry	X	M	R	Additive (equiv.)	T	Time [h]	Yield [%]
1	OTf	MgBr	H	—	rt	20	0
2	OTf	MgBr	H	—	60 °C	3	0
3	OTf	MgBr	H	$CeCl_3$ (3.0)[a]	rt	52	0
4	OTf	MgBr	H	CuI (20 mol%)[a]	60 °C	3	trace
5	OTf	Li	TMS	—	−78 °C → rt	5	16
6	**OTf**	**Li**	**TMS**	**CuI (20 mol%)[a]**	**−78 °C → rt**	**8.5**	**29**
7	OTf	Li	TMS	CuI (50 mol%)[a]	−78 °C → rt	23	trace
8	OTf	Li	TMS	CuI (150 mol%)[a]	−78 °C → rt	8	0
9	I	Li	TMS	—	−78 °C → rt	26	12
10	I	Li	TMS	CuI (20 mol%)[a]	−78 °C → rt	25	16

[a] With respect to the nucleoside.

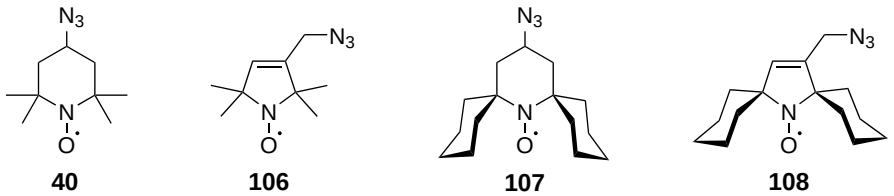
of ethynylmagnesium bromide (Entry 1) led to no conversion, even at elevated temperatures (Entry 2). Organocerium compounds have been shown to exhibit lower basicity than their corresponding Grignard reagents;[182] however, pretreatment of ethynylmagnesium bromide with $CeCl_3$ provided no conversion (Entry 3), even at extended reaction times. Encouragingly, however, performing the reaction in the presence of 20 mol% CuI (Entry 4) resulted in a mixture of products, in which a trace amount of the desired alkyne was detected. Reaction with a lithium acetylide, formed *in situ* by deprotonation of trimethylsilylacetylene with *n*-butyllithium, provided a small amount of alkyne **105** (R = TMS, Entry 5). In the presence of 20 mol% CuI, the yield increased slightly (Entry 6), although partial loss of the TMS group was also observed; however, further increasing the amount of CuI was detrimental to the reaction (Entries 7 and 8). Using the conditions of Entries 5 and 6 with an iodide leaving group (**97**, Entries 9 and 10) also permitted alkyne **105** to be isolated, albeit in lower yields. At this stage, the nucleophilic alkynylation strategy was abandoned to focus on other aspects of the project.

3 Synthesis of nitroxyl spin labels

The realisation of the novel CuAAC 'click' spin labelling strategy discussed in Section 1.5 requires not only the 2′-ethynyl-2′-deoxynucleoside building blocks which were discussed in Chapter 2, but also azide-bearing spin labels as 'click' coupling partners. As discussed in Section 1.2, the chemical structures of spin labels have important consequences for their properties, and ultimately for their suitability as EPR probes in a particular application, such as high-temperature DEER measurements or performing EPR experiments *in vivo*. Section 1.4 provided a few examples of how the structure of the label and linker affects the stability and spectroscopic properties of the spin labelled system. As mentioned, it is a stated goal to develop EPR probes which are as conformationally restricted as possible, while at the same time causing minimal structural distortion in the labelled oligonucleotide. Taking advantage of the late-stage divergence in installing the spin labels post-nucleotide synthesis, one aim of this project is to investigate the effect of label structure on the DNA duplex stability and the EPR spectra obtained from these duplexes. This chapter discusses the identification and synthesis of a small library of spin labels, selected to enable the exploration of how structural features of the spin label influence these central aspects of the 2′-triazolyl oligonucleotide SDSL strategy.

The 2,2,6,6-tetramethylpiperidinyl 1-oxyl scaffold, e.g. in azide **40** (Figure 3.1) is ubiquitous in the SDSL literature as one of the most widely used spin label frameworks. As such, it provides a convenient way to evaluate the 2′-triazolyl system against existing SDSL methods, albeit any direct comparisons based purely on the label scaffold are of limited value as many factors (e.g. nucleotide sequence, duplex length, or interspin distance) may affect the outcome. Nevertheless, the six-membered, tetramethyl-shielded nitroxyl **40** is one of the structurally (and synthetically) simplest spin labels, and can thus be used as a benchmark for direct comparisons between different spin labels in the proposed 2′-triazolyl strategy.

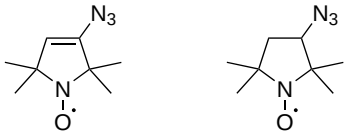
As outlined in Section 1.2, in simplified terms, three components of the fundamental spin label structure can be considered for optimisation of the spin label properties: The size and nature of the nitroxyl-bearing ring; the size and nature of the α,α′-substituents; and the presence, identity and position of any substituents on the ring and/or the α,α′-substituents. To explore the effect of the ring size, a five-membered, tetramethyl-substituted pyrrolinyl nitroxyl **106** was identified. The more reduction-resistant pyrrolinyl scaffold is also well-known in previous SDSL strategies; although not as stable as the saturated pyrrolidinyl nitroxyls,[23,24] the pyrrolinyl (unlike the pyrrolidinyl) framework benefits from being achiral, and thus does not lead to the formation of diastereomers upon attachment to the chiral oligonucleotide strands. Variation of the α,α′-substituents can impart additional reduction stability (especially for tetraethyl-substituted nitroxyls) or extended phase coherence times T_m (with bis(spirocyclohexyl)-derived scaffolds). Replacement of the tetramethyl substituents in **40** with spirocyclohexyl groups leads to the novel spin label **107**; comparison between these two labels may show whether increasing the steric bulk of the spin label to enhance its spectroscopic properties leads to unacceptable levels of destabilisation of the oligonucleotide structure. Variation of both the ring size and α,α′-substituents is possible with five-membered bis(spirocyclohexyl)-substituted nitroxyl **108**; although other bis(spirocyclohexyl) pyrrolinyl nitroxyls are known, this azide has not been previously reported. Comparison between **108** and **107** may show whether the presence of an extra methylene group in the linker allows the more bulky spin labels to be better accommodated by the duplex. Although this methylene group is also present in the tetramethyl-substituted label **106**, any difference in destabilisation can be expected to be more pronounced for the bulkier bis(spirocyclohexyl) nitroxyls.



40 **106** **107** **108**

Figure 3.1: Proposed library of spin labels for evaluation of the novel SDSL strategy.

It should be noted that the effect of the extra methylene group in the linker and the effect of the five- vs. six-membered rings cannot be disentangled with this library of spin labels. As the preparation of five-membered nitroxyls with the azide attached directly to the nitroxyl-bearing ring (e.g. **109** or **110**, Figure 3.2) requires considerable additional synthetic effort, these spin labels were not included in the label library at this stage.

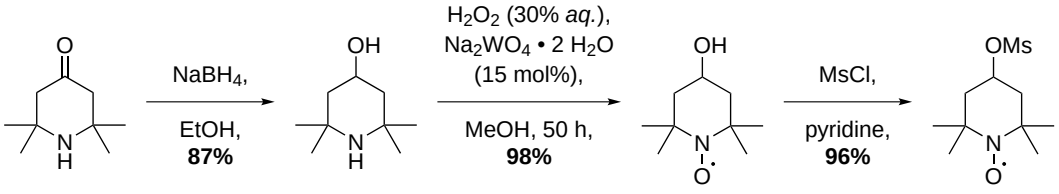


109 **110**

Figure 3.2: Five-membered ring spin labels without a methylene linker group were not included in the library of spin labels at this stage.

3.1 Synthesis of tetramethylpiperidinyl nitroxyl 40

Although the known tetramethyl-substituted piperidine nitroxyl **40** (also known as 4-azido-TEMPO) is commercially available, it was decided to synthesise this spin label to gain experience with the chemistry involved.* The synthetic route, based on literature procedures,[159] starts with reduction of aminoketone **111** (Scheme 3.1) to aminoalcohol **112**, which was subsequently oxidised to the nitroxyl radical **7** at this stage by treatment with an excess of H_2O_2 in the presence of a Na_2WO_4 catalyst.[20] As this reaction requires very polar solvents (i.e. a water/alcohol mixture) to solubilise the catalyst, poor substrate solubility can lead to poor conversion and long reaction times.[183] For this reason, the amine was oxidised to the nitroxyl at this (most polar) stage rather than later in the synthetic sequence,



111 **112** **7** **113**

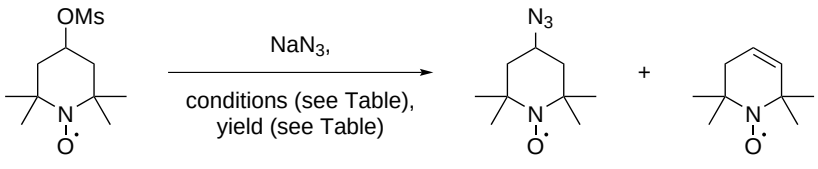
Scheme 3.1: Synthetic route towards a tetramethylpiperidinyl nitroxyl spin label.

*Spin label **40** was successfully synthesised by Peña, although the synthesis was not optimised.[159]

even though this complicated the characterisation of the following synthetic intermediates (as paramagnetic species cannot be characterised by NMR). Following *N*-oxidation, the alcohol was converted into a mesylate leaving group (**113**).

The subsequent S_N2 reaction with sodium azide required some optimisation (Table 3.1). Refluxing mesylate **113** with two equivalents of sodium azide led to complete conversion within hours (Entry 1). However, the isolated yield of azide **40** was low, and a closely related compound which co-eluted with the product was identified as the elimination product **114**.[†] Alkene **114** is however volatile, and was easily removed from azide **40** by sublimation on the Schlenk line. The formation of alkene **114** is not surprising, given that the methyl substituents hinder backside attack on the mesylate, which is presumably primarily in an equatorial conformation; the more reactive conformer with the mesylate in an axial position is destabilised by 1,3-diaxial interactions and hence populated to a much smaller extent. In contrast, an E1 elimination to form alkene **114** may however take place from either conformer (although admittedly also more readily when the mesylate is axial, to alleviate 1,3-diaxial strain). To increase the substitution to elimination ratio, the reaction was performed at lower temperature (Entry 2). Although the reaction time increased, the yield of azide **40** was also pleasingly enhanced. Increasing the excess of the nucleophile

Table 3.1: Optimisation of the nucleophilic azidation of mesylate **113**.



Entry	Equiv. NaN_3	Solvent	T [°C]	Time [h]	Yield 40 [%]
1	2.0	DMF	160	4	16
2	2.0	DMF	80	22	41
3	6.0	DMF	80	26	69
4	2.0	DMSO	110	2	51

[†]Although this compound was not isolated and characterised, its presence in the crude product was deduced from ^{1}H NMR and LRMS data.

(Entry 3) further improved the yield; however, it was noted that not all of the sodium azide was soluble in DMF under these conditions. To further enhance the effective concentration of azide, the use of the more polar solvent DMSO was attempted (Entry 4); pleasingly, this enhanced the yield and reaction time compared to Entry 2. Further optimisation of this reaction was not performed, as sufficient quantities of azide **40** had been obtained.

In summary, tetramethylpiperidinyl azide spin label **40** was synthesised in a total yield of 56% over four steps from piperidone **111**. The nitroxyl radical **40** is consistent with the observed triplet EPR spectrum of this compound (Figure 3.3).

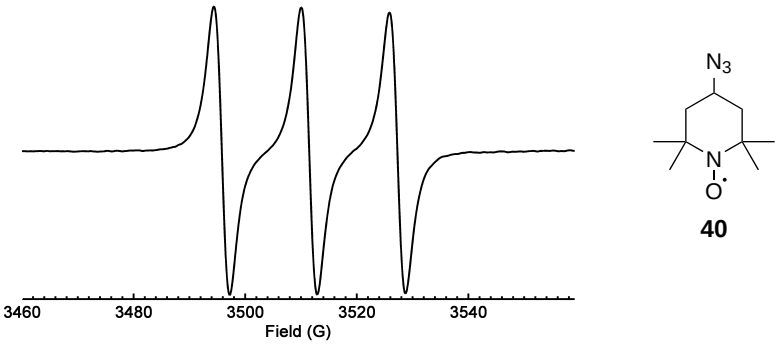
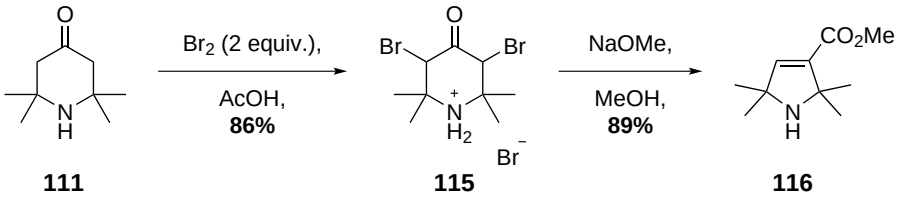


Figure 3.3: Room temperature X-band CW EPR spectrum of **40** (100 μM in $CHCl_3$).

3.2 Synthesis of tetramethylpyrrolinyl nitroxyl 106

The tetramethyl-substituted pyrrolinyl nitroxyl **106** has also been previously reported.[184] To access the unsaturated five-membered ring system, piperidone **111** was subjected to a double α,α′-bromination followed by a Favorskii rearrangement and dehydrohalogenation (Scheme 3.2).[185] Dibromide **115** (a mixture of the *cis* and *trans* diastereomers) is unstable in solution, but the hydrobromide salt precipitates out of the reaction mixture and was isolated as such;[186] attempts at neutralisation and purification of this compound resulted in decomposition products, including aziridines formed by transannular substitution of bromide by nitrogen. The Favorskii rearrangement and elimination to enoate **116** was effected by adding the ammonium salt **115** to a concentrated, freshly prepared solution of sodium methoxide in methanol. Addition of **115** in small portions was found to be beneficial to this reaction; presumably, rapid neutralisation of the ammonium bromide

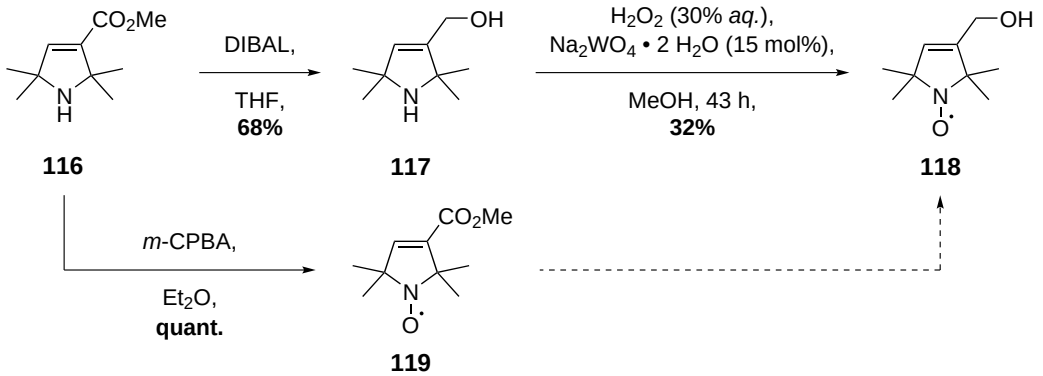


111 **115** **116**

Scheme 3.2: Synthetic route to access the 3-carboxylated tetramethylpyrroline framework from the corresponding piperidone.

liberates the unstable dibromoamine, which decomposes to a larger extent if the relative concentration of methoxide in the reaction mixture is low.

After the rearrangement, the ester was reduced to the allylic alcohol **117** (Scheme 3.3) in preparation for *N*-oxidation; it was suspected that the electron deficient double bond in **116** might be epoxidised under the H_2O_2/Na_2WO_4 oxidation conditions, and the aminoalcohol was furthermore expected to be polar enough to react under the conditions required for this oxidation. However, submission of aminoalcohol **117** to the previously employed conditions only led to low yields of nitroxyl radical **118**, even after extended reaction times. An alternative method for the oxidation of amines to nitroxyl radicals is treatment with 1.5–2 equivalents of *m*-CPBA, which permits the reaction to be performed in organic solvents of lower polarity than the H_2O_2/Na_2WO_4 method, thereby avoiding problems with poor substrate solubility.[187–189] To avoid potential epoxidation of the double bond in the allylic alcohol **117**, this oxidation was performed on the more electron deficient enoate **116**. Pleasingly, nitroxyl radical **119** was obtained in quantitative yields after only 1.5 hours.

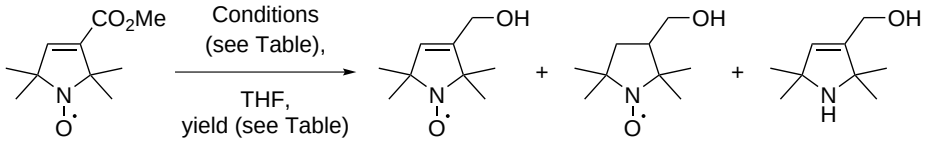


116 **117** **118** **119**

Scheme 3.3: Synthetic routes for *N*-oxidation and carbonyl reduction of tetramethylpyrroline substrates.

Following oxidation to the nitroxyl radical, the ester functionality in **119** required reduction to alcohol **118** (Table 3.2). Reduction of similar carboxylic acids or carboxylic acid derivatives to their corresponding alcohols has previously been identified as a challenging transformation;[190] in addition to the desired carbonyl reduction, conjugate reduction (**120**) or reduction of the nitroxyl radical to the corresponding secondary amine (**117**) may also occur. Submitting enoate **119** to literature conditions[191] (Entry 1) resulted in an acceptable yield of allylic alcohol **118**, but pyrrolidine **120** was also observed, which complicated the chromatographic purification of **118**. Reduction with lithium aluminium hydride (Entry 2), another previously reported method,[190] led to increased formation of side products; although amine **117** was observed, it could not be isolated. Using DIBAL while warming the reaction mixture slowly to room temperature (Entry 3) resulted in similar yields; however, it was noted that conjugated reduction product **120** was not formed, and that formation of amine **117** only took place after the reaction mixture reached temperatures above -40 °C. Pleasingly, maintaining the reaction mixture around -50 °C until full conversion was achieved (Entry 4) resulted in clean conversion to allylic alcohol **118** in high yields.

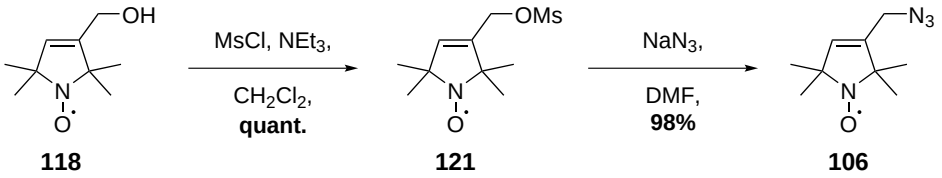
Table 3.2: Optimisation of the chemoselective reduction of the ester group in nitroxyl radical **119**.



119 **118** **120** **117**

Entry	Reagent	T	Time [h]	Yields [%]		
				118	**120**	**117**
1	Red-Al	-78 °C → rt	7.5	65	17	0
2	$LiAlH_4$	0 °C → rt	5	51	24	n/d
3	DIBAL	-78 °C → rt	4.5	48	0	n/d
4	**DIBAL**	**-78 °C → -50 °C**	**4.5**	**96**	**0**	**0**

The allylic alcohol **118** was straightforwardly converted into mesylate **121** (Scheme 3.4); although the material was unstable to column chromatography, the reaction proceeded very cleanly and only an aqueous workup was required to isolate pure mesylate **121** in



Scheme 3.4: Installation of the required azide functionality in tetramethylpyrrolinyl spin label **106**.

quantitative yield. This compound was immediately submitted to a nucleophilic substitution with sodium azide to form the target azide spin label **106**. As the electrophile is much less hindered than the corresponding piperidinyl **113**, as well as electronically activated, the reaction proceeded smoothly at room temperature to produce azide **106** in high yields.

In summary, tetramethylpyrrolinyl azide spin label **106** was synthesised in a total yield of 72% over six steps from piperidone **111**. The nitroxyl radical **106** is consistent with the observed triplet EPR spectrum of this compound (Figure 3.4).

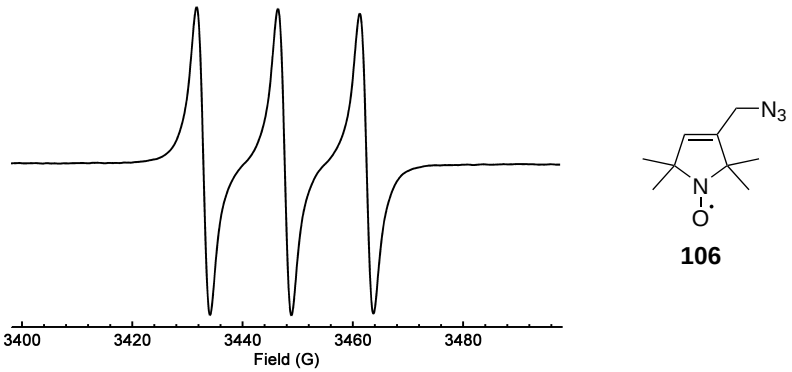


Figure 3.4: Room temperature X-band CW EPR spectrum of **106** (100 μM in $CHCl_3$).

3.3 Synthesis of bis(spirocyclohexyl)piperidinyl nitroxyl 107

Relatively few nitroxyl radicals of the bis(spirocyclohexyl)piperidine scaffold are known. Of these, only two have been used for SDSL of biomolecules: the protected α-amino acid **122** (Figure 3.5), which can be incorporated into the peptide backbone of proteins,[32] and the α-iodoacetamide **123** which was recently used to label cysteines in a lysozyme.[192] The proposed azide **107** has not previously been reported.

A convenient way to access these spirocyclic scaffolds was reported in 2010 by the group of Utsumi,[193] where the readily available starting material 2,2,6,6-tetramethylpiperidone

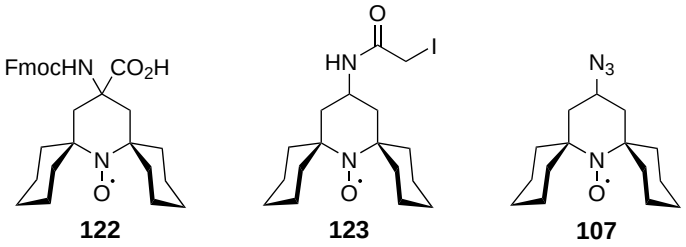
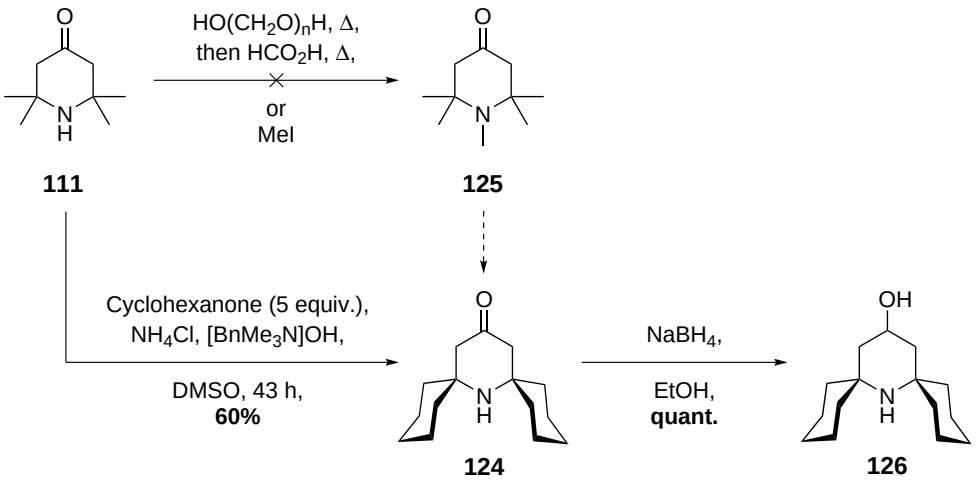


Figure 3.5: Known and proposed bis(spirocyclohexyl)piperidine-based nitroxyls for SDSL.

(**111**, Scheme 3.5) undergoes a formal exchange of acetone for a six-membered cyclic ketone, such as cyclohexanone, to form the spirocyclic aminoketone **124**. The authors found that this reaction proceeds in higher yields from 1,2,2,6,6-pentamethylpiperidone (**125**), with the secondary amine nitrogen atom in the product originating from ammonium chloride; however, in our hands, the *N*-methylated compound **125** could surprisingly not be prepared from piperidone **111**, neither *via* a reductive amination with paraformaldehyde, nor by treatment with methyl iodide. However, it was found that the spirocyclic piperidone **124** could be formed directly from **111** in good yields using prolonged reaction times.

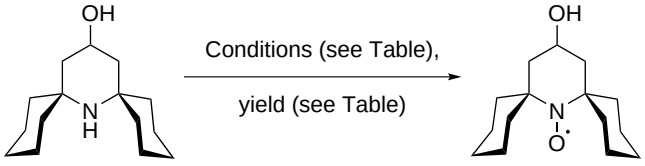
With aminoketone **124** in hand, spin label **107** was synthesised *via* a route analogous to the synthesis of tetramethylpiperidinyl spin label **40** (cf. Section 3.1). Reduction of the ketone functionality to the alcohol **126** proceeded smoothly and in high yields. However, the subsequent *N*-oxidation to nitroxyl radical **8** proved more challenging (Table 3.3). Submitting the spirocyclic aminoalcohol to conditions previously employed for the tetramethyl-



Scheme 3.5: Synthetic route towards the bis(spirocyclohexyl)piperidinyl spin label **107**.

substituted piperidine **112** (except substituting methanol with ethanol as the reaction solvent, Entry 1) resulted in low conversion, even after long reaction times. Adopting the conditions of another previous study,[194] disodium EDTA was added to the reaction mixture (Entry 2); this additive is frequently used in the literature to prevent degradation of H_2O_2 by traces of transition metals present in commercial Na_2WO_4.[195] An increase in the yield was observed; however, reaction times remained excessively long in spite of the increased concentration of **126**, perhaps due to the lower catalyst loading. It was at this stage hypothesised that both substrate solubility and increased steric hindrance around the amine moiety contributed to a reduction of the reaction rate. Increasing the catalyst loading to 50 mol% (Entry 3) and addition of phase-transfer catalyst benzyltrimethylammonium hydroxide[183] pleasingly led to higher conversion. After ∼48 h reaction time, the oxidation appeared to have stalled; however, addition of fresh hydrogen peroxide allowed the reaction to reach completion. Pleasingly, nitroxyl radical **8** was isolated in high yield, although a reaction time of 3.5 days was still required. Oxidation with *m*-CPBA (Entry 4) could be performed in dichlorometh-

Table 3.3: Optimisation of the *N*-oxidation of amine **126**.

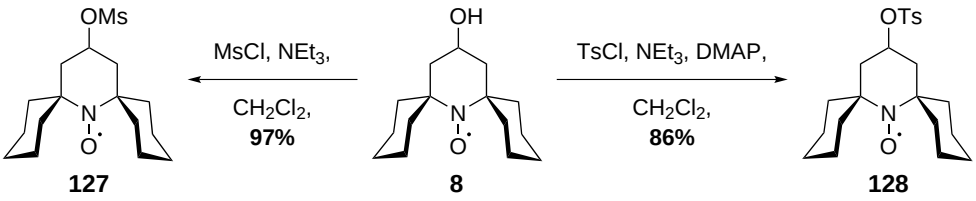


126 **8**

Entry	Conditions	Concentration 126 [M]	Time [h]	Yield [%]
1	$Na_2WO_4{\cdot}2H_2O$ (10 mol%), H_2O_2 (30% *aq.*, 20 equiv.), EtOH	0.1	71	38
2	$Na_2WO_4{\cdot}2H_2O$ (5 mol%), H_2O_2 (30% *aq.*, 7 equiv.), Na_2EDTA (5 mol%), H_2O	1.0	191	47
3	**$Na_2WO_4{\cdot}2H_2O$ (50 mol%), H_2O_2 (30% *aq.*, 2 × 30 equiv.), [$BnMe_3N$]OH (3 equiv.), EtOH**	**0.2**	**84**	**83**
4	*m*-CPBA (2.0 equiv.), CH_2Cl_2	0.15	2	65

ane, and allowed nitroxyl radical **8** to be prepared in a matter of hours, albeit in somewhat lower yields.

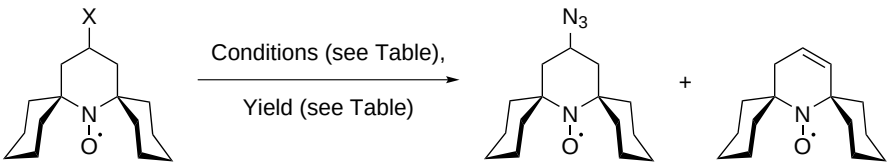
The nitroxyl alcohol **8** was further converted into a leaving group (Scheme 3.6). In connection with the optimisation of the subsequent nucleophilic substitution with sodium azide (see below), both mesylate **127** and tosylate **128** were prepared.



Scheme 3.6: Conversion of the alcohol in nitroxyl radical **8** into a leaving group.

Nucleophilic installation of the azide functionality again proved a challenging transformation (Table 3.4); the two spirocyclohexyl groups presumably increase the steric shielding of the leaving group compared to the tetramethyl-substituted mesylate **113** (see Section 3.1), and potentially also increase the activation energy barrier of a ring-flip of the piperidine ring to place the leaving group in a more reactive axial conformation. Submitting the mesylate **127** to conditions optimised for the tetramethyl-substituted system **113** (Entries 1 and 2) led to complete conversion, but also a mixture of the desired azide **107** and elimination product **129**. As alkene **129** is not volatile, the products were only separable by column chromatography with a very slow gradient; attempts at submitting the mixture of **107** and **129** to an Upjohn dihydroxylation of the alkene (and thereby simplify the purification) did not lead to any reaction taking place. Replacing the mesylate leaving group with a tosylate (Entries 3 and 4) reduced the selectivity for substitution over elimination. Decreasing the reaction temperature (Entries 5 and 6) only led to a moderate decrease in the formation of elimination product **129**; admittedly, these reactions did not reach completion and the product ratio could deteriorate as the reaction reaches high conversion. Further decreasing the reaction temperature (Entry 7) lowered the azide to alkene ratio, and the reaction took much longer to reach completion. Increasing the excess of sodium azide (Entry 8) doubled the reaction rate, but the selectivity for substitution observed in Entry 2 could

Table 3.4: Optimisation of the nucleophilic azidation of mesylate **127** or tosylate **128**.



Entry	X	Equiv. NaN_3	Solvent	T [°C]	Time [h]	Crude ratio 127/128 : 107 : 129	Yield 107 [%]
1[a]	OMs	6.0	DMF	80	2	0 : 1.0 : 0.24	59
2[a]	**OMs**	**2.0**	**DMSO**	**80**	**2**	**0 : 1.0 : 0.10**	**90**
3[b]	OTs	6.0	DMF	80	3	0 : 1.0 : 0.34	n/d
4[b]	OTs	2.0	DMSO	80	3	0 : 1.0 : 0.45	n/d
5[b]	OMs	6.0	DMF	70	2	0.92 : 1.0 : 0.15	n/d
6[b]	OMs	2.0	DMSO	70	2	0.76 : 1.0 : 0.13	n/d
7[b]	OMs	2.0	DMSO	60	47	0 : 1.0 : 0.22	n/d
8[b]	OMs	6.0	DMSO	60	24	0 : 1.0 : 0.17	n/d
9[c]	OMs	5.0	DMSO	80	2	0 : 1.0 : 0.20	65

[a] 0.3 mmol scale. [b] 0.06 mmol scale. [c] 1.4 mmol scale.

not be matched. Scaling up the reaction with the conditions of Entry 2, except with an increased amount of nucleophile to further favour S_N2 over E1 (Entry 9) surprisingly led to a deterioration of the azide to alkene ratio and lower isolated yield of azide **107**.

In summary, the novel bis(spirocyclohexyl)piperidinyl azide spin label **107** was prepared in a total yield of 43% over five steps from piperidone **111**. The structure of the spin label is verified by its X-ray crystal structure (Figure 3.6; crystallised by Dr Janet Lovett, analysed

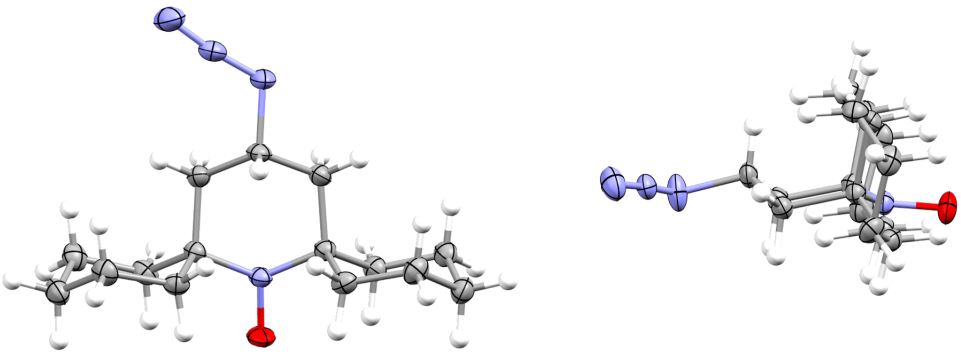


Figure 3.6: X-ray crystal structure of spin label **107**. The sample was crystallised by Dr Janet Lovett and analysed and refined by Prof. Alexandra Slawin (both at the University of St Andrews).

and refined by Prof. Alexandra Slawin (both at the University of St Andrews)) and is consistent with the observed triplet EPR spectrum of this compound (Figure 3.7).

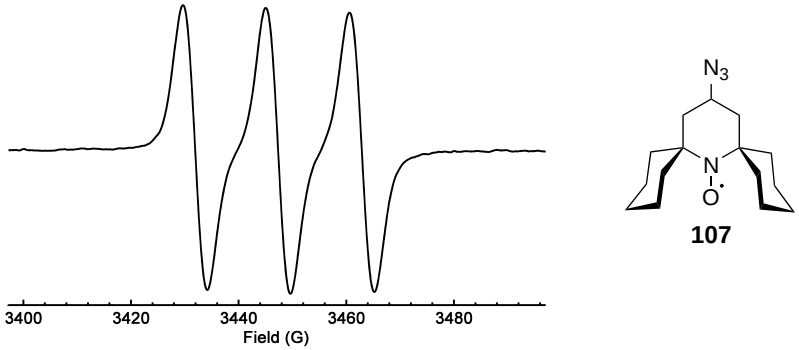
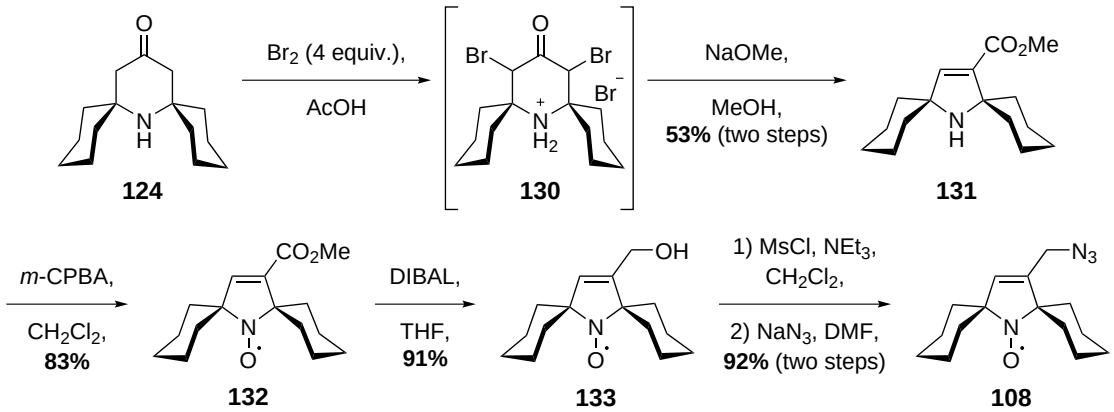


Figure 3.7: Room temperature X-band CW EPR spectrum of **107** (100 μM in $CHCl_3$).

3.4 Synthesis of bis(spirocyclohexyl)pyrrolinyl nitroxyl 108

From bis(spirocyclohexyl)-substituted aminoketone **124** (Scheme 3.7), bis(spirocyclohexyl)pyrrolinyl spin label **108** can be synthesised in analogy to the route towards tetramethylpyrroline label **106** (cf. Section 3.2). The increased rigidity and steric bulk of aminoketone **124** required an excess of bromine to effect the double α,α′-bromination; monitoring this reaction by LRMS revealed that full conversion was only achieved with four equivalents of Br_2. Small amounts of both mono-, tri- and tetrabrominated aminoketone were observed, although the dibromide **130** was the predominant species in the product mixture. As these compounds are unstable in solution, the mixture of hydrobromide salts



Scheme 3.7: Synthetic route towards bis(spirocyclohexyl)pyrroline spin label **108**.

which precipitated from the reaction mixture was not purified. Rather, the crude mixture of bromination products was submitted directly to the following Favorskii reaction/elimination with sodium methoxide; it was found that slow addition of solid **130** to a concentrated, freshly prepared solution of NaOMe afforded superior yields of methyl enoate **131**, which was purified at this stage. Subsequent *N*-oxidation to nitroxyl radical **132** using the *m*-CPBA protocol was followed by chemoselective reduction of the ester to the allylic alcohol **133**. Finally, the alcohol was mesylated and, without chromatographic purification, treated with sodium azide to afford the azide spin label **108** in excellent yields.

In summary, the novel bis(spirocyclohexyl)pyrrolinyl azide spin label **108** was synthesised from piperidone **111** in a total yield of 22% over seven steps. The structure of the spin label is verified by its X-ray crystal structure (Figure 3.8; crystallised by Dr Janet Lovett, analysed and refined by Prof. Alexandra Slawin (both at the University of St Andrews)) and is consistent with the observed triplet EPR spectrum of this compound (Figure 3.9).

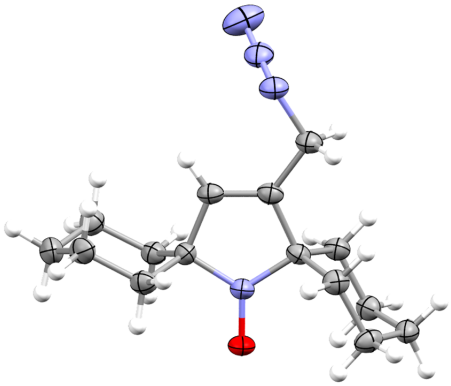


Figure 3.8: X-ray crystal structure of spin label **108**. The sample was crystallised by Dr Janet Lovett and analysed and refined by Prof. Alexandra Slawin (both at the University of St Andrews).

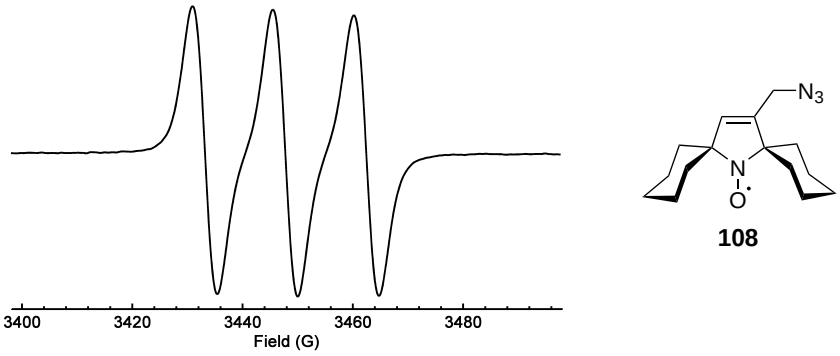
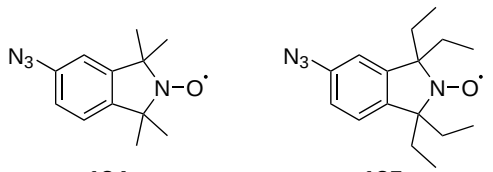


Figure 3.9: Room temperature X-band CW EPR spectrum of **108** (100 μM in $CHCl_3$).

3.5 Isoindolinyl spin labels

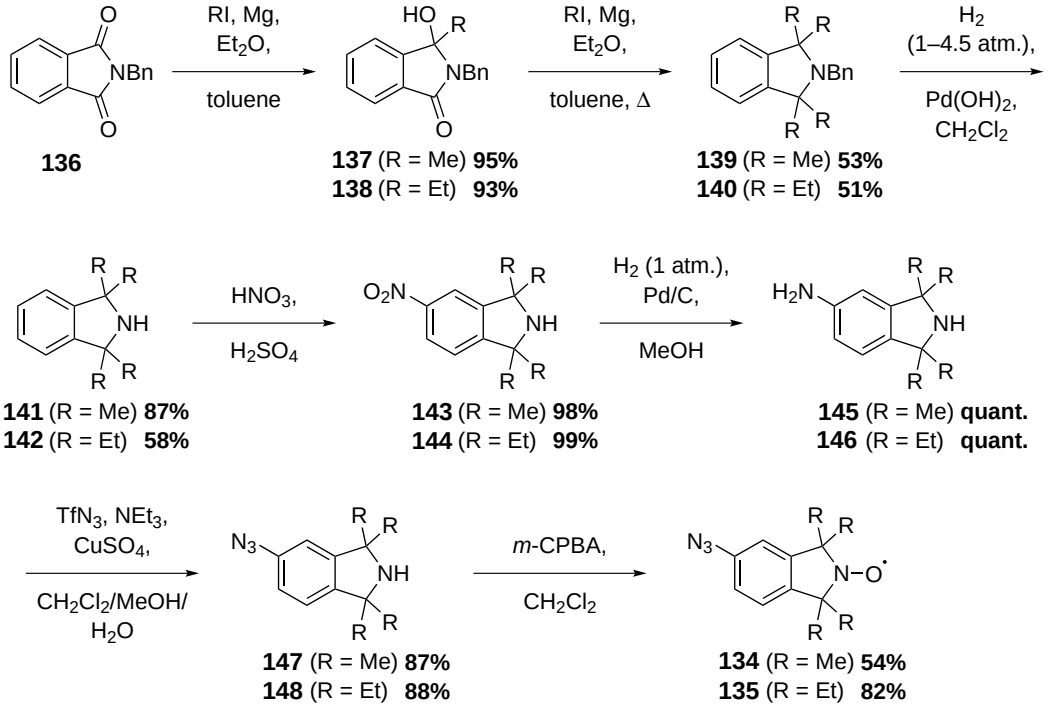
In addition to the four spin labels described so far, the spin label library was expanded with two isoindolinyl spin labels (**134** and **135**, Figure 3.10). The isoindoline scaffold is inherently rigid, and labels of this type have previously been used in highly successful approaches to SDSL of nucleic acids.[28,94,117,196,197] The novel tetraethyl-shielded label **135** is of particular interest as similar derivatives have been shown to exhibit very high stability towards reducing environments;[27] despite this, a tetraethyl-substituted isoindolinyl spin label was only recently incorporated into a nucleic acid.[28] The synthesis of spin labels **134** and **135** was performed by Part II student Rachel Porter.[198]



134 **135**

Figure 3.10: Isoindolinyl spin labels synthesised by Rachel Porter.[198]

In accordance with a published route towards **134**,[117] the synthesis of both of the isoindolinyl spin labels[198,199] started from *N*-benzylphthalimide (**136**, Scheme 3.8) by installation of the four α-substituents *via* a challenging quadruple Grignard addition. Resubmission of the monoaddition hemiaminal products (**137** and **138**) to an excess of organomagnesium reagent enabled the tetraalkylated compounds (**139** and **140**) to be isolated in respectable yields after several days of high-temperature reflux. The amine was subsequently debenzylated by hydrogenolysis, where the tetraethyl-substituted compound **140** required more forcing conditions (i.e. 4.5 atm. H_2). The resulting secondary amines (**141** and **142**) were further nitrated under classic conditions (**143** and **144**), and the nitro group was hydrogenated to afford the corresponding anilines (**145** and **146**) in excellent yields. The anilines were transformed into aromatic azides (**147** and **148**) using a Cu(II)-catalysed diazo transfer reaction, and finally the amine functionalities were oxidised by treatment with *m*-CPBA to the nitroxyl radicals (**134** and **135**).



Scheme 3.8: Synthesis of isoindolinyl spin labels performed by Rachel Porter.[198]

The isoindolinyl spin labels **134** and **135** were both synthesised in total yields of 20% over seven steps from *N*-benzylphthalimide (**136**). The nitroxyl radicals **134** and **135** are consistent with the observed triplet EPR spectra of these compounds (Figure 3.11).

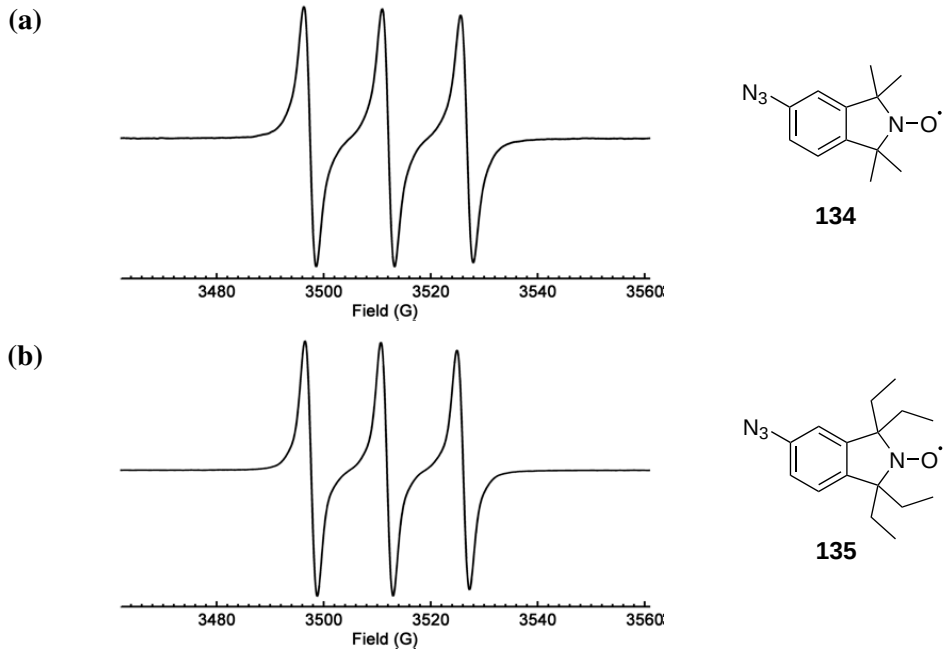


Figure 3.11: Room temperature X-band CW EPR spectra of **(a) 134** and **(b) 135** (100 μM, $CHCl_3$).

4 Site-directed spin labelling of oligodeoxynucleotides

With 2′-ethynyl-2′-deoxynucleoside phosphoramidite building blocks of uridine, cytidine and adenosine in hand (see Chapter 2), site-specifically modified 2′-alkynyl oligonucleotides were accessible through solid-phase synthesis by the phosphoramidite method. To facilitate the interpretation of EPR data, a regular model system of known structure was desirable; for this purpose one could use duplexes of either DNA (B-form double helix) or RNA (A-form). As the 2′-hydroxyl functionality in ribonucleic acids render RNA strands vulnerable to strand cleavage,[51] DNA was selected as a more stable system to carry out the initial evaluation of the proposed SDSL strategy. A 16-mer dsDNA system (Figure 4.1) was designed, in which a wide range of positions – both internal and terminal – could be functionalised using the available U-resin (**68**) and U, C and A phosphoramidites (**70**, **75** and **92**, respectively).

Strand A 5'—**A**-**C**-**T**-**A**-G-**C**-G-**C**-G-G-**A**-**C**-**T**-**C**-**T**-**T**—3'

Strand B 3'—**T**-G-**A**-**T**-**C**-G-**C**-G-**C**-**C**-**T**-G-**A**-G-**A**-**A**—5'

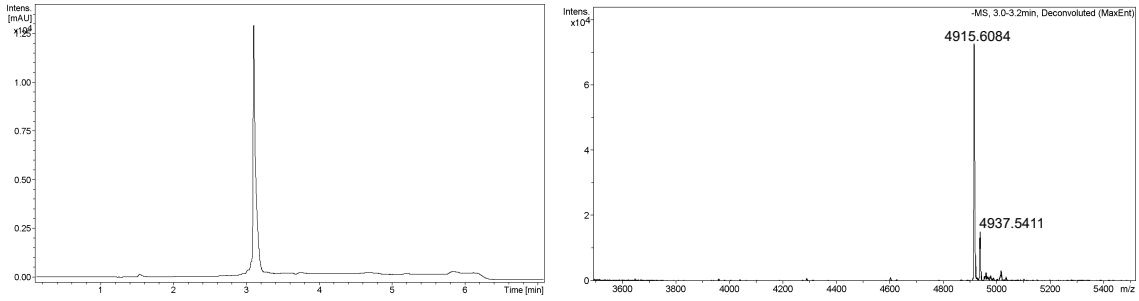
Figure 4.1: The non-self-complementary dsDNA system designed to evaluate the proposed SDSL strategy. For convenience, the top strand is named 'Strand A', while the bottom sequence is called 'Strand B'. Positions which can be spin labelled using the synthesised resin and phosphoramidites are indicated in bold.

4.1 Functionalisation of DNA at dT residues

Initial studies focused on the spin labelling of dT residues in the model duplex by substitution with 2′-ethynyl-2′-deoxyuridine. All DNA syntheses were kindly performed by Dr Afaf H. El-Sagheer,* on a 1.0 μmol scale using a standard protocol for solid-phase

*Specifically, Dr El-Sagheer programmed and operated the DNA synthesiser, cleaved the oligonucleotides from the resin and deprotected them.

DNA synthesis *via* the phosphoramidite method (see Section 7.7 for details); the only modification to the DNA synthesis conditions was increasing the coupling times for the 2′-alkynylated phosphoramidites to 600 s. This is routinely done even with commercially available phosphoramidites of modified nucleosides to improve the coupling yield, especially where there is increased steric hindrance around the phosphoramidite functionality (such as a 2′-modification). After cleavage from the resin and deprotection, the oligodeoxynucleotides were purified by RP-HPLC and characterised by LC-HRMS (Table 4.1); a representative HPLC chromatogram and deconvoluted ESI mass spectrum of a purified 2′-alkynylated DNA strand are shown in Figure 4.2.



(a) **(b)**

Figure 4.2: Representative HPLC-HRMS analysis of Strand **B2** verifying oligonucleotide purity and identity. **(a)** HPLC chromatogram with UV detection at 255–265 nm. **(b)** Deconvoluted ESI mass spectrum showing the $[M-H]^-$ and $[M-2H+Na]^-$ ions.

Initially, a number of DNA strands containing 2′-alkynyluridine residues were prepared (Table 4.1). In addition to the two non-functionalised DNA strands, **A1** and **B1**, analogues of Strands A and B were prepared (using the resin-bound 2′-alkynyluridine derivative **68**, Scheme 2.5) in which the T in the terminal position 16 was replaced with 2′-ethynyl-2′-deoxyuridine (**48**; indicated U, Strands **A2** and **B2**). Furthermore, using the 2′-alkynyluridine phosphoramidite building block **70** (Scheme 2.5), internal positions were functionalised at residue number 13 (Strands **A3** and **B3**). This set of modified oligonucleotides enables the incorporation of one or two spin labels in terminal or internal positions, or a combination of these, in a DNA duplex.

Following the preparation of alkynylated DNA strands, the site-directed spin labelling

Table 4.1: Synthesised non-modified and 2′-alkynyluridine-containing DNA strands. The alkyne-bearing residue is indicated in bold and underlined.

Strand	Sequence ($5' \rightarrow 3'$)	Mass $[M-H]^-$ [g/mol]		Isolated yield [%]
		Calc.	Found	
A1	ACTAGCGCGGACTCTT	4856	4856	19
B1	AAGAGTCCGCGCTAGT	4905	4905	22
A2	ACTAGCGCGGACTCT**U**	4866	4866	33
B2	AAGAGTCCGCGCTAG**U**	4915	4915	24
A3	ACTAGCGCGGAC**U**CTT	4866	4866	32
B3	AAGAGTCCGCGC**U**AGT	4915	4915	29

via CuAAC 'click' chemistry[200,201] could be attempted. The 'standard' protocol for CuAAC reactions involves *in situ* generation of catalytically active Cu(I) by reduction of Cu(II) with sodium ascorbate.[200] However, as ascorbate is known to reduce nitroxyl radicals to hydroxylamines (see Section 1.2), which are diamagnetic and thus EPR-silent, alternative conditions were considered. Copper(I) salts such as CuI have previously been directly used as CuAAC catalysts,[202] including for the purpose of SDSL of oligonucleotides before[117] or after[118,119,153] strand deprotection and cleavage from the resin.

One caveat with these Cu(I) salts is however their low solubility in water. As labelling reactions with protected, resin-bound oligonucleotides are carried out in polar organic solvents, in which both Cu(I) salts and the (often hydrophobic) spin label are soluble, reaction homogeneity is normally not an issue. Although on-column 'click' labelling would in all probability be possible with the 2′-ethynyl-2′-deoxynucleotide SDSL approach, it is useful to be able to perform 'click' reactions on DNA in aqueous solutions; as the designed sequence contained the alkyne on a residue close to the 3′-terminus and therefore the resin surface, the system might prove inaccessible to the catalyst and spin label and thus result in low rates for the 'click' reaction. Furthermore, a solution-based 'click' protocol can be further developed to enable other applications of oligonucleotide labelling, e.g. *in vivo* SDSL (albeit other considerations such as the cytotoxicity of copper must also be taken into account). Thus, performing the 'click' reaction in aqueous solutions was desirable. To this end, mixtures of water and organic solvents can be used to solubilise both the (hydrophilic)

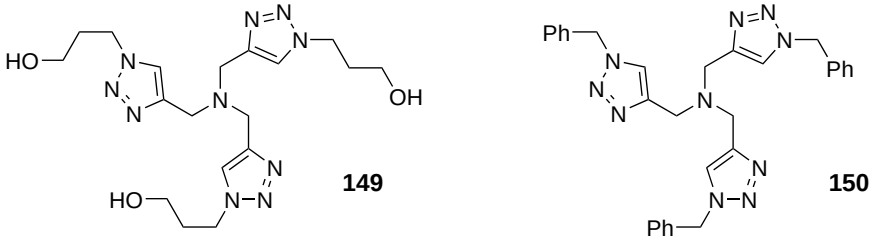
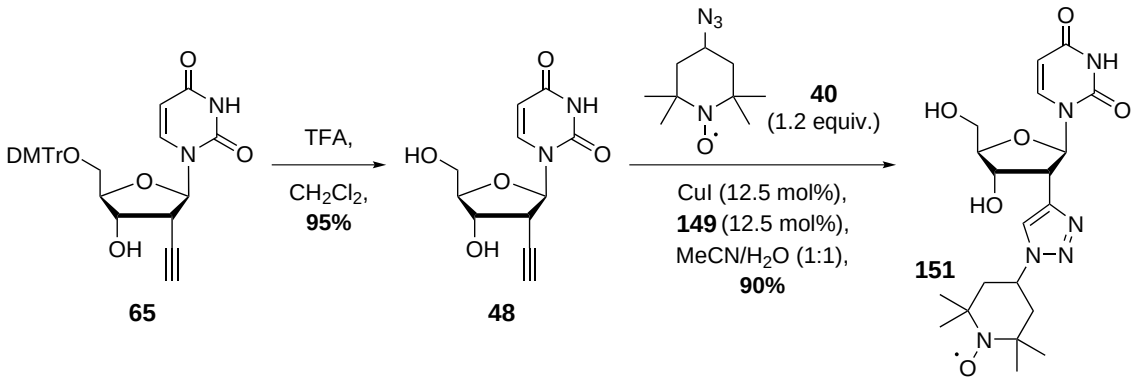


Figure 4.3: Structure of the tris(triazolylmethyl)amine ligands THPTA and TBTA.

nucleic acid, the water-insoluble catalyst, and hydrophobic spin labels. Acetonitrile, in which CuI is highly soluble, was identified as a suitable solvent to this end.

The use of tris(triazolylmethyl)amine ligands is a well-established way to enhance the rate of biomolecule CuAAC 'click' reactions;[203,204] the water-soluble ligand tris(hydroxypropyltriazolylmethyl)amine (THPTA, **149**, Figure 4.3) was further expected to enhance the catalyst solubility in the system. Tris(benzyltriazolylmethyl)amine (TBTA, **150**) is more commonly used in 'click' reactions performed in organic solvents. Ligand **149** has moreover been shown to act as a sacrificial reducing agent to scavenge reactive oxygen species (ROS),[203,205,206] the generation of which is catalysed by copper ions, which may lead to DNA damage.[207]

To investigate the suitability of the catalytic system and the stability of the nitroxyl radical under the 'click' labelling conditions, a test reaction was first performed on detritylated 2′-alkynyluridine (**48**, Scheme 4.1), which was prepared from trityl ether **65** by treatment with acid. Reaction with tetramethylpiperidinyl spin label **40**, the least reduction-resistant



Scheme 4.1: Preliminary investigation of the CuAAC 'click' reaction conditions on a nucleoside level.

spin label in the selected label library, in the presence of copper(I) iodide and ligand **149** pleasingly led to clean formation of 2′-triazolyluridine derivative **151** in high yields.

To verify the integrity of the nitroxyl radical in **151**, the radical was quantified by CW EPR spectroscopy. A series of solutions at different concentrations of spin label **40** and 'click' product **151** were prepared in precision quartz EPR tubes, and the CW EPR spectra were acquired under non-saturating conditions (i.e. within the linear range of the detector). The spectra, normalised with respect to the EPR acquisition parameters[†] are displayed in Figure 4.4a–b. These spectra are also normalised with respect to concentration; hence, in an ideal data set, their intensities would be identical. The spin concentration of the samples

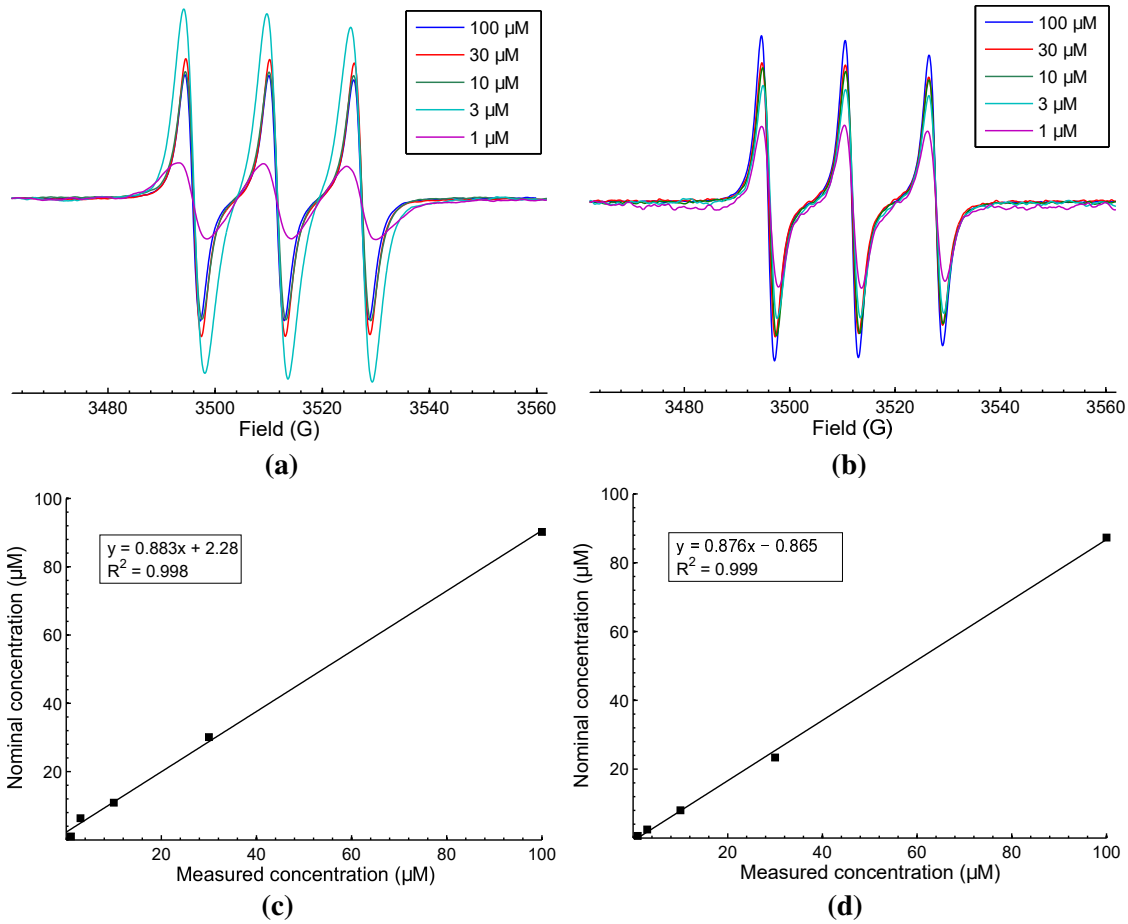


Figure 4.4: Spin concentration measurement by CW EPR. X-band CW EPR spectra of **(a) 40**, and **(b) 151**, at a range of concentrations in $CHCl_3$. The spectra are normalised with respect to concentration. The nominal concentration was plotted against measured concentration for **(c) 40** and **(d) 151**.

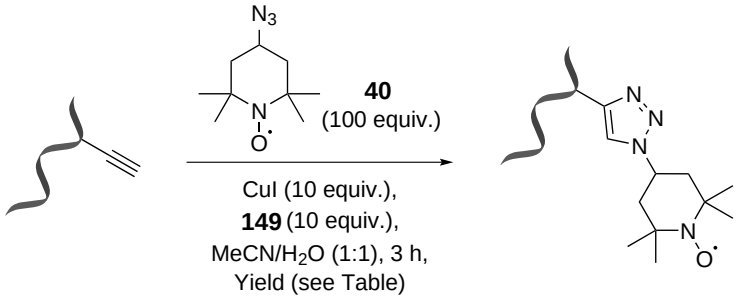
[†]Receiver gain, conversion time, number of scans, microwave power, modulation amplitude, and Q value.[9,208]

was determined by double integration of the spectra, and the nominal concentration of the samples was plotted against the measured values for the dilution series (Figure 4.4c–d). Linear regression provided a trendline with a good fit; the gradient of this line is the measured spin concentration (as a molar fraction). Spin densities were estimated to be 88% both for spin label **40** and for the 'click' product **151**; this indicates that the nitroxyl radical is not significantly degraded by the 'click' reaction conditions.

It is worth noting that quantitative measurements by EPR remains a challenging technique; as very low concentrations are required to avoid saturation effects and get a linear relationship between spin concentration and detector output, the method is sensitive to small inaccuracies in concentration.[9] This inaccuracy is apparent from the plotted CW EPR spectra in Figure 4.4, where especially samples at 1 μM appear to be too dilute. Furthermore, many environmental variables which are difficult to control precisely – such as sample temperature and solvent loss – can impact on the measurement. Considering the above, it is not unreasonable to expect an error of $\pm 10\%$; thus, the *de facto* values of the spin densities above may well be higher.

Having verified the suitability of the 'click' labelling methodology, the reaction was

Table 4.2: Spin labelling of 2′-ethynyl-dU containing DNA with spin label **40**. The spin labelled positions are indicated.



Strand	Sequence ($5' \rightarrow 3'$)	Mass $[M-H]^-$ [g/mol]		Isolated yield [%]
		Calc.	Found	
A2-6-Me	A C T A G C G C G G A C T C T **U**	5064	5064	57
B2-6-Me	A A G A G T C C G C G C T A G **U**	5113	5113	27
A3-6-Me	A C T A G C G C G G A C **U** C T T	5064	5064	81
B3-6-Me	A A G A G T C C G C G C **U** A G T	5113	5113	46

applied to label the alkyne-bearing DNA strands (Table 4.2) with azide **40**. Reactions were typically performed on a 50–100 nmol scale; thus, even using minimal reaction volumes (typically 30–50 μL), the reactions were very dilute with respect to the alkyne (∼2 mM). To achieve acceptable 'click' reaction rates, a large excess (100 equivalents) of azide, 10 equivalents of CuI catalyst and 10 equivalents of ligand **149** were used. Pleasingly, the reactions reached full conversion to 2′-triazole-linked spin labelled DNA within three hours as indicated by LC-HRMS analysis (Figure 4.5). Although full conversion was achieved in all cases, the isolated yields varied, as the small scale makes these reactions sensitive to sample loss during purification. For simplicity, DNA strands spin labelled with **40** are named with the more descriptive term "**-6-Me**" (indicating the ring size and substituents on the label).

To investigate the effect of these previously unknown modifications on the stability

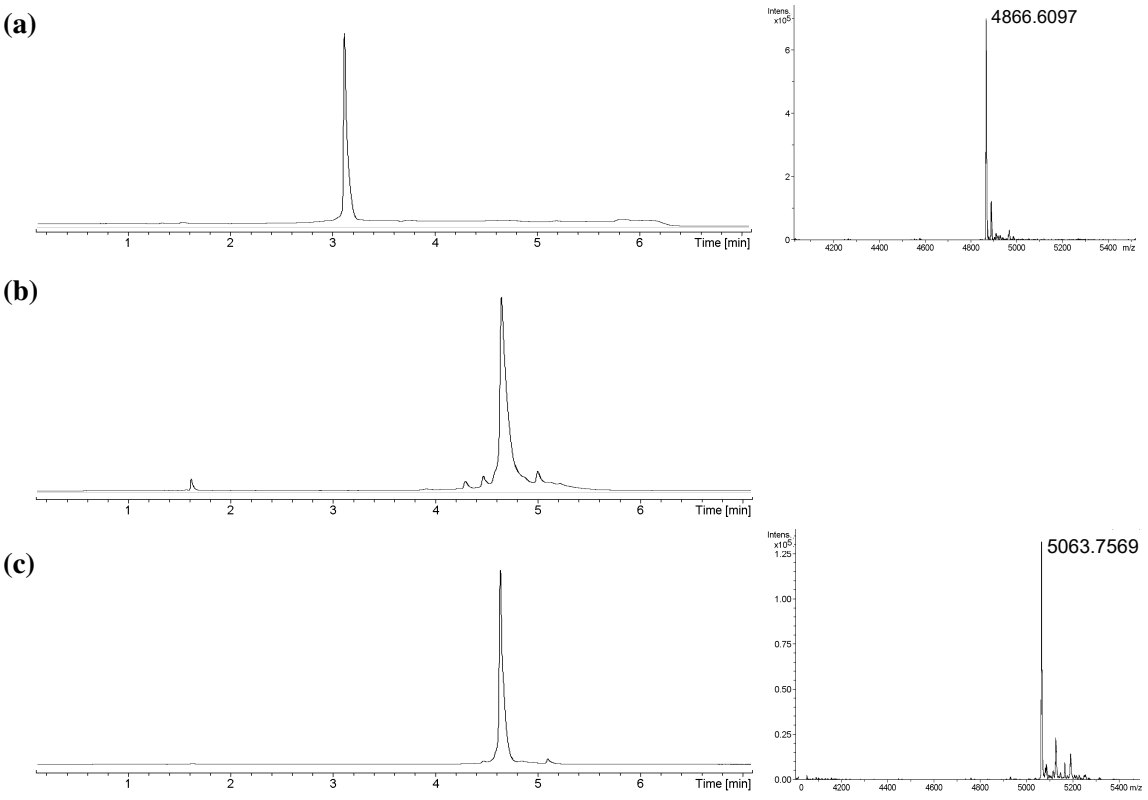


Figure 4.5: Chromatograms (255-292 nm) and HRMS ESI spectra showing **(a)** the starting material **A3**, **(b)** the crude 'click' reaction mixture after three hours, and **(c)** the purified spin labelled product **A3-6-Me**.

of the DNA structure, UV denaturation studies were performed. By monitoring the UV absorbance at 260 nm of a solution of a 1 : 1 mixture of Strands A and B at varying temperatures, a characteristic sigmoidal graph was obtained (Figure 4.6). This graph is indicative of a duplex formed between Strands A and B; the base stacking in a duplex (formed at lower temperatures) decreases the net UV absorbance of the nucleobases – a hypochromic shift.[209] As the temperature increases, the DNA strands dissociate, which gives rise to a net increase in the UV absorbance, in this case over a range of ∼60–75 °C. The UV melting temperature (T_m^{260}) is defined as the temperature at which 50% of the DNA duplex is dissociated, and is a measure of the overall thermodynamic favourability of duplex formation. The value of T_m^{260} is however strongly dependent on the sequence and duplex length, and is also influenced by factors such as DNA concentration, pH and the composition and ionic strength of the buffer solution.[209] For this reason, the *difference* (ΔT_m^{260}) in the UV melting temperature of a modified duplex compared to the corresponding non-modified duplex is a more useful parameter to characterise the biophysical consequences of DNA modifications.

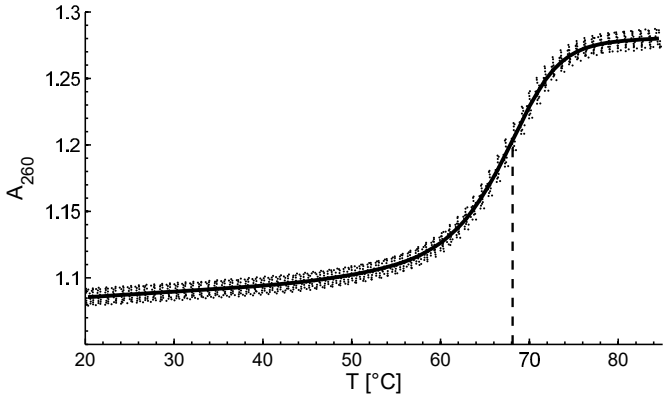


Figure 4.6: UV absorbance at 260 nm (A_{260}) of non-modified DNA duplex **A1:B1** (3.0 µM, 200 mM NaCl, 10 mM phosphate buffer, pH 7.3) plotted against temperature gives a sigmoidal curve, showing how the strands of the DNA duplex, which is favoured at low temperatures, dissociate upon heating. T_m^{260}, the temperature at which 50% of the duplex is dissociated, is in this case 68.1 ± 0.4 °C (dashed line).

T_m^{260} values were obtained for duplexes made up of non-modified DNA strands, as well as strands containing 2′-ethynyl-2′-deoxyuridine residues, and strands spin labelled with **40** (**6-Me**; Table 4.3). Introduction of two terminal 2′-alkynyluridine residues

(**A2:B2**) made no significant change to the duplex stability; as the ethynyl group is a very small modification, this is not surprising. However, one internal and one terminal 2′-alkynyluridine residue (**A3:B2** and **A2:B3**) led to a small decrease in ΔT_m^{260} of -2.80 °C and -2.99 °C, respectively, indicating a destabilising effect. Two internal alkynylated residues (**A3:B3**) led to a moderate destabilisation (-6.51 °C); interestingly, this effect is greater than the sum of the contributions of each modification.

A similar trend is observed for the spin labelled duplexes; both for singly (**A2-6-Me:B1** and **A1:B2-6-Me**) and doubly (**A2-6-Me:B2-6-Me**) terminally labelled duplexes, an insignificant to small destabilisation (up to -0.81 °C) was observed; the destabilisation of other doubly labelled duplexes (**A3-6-Me:B2-6-Me** and **A2-6-Me:B3-6-Me**) is dominated by the contribution of the internally labelled position. Notably, spin labelling did not increase the destabilisation of duplexes with Strand **B3-6-Me** compared to alkyne-bearing **B3**; on the other hand, internal spin labelling of Strand **A3** led to an increase in ΔT_m^{260} for duplexes of **A3-6-Me** from -2.80 °C to around -5 °C. It is possible that this increase indicates a sequence dependence on the destabilising effect of the 2′-triazolyl-linked spin label, where a more stable GC base pair on the terminal side of the modification is disrupted in duplexes of Strand **A3-6-Me** compared to an AT base pair in duplexes of Strand **B3-6-Me**. A more systematic investigation of the sequence dependence is, however, required before any conclusions can be drawn; nevertheless, the sequence flexibility of this SDSL technique could be exploited to minimise duplex disruption. The doubly internally labelled duplex **A3-6-Me:B3-6-Me** exhibited a significant depression of T_m^{260} of -9.79 °C, which is again larger than the sum of the depressions caused by each internal modification. This cooperative destabilising effect may be explained by the relative proximity of the modifications in this duplex, but no firm conclusions can be made without further studies.

It was hypothesised that the substitution of the native thymine for a uracil nucleobase might contribute to the ΔT_m^{260} discussed above. The 5-methyl substituent is known to enhance the base-stacking ability of thymine compared to uracil, and thus contribute to increasing the T_m^{260} of nucleic acids.[210] The magnitude of this effect is dependent on the

Table 4.3: UV denaturation studies on 2′-alkynyl-bearing DNA and the corresponding sequences spin labelled with azide **40** (3.0 μM, 200 mM NaCl, 10 mM phosphate buffer, pH 7.3). The modified positions are indicated.

Duplex	Sequence	ΔT_m^{260} [°C]
A1:B1	5′–A C T A G C G C G G A C T C T T–3′ 3′–T G A T C G C G C C T G A G A A–5′	—
A2:B2	5′–A C T A G C G C G G A C T C T **U**–3′ 3′–**U** G A T C G C G C C T G A G A A–5′	$+0.23 \pm 0.34$
A3:B2	5′–A C T A G C G C G G A C **U** C T T–3′ 3′–**U** G A T C G C G C C T G A G A A–5′	-2.80 ± 0.39
A2:B3	5′–A C T A G C G C G G A C T C T **U**–3′ 3′–T G A **U** C G C G C C T G A G A A–5′	-2.99 ± 0.46
A3:B3	5′–A C T A G C G C G G A C **U** C T T–3′ 3′–T G A **U** C G C G C C T G A G A A–5′	-6.51 ± 0.47
A2-6-Me:B1	5′–A C T A G C G C G G A C T C T **U**–3′ 3′–T G A T C G C G C C T G A G A A–5′	-0.80 ± 0.38
A1:B2-6-Me	5′–A C T A G C G C G G A C T C T T–3′ 3′–**U** G A T C G C G C C T G A G A A–5′	-0.12 ± 0.41
A3-6-Me:B1	5′–A C T A G C G C G G A C **U** C T T–3′ 3′–T G A T C G C G C C T G A G A A–5′	-4.94 ± 0.44
A1:B3-6-Me	5′–A C T A G C G C G G A C T C T T–3′ 3′–T G A **U** C G C G C C T G A G A A–5′	-3.13 ± 0.47
A2-6-Me:B2-6-Me	5′–A C T A G C G C G G A C T C T **U**–3′ 3′–**U** G A T C G C G C C T G A G A A–5′	-0.81 ± 0.32
A3-6-Me:B2-6-Me	5′–A C T A G C G C G G A C **U** C T T–3′ 3′–**U** G A T C G C G C C T G A G A A–5′	-5.24 ± 0.37
A2-6-Me:B3-6-Me	5′–A C T A G C G C G G A C T C T **U**–3′ 3′–T G A **U** C G C G C C T G A G A A–5′	-3.06 ± 0.46
A3-6-Me:B3-6-Me	5′–A C T A G C G C G G A C **U** C T T–3′ 3′–T G A **U** C G C G C C T G A G A A–5′	-9.79 ± 0.37

neighbouring base pairs and the overall sequence; hence, it is difficult to estimate how much it contributes to the observed T_m^{260} depressions. Therefore, to evaluate the impact of substitution of dT with dU, duplexes were prepared with 2′-deoxyuridine incorporated in place of the spin labelled sites, and their ΔT_m^{260} compared to non-modified duplex **A1:B1** were acquired (Table 4.4). In all cases the change in melting temperature was found to be insignificant ($\leq +0.31$ °C and within the error margins); any contribution from the

Table 4.4: UV denaturation studies on DNA containing 2′-deoxyuridine (3.0 μM, 200 mM NaCl, 10 mM phosphate buffer, pH 7.3).

Duplex	Sequence	ΔT_m^{260} [°C]
A1:B1	5′–A C T A G C G C G G A C T C T T–3′ 3′–T G A T C G C G C C T G A G A A–5′	—
A4:B4	5′–A C T A G C G C G G A C T C T U–3′ 3′–U G A T C G C G C C T G A G A A–5′	$+0.11 \pm 0.36$
A5:B4	5′–A C T A G C G C G G A C U C T T–3′ 3′–U G A T C G C G C C T G A G A A–5′	$+0.03 \pm 0.23$
A4:B5	5′–A C T A G C G C G G A C T C T U–3′ 3′–T G A U C G C G C C T G A G A A–5′	$+0.31 \pm 0.31$
A5:B5	5′–A C T A G C G C G G A C U C T T–3′ 3′–T G A U C G C G C C T G A G A A–5′	$+0.09 \pm 0.23$

substitution of dU for dT in the spin labelled duplexes (Table 4.3) can thus be discounted.

4.1.1 Variation of the spin label at dU

Following the successful incorporation of tetramethylpiperidinyl spin label **40** into the 2′-alkynyluridine containing DNA strands, the feasibility and consequences of using other spin labels were assessed. To facilitate the discussion below, each nitroxyl in the spin label library was given a recognisable descriptor (Figure 4.7).

To limit the amount of data produced in this extensive study, the terminally alkynylated strand **B2** was not investigated further; only one duplex containing one terminal and

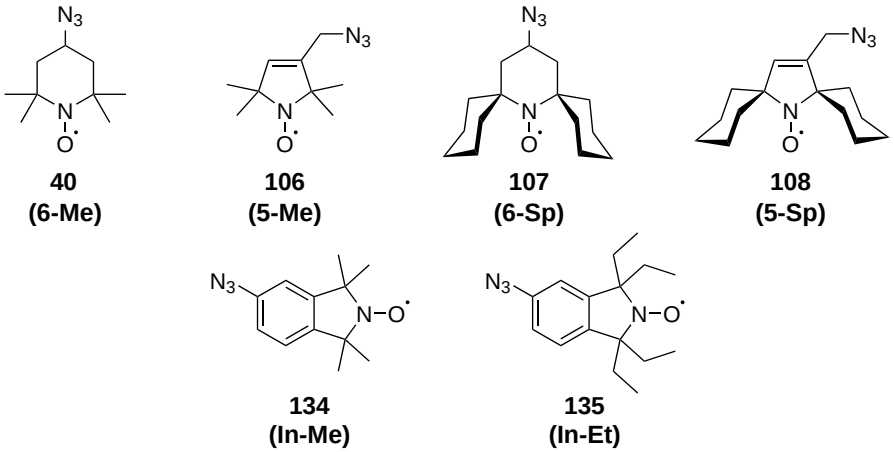
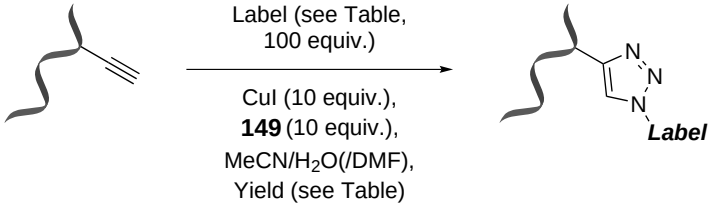


Figure 4.7: Library of spin labels to be investigated.

one internal spin label (i.e. derivatives of **A2:B3**) was required. Preliminary EPR results moreover indicated a relatively high degree of conformational mobility in doubly terminally labelled systems (**A2-6-Me:B2-6-Me**, Table 4.3; see Chapter 5 for a full discussion of results from EPR spectroscopy), making these duplexes less interesting for further study. The remaining DNA strands containing 2′-alkynyluridine (**A2**, **A3** and **B3**) were site-selectively spin labelled by submission to the previously developed reaction conditions (Table 4.5). For the more lipophilic spin labels **5-Sp**, **In-Me** and **In-Et**, the reaction time was increased to 4 h, and the solvent composition required adjustment (up to a 7 : 3 ratio of MeCN/H_2O) to solubilise the spin labels. The least soluble label, **6-Sp**, only reacted

Table 4.5: Spin labelling of 2′-ethynyl-dU containing DNA with azides **106**, **107**, **108**, **134** and **135**. The spin labelled positions are indicated.



Strand	Sequence (5′ → 3′)	Label	Mass $[M-H]^-$ [g/mol]		Isolated yield [%]
			Calc.	Found	
A2-5-Me	A C T A G C G C G G A C T C T **U**	**106**	5062	5062	64
A3-5-Me	A C T A G C G C G G A C **U** C T T	**106**	5062	5062	61
B3-5-Me	A A G A G T C C G C G C **U** A G T	**106**	5111	5111	65
A2-6-Sp	A C T A G C G C G G A C T C T **U**	**107**	5144	5144	59
A3-6-Sp	A C T A G C G C G G A C **U** C T T	**107**	5144	5144	42
B3-6-Sp	A A G A G T C C G C G C **U** A G T	**107**	5193	5193	50
A2-5-Sp	A C T A G C G C G G A C T C T **U**	**108**	5142	5142	68
A3-5-Sp	A C T A G C G C G G A C **U** C T T	**108**	5142	5142	44
B3-5-Sp	A A G A G T C C G C G C **U** A G T	**108**	5191	5191	63
A2-In-Me	A C T A G C G C G G A C T C T **U**	**134**	5097	5098	36[a]
A3-In-Me	A C T A G C G C G G A C **U** C T T	**134**	5097	5098	61[a]
B3-In-Me	A A G A G T C C G C G C **U** A G T	**134**	5146	5147	41[a]
A2-In-Et	A C T A G C G C G G A C T C T **U**	**135**	5154	5154	58
A3-In-Et	A C T A G C G C G G A C **U** C T T	**135**	5154	5154	46
B3-In-Et	A A G A G T C C G C G C **U** A G T	**135**	5203	5203	20[a]

[a] Reaction performed by Rachel Porter.[198]

when dissolved in DMF (final solvent composition 22 : 1 : 11 DMF/MeCN/H_2O), in spite of the increased dilution of these solutions. Even with adjustment of the solvent mixture, homogeneous mixtures could not always be obtained. In these cases, the reaction mixture was agitated and sonicated regularly throughout the reaction to ensure sufficient mixing; full conversion was observed and spin labelled DNA strands were pleasingly isolated in good yields.

The spin labelled DNA strands were mixed to form duplexes containing one or two spin labels (but limited to one type of spin label per duplex), and the effect of introducing the various triazole-linked spin labels was investigated by UV denaturation studies (Table 4.6). In general, all the sets of duplexes with the various labels displayed similar trends to the duplexes labelled with **6-Me**: The effect of terminal labelling is either insignificant (i.e. within the margins of error, given as standard deviation), or indeed for some labels weakly *stabilising* ($\leq +0.69$ °C). Furthermore, internal labelling of Strand A is more destabilising than internal labelling of Strand B by around 1.3–2.6 °C. Finally, the doubly internally labelled duplexes were of the lowest stability (varying from -3.73 to -10.40 °C), and in most cases the ΔT_m^{260} of this duplex was larger than the sum of the individual contribution from each spin label.

More surprising results were found when comparing duplexes with the same labelling patterns, but where different labels had been used (including comparison to the data for **6-Me** labelling, Table 4.3). Comparing the datasets for **6-Me** with **6-Sp** and **5-Me** with **5-Sp** indicates that for a given site of modification, the tetramethyl-substituted spin labels are *more* destabilising than the bis(spirocyclohexyl)-substituted labels. This is unexpected considering that the larger bulk of the latter might be expected to increase distortion of the double helix structure, purely on steric grounds. On the other hand, these results can be rationalised by a hydrophobic effect: the lipophilic spin labels will presumably associate with the DNA surface (as far as the conformationally restricting triazole linker allows) to minimise the total hydrophobic surface area exposed to water. One driving force for this is minimising the entropic cost of forming a highly ordered solvation shell

Table 4.6: UV denaturation studies on DNA sequences spin labelled with azides **106**, **107**, **108**, **134** and **135** (3.0 µM, 200 mM NaCl, 10 mM phosphate buffer, pH 7.3). The modified positions are indicated.

Duplex	Sequence	ΔT_m^{260} [°C]
A1:B1	5′–A C T A G C G C G G A C T C T T–3′ 3′–T G A T C G C G C C T G A G A A–5′	—
A2-5-Me:B1	5′–A C T A G C G C G G A C T C T **U**–3′ 3′–T G A T C G C G C C T G A G A A–5′	$+0.15 \pm 0.40$
A3-5-Me:B1	5′–A C T A G C G C G G A C **U** C T T–3′ 3′–T G A T C G C G C C T G A G A A–5′	-4.87 ± 0.34
A1:B3-5-Me	5′–A C T A G C G C G G A C T C T T–3′ 3′–T G A **U** C G C G C C T G A G A A–5′	-3.62 ± 0.23
A2-5-Me:B3-5-Me	5′–A C T A G C G C G G A C T C T **U**–3′ 3′–T G A **U** C G C G C C T G A G A A–5′	-3.46 ± 0.45
A3-5-Me:B3-5-Me	5′–A C T A G C G C G G A C **U** C T T–3′ 3′–T G A **U** C G C G C C T G A G A A–5′	-10.40 ± 0.51
A2-6-Sp:B1	5′–A C T A G C G C G G A C T C T **U**–3′ 3′–T G A T C G C G C C T G A G A A–5′	$+0.41 \pm 0.33$
A3-6-Sp:B1	5′–A C T A G C G C G G A C **U** C T T–3′ 3′–T G A T C G C G C C T G A G A A–5′	-2.27 ± 0.45
A1:B3-6-Sp	5′–A C T A G C G C G G A C T C T T–3′ 3′–T G A **U** C G C G C C T G A G A A–5′	-0.56 ± 0.75
A2-6-Sp:B3-6-Sp	5′–A C T A G C G C G G A C T C T **U**–3′ 3′–T G A **U** C G C G C C T G A G A A–5′	-0.56 ± 0.41
A3-6-Sp:B3-6-Sp	5′–A C T A G C G C G G A C **U** C T T–3′ 3′–T G A **U** C G C G C C T G A G A A–5′	-3.73 ± 0.41
A2-5-Sp:B1	5′–A C T A G C G C G G A C T C T **U**–3′ 3′–T G A T C G C G C C T G A G A A–5′	$+0.55 \pm 0.37$
A3-5-Sp:B1	5′–A C T A G C G C G G A C **U** C T T–3′ 3′–T G A T C G C G C C T G A G A A–5′	-4.05 ± 0.39
A1:B3-5-Sp	5′–A C T A G C G C G G A C T C T T–3′ 3′–T G A **U** C G C G C C T G A G A A–5′	-2.11 ± 0.32
A2-5-Sp:B3-5-Sp	5′–A C T A G C G C G G A C T C T **U**–3′ 3′–T G A **U** C G C G C C T G A G A A–5′	-1.07 ± 0.75
A3-5-Sp:B3-5-Sp	5′–A C T A G C G C G G A C **U** C T T–3′ 3′–T G A **U** C G C G C C T G A G A A–5′	-8.03 ± 0.30

(Continued on next page)

Table 4.6 *(continued from previous page)*

Duplex	Sequence	ΔT_m^{260} [°C]
A2-In-Me:B1	5′–A C T A G C G C G G A C T C T **U**–3′ 3′–T G A T C G C G C C T G A G A A–5′	$+0.35 \pm 0.27$[a]
A3-In-Me:B1	5′–A C T A G C G C G G A C **U** C T T–3′ 3′–T G A T C G C G C C T G A G A A–5′	-3.95 ± 0.54[a]
A1:B3-In-Me	5′–A C T A G C G C G G A C T C T T–3′ 3′–T G A **U** C G C G C C T G A G A A–5′	-1.42 ± 0.34[a]
A2-In-Me:B3-In-Me	5′–A C T A G C G C G G A C T C T **U**–3′ 3′–T G A **U** C G C G C C T G A G A A–5′	-0.55 ± 0.57[a]
A3-In-Me:B3-In-Me	5′–A C T A G C G C G G A C **U** C T T–3′ 3′–T G A **U** C G C G C C T G A G A A–5′	-6.40 ± 0.47[a]
A2-In-Et:B1	5′–A C T A G C G C G G A C T C T **U**–3′ 3′–T G A T C G C G C C T G A G A A–5′	$+0.17 \pm 0.52$[a]
A3-In-Et:B1	5′–A C T A G C G C G G A C **U** C T T–3′ 3′–T G A T C G C G C C T G A G A A–5′	-3.21 ± 0.56[a]
A1:B3-In-Et	5′–A C T A G C G C G G A C T C T T–3′ 3′–T G A **U** C G C G C C T G A G A A–5′	-0.97 ± 0.40[a]
A2-In-Et:B3-In-Et	5′–A C T A G C G C G G A C T C T **U**–3′ 3′–T G A **U** C G C G C C T G A G A A–5′	$+0.69 \pm 0.43$[a]
A3-In-Et:B3-In-Et	5′–A C T A G C G C G G A C **U** C T T–3′ 3′–T G A **U** C G C G C C T G A G A A–5′	-4.27 ± 0.44[a]

[a] Measurement performed by Rachel Porter.[198]

at the DNA/label-water interface. It is possible that the spirocyclic labels **6-Sp** and **5-Sp** are capable of adapting a conformation with a lower overall hydrophobic surface area. Alternatively it can be envisaged that the bulky labels cause a larger aqueous/hydrophobic interface in both the ssDNA and the dsDNA, whereas the disordered ssDNA is more able to envelop the smaller tetramethyl-substituted spin labels than the ordered dsDNA; this would manifest itself as a relatively larger thermodynamic destabilisation in the latter case. It is, however, impossible to draw conclusions without detailed structural insight into the conformations adopted by the spin labelled system.[211]

Another trend, apparent when comparing the datasets of **6-Me** and **6-Sp** with **5-Me** and **5-Sp**, respectively, is that the six-membered piperidinyl spin labels are less destabilising

than the corresponding five-membered pyrrolinyl spin labels. This was again unexpected; as the pyrrolinyl spin labels have an additional methylene group between the triazole linker and the nitroxyl-bearing ring, it was anticipated that these systems would be more flexible and so allow the label to adopt a less disrupting conformation. It is difficult to explain this finding without further investigation of the conformations adopted by these systems. This effect is however smaller in magnitude than the impact of the α,α'-substituents.

The tetramethyl-substituted isoindolinyl spin label **In-Me** was surprisingly found to be *more* destabilising than the more sterically demanding tetraethyl-substituted label **In-Et**; a hydrophobic effect may again be invoked to explain this. This is however in contrast to a previous study, where 2′-aminouridine residues (admittedly in RNA) were labelled with an isothiocyanate analogue of **In-Et**, which proved more destabilising than the corresponding **In-Me**.[28] Compared to the majority of the other labels, the isoindoline derivatives exhibited relatively low destabilising effects; this is in accordance with previous reports.[28] It may be that the linked aromatic rings in these systems, a feature shared with many minor groove binders,[59] allow these labels to interact with the DNA backbone in a manner fundamentally different to saturated labels.

In summary, where differences are significant (in terms of the error margins, given as standard deviation), the destabilising effect of the various spin labels in the model system can be ordered as follows:

5-Me > **6-Me** > **5-Sp** > **In-Me** > **In-Et** > **6-Sp**

Intriguingly, derivatives of duplex **A2:B3** (containing one terminal and one internal alkyne) with spin labels **6-Sp**, **5-Sp**, **In-Me** and **In-Et** are *less* destabilised than the parent alkyne-bearing duplex (cf. Table 4.3). For the double internal alkynyl duplex **A3:B3**, this relative stabilisation was only observed with labels **6-Sp** and **In-Et**. The origin of this effect is not understood at present.

4.1.2 Comparison to other SDSL methods

Only one previous example of a 'click' chemistry approach to achieve SDSL of the 2′-position in nucleic acids has been reported, wherein a uridine carrying a more flexible 2′-*O*-propargyl ether was labelled with **6-Me** (see **38**, Section 1.4).[153] To evaluate whether the novel 2′-alkynylnucleoside strategy offers an improvement over the previously reported approach, DNA strands of the model sequence were prepared in which dT in position 13 was substituted with 2′-*O*-propargyluridine using the corresponding, commercially available phosphoramidite (Table 4.7). The isolated yields of these strands were comparable to the yields of 2′-alkynyluridine-containing strands (cf. Table 4.1).

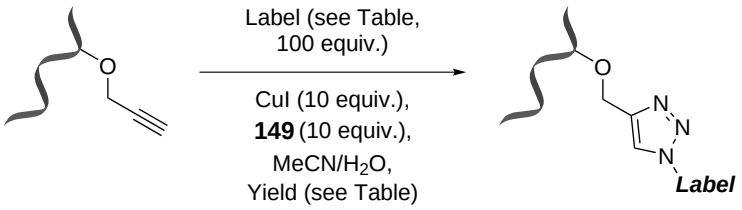
With the propargyl-bearing DNA strands in hand, 'click' reactions were performed with label **6-Me**, **5-Sp** and **In-Et** (Table 4.8), under the conditions developed for the 2′-alkynyluridine labelling. The isolated yields of 'click' products were overall similar or slightly better compared to the respective 2′-triazolyl DNA strands; however, these reactions are, as mentioned, sensitive to sample loss during purification, making it hard to conclude whether the higher yields are a result of the 2′-*O*-propargyl system itself.

After 'click' labelling, duplexes of the above strands were formed to investigate the effect of the increased flexibility of the linker group (Table 4.9). All three duplexes demonstrated that the 2′-*O*-propargyl-derived systems are less destabilising than the corresponding 2′-ethynyl-derived systems; this is unsurprising given that the longer and more flexible linker group should allow the duplexes to better accommodate the spin label without structural disruption. Interestingly, the relative order of destabilisation amongst the spin labels is preserved; although the difference between them is much smaller, this suggests that the

Table 4.7: Synthesised 2′-*O*-propargyluridine-containing DNA strands. The propargyl-bearing residue is indicated in bold and underlined.

Strand	Sequence (5′ → 3′)	Mass $[M-H]^-$ [g/mol]		Isolated yield [%]
		Calc.	Found	
A6	A C T A G C G C G G A C **U** C T T	4896	4897	33
B6	A A G A G T C C G C G C **U** A G T	4945	4946	30

Table 4.8: Spin labelling of 2′-*O*-propargyluridine containing DNA with azides **40**, **108** and **135**. The spin labelled positions are indicated.



Strand	Sequence (5′ → 3′)	Label	Mass $[M-H]^-$ [g/mol]		Isolated yield [%]
			Calc.	Found	
A6-6-Me	A C T A G C G C G G A C **U** C T T	**40**	5094	5094	70
B6-6-Me	A A G A G T C C G C G C **U** A G T	**40**	5143	5143	76
A6-5-Sp	A C T A G C G C G G A C **U** C T T	**108**	5172	5172	55
B6-5-Sp	A A G A G T C C G C G C **U** A G T	**108**	5221	5221	63
A6-In-Et	A C T A G C G C G G A C **U** C T T	**135**	5183	5184	67
B6-In-Et	A A G A G T C C G C G C **U** A G T	**135**	5232	5233	60

structure of the spin label is still significant with respect to the interactions between the label and the DNA backbone, even with a long and more flexible linker.

The ΔT_m^{260} values, although relevant, are in themselves not sufficient to evaluate the performance of 2′-ethynylnucleoside derivatives compared to the 2′-*O*-propargylnucleoside derivatives. The characteristics of their respective EPR spectra, discussed in Sections 5.1.1 and 5.3.1, are arguably of greater significance in some applications, and therefore important for the comparative analysis of these two SDSL techniques.

Table 4.9: UV denaturation studies on spin labelled derivatives of propargyl-bearing DNA strands (3.0 µM, 200 mM NaCl, 10 mM phosphate buffer, pH 7.3). Spin labelled positions are indicated.

Duplex	Sequence	ΔT_m^{260} [°C]
A1:B1	5′–A C T A G C G C G G A C T C T T–3′ 3′–T G A T C G C G C C T G A G A A–5′	—
A6-6-Me:B6-6-Me	5′–A C T A G C G C G G A C **U** C T T–3′ 3′–T G A **U** C G C G C C T G A G A A–5′	-4.72 ± 0.38
A6-5-Sp:B6-5-Sp	5′–A C T A G C G C G G A C **U** C T T–3′ 3′–T G A **U** C G C G C C T G A G A A–5′	-3.06 ± 0.51
A6-In-Et:B6-In-Et	5′–A C T A G C G C G G A C **U** C T T–3′ 3′–T G A **U** C G C G C C T G A G A A–5′	-2.67 ± 0.47

4.2 Functionalisation of DNA at dC and dA residues

Having established the feasibility of labelling 2′-ethynyl-2′-deoxyuridine residues in DNA with a range of spin labels, attention turned to the functionalisation other nucleotides. Using the (cyanoethyl)phosphoramidite building blocks of 2′-ethynyl-2′-deoxycytidine (**75**, Scheme 2.7) and -adenosine (**92**, Scheme 2.12), DNA strands bearing alkynyl groups on dC and dA were synthesised (Table 4.10). Yields could not be calculated for 2′-alkynyladenosine-containing strands **A7** and **B7** as these oligonucleotides contained a large amount of side product (Figure 4.8), which could only be partially separated from the product strand on a preparative scale. Given the large quantity of the side products, the yields are likely to be lower than for 2′-alkynylcytidine strand **B8**. Interestingly, in both strands, the side product appears to be the result of a strand break, giving rise to one fragment with a 3′-terminal enyne adenosine derivative and another with a 5′-phosphate. As these fragments can only arise from the full length oligonucleotide, this may indicate that the side products are the result of degradation during deprotection of the oligonucleotide (conc. NH_3 (*aq.*), 55 °C, 5 h), and are not caused by degradation or insufficient coupling of 2′-alkynyladenosine phosphoramidite **92**. It is not clear why this degradation was not observed with DNA strands containing alkynylated pyrimidine nucleotides.

In spite of the varying degrees of purity obtained for the alkynylated DNA strands, 'click' reactions were performed with azides **40**, **108** and **135** (**6-Me**, **5-Sp** and **In-Et**, respectively). Although yields could not be calculated in cases where impure alkynylated strands were used, 'click' labelled oligonucleotides were isolated in sufficient quantities

Table 4.10: Synthesised DNA strands containing 2′-ethynyl-2′-deoxyadenosine and -cytidine. The alkynylated residue is indicated in bold and underlined.

Strand	Sequence (5′ → 3′)	Mass $[M-H]^-$ [g/mol]		Isolated yield [%]
		Calc.	Found	
A7	A C T **A** G C G C G G A C T C T T	4880	4881	n/d
B7	A A G A G T C C G C G C T **A** G T	4929	4930	n/d
B8	A A G A G T C C G C G **C** T A G T	4929	4930	25

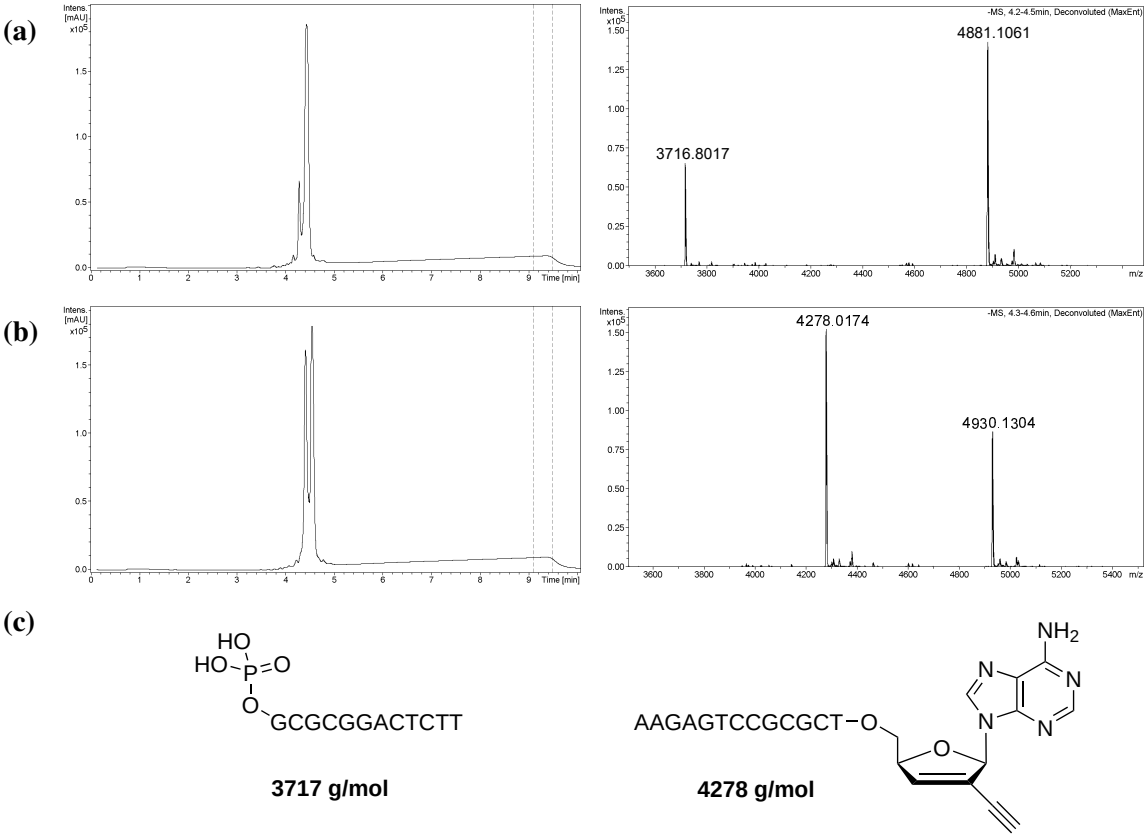
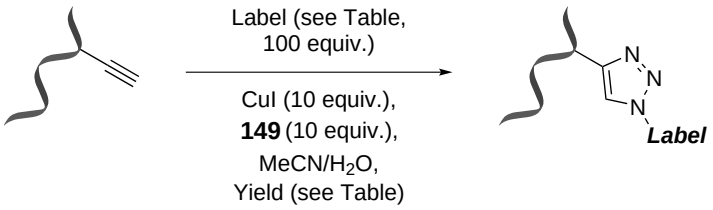


Figure 4.8: Chromatograms (255–292 nm) and deconvoluted mass spectra for the most concentrated fractions of **(a) A7**, and **(b) B7**, after HPLC purification. **(c)** The mass of the side products suggests a strand break has taken place.

(Table 4.11). Pleasingly, purification of the 'click' labelled strands was simplified by a relatively large change in retention time upon introduction of the hydrophobic spin labels; the spin labelled DNA strands were thus obtained in high purity.

As with the DNA strands labelled at 2′-ethynyl-2′-deoxyuridine, duplexes of the spin labelled strands were formed, and the destabilising effect of the spin labels at different nucleotides was assessed by ΔT_m^{260} (Table 4.12). In general, spin labelling at dC appears to be comparable to or slightly more destabilising (by up to 0.7 °C) than labelling at the neighbouring dT/dU (cf. Table 4.6), irrespective of which label was used. On the contrary, labelling at dA seems to be markedly less destabilising (by up to 2.7 °C) than at the neighbouring dT, except when using the **In-Et** label. It should be noted that these trends may equally be explained by the distance of the modification site from the duplex terminus. However, the results clearly demonstrate that the structure of the spin label has a larger

Table 4.11: Spin labelling of 2′-ethynyl-dC and -dA containing DNA with azides **40**, **108** and **135**. The spin labelled positions are indicated.



Strand	Sequence (5′ → 3′)	Label	Mass $[M-H]^-$ [g/mol]		Isolated yield [%]
			Calc.	Found	
B7-6-Me	A A G A G T C C G C G C T **A** G T	**40**	5127	5127	59
B8-6-Me	A A G A G T C C G C G **C** T A G T	**40**	5127	5127	58
A7-5-Sp	A C T **A** G C G C G G A C T C T T	**108**	5156	5156	n/d
B7-5-Sp	A A G A G T C C G C G C T **A** G T	**108**	5205	5205	56
B8-5-Sp	A A G A G T C C G C G **C** T A G T	**108**	5205	5205	55
B7-In-Et	A A G A G T C C G C G C T **A** G T	**135**	5217	5218	57
B8-In-Et	A A G A G T C C G C G **C** T A G T	**135**	5217	5217	59

impact on the ΔT_m^{260} than the position and identity of the spin labelled nucleotide; as such, the 2′-ethynyl-2′-deoxynucleotide SDSL strategy should in principle be suitable to label any position of a given oligonucleotide sequence.

Two particularly interesting cases in Table 4.12 are the duplexes of Strand **A7-5-Sp**, which are the only examples so far of a spin labelled nucleotide positioned further towards the 5′-terminus than the 3′-terminus. The depression in T_m^{260} for the singly labelled duplex **A7-5-Sp:B1** is smaller than for the duplex with the same modification on dT (dU) in position 13 (**A3-5-Sp:B1**; $\Delta T_m^{260} = -4.05 \pm 0.39$ °C), perhaps indicating an enhanced hydrophobic interaction between the label and the DNA backbone, or a reduced fraying effect. Even more interesting, however, is the doubly labelled duplex **A7-5-Sp:B3-5-Sp**, wherein the complementary strands have been labelled on the opposing nucleotides of the same base pair. This duplex displays a surprisingly small ΔT_m^{260}, even smaller than the singly labelled **A7-5-Sp:B1**, which might suggest a complementary conformational shift in both strands induced by the modification in the same position, thus leading to a net reduction in destabilisation.

Table 4.12: UV denaturation studies on DNA containing 2′-ethynyl-dC or -dA (3.0 µM, 200 mM NaCl, 10 mM phosphate buffer, pH 7.3).

Duplex	Sequence	ΔT_m^{260} [°C]
A1:B1	5′–A C T A G C G C G G A C T C T T–3′ 3′–T G A T C G C G C C T G A G A A–5′	—
A1:B7-6-Me	5′–A C T A G C G C G G A C T C T T–3′ 3′–T G **A** T C G C G C C T G A G A A–5′	-1.98 ± 0.47
A2-6-Me:B7-6-Me	5′–A C T A G C G C G G A C T C T **U**–3′ 3′–T G **A** T C G C G C C T G A G A A–5′	-1.70 ± 0.36
A3-6-Me:B7-6-Me	5′–A C T A G C G C G G A C **U** C T T–3′ 3′–T G **A** T C G C G C C T G A G A A–5′	-7.07 ± 0.35
A1:B8-6-Me	5′–A C T A G C G C G G A C T C T T–3′ 3′–T G A T **C** G C G C C T G A G A A–5′	-3.26 ± 0.47
A2-6-Me:B8-6-Me	5′–A C T A G C G C G G A C T C T **U**–3′ 3′–T G A T **C** G C G C C T G A G A A–5′	-3.08 ± 0.43
A3-6-Me:B8-6-Me	5′–A C T A G C G C G G A C **U** C T T–3′ 3′–T G A T **C** G C G C C T G A G A A–5′	-9.57 ± 0.32
A1:B7-5-Sp	5′–A C T A G C G C G G A C T C T T–3′ 3′–T G **A** T C G C G C C T G A G A A–5′	-1.27 ± 0.48
A2-5-Sp:B7-5-Sp	5′–A C T A G C G C G G A C T C T **U**–3′ 3′–T G **A** T C G C G C C T G A G A A–5′	-0.82 ± 0.35
A3-5-Sp:B7-5-Sp	5′–A C T A G C G C G G A C **U** C T T–3′ 3′–T G **A** T C G C G C C T G A G A A–5′	-6.64 ± 0.39
A1:B8-5-Sp	5′–A C T A G C G C G G A C T C T T–3′ 3′–T G C T **C** G C G C C T G A G A A–5′	-2.37 ± 0.37
A2-5-Sp:B8-5-Sp	5′–A C T A G C G C G G A C T C T **U**–3′ 3′–T G A T **C** G C G C C T G A G A A–5′	-1.82 ± 0.45
A3-5-Sp:B8-5-Sp	5′–A C T A G C G C G G A C **U** C T T–3′ 3′–T G A T **C** G C G C C T G A G A A–5′	-8.93 ± 0.49
A7-5-Sp:B1	5′–A C T **A** G C G C G G A C T C T T–3′ 3′–T G A T C G C G C C T G A G A A–5′	-2.39 ± 0.23
A7-5-Sp:B3-5-Sp	5′–A C T **A** G C G C G G A C T C T T–3′ 3′–T G A **U** C G C G C C T G A G A A–5′	-1.18 ± 0.32
A1:B7-In-Et	5′–A C T A G C G C G G A C T C T T–3′ 3′–T G **A** T C G C G C C T G A G A A–5′	-1.23 ± 0.40
A2-In-Et:B7-In-Et	5′–A C T A G C G C G G A C T C T **U**–3′ 3′–T G **A** T C G C G C C T G A G A A–5′	-0.29 ± 0.35

(Continued on next page)

Table 4.12 *(continued from previous page)*

Duplex	Sequence	ΔT_m^{260} [°C]
A3-In-Et:B7-In-Et	5′–A C T A G C G C G G A C **U** C T T–3′ 3′–T G **A** T C G C G C C T G A G A A–5′	-4.24 ± 0.43
A1:B8-In-Et	5′–A C T A G C G C G G A C T C T T–3′ 3′–T G A T **C** G C G C C T G A G A A–5′	-0.96 ± 0.40
A2-In-Et:B8-In-Et	5′–A C T A G C G C G G A C T C T **U**–3′ 3′–T G A T **C** G C G C C T G A G A A–5′	$+0.08 \pm 0.48$
A3-In-Et:B8-In-Et	5′–A C T A G C G C G G A C **U** C T T–3′ 3′–T G A T **C** G C G C C T G A G A A–5′	-4.26 ± 0.47

4.3 Circular dichroism studies

The destabilising effect of several of the 2′-triazole-linked spin labels was found to be relatively high in several cases, especially for doubly internally labelled duplexes (derivatives of **A3:B3**; see above). Prompted by concerns that this indicated a large distortion of the duplex structure, circular dichroism (CD) spectroscopy was performed on a selection of the spin labelled duplexes. CD measurements provide a description of the *overall* conformation of an oligonucleotide by measuring the difference in absorption of left- and right-handed circularly polarised light ($\Delta\varepsilon$) across a range of wavelengths (λ), normally in the near-UV region.[212] The observed spectra are the sum of a large number of transitions of either negative or positive sign, many of which overlap; thus, the technique cannot be used to provide locally detailed structural information. Furthermore, the transitions and therefore the total spectra are dependent on the base identity, composition and sequence (both with respect to base stacking and hydrogen bonding). The upside to this is that CD spectroscopy is sensitive to small changes in the nucleic acid conformation, and can report accurately on processes such as the binding of intercalators, or a transition between B- and A-DNA.[213] An example of the latter is shown in Figure 4.9, where the transition from B-form DNA (black curve) to A-DNA (solid blue curve) is driven by titration with trifluoroethanol; the two conformations have significantly different CD spectra.

The CD spectra of the non-modified control duplex **A1:B1**, doubly internally al-

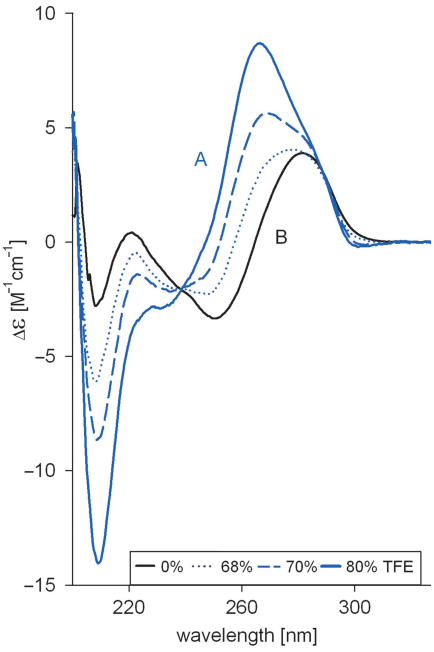
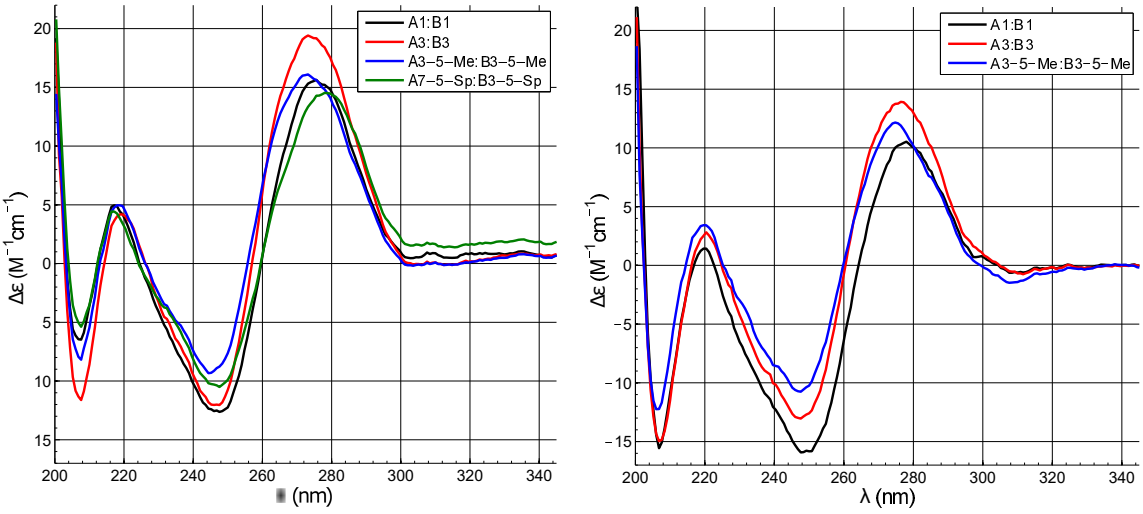


Figure 4.9: The transition from B-form (black) to A-form (solid blue) DNA driven by increasing concentration of trifluoroethanol, as monitored by CD spectroscopy. From Ref. 212, licenced under CC BY-NC 2.0 UK (cropped).

kynylated duplex **A3:B3**, and the two doubly spin labelled duplexes **A3-5-Me:B3-5-Me** (largest negative ΔT_m^{260}) and **A7-5-Sp:B3-5-Sp** (labelling opposing nucleotides) in aqueous buffer are shown in Figure 4.10a. The overall shape of all four spectra, with a positive band at ∼270–280 nm and a negative band at ∼245 nm, is characteristic of a B-form



(a) **(b)**

Figure 4.10: CD spectra of selected duplexes (3.0 µM) at 20 °C, in **(a)** 200 mM NaCl, 10 mM phosphate buffer, pH 7.3; **(b)** glycerol/[400 mM NaCl, 20 mM phosphate buffer] (1 : 1), pH 7.3.

double helix.[212] By contrast, A-DNA displays a more intense positive band at ∼260 nm and an intense negative band at ∼210 nm (cf. Figure 4.9). Compared to **A1:B1**, the alkyne-containing **A3:B3** exhibits a blueshift and increased intensity of the positive band (∼275 nm) and increased intensity of the negative band at ∼210 nm, and may thus appear to have undergone a slight partial transition towards a more A-like conformation. It must be kept in mind that change of the nucleobases in the modified systems will likely also exert an influence on the spectra; the substitution of dT with dU has previously been shown to cause a blueshift of the positive band, as well as a shallowing of the negative band at ∼245 nm,[214] and may thus also partly explain this spectral change.

Interestingly, however, this effect appears to be smaller or absent in the spin labelled duplexes. The similar intensity of the positive band of the spin labelled duplexes compared to **A1:B1** may at first glance suggest that base stacking is not significantly affected by spin labelling.[213] It may however be argued that the spin labelled duplexes should rather be compared to alkyne-containing duplex **A3:B3**, being derivatives of the latter; in that case, introduction of spin labels at the 2′-alkynylnucleotide can appear to have a small adverse effect on the base stacking and/or -pairing ability of the nucleic acid. The simplest explanation may however be that there is a smaller and less significant transition from one type of B-form DNA to another. B-type double helices are known to occur with a number of variations in the structural parameters (e.g. groove dimensions, base tilt, etc.; see Section 1.3) and should as such be considered a family of conformations.[59] This adaptability may allow the duplex to accommodate a 2′-triazole-linked spin label without any dramatic change in its secondary structure.

Figure 4.10b shows CD spectra of duplexes in a 1 : 1 mixture of aqueous buffer and glycerol (with the same total salt concentration as in Figure 4.10a), which is the solvent used for the majority of the EPR spectroscopic investigations (see Chapter 5). Similar overall spectra and trends between the duplexes are obtained in this solvent mixture, indicating that the B-DNA double helix is also conserved under the conditions used for EPR measurements (albeit the low temperatures used for many EPR experiments could not be achieved for

CD measurements). One difference encountered for all duplexes upon introduction of 50% glycerol is a diminished intensity and slight redshift of the positive band; although this is known to occur with the introduction of a high alcohol content in solutions of dsDNA, it is generally agreed that these duplexes still adopt a B-type double helix structure.[213]

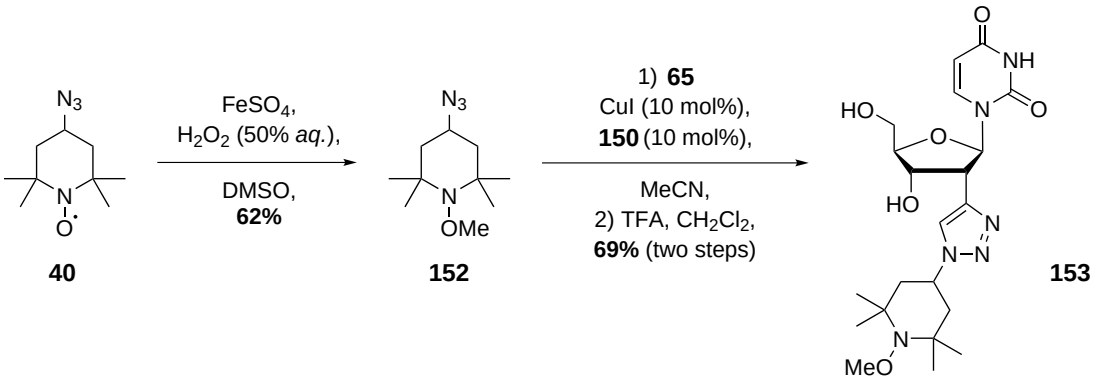
It should be noted that authoritative conclusions cannot be drawn from only one CD spectrum of each duplex. Rather, it has been suggested that detailed CD studies should be performed over a variation of conditions such as pH, temperature and buffer composition, which also affect the appearance of the CD spectra of nucleic acids.[212] A fuller study was not performed due to time constraints; thus, further CD spectroscopic investigation of the spin labelled DNA duplexes is required to enable unambiguous interpretation.

4.4 The effect of sugar puckering

It is known that the puckering of the furanose ring can impact on the stability of oligonucleotide duplexes. For example, incorporation of 2′-*ribo*-fluoronucleotides can be used to stabilise DNA-RNA or RNA-RNA duplexes, both of which normally adopt A-type double helices.[215,216] It is thought that this stabilising contribution can in part be explained by preferential preorganisation of 2′-*ribo*-fluoronucleotides into N-type sugar conformations, which is the family of sugar puckers required in A-type double helices; the unfavourable decrease in entropy upon duplex formation can thus be reduced. On the contrary, the incorporation of a single 2′-*ribo*-fluoronucleotide have been found to slightly destabilise B-form DNA duplexes, which require S-type furanose conformations.[217]

On the basis of these reports, it is not unreasonable to partially ascribe the reduction in T_m^{260} of the spin labelled duplexes to an altered conformational preference of the ribose. ^{1}H NMR coupling constants have previously been used to calculate the conformational distribution of various nucleosides;[60] however, this technique is not suitable for paramagnetic derivatives, as the unpaired electron spin causes rapid relaxation and consequent line broadening and loss of intensity in ^{1}H NMR spectra.[218] To enable the conformational analysis of the novel ‘click’ derivatives of 2′-ethynyl-2′-deoxyuridine on the nucleoside

level, a diamagnetic analogue to the spin labelled nucleoside was required. To this end, the nitroxyl radical **40** (Scheme 4.2) was subjected to a Fenton reaction wherein Fe(II) catalyses the decomposition of hydrogen peroxide into high-energy radicals (e.g. hydroxyl), which upon reaction with DMSO generate methyl radicals that can combine with nitroxyl **40**.[218] The resulting *N*-methoxy compound **152**, which could not be isolated in sufficiently high purity for characterisation, was submitted to a 'click' reaction with DMTr-protected 2′-alkynyluridine (**65**). The intermediate DMTr-protected 'click' product could not be obtained in pure form, but deprotection of the dimethoxytrityl ether allowed the nucleoside derivative **153** to be isolated in good yield and high purity.



Scheme 4.2: Preparation of a diamagnetic analogue of a spin labelled nucleoside.

With a diamagnetic model compound in hand, ^{1}H NMR coupling constants could be acquired (Table 4.13). Using Equation 2.2, the molar fraction of each nucleoside in the N-conformation (χ_N) in an assumed N $\rightleftharpoons$ S equilibrium could be estimated from the coupling constants. The values of χ_N for 2′-deoxyuridine and uridine only showed small deviations from literature values, indicating that the approximation of Equation 2.2 gives a valid indication of the conformational distribution for ribo- and 2′-deoxyribonucleosides. As expected, these values show a preference for the S-conformer for the deoxynucleoside, whereas the ribonucleoside exhibits a slight preference for the N-conformation. In CD_3OD, in which all the nucleosides studied were soluble, the equilibrium of both nucleosides shifted slightly towards the S-conformer.

The estimated χ_N for detritylated 2′-ethynyluridine **48** showed a large preference for

Table 4.13: Estimation of conformer populations for 2′-deoxyuridine, uridine, and synthesised 2′-ethynyluridine (**48**) and triazole derivative (**153**), using ^{1}H NMR coupling constants (500 MHz, sample concentration 15 mM) at 298 K.

Compound	**Solvent**	^3J **[Hz]**		χ_N	
		H1′-H2′	H3′-H4′	Calc.	Lit.
2′-Deoxyuridine	D_2O	6.6	3.9	0.37	0.39[61]
2′-Deoxyuridine	CD_3OD	6.2	3.2	0.34	—
Uridine	D_2O	4.6	5.4	0.54	0.53[61]
Uridine	CD_3OD	4.7	4.6	0.49	—
48	D_2O	8.2	3.0	0.27	—
48	CD_3OD	8.5	2.2	0.21	—
153	CD_3OD	9.4	1.4	0.13	—

the S-conformer (73% in D_2O); moreover, the 'click' labelled nucleoside **153** exhibited an even larger preference for S-type conformations (87%). These results are surprising, given that nucleosides substituted at the 2′-position in a *ribo*-configuration normally prefer N-type conformers (see Section 1.3). It may be that Equation 2.2, which is based on an empirical trend amongst ribo- and 2′-deoxynucleosides, does not apply to carbon branched nucleosides; it is known that substituents of varying electronegativities can influence the coupling constants.[219] Another possibility is that the assumption of a two-state N $\rightleftharpoons$ S conformational equilibrium does not hold for the 2′-ethynyl- and -triazolyl-nucleosides, and that these nucleosides adopt entirely different conformations.

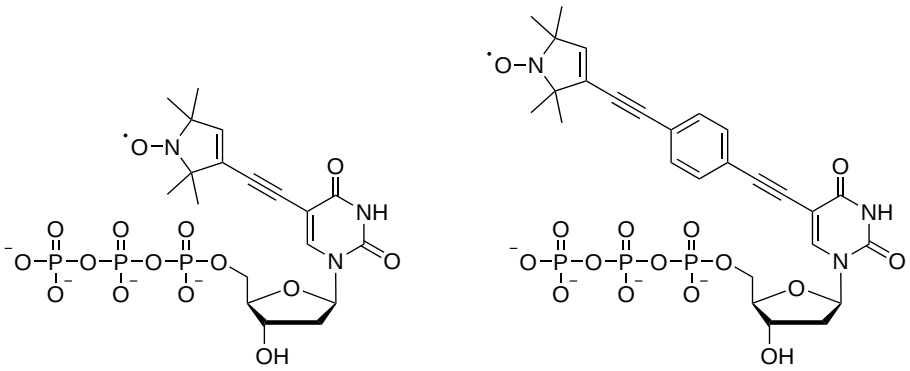
Preliminary attempts to use specialised computational software[220] to fit the observed ^3J values to one or more nucleoside conformations, across the entire pseudorotation wheel (see Figure 1.8a), did not lead to any meaningful results. This method builds on comparison of the observed coupling constants to values calculated for different conformers using an extended version of the Karplus equation.[221,222] It may be that these initial computational attempts failed because the relevant equation has not been parametrised for alkynyl- or triazolyl-substituted nucleosides.[219,223] However, this may also be a further indication that the synthesised nucleosides do not exist in a two-state equilibrium in solution. Due to time constraints, these efforts were not pursued further.

4.5 2′-Ethynyl-2′-deoxyuridine 5′-triphosphate

All of the relatively short oligonucleotides in this thesis have been prepared by the solid-supported phosphoramidite method. High coupling yields and absolute control over the position and number of modified residues make this a powerful technique for the site-specific insertion of modified nucleotides; however, as coupling yields are not quantitative for every step, the upper limit to the DNA strand lengths accessible *via* this method is ∼100 nucleotides.[224] A modified technique which reduces the impact of acid-catalysed depurination permits DNA strands up to 150 nucleotides long to be prepared, albeit on small scales.[225]

Additional steric hindrance around the phosphoramidite functionality imposed by the protected 2′-alcohol in ribonucleoside phosphoramidites can reduce coupling yields, thereby making the synthesis of long, modified RNAs even more challenging than their DNA counterparts. Moreover, once deprotected, the inherent propensity of RNA strands to undergo $3' \rightarrow 2'$ phosphodiester migration or strand cleavage, which increases in probability with every additional nucleotide introduced, results in an effective upper limit of ∼50 nucleotides for synthetic RNAs.[226]

The limitations of the phosphoramidite method means that many naturally occurring nucleic acids (especially RNAs), which are generally longer polymers, cannot be spin labelled *via* incorporation of modified nucleotide phosphoramidites. Introduction of modified nucleotides into such nucleic acids can however still be possible using enzymatic primer extension techniques, where a DNA or RNA polymerase with the ability to accept a modified nucleoside 5′-triphosphate incorporates the modified residue into the growing oligonucleotide strand in place of its natural analogue.[227] This method however results in 'global labelling' – i.e. substitution of *all* the natural nucleotides of a particular kind with the modified version – and therefore offers limited control over the site-selectivity. Indeed, enzymatic spin labelling of DNA has previously been achieved by incorporation of triphosphates **154** and **155** (Figure 4.11) by DNA polymerases.[228] By controlling the template sequence, one or several spin labelled residues could be incorporated into the



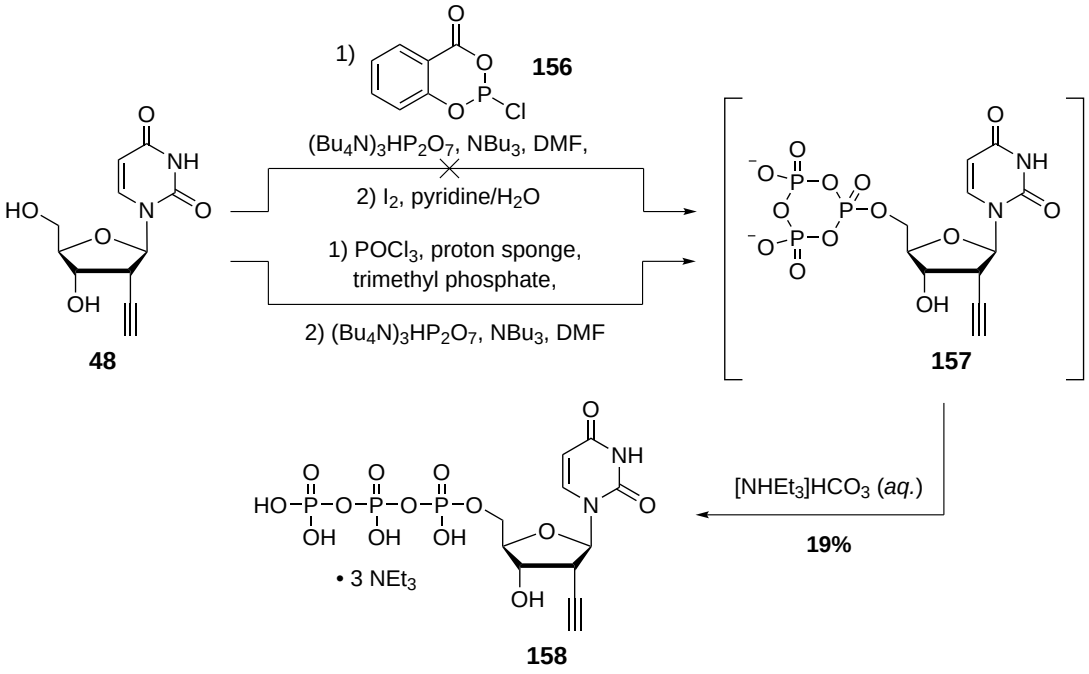
154 **155**

Figure 4.11: Spin labelled triphosphates for enzymatic incorporation.

same DNA strand, but global spin labelling was always the result. However, the advent of new technologies for synthesising long, site-specifically modified RNAs on preparative scales makes enzymatic SDSL of nucleic acids a more realistic prospect.[229,230]

2′-Ethynyl-2′-deoxynucleosides are promising candidates for acceptance by polymerases, because the 2′-ethynyl group is a relatively small and chemically innocuous modification. Several other 2′-modifications, e.g. azides, have previously been reported to be incorporated into nucleic acids through primer extension, especially by mutants of T7 RNA polymerase.[231] To function as polymerase substrates, the 2′-alkynylnucleosides must necessarily be functionalised with a 5′-triphosphate. This was first attempted by reaction of nucleoside **48** (Scheme 4.3) with a mixture of salicyl chlorophosphite **156** and tris(tetrabutylammonium) hydrogen pyrophosphate, which forms a bulky, 5′-OH selective phosphitylating reagent *in situ*,[232] followed by I_2-mediated oxidation to intermediate cyclic trimetaphosphate ester **157**; subsequent hydrolysis would lead to the open-chain triphosphate **158**. However, no conversion was observed in this reaction. An alternative literature method[233] under more forcing conditions was therefore attempted, wherein nucleoside **48** was reacted with phosphorus oxychloride, followed by addition of pyrophosphate and subsequent hydrolysis of intermediate **157**. In this case, regioselectivity is achieved using the unusual solvent trimethyl phosphate; the origin of this effect is not clear.[234,235] Pleasingly, the tris(triethylammonium) salt of triphosphate **158** was obtained in a yield of 19% (respectable for this type of transformation) after purification by RP-HPLC. The

synthesised 2′-ethynyl-2′-deoxyuridine 5′-triphosphate **158** is currently being screened for activity as a polymerase substrate in collaboration with the research group of Prof. Tom Brown.



Scheme 4.3: Preparation of a 5′-triphosphate of 2′-alkynyluridine.

5 EPR analysis of spin labelled DNA

Having prepared a wide array of DNA spin labelled at dT (dU), dC and dA, in internal and terminal positions, using six different spin labels, attention turned to exploring their properties when studied by CW and pulsed EPR spectroscopy. Of particular interest was the rigidity of the 2′-triazole-linked spin labels in terms of dynamics in CW EPR and signal width in pulsed EPR, and whether there was any correlation between these and the destabilising effect of the spin labels (as measured by ΔT_m^{260}, see Chapter 4). Also of special interest was the effect of the bis(spirocyclohexyl) substituents, which have previously been found to display longer T_m phase coherence times.

All measurements in this chapter were performed by Dr Janet Lovett, at the University of St Andrews, or at the EPSRC National Service for EPR at the University of Manchester.

5.1 CW EPR of 2′-triazolyl spin labelled DNA

Room temperature CW EPR spectra can reveal information about the dynamic mobility of the spin labelled system on the ns timescale. For the purposes of this work, a qualitative discussion of these measurements is sufficient. Initial efforts looked at the changes in dynamics when a spin labelled ssDNA associates with its complementary strand. Whereas the spectra of the free azide spin labels (see Chapter 3) are almost completely isotropic (equal height and width of all three spectral lines), a higher degree of anisotropy is apparent for spin labels incorporated into DNA (Figure 5.1). This is only to be expected when the labels are conjoined to large, more slowly tumbling biomolecules. The room temperature X-band CW EPR spectra of singly terminally labelled ssDNA and dsDNA (Figure 5.1a) reveal that the CW spectrum is slightly broadened upon duplex formation, which is indicative of the increased molecular weight and therefore tumbling time of the bimolecular complex. Interestingly, though, a larger degree of broadening is observed when internally labelled ssDNA is hybridised with its complementary strand (Figure 5.1b); this suggests that

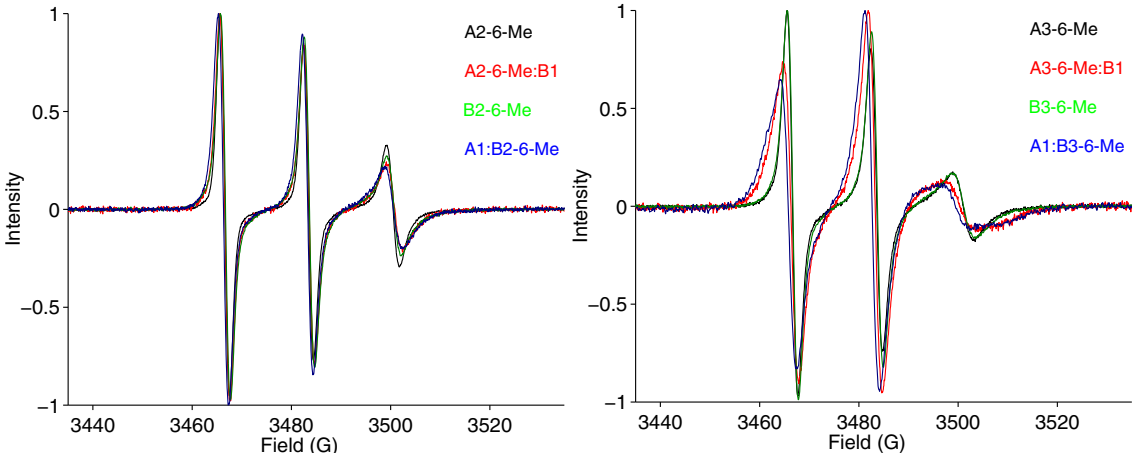


Figure 5.1: Room temperature X-band CW EPR spectra of ssDNA and dsDNA for **(a)** terminally, and **(b)** internally labelled strands. 100 µM in phosphate buffer (12 mM, pH 7.4, 100 mM NaCl) in D_2O and 30% glycerol.

internally positioned labels are inherently more conformationally restricted.

Prompted by concerns over the destabilisation (in terms of ΔT_m^{260}) of doubly internally labelled duplexes, their CW EPR spectra were overlaid with the corresponding singly labelled duplexes. The spectra for singly and doubly *terminally* labelled duplexes (Figure 5.2a) are identical, perhaps unsurprisingly; these duplexes showed very small changes in T_m^{260}. Pleasingly, the difference in dynamics between doubly and singly *internally* labelled

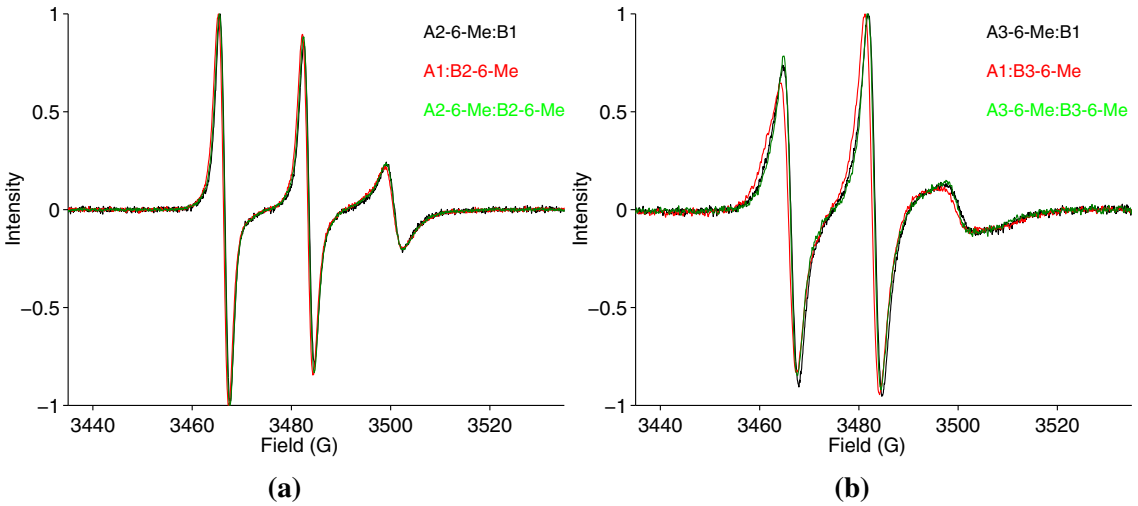


Figure 5.2: Room temperature X-band CW EPR spectra of singly and doubly labelled dsDNA for **(a)** terminally, and **(b)** internally labelled duplexes. 100 µM in phosphate buffer (12 mM, pH 7.4, 100 mM NaCl) in D_2O and 30% glycerol.

duplexes (Figure 5.2b) appears to be very small; although the former duplex exhibits a large destabilisation ($\Delta T_m^{260} - 9.79 \pm 0.37$ °C), the structural perturbation seems to be of a local nature, which not necessarily increases the mobility of the spin label to a significant degree.

The spectra for duplexes singly labelled with **6-Me** in various positions were also compared with each other (Figure 5.3a). When **6-Me** is attached to a terminal nucleotide (red and green spectra), the system still displays a relatively large degree of mobility, intermediate between the fast- and slow-motion regimes. The dynamics of this label decrease when it is attached to an internal position (blue and black spectra), as shown by the change in intensity and width, especially by the high- and low-field lines. This may be attributable to duplex fraying, where unwinding of the ends of the double helix increases the dynamic mobility of terminally positioned spin labels; but equally, if the label is able to nest in a groove or otherwise associate with the DNA backbone in an internal position, this can contribute to restricting its dynamic motion. The effect is seen irrespective of which strand is labelled.

The general trend with internal labels being less mobile than terminal labels is observed for all the different spin labels (Figure 5.3b–f). Interestingly, the pyrrolinyl spin labels **5-Me** and **5-Sp** exhibit slightly lower dynamic mobility than piperidinyl labels **6-Me** and **6-Sp**, respectively, in spite of having a conformationally flexible methylene group in the linker between the nitroxyl and the DNA backbone; the larger mobility of the 6-membered ring labels is likely due to internal motion in the label framework (such as ring flipping), which cannot take place in 5-membered rings. Of greater significance is the decreased dynamic mobility of the bis(spirocyclohexyl)-substituted spin labels **6-Sp** and **5-Sp** compared to **6-Me** and **5-Me**, respectively, where the internally labelled duplexes have spectra well within the slow-motion regime. This can be explained by the larger size of the spin labels themselves (and thereby longer local tumbling correlation time of the label and linker, independent of the duplex), but may also indicate an enhanced hydrophobic interaction between the spin label and the DNA backbone compared to tetramethyl-substituted labels. A similar effect is seen with isoindolinyl spin labels **In-Me** and **In-Et**. Overlaying the

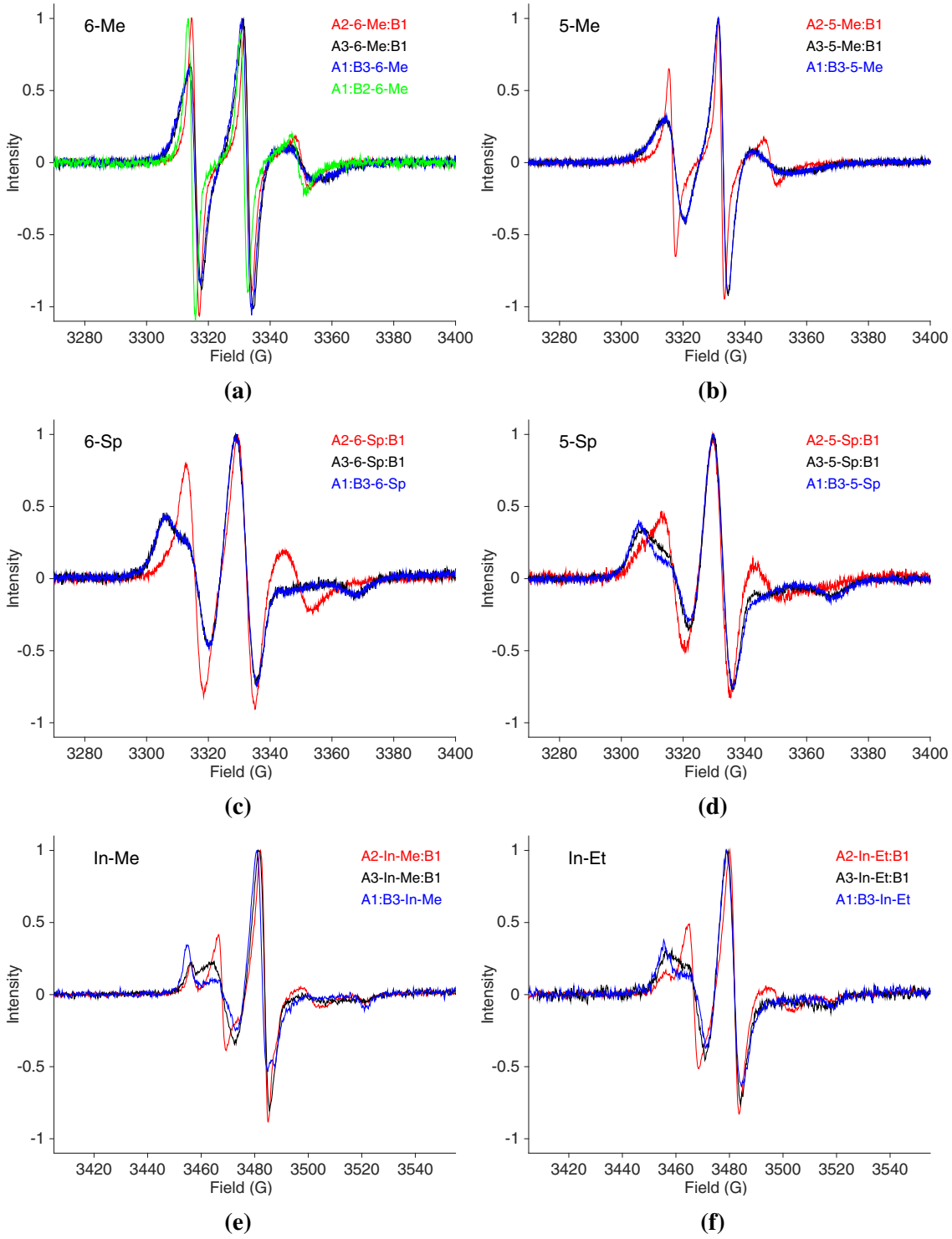


Figure 5.3: Room temperature X-band CW EPR spectra of dsDNA singly labelled with **(a) 6-Me**, **(b) 5-Me**, **(c) 6-Sp**, **(d) 5-Sp**, **(e) In-Me**, and **(f) In-Et**. 100 µM in phosphate buffer (10 mM, pH 7.4, 150 mM NaCl) in D_2O and 50% glycerol.

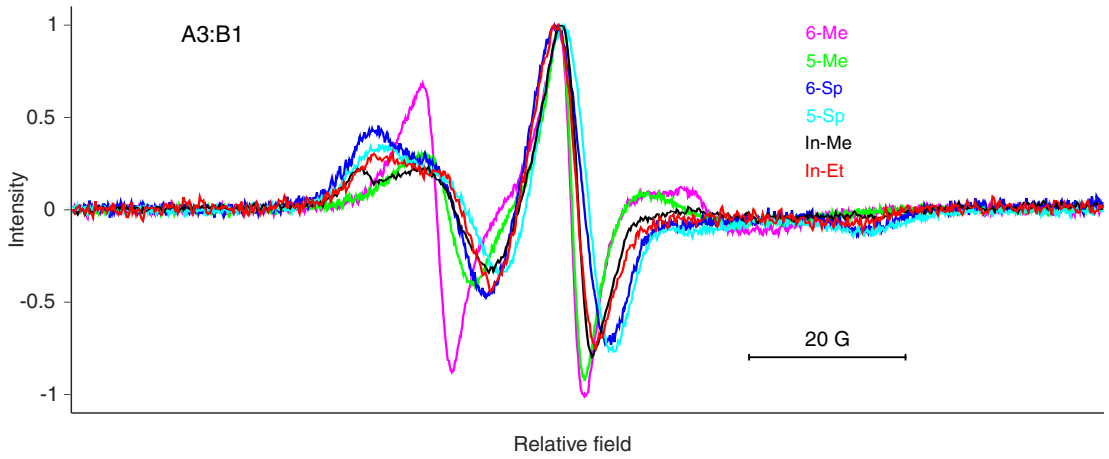


Figure 5.4: Normalised room temperature X-band CW EPR spectra of spin labelled derivatives of duplex **A3:B1** with various labels. 100 µM in phosphate buffer (10 mM, pH 7.4, 150 mM NaCl) in D_2O and 50% glycerol.

spectra for duplexes internally labelled with the various labels (Figure 5.4) suggests the following order of dynamic mobility for the spin labels:

$$\textbf{5-Sp} \approx \textbf{6-Sp} < \textbf{In-Me} \approx \textbf{In-Et} < \textbf{5-Me} \ll \textbf{6-Me}$$

The CW EPR spectra of duplexes spin labelled at internal 2′-alkynyl-dU (**A1:B3**), -dA (**A1:B7**) and -dC (**A1:B8**) residues are overlaid in Figure 5.5. Pleasingly, it appears that the identity of the labelled nucleotide is of minor significance to the dynamics of the system. Overall, very similar dynamics are observed, with only a small increase in mobility of **6-Me** spin labels at dC and dA compared to dU, and **In-Me** at dA being slightly more mobile than at dC or dU. It can be envisaged that the small increase in mobility when labelling at dA is a result of duplex fraying or reduced hydrophobic interaction between the label and the DNA backbone, this residue being only the third from the 3′-terminus. However, the differences in mobility based on nucleotide identity are small, and more systematic investigations (e.g. simulations) are required to draw further conclusions.

5.1.1 Comparison to 2′-*O*-propargyl spin labelling

The room temperature CW EPR spectra of duplexes of 2′-*O*-propargyl-derived 'click' labelled DNA (derivatives of Strand **B6** with **6-Me**, **5-Sp** and **In-Et**) were also acquired (Figure 5.6). Overlaying these spectra with the corresponding 2′-ethynyl-derived system

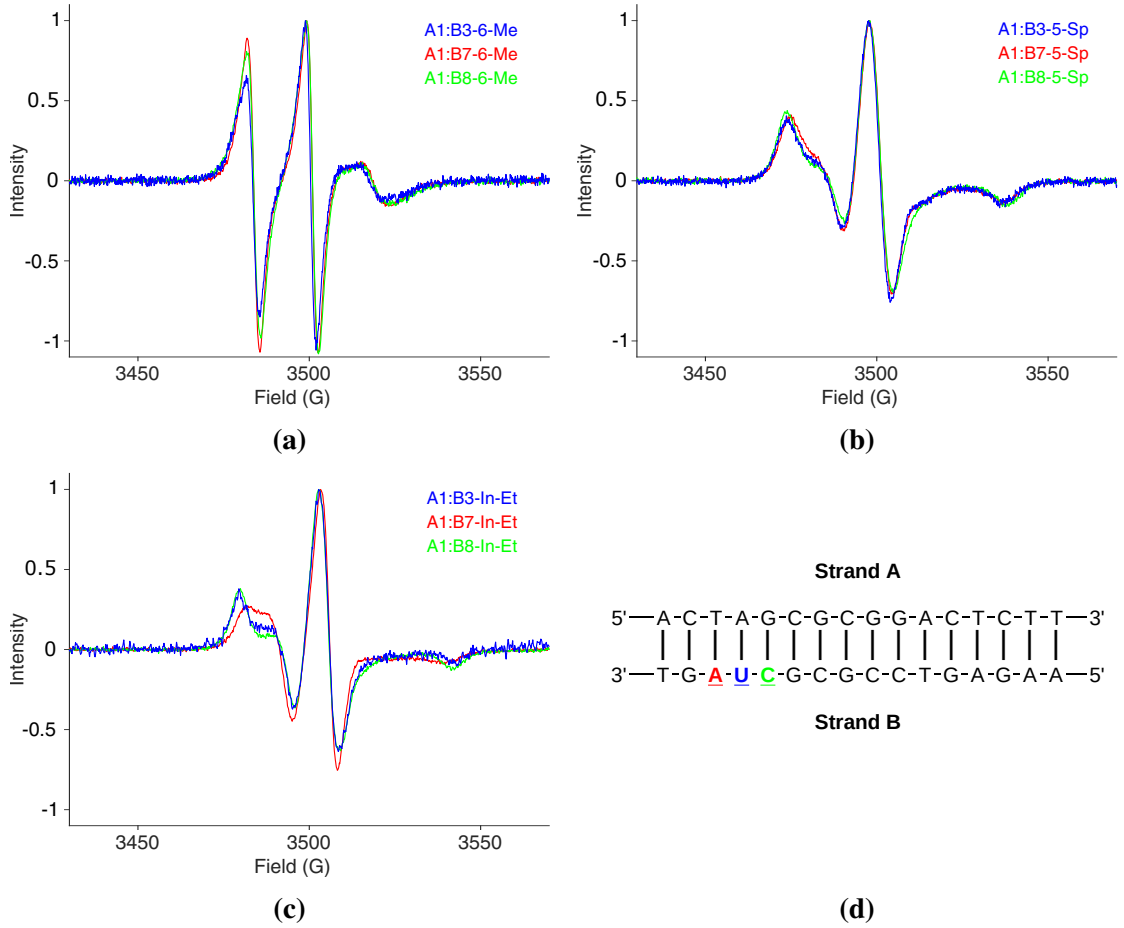


Figure 5.5: Normalised room temperature X-band CW EPR spectra of spin labelled derivatives of duplexes containing 2′-alkynyl-dU (**B3**), -dA (**B7**) and -dC (**B8**), with **(a) 6-Me**, **(b) 5-Sp**, and **(c) In-Et**; 100 µM in phosphate buffer (10 mM, pH 7.4, 150 mM NaCl) in D_2O and 50% glycerol. **(d)** Duplex showing the positioning of the labels with colours corresponding to the spectra.

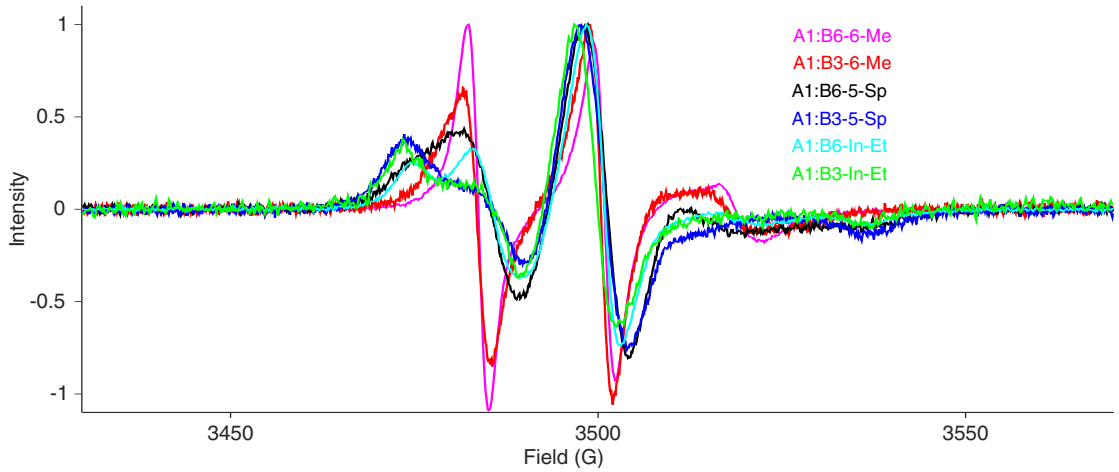


Figure 5.6: Normalised room temperature X-band CW EPR spectra of spin labelled derivatives of 2′-*O*-propargyl bearing duplex **A1:B6** and 2′-ethynyl bearing duplex **A1:B3** (100 µM in phosphate buffer (10 mM, pH 7.4, 150 mM NaCl) in D_2O and 50% glycerol).

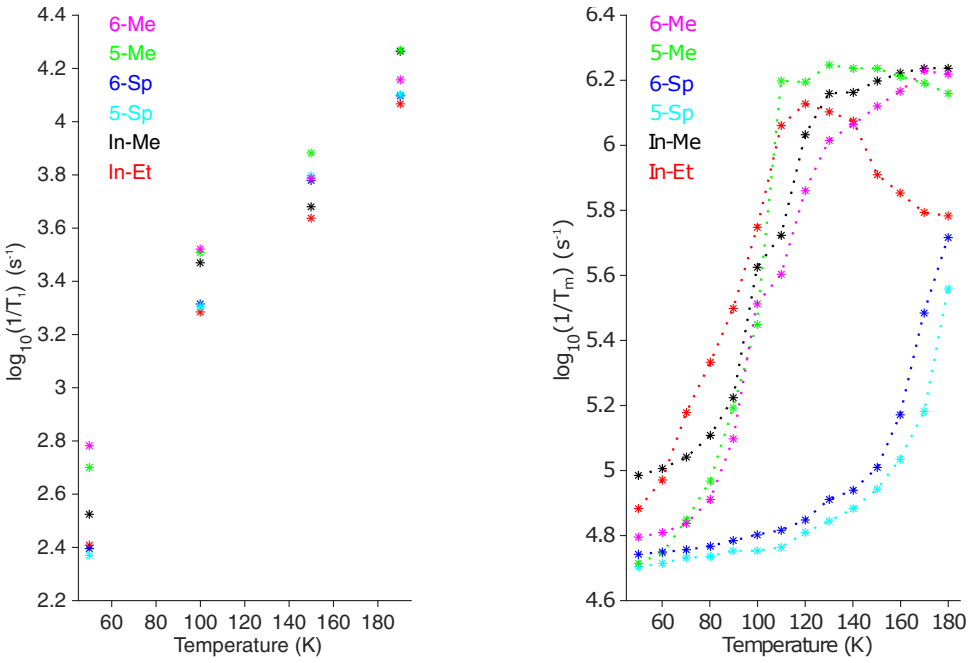
(Strand **B3**) reveals that the latter, novel system displays significantly slower dynamics than the commercially available propargyl-derived spin labelled DNA. The slower tumbling of the bulkier spin labels **5-Sp** and **In-Et** compared to **6-Me** is apparent even in the more flexible system, thus emphasising that the spin label scaffold itself, and not only the length and flexibility of the linker, plays an important part in determining the EPR spectroscopic properties of the spin labelled system as a whole.

5.2 Determination of relaxation rates

One goal of this project is exploring labelling nucleic acids with bis(spirocyclohexyl)-substituted spin labels such as **6-Sp** and **5-Sp**; similar derivatives have previously been found to exhibit longer T_m phase coherence times, making such labels potentially suitable for the measurement of longer distances, and/or measurement at higher temperatures, using pulsed EPR techniques.[31,32,35] In preparation for using these novel spin labels for distance measurements in the 2′-triazolyl system, the relaxation rates of 'click' labelled derivatives of the terminally alkynylated duplex **A2:B1** with all the different spin labels were determined at different temperatures. This work was performed by Dr Janet Lovett; detailed information about the spectroscopic measurements is available in the literature.[199]

Using an inversion recovery sequence, monitoring the amplitude of a Hahn echo as a function of the delay time between an initial inversion π pulse and a Hahn echo sequence (see Section 1.1.1), the longitudinal relaxation rate T_1^{-1} was determined by fitting with exponential functions; this experiment was performed at various temperatures (Figure 5.7a). Echo dephasing rates (T_m^{-1}) were similarly found by fitting exponential functions to the overall decay of the Hahn echo by varying the interpulse delay in a regular Hahn echo sequence; measured relaxation rates at different temperatures are displayed in Figure 5.7b.

As expected, T_m^{-1} rates are higher than T_1^{-1} at all temperatures; transverse relaxation is limiting in terms of acquisition time, while the repetition rate of the experiments is dictated by T_1^{-1}. Further, T_1^{-1}, while increasing with temperature, exhibits a relatively small and non-systematic variance among the different labels. The case is however dif-



(a) **(b)**

Figure 5.7: Determination of relaxation rates **(a)** T_1^{-1} and **(b)** T_m^{-1} at Q-band at various temperatures for all spin labels conjoined to duplex **A2:B1**. 100 µM in phosphate buffer (10 mM, pH 7.4, 150 mM NaCl) in D_2O and 50% glycerol-d_8.

ferent for T_m^{-1}: Whereas the transverse relaxation rates are similar at 50 K, increasing the temperature leads to a dramatic increase in T_m^{-1} for α,α′-tetramethyl substituted nitroxyls, including **In-Et**, which is attributed to rotation of the methyl groups. In comparison, the rigid bis(spirocyclohexyl)-substituted nitroxyls **6-Sp** and **5-Sp** exhibit low relaxation rates, which slowly increase with temperature until a rapid increase is observed at temperatures above ∼150 K, presumably when the glycerol-water glass begins to melt.[31] These results are in line with previously published relaxation rate studies from other groups.[31,32,35] However, whereas previous studies have found T_m^{-1} for tetramethyl-substituted spin labels to be decreasing around 120–160 K, attributed to rapid averaging of the hyperfine anisotropy imparted by the methyl groups,[35] this effect is only observed for the tetra*ethyl*-substituted spin label **In-Et** in the present work. The significance of this is not clear without performing measurements at even higher temperatures; however, it can be hypothesised that association to the DNA backbone dampens the rate increase of methyl rotation with increasing temperature. This would result in the expected decrease in T_m^{-1} for **6-Me**, **5-Me** and **In-Me** only being observable at temperatures beyond 180 K, whereas it can still be seen at the

expected temperature range for **In-Et**; the methyl groups (i.e. part of the ethyl substituents) of which have a lower energy barrier to rotation.

5.3 Pulsed EPR of 2′-triazolyl spin labelled DNA

One of the most exciting applications of the novel 2′-ethynyl-2′-deoxynucleoside SDSL strategy is performing distance measurements on nucleic acids, with the aim to discern their tertiary structure in solution. To this end, the pulsed EPR experiment DEER is an invaluable tool (see Section 1.1.1). To investigate the suitability of the new 2′-alkynylnucleoside SDSL strategy for such measurements, DEER experiments were first performed on model duplexes doubly spin labelled with **6-Me** at dU, at Q-band frequencies and 50 K; further details of the data acquisition and processing are available in the literature.[199] The background-corrected DEER time traces (Figure 5.8a) show around 1–2 frequency modulations, suggesting that the labels are spatially confined, and that meaningful data can be extracted from the DEER measurements. Tikhonov regularisation of the time traces led to the distance

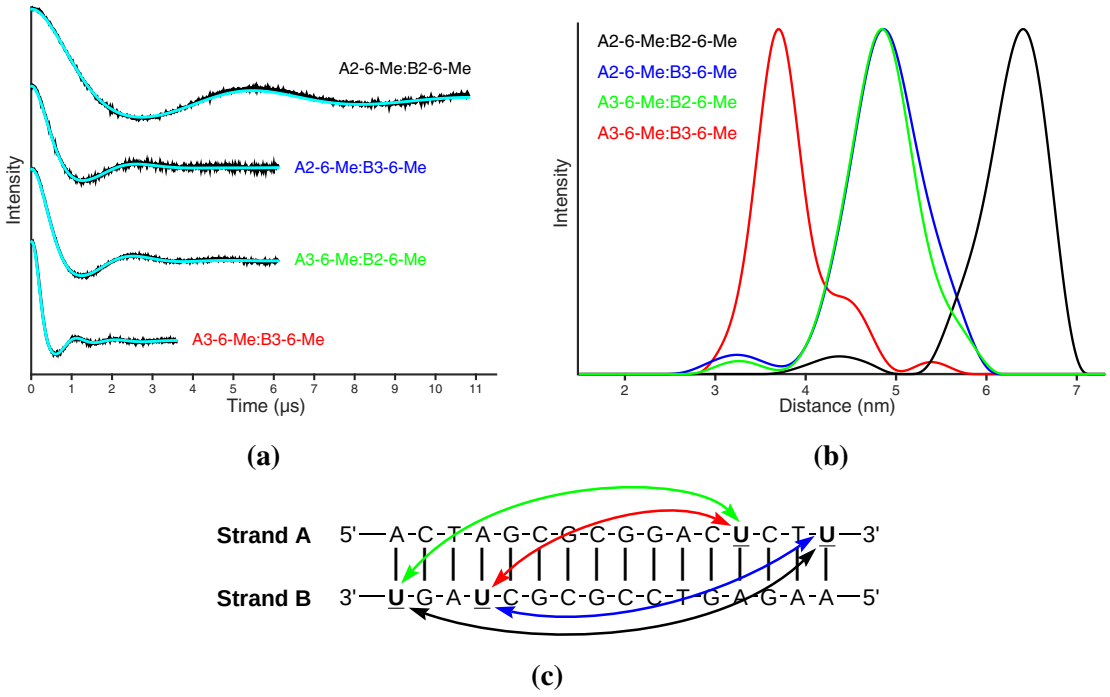


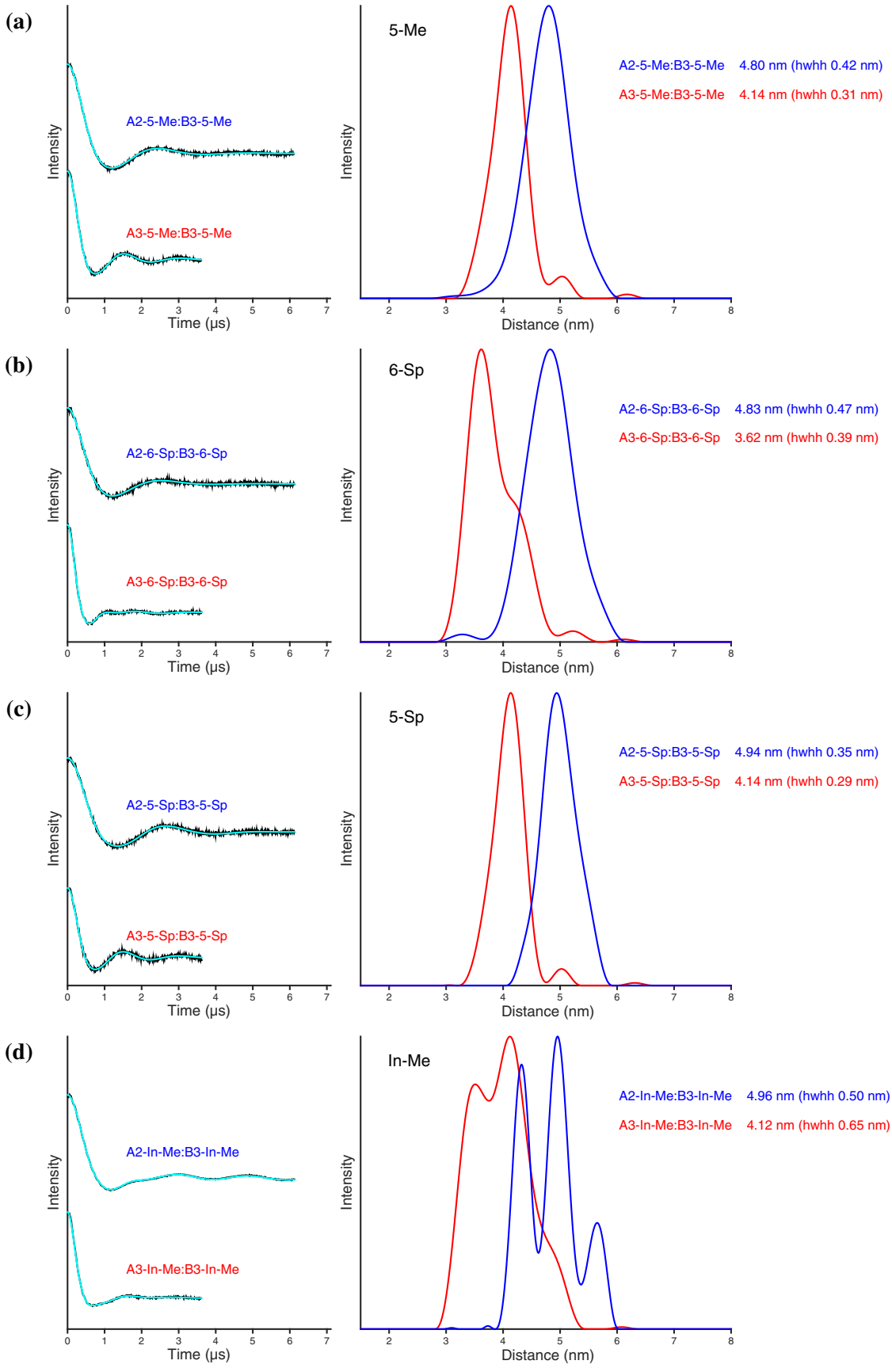
Figure 5.8: **(a)** Background-corrected Q-band DEER time traces with fit (cyan), and **(b)** distance distributions, for duplexes labelled with **6-Me** at dU, at 50 K. 100 µM in phosphate buffer (10 mM, pH 7.4, 150 mM NaCl) in D_2O and 50% glycerol-d_8. **(c)** Duplex showing the positioning of labelled residues; the colour of the arrows corresponds to the distance distributions.

distributions shown in Figure 5.8b. Pleasingly, double terminal labelling gave the longest distance (6.42 nm, hwhh 0.38 nm), one terminal and one internal label gave an intermediate distance (**A2-6-Me:B3-6-Me** 4.87 nm, hwhh 0.47 nm; **A3-6-Me:B2-6-Me** 4.86 nm, hwhh 0.42 nm), and the shortest distance (3.70 nm, hwhh 0.29 nm) was observed for the doubly internally labelled duplex.* Interestingly, the half-width at half-height (hwhh) of the latter signal was the smallest, suggesting that internal spin labels are more conformationally restricted, leading to a smaller ensemble of conformations being observed. This is also supported by the near-perfect overlap between the pseudosymmetric **A2-6-Me:B3-6-Me** and **A3-6-Me:B2-6-Me**, each carrying one internal and one terminal spin label.

Next, the performance of the various labels in DEER was evaluated by comparison of their various distance distributions (Figure 5.9); the colour of the distance distributions correspond to the duplex in Figure 5.8c. For all sets of doubly labelled duplexes, the distance between one terminal and one internal label (derivatives of **A2:B3**) was found to be longer than the distance between two internal labels (derivatives of **A3:B3**). Interestingly, however, subtle differences appear to be present between the labels; although the distances for derivatives of duplex **A2:B3** (one terminal and one internal label) appear to be in reasonably good agreement (4.80–4.96 nm), the distances measured for the doubly internally labelled duplex **A3:B3** varies depending on which spin label is used. The latter distance distributions also appear to have a shoulder, but only when the spin label is a six-membered piperidinyl nitroxyl. Overall, there is no correlation between the width of distance distributions in terms of hwhh and the destabilisation of the duplexes as measured by ΔT_m^{260}.

Surprisingly, spin labelling with **In-Me** (Figure 5.9d) revealed an ensemble of three distance distributions, presumably three distinctly different conformations of the label, which are well-resolved in the duplex **A2-In-Me:B3-In-Me**. Although the modal distances (4.96 and 4.12 nm) are in agreement with distances measured by the pyrrolinyl labels, the presence of multiple peaks causes an apparent broadening of the overall distance distribution (hwhh 0.50 and 0.65 nm, respectively). However, individual resolved distance

*Distances are given throughout as modal distances, i.e. distance at maximum intensity.



(Figure continues on next page)

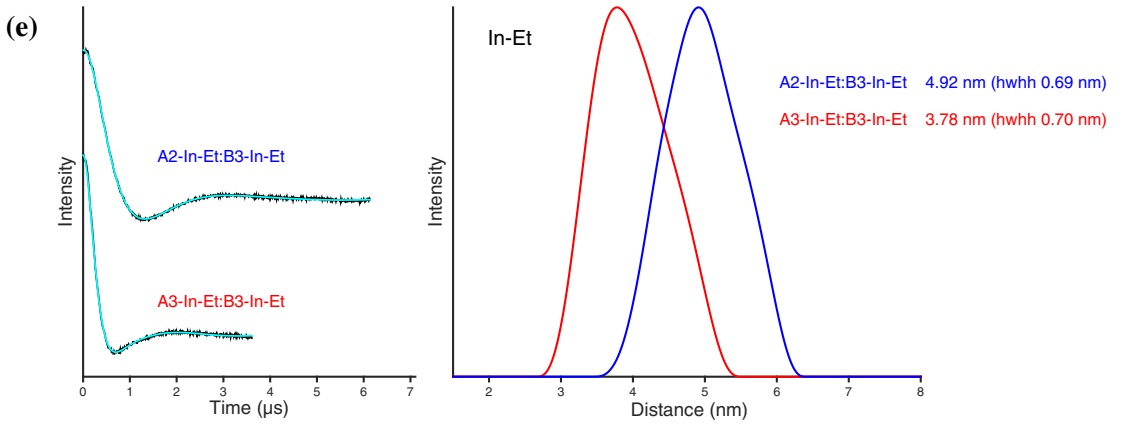


Figure 5.9: Background-corrected Q-band DEER time traces with fit (cyan) and distance distributions for duplexes doubly labelled with **(a) 5-Me**, **(b) 6-Sp**, **(c) 5-Sp**, **(d) In-Me**, and **(e) In-Et** at dU, at 50 K. 100 µM in phosphate buffer (20 mM, pH 7.4, 300 mM NaCl) in D_2O and 50% glycerol-d_8.

distributions appear *narrower* than distributions from other labels – e.g., compare the tallest distribution of **A2-In-Me:B3-In-Me** with **A2-5-Sp:B3-5-Sp**, the narrowest distance distribution for this duplex (hwhh 0.35 nm). Possibly, the larger size of the **In-Me** label, and hence its larger cone of rotation around the bonds attaching it to the DNA backbone, makes the interspin distances of these conformations different enough to be resolved using this label. It is also conceivable that the aromatic character of the spin label framework enables it to adopt conformations which are not accessible to the piperidinyl and pyrrolinyl spin labels.

The bulky spin label **In-Et** (Figure 5.9e) showed broad distance distributions for both the doubly internally and the terminally-internally labelled duplex (hwhh ∼0.70 nm). This was unexpected, given that the CW EPR spectra of duplexes carrying this spin label exhibited relatively rigid dynamics (see Figures 5.3f and 5.5c). It may simply be that this spin label is too sterically obstructed to enable it to adopt well-defined conformations within the local environment around the DNA backbone, and that it rather adopts a number of ill-defined, but "hydrophobically rigid" positions.

Superimposing the DEER distance distributions from Figure 5.9 for duplexes carrying one internal and one terminal label (derivatives of **A2:B3**, Figure 5.10a) confirms that there is good agreement across the labels for this interspin distance (∼4.9 nm), and that **5-Sp**

gives the narrowest overall distance distribution. However, the corresponding overlay for duplexes containing two internal labels (derivatives of **A3:B3**, Figure 5.10b) emphasises that there are notable differences between labels. The pyrrolinyl labels **5-Me** and **5-Sp** seem to be in excellent accord, giving a modal distance of 4.14 nm. Piperidinyl labels **6-Me** and **6-Sp**, however, give modal distances of 3.70 and 3.62 nm, respectively, and both exhibit a shoulder at a higher distance. It seems like the latter labels are able to adopt two distinct conformations, and that the conformations which give the longer distance is populated to a larger extent for **6-Sp**. This conformation may give a modal distance similar to the one measured for **5-Me** and **5-Sp**.

Interestingly, the modal distance for **In-Me** (4.12 nm) coincides with the distance measured for **5-Me** and **5-Sp**, with a local maximum at lower distance similar to the modal distances for **6-Me** and **6-Sp**. There is also an unresolved shoulder at higher distance, perhaps attributable to a third conformation. The resolved distributions observed for **In-Me** might be suggestive of fixed relative orientations of the pair of labels; more detailed investigations, e.g. higher field orientation-selective DEER measurements and computer simulations, are however required to substantiate this hypothesis. **In-Et**, in contrast, shows the widest distance distribution (hwhh 0.70 nm), which may be interpreted as an unresolved

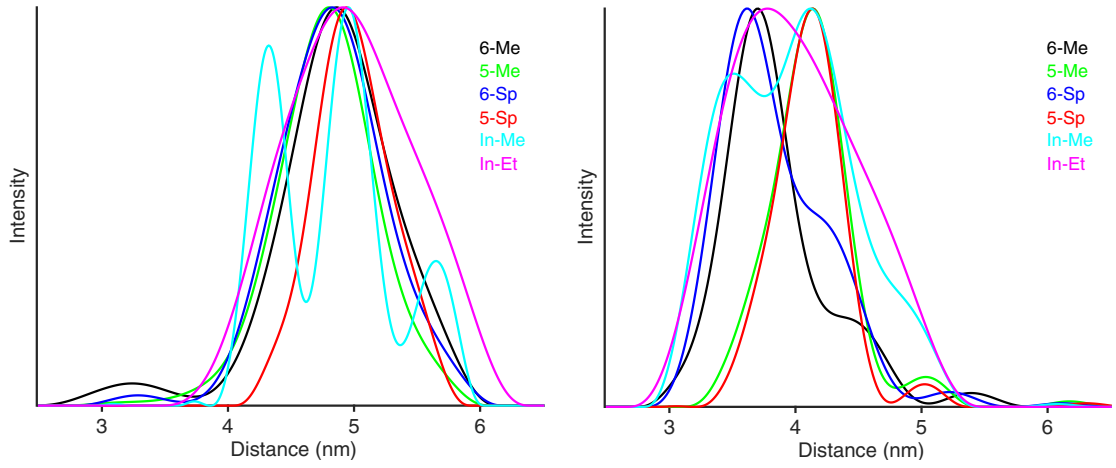


Figure 5.10: Expanded superimposition of Q-band DEER distance distributions from Figure 5.9, sorted by duplex. **(a)** Derivatives of duplex **A2:B3**. **(b)** Derivatives of duplex **A3:B3**.

average of the distributions for **In-Me**, or simply a near-normal distribution of less restricted conformers.

Having investigated the effect of the spin label, attention turned to the consequence of changing the labelling site by positioning the label on different nucleotides. DEER experiments were performed on doubly labelled duplexes where strand B carried the spin label on a 2′-triazolyl-dA or -dC residue (derivatives of **B7** and **B8**, respectively), and the resulting distance distributions were superimposed on the distributions obtained from duplexes carrying both spin labels on 2′-ethynyl-dU (Figure 5.11). For all sets of duplexes the measured modal distances increased with the number of base pairs separating the labels. However, greater variance was observed between the different labels at dC and dA, compared to dU. Surprisingly, the hwhh of the distance distributions were consistently found to be highest for duplexes labelled at 2′-ethynyl-dC, i.e. the position furthest from the terminus; this may be a consequence of changing the relative orientation of the labels through the helical turn. Moreover, the distribution of duplex **A2-In-Et:B8-In-Et** (Figure 5.11d) unexpectedly exhibited two shoulders, suggestive of three unresolved distributions as previously observed for **In-Me**.

Similarly, distances were measured for doubly labelled duplexes where the label on strand A was in an internal position (Figure 5.12). The modal distances also increased as expected for these duplexes, albeit more unevenly; the difference between the spin labelled derivatives of **A3:B3** and **A3:B7** was only 0.16 nm for both **6-Me** and **5-Sp**, whereas with **In-Et** the duplexes **A3:B3** and **A3:B8** were the closest with only a 0.13 nm difference. The origin of this asymmetry is not clear, but it may be related to the relative angle of the two labels imposed by the turn of the helix.[147] Moreover, the lineshape of the distance distribution of **A3-6-Me:B7-6-Me** may suggest two distinct conformations populated to a similar extent.

There is again no apparent correlation between the changes in UV melting temperature of a duplex upon spin labelling, and the width of the distance distributions obtained from DEER measurements. As a significant variance is found amongst the different labels

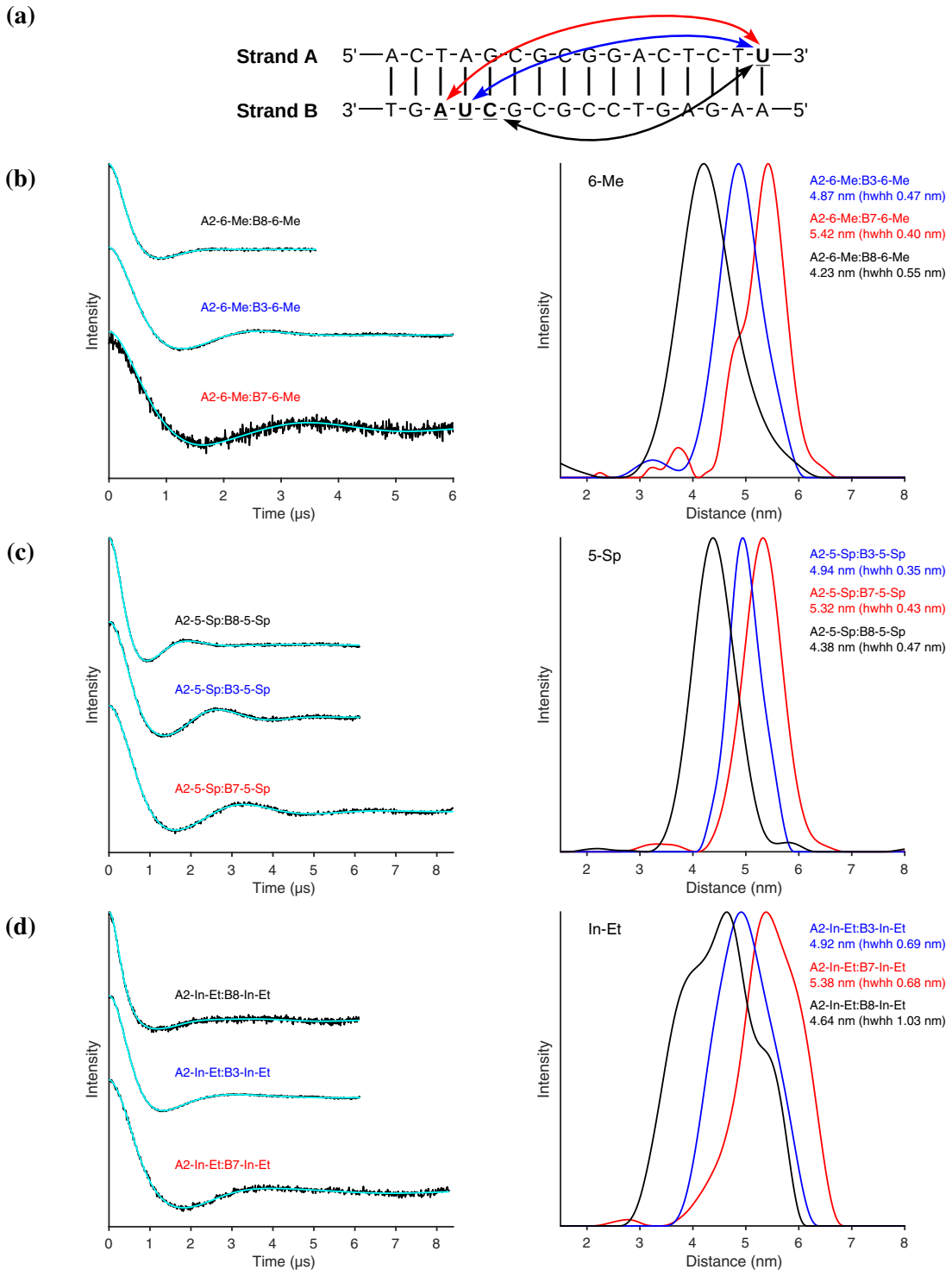


Figure 5.11: Background-corrected Q-band DEER time traces with fitting (cyan) and normalised distance distributions for duplexes of labelled derivatives of **A2** and B-strands carrying the spin label on 2′-triazolyl-dU (**B3**), -dA (**B7**), or -dC (**B8**), at 50 K, in phosphate buffer (10 mM, pH 7.4, 150 mM NaCl) in D_2O and 50% glycerol-d_8. Sample concentrations and the ratio of protonated to deuterated glycerol varied.[199] **(a)** Duplex showing the positioning of labelled residues; the colour of the arrows corresponds to the distance distributions. **(b)** Duplexes labelled with **6-Me**. **(c)** Duplexes labelled with **5-Sp**. **(d)** Duplexes labelled with **In-Et**.

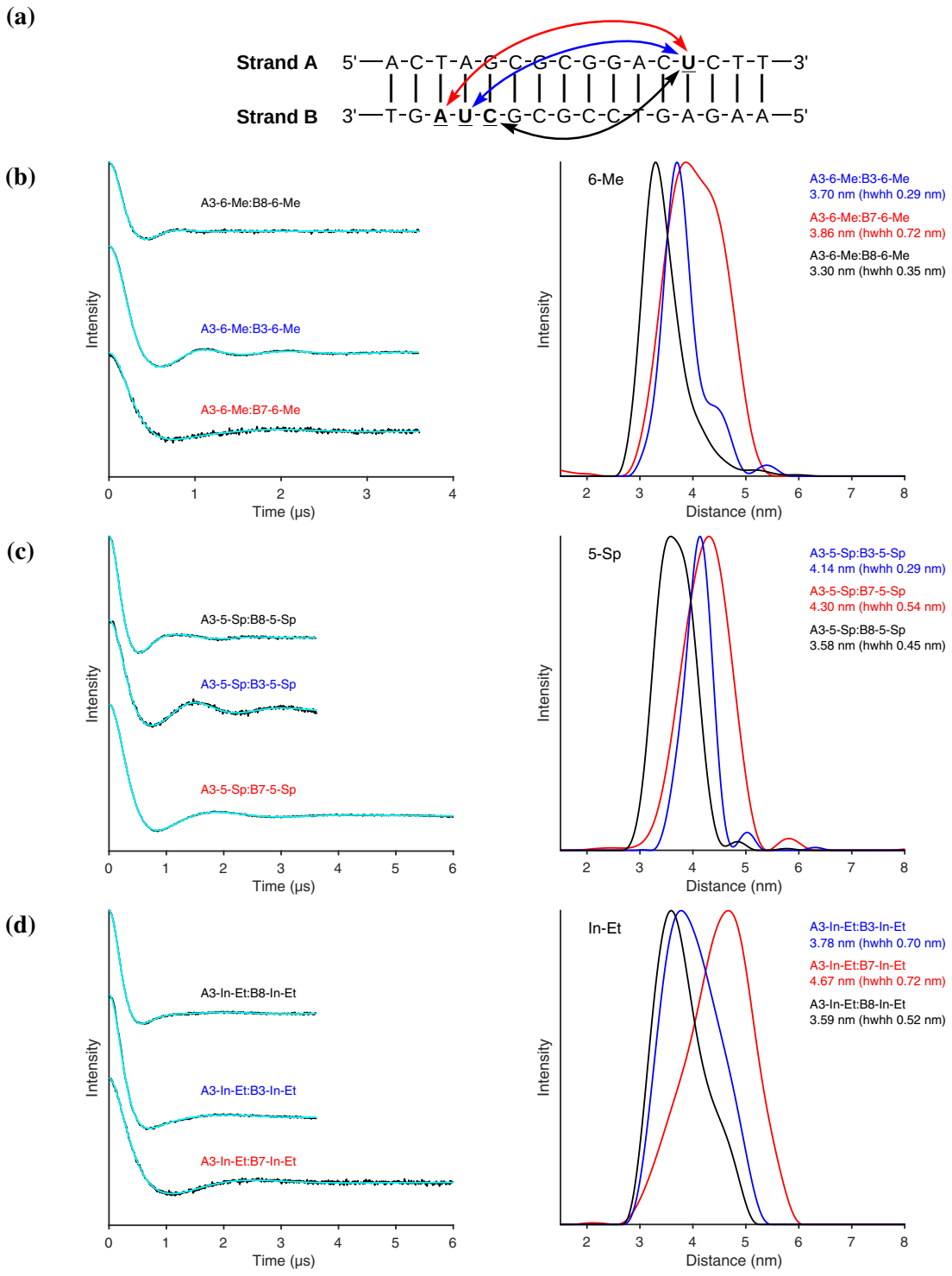


Figure 5.12: Background-corrected Q-band DEER time traces with fitting (cyan) and normalised distance distributions for duplexes of labelled derivatives of **A3** and B-strands carrying the spin label on 2′-triazolyl-dU (**B3**), -dA (**B7**), or -dC (**B8**), at 50 K, in phosphate buffer (10 mM, pH 7.4, 150 mM NaCl) in D_2O and 50% glycerol-d_8. Sample concentrations and the ratio of protonated to deuterated glycerol varied.[199] **(a)** Duplex showing the positioning of labelled residues; the colour of the arrows corresponds to the distance distributions. **(b)** Duplexes labelled with **6-Me**. **(c)** Duplexes labelled with **5-Sp**. **(d)** Duplexes labelled with **In-Et**.

in a given duplex, as well as variance for the same label at different but spatially close nucleotides, it is possible that the 2′-alkynylnucleoside SDSL strategy is sensitive to the microenvironment of the DNA backbone. Further systematic studies of the sequence dependence are, however, required to distinguish the effects of varying both the flanking sequence and the position of labelling. It is difficult to interpret these results in more detail without deeper insight into the conformational space available to the spin label and the nucleic acid. This is the objective of ongoing work in the Anderson group to investigate the spin labelled 2′-triazolyl DNA computationally, as well as analysing a spin labelled self-complementary DNA sequence by X-ray crystallography.

5.3.1 Comparison to 2′-*O*-propargyl spin labelling

Having previously found that installing the spin labels on a commercially available 2′-*O*-propargyl-dU residue resulted in dynamically more mobile spin labels (see Section 5.1.1), distance measurements were performed on doubly labelled propargyl-appended duplexes (derivatives of **A6:B6**, Figure 5.13). The distance distributions are superimposed on the distributions from the duplexes doubly internally labelled on a 2′-ethynylnucleotide

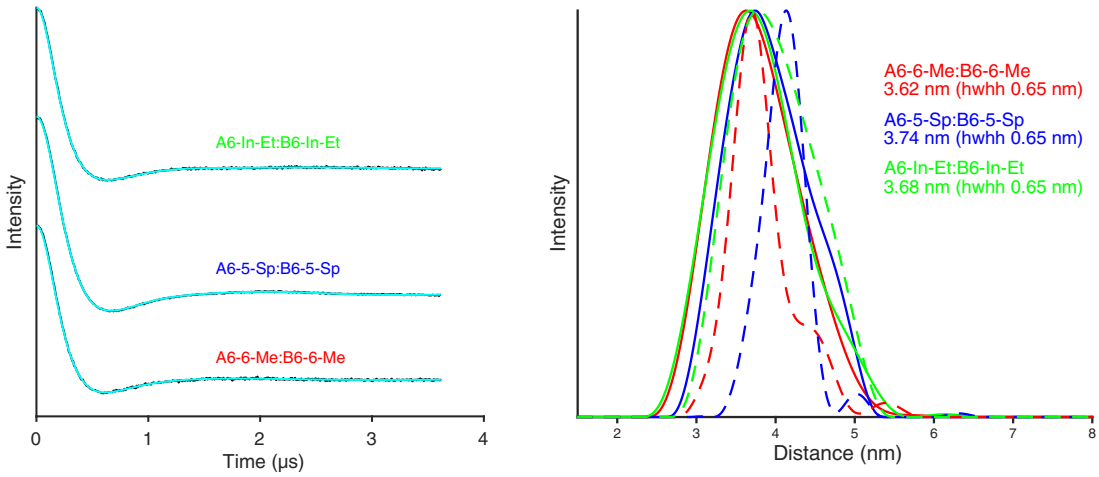


Figure 5.13: (a) Background-corrected Q-band DEER time trace with fit (cyan) and **(b)** distance distribution, for propargyl-appended duplex **A6:B6** doubly labelled with **6-Me**, **5-Sp** and **In-Et**, at 50 K. Superimposed dashed distributions are the labelled products of ethynyl-appended duplex **A3:B3**. 67 µM in phosphate buffer (10 mM, pH 7.4, 150 mM NaCl) in D_2O and 50% glycerol-d_8.

with the corresponding spin labels (derivatives of **A3:B3**, dashed). Pleasingly, the 2′-ethynylnucleoside system clearly affords much more narrow distance distributions in the case of **6-Me** and **5-Sp**, indicating more well-defined conformations for these spin labels. For **In-Et** there is not much difference, perhaps lending some support to the hypothesis that this spin label is too sterically demanding to enable it to adopt preferred conformations while appended through a 2′-triazole. Interestingly, appendage through an extended linker significantly shifts the modal distance of the **5-Sp** labelled duplex, from 4.14 nm for **A3-5-Sp:B3-5-Sp** to 3.74 nm for **A6-5-Sp:B6-5-Sp**. This suggests that the longer linker allows all the spin labels to adopt similar conformations, thereby attenuating the previously observed difference between five- and six-membered nitroxyls.

5.4 Measuring short interspin distances

DNA Strand **A7-5-Sp** is unique in this study, in that it carries the spin label on a dA residue close to the 5′-terminus. Thus, hybridisation of this strand with the various spin labelled derivatives of Strand B (Figure 5.14) will enable the measurement of very short interspin distances. It was hoped that this data could reveal details of the conformational arrangement(s) of the spin labels.

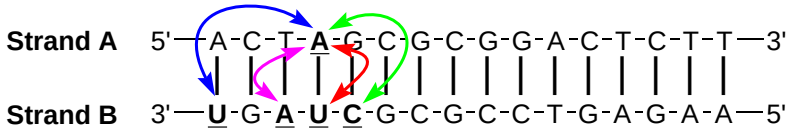


Figure 5.14: Duplexes of Strand **A7-5-Sp** would enable very short interspin distances to be measured.

DEER measurements performed on these doubly spin labelled duplexes show that the distances are indeed very short. Only for the duplex carrying one terminal and one internal label (Figure 5.15a) could a meaningful distance be obtained; the duplexes with internal spin labels on opposing base pairs (Figure 5.15b) had interspin distances too short to be accurately measurable by DEER. The DEER time traces for these duplexes show that the modulation depth is very small and rapidly deteriorates, meaning that Tikhonov regularisation of the fit (cyan) is likely to result in erroneous and broadened distance

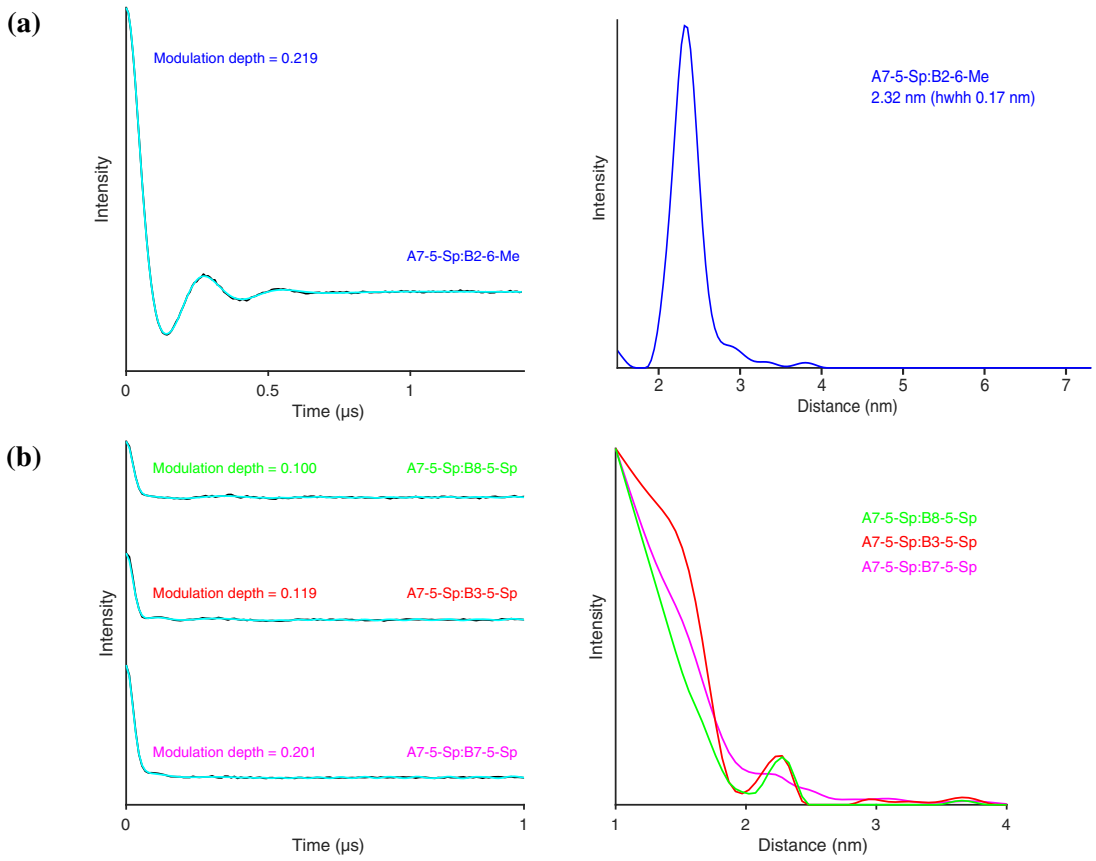


Figure 5.15: Background-corrected Q-band DEER time traces with fitting (cyan) and normalised distance distributions for **(a)** the duplex of **A7-5-Sp** and a terminally labelled B-strand, and **(b)** **A7-5-Sp** and B-strands carrying the spin label on internal 2′-triazolyl-dU (**B3**), -dA (**B7**), or -dC (**B8**), at 50 K, in phosphate buffer (12 mM, pH 7.4, 100 mM NaCl) in D_2O and 50% glycerol-d_8. Sample concentrations and the ratio of protonated to deuterated glycerol varied.[199]

distributions.[11] Through-space exchange coupling may also introduce errors in DEER measurements on distances <2 nm.[12]

As mentioned in Section 1.1, line broadening of the CW EPR spectra of immobilised samples can also be used to measure interspin distances. To this end, CW EPR spectra of the spin labelled duplexes were acquired in a water/glycerol glass at 130 K (Figure 5.16a); this work was performed by Dr Janet Lovett.[199] Compared to the singly terminally labelled duplex **A1:B3-5-Sp** (black), the doubly labelled duplexes showed varying degrees of line broadening attributable to the dipolar coupling between the two spins. The difference between the spectra is more easily discerned from the absorption spectrum (Figure 5.16b), obtained by single integration of the field-swept spectrum. The widest signal corresponds

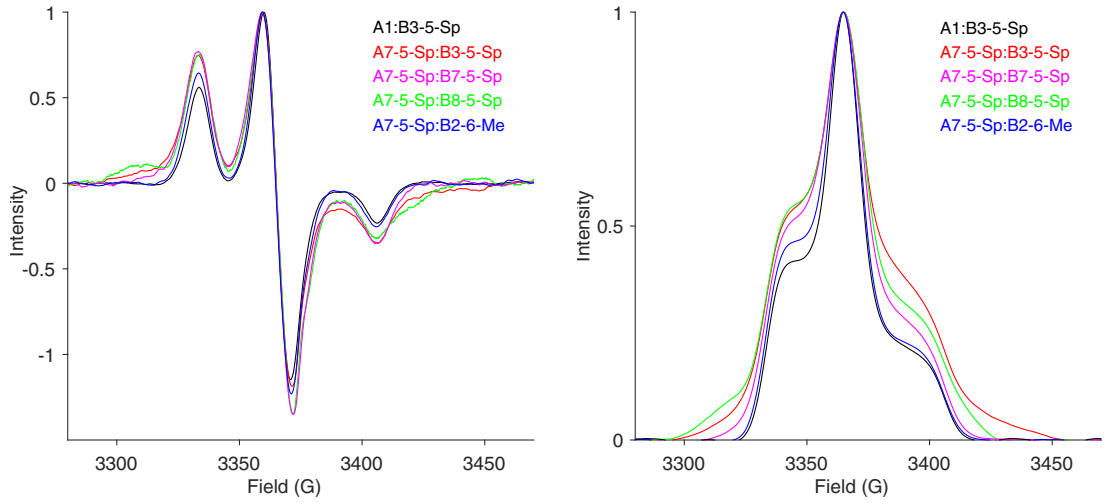


Figure 5.16: Background-corrected **(a)** field-sweep and **(b)** absorption (i.e. singly integrated) X-band CW EPR spectra of doubly labelled duplexes of Strand **A7-5-Sp** at 130 K in phosphate buffer (12 mM, pH 7.4, 100 mM NaCl) in D_2O and 50% glycerol. Sample concentrations varied.[199]

to duplex **A7-5-Sp:B3-5-Sp** (red), which therefore has the shortest interspin distance; this makes sense given that this duplex has the spin labels attached to the opposing nucleotides of the same base pair. Thereafter follows **A7-5-Sp:B8-5-Sp** (green, strand B labelled at dC) and **A7-5-Sp:B7-5-Sp** (magenta, strand B labelled at dA). The duplex with a terminal label on strand B (**A7-5-Sp:B2-6-Me**, blue) exhibits very small line broadening, suggesting that this distance (which was measurable by DEER, Figure 5.15a) is too long to be measured by CW EPR.

Comparing the line width of the doubly labelled duplexes in Figure 5.16 with the corresponding singly labelled duplexes, the line broadening contribution of the dipolar coupling was extracted and and the interspin distances were thus calculated.[11] The interspin distance for duplex **A7-5-Sp:B3-5-Sp**, where the opposing nucleotides of the same base pair are labelled, was 0.92 ± 0.02 nm; for duplex **A7-5-Sp:B8-5-Sp** (strand B labelled on dC) the distance was 1.01 ± 0.04 nm; and for duplex **A7-5-Sp:B7-5-Sp** (strand B labelled on dA) the interspin distance was measured to 1.30 ± 0.22 nm.[†] The significant difference

[†]Error margins are based on the standard deviation in the second moments of singly labelled duplexes, and do not account for differences in baseline due to varying sample concentrations; they are as such only approximate.

between the measured distances of the two latter duplexes, corresponding to the green and magenta distances, respectively, in Figure 5.14, seems to indicate that the labels are preferentially oriented towards the 3′-terminus of the strand to which they are attached. A label orientation perpendicular to the helical axis would, in the idealised case, have led to identical distances measured for these two duplexes, whereas labels protruding towards the 5′-terminus and therefore towards each other in duplex **A7-5-Sp:B7-5-Sp** would have given the shorter distance for this duplex.

6 Conclusions and future work

Site-directed spin labelling (SDSL) is a powerful method to investigate the tertiary structure of biomolecules in solution. In this work, the development of a novel method to achieve SDSL of nucleic acids by CuAAC 'click' labelling of nucleotides bearing a 2′-ethynyl functionality has been described. This research formed the basis of a publication in the *Journal of the American Chemical Society* in 2016.[199]

Alkyne-bearing analogues of 2′-deoxyuridine, 2′-deoxycytidine and 2′-deoxyadenosine were synthesised in a stereospecific fashion *via* a radical atom transfer reaction (Chapter 2). The nucleoside derivatives were protected and derivatised into 3′-(cyanoethyl)phosphoramidites or immobilised on a resin to enable their incorporation into DNA oligonucleotides. In parallel, a set of four nitroxyl spin labels carrying azide functionalities were synthesised (Chapter 3), enabling spin labels with various structural features such as the size of the nitroxyl-bearing ring and the nature of the substituents to be evaluated.

In collaboration with the group of Prof. Tom Brown (University of Oxford), the 2′-ethynyl-functionalised nucleosides were site-specifically incorporated into 16-mer DNA oligonucleotides using the automated solid-supported phosphoramidite method under standard conditions (Chapter 4). Taking advantage of the highly divergent nature of the SDSL strategy, the alkynylated DNA strands were subsequently spin labelled with several azide spin labels using CuAAC 'click' chemistry. In addition to the four labels prepared in this work, two azide-bearing isoindoline-derived nitroxyls prepared by Rachel Porter[198] were also used. Through a wide range of DNA duplexes, the impact of the identity and positioning of the spin label on duplex stability (as measured by ΔT_m^{260}) was explored. It was found that incorporation of a spin label *via* a 2′-triazole linker caused a destabilisation of the duplex, with labels in internal positions exerting a larger effect than terminal labels. Whereas the identity of the nucleotide was found to be of minor importance, the duplex destabilisation varied dramatically and systematically with the identity of the spin label.

However, evidence from CD spectroscopy suggests that only local disruption is caused to the duplex structure.

EPR spectroscopic investigations of the spin labelled DNA (Chapter 5) were performed by Dr Janet Lovett (University of St Andrews); preliminary results suggest that the novel SDSL technique shows promise to enable the deduction of information about the tertiary structure of nucleic acids. Room temperature X-band CW EPR spectra showed that labels in internal positions are more conformationally restricted than terminal labels, and that the structure of the label plays an important role towards minimising the dynamic mobility of the system. Relaxation rates were measured at Q-band and found to be superior for the novel bis(spirocyclohexyl)-substituted spin labels. Q-band DEER measurements on doubly labelled duplexes showed that the 2′-alkynylnucleotides provide narrower distance distributions than commercially available 2′-*O*-propargyl nucleotides for spin labelling DNA, at the cost of causing a slightly larger destabilisation of the duplex structure. Terminally attached spin labels generally gave wider distance distributions than spin labels attached to internal nucleotides. Notably, the measured modal distances were found to vary systematically with the size of the nitroxyl-bearing ring. However, no systematic correlation was found between the width of distance distributions and duplex T_m^{260}. Distribution widths were also found to vary non-systematically with the site of spin labelling; it is however not clear whether this variance originates from a sequence dependence or variation of the labelling site in the duplex.

Detailed interpretation of the DEER distance distributions requires an understanding of the conformations adopted by the spin label and the nucleic acid backbone. The measurement of short distances by frozen CW EPR indicated that the labels preferentially protrude towards the 3′-terminus of the DNA strand they are attached to. However, further investigations are required to refine the understanding of the conformational space available to the spin labelled nucleic acids. Current work in the Anderson group aims to obtain crystal structures of spin labelled DNA, which it is hoped will indicate any DNA backbone distortions and suggest one or more preferred conformations of the spin labels. In collaboration

with Dr Frank Beierlein (Friedrich-Alexander Universität Erlangen-Nürnberg, Germany), computational investigations of the spin labelled system are currently underway. Further, more detailed UV denaturation studies can separate the enthalpic and entropic contributions of the duplex destabilisation, which may reveal the significance of the hydrophobic effect in the novel SDSL strategy. More detailed and systematic investigations by CD spectroscopy (in particular, investigation of the cooperativity of the transition from B-form to A-form DNA upon titration with trifluoroethanol), as well as NMR studies, could also shed light on the structural changes associated with the introduction of spin labels into the DNA duplex.

7 Experimental

7.1 General considerations

Materials: All reagents, obtained from Acros, Alfa, CarboSynth, Fluorochem, Lancaster, Strem, Sigma-Aldrich and TCI, were used directly as supplied unless otherwise noted. Anhydrous solvents were dried by pre-storing over activated 3 Å molecular sieves before being passed through an activated alumina column on a solvent tower under N_2 pressure. Diethylamine, triethylamine, DIPEA and pyridine were distilled and stored over 3Å molecular sieves or KOH under N_2. PCl_3 and $POCl_3$ were distilled immediately before use.

Chromatography: Thin layer chromatography (TLC) was used to monitor reaction progress, and was performed on pre-coated aluminium based plates (0.2 mm Merck Kieselgel 60 with F_{254}); plates were developed under UV irradiation (254 nm) or with vanillin or $KMnO_4$ staining and heating. Column chromatography was performed with silica gel (Macherey-Nagel Kieselgel 60 M, 0.040–0.063 mm) unless otherwise specified.

Nuclear magnetic resonance spectroscopy: ^{1}H Nuclear magnetic resonance (NMR) spectra were recorded at ambient probe temperatures on the following instruments: Bruker AVII500 with ^{13}C cryoprobe (500 MHz), Bruker AVIII400HD (400 MHz), or Bruker DPX200 (200 MHz). Spectra were referenced to residual protons in $CDCl_3$ (δ 7.26), DMSO-d_6 (δ 2.50), CD_3OD (δ 3.31) or D_2O (δ 4.79). Chemical shifts (δ) are reported as parts per million (ppm). Coupling constants (J) are given in Hz to an accuracy of 0.1 Hz. Assignment of ^{1}H resonances were determined on the basis of unambiguous chemical shift, coupling patterns, by analysis of 2D NMR (COSY, HSQC and/or HMBC) and/or by analogy to fully interpreted spectra of closely structurally related compounds. ^{13}C NMR spectra (^{1}H decoupled) were recorded at ambient probe temperatures on the instruments mentioned above (125 MHz, 100 MHz and 50 MHz, respectively), and referenced to the solvents $CDCl_3$ (δ 77.16), DMSO-d_6 (δ 39.52) or CD_3OD (δ 49.00). Samples in D_2O were referenced to one drop of added CD_3OD (δ 49.50). ^{31}P NMR spectra (^{1}H decoupled) were

recorded at ambient probe temperatures on the Bruker AVIII400HD instrument (162 MHz), and referenced to triphenylphosphine (δ –6.00).

Mass spectrometry: Low resolution mass spectra were recorded on an Agilent 6120 Quadrupole mass spectrometer with an Agilent pump and a CTC autosampler, using positive electrospray ionisation (ES+). High-resolution mass spectra (HRMS) were recorded by the Departmental Mass Spectrometry Service, Department of Chemistry, University of Oxford. Data were obtained on a Thermo Scientific Exactive mass spectrometer with a Waters Acquity autosampler and pump (positive electrospray ionisation, ES+), on a Bruker micrOTOF II focus ESI-TOF (negative electrospray ionisation, ES−), or on an Agilent 7200 Accurate Mass QTOF GCMS using a SIM Direct Insertion Probe or a Waters GCT mass spectrometer using a Temperature Programmed Solids Probe (electron impact, EI+, or field ionisation, FI+) in positive mode. The parent ion $[M]^+$ or adduct ($[M+H]^+$, $[M+Na]^+$) are calculated to at least four decimal places. All values are within an error of 5 ppm.

Infrared spectroscopy: All IR spectra were recorded as solids or thin films on a Bruker Tensor 27 FTIR instrument with a Pike Miracle ATR ZnSe module. Wavelengths of maximum absorbance (ν_{max}) are reported in wavenumbers (cm^{-1}). Only a selection of characteristic resonances are reported.

Polarimetry: Optical rotation measurements were performed on a Perkin-Elmer 241 or 341, or a Schmidt+Haensch UniPol L 2000 polarimeter using a 1 dm path length cell, at the sodium D line (589 nm). Specific rotations are given as $[\alpha]_D^T$ in units of 10^{-1} °dm^2g^{-1}, where T is the temperature in °C. The concentration (c) is reported in g/100 mL.

Melting points: Melting points were obtained using a Leica Galen III hot stage microscope and are uncorrected. For thermally labile compounds, the decomposition temperature (decomp.) is quoted.

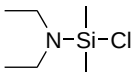
Elemental analysis: Combustion elemental analysis was performed by Mr Stephen Boyer, London Metropolitan University.

Circular dichroism: Circular dichroism (CD) spectra were recorded on a ChiraScan qCD spectrometer (Applied Photophysics Ltd.), using a 1 mm path length quartz cuvette.

EPR spectroscopy: The CW EPR spectra in Chapters 3 and 4 were acquired at the Centre for Advanced Electron Spin Resonance (CAESR) in the Department of Chemistry, University of Oxford, on a Bruker EMXmicro X-band spectrometer using either an EMX High Sensitivity or Super High Sensitivity resonator. All other EPR measurements were performed by Dr Janet Lovett (University of St Andrews).[199]

7.2 Synthesis of reagents

7.2.1 Chloro(diethylamino)dimethylsilane, 56



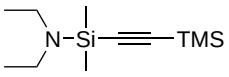
56

Triethylamine (25.5 mL, 0.183 mol, 1.1 equiv.) and Me_2SiCl_2 (20.0 mL, 0.166 mol, 1.0 equiv.) were suspended in dry THF (21 mL) under N_2. A solution of diethylamine (17.5 mL, 0.169 mol, 1.0 equiv.) in dry THF (20.5 mL) was added over 2 h at 0 °C. The resulting thick suspension was diluted with dry THF (50 mL). The cooling bath was removed and the reaction mixture stirred at room temperature for an additional 20 h. Dry pentane (20 mL) was added, and the resulting suspension was filtered through oven-dried celite under N_2. The solvent was removed carefully *in vacuo* at room temperature, and chloroaminosilane **56** was isolated by vacuum distillation (78–80 °C at 90 mbar, lit.[236] 82–84 °C at 90 mmHg) as a white, opaque oil (15.9 g, 95.9 mmol, 58%).

^{1}H NMR (400 MHz, $CDCl_3$) δ_H 2.88 (4H, q, $J = 7.1$ Hz, CH_2CH_3), 1.03 (6H, t, $J = 7.1$ Hz, CH_2CH_3), 0.45 (s, 6H, $Si(CH_3)_2$); **^{13}C NMR** (100 MHz, $CDCl_3$) δ_C 39.9, 15.4, 2.0.

Data consistent with literature values.[236]

7.2.2 Trimethylsilylethynyl(diethylamino)dimethylsilane, 57



57

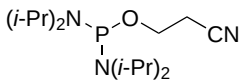
To a solution of trimethylsilylacetylene (13.5 mL, 95.8 mmol, 1.0 equiv.) in dry THF

(150 mL), a solution of *n*-butyllithium (2.5 M in hexane, 42.0 mL, 105 mmol, 1.1 equiv.) was added dropwise over 20 min under N_2. After stirring for 30 min, the solution was added dropwise to a solution of chloroaminosilane **56** (15.9 g, 95.8 mmol, 1.0 equiv.) at −78 °C under Ar over 30 min *via* cannula. The reaction mixture was allowed to reach room temperature while stirring overnight, diluted with dry pentane (10 mL) and concentrated *in vacuo*. Aminosilane **57** was isolated by vacuum distillation (50–52 °C at 1.7 mbar, lit.[237] 47–48 °C at 0.5 mmHg) as a colourless oil (17.2 g, 75.7 mmol, 79%).

IR (thin film, ν_{max} / cm^{-1}) 2963, 1250, 1029, 832, 816, 752; **^{1}H NMR** (200 MHz, $CDCl_3$) δ_H 2.85 (4H, q, $J = 7.0$ Hz, CH_2CH_3), 1.02 (6H, t, $J = 7.0$ Hz, CH_2CH_3), 0.20 (6H, s, $Si(CH_3)_2$), 0.16 (9H, s, $Si(CH_3)_3$); **^{13}C NMR** (50 MHz, $CDCl_3$) δ_C 114.1, 112.5, 40.3, 15.6, 0.3, 0.1.

Data consistent with literature values.[237]

7.2.3 2-Cyanoethyl *N,N,N′,N′*-tetraisopropylphosphordiamidite, 69



69

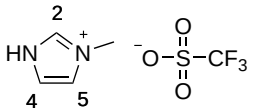
Dry pyridine (2.8 mL, 34.4 mmol, 1.0 equiv.) was added to a solution of freshly distilled PCl_3 (3.0 mL, 34.4 mmol, 1.0 equiv.) in dry diethyl ether (35 mL) under Ar. The solution was cooled to −78 °C and 3-hydroxypropionitrile (2.35 mL, 34.4 mmol, 1.0 equiv.) was added dropwise over 1 h. The reaction mixture was stirred at −78 °C for 1.5 h, before the cooling bath was removed and the mixture stirred for 24 h at room temperature. Precipitated pyridinium chloride salt was removed by filtration through dry celite under Ar. The precipitate was washed with dry diethyl ether under Ar. The combined filtrates were concentrated *in vacuo* and dried under high vacuum for 1 h. The residue was redissolved in dry diethyl ether (35 mL) under Ar. The solution was cooled to −40 °C and diisopropylamine (24.1 mL, 172 mmol, 5.0 equiv.) was added dropwise over 1 h. The reaction mixture was stirred at −10 °C for 1 h, and the cooling bath was allowed to warm up to room temperature overnight. After 14 h, the thick suspension was diluted with dry

diethyl ether (30 mL) and filtered through dry celite under Ar. The filtrand was washed with dry diethyl ether (3 × 30 mL) and the combined filtrates were concentrated *in vacuo*. Phosphordiamidite **69** was obtained by vacuum distillation (124–145 °C at 0.64–1.8 mbar, lit.[238] 116–135 °C at 0.2–0.5 mmHg) as a colourless oil (5.22 g, 17.3 mmol, 50%).

IR (liquid, ν_{max} / cm^{-1}) 2967, 2253, 1459, 1363, 1183, 954, 717; **^{1}H NMR** (400 MHz, $CDCl_3$) δ_H 3.74 (2H, q, $J = 6.7$ Hz, OCH_2), 3.51 (4H, dsept, $J = 17.6, 6.7$ Hz, 4 × $(CH_3)_2CHN$), 2.59 (2H, t, $J = 6.3$ Hz, CH_2CN), 1.16–1.13 (24H, 2 × d, $J = 6.8, 7.0$ Hz, 4 × $(CH_3)_2$CHN); **^{13}C NMR** (100 MHz, $CDCl_3$) δ_C 118.0, 59.3 (d, $^2J_{CP} = 24.9$ Hz), 44.6 (d, $^2J_{CP} = 12.5$ Hz), 24.6 (d, $^3J_{CP} = 8.4$ Hz), 23.9 (d, $^3J_{CP} = 5.7$ Hz), 20.7 (d, $^3J_{CP} = 8.9$ Hz); **^{31}P NMR** (162 MHz, $CDCl_3$) δ_P 122.9.

Data consistent with literature values.[238]

7.2.4 *N*-Methylimidazolium triflate, 159



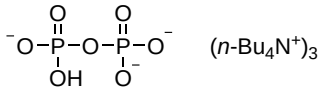
159

Trifluoromethanesulfonic acid (1.00 mL, 11.3 mmol, 1.0 equiv.) was dissolved in dry CH_2Cl_2 (3 mL) under Ar and cooled to 0 °C. A solution of *N*-methylimidazole (0.90 mL, 11.3 mmol, 1.0 equiv.) in dry CH_2Cl_2 (3 mL) was added over 1 h. The reaction mixture was stirred for 1 h at room temperature, before being filtered under Ar. The collected crystals were washed with dry CH_2Cl_2 (2 × 10 mL) and dried under high vacuum at 40 °C. The white, crystalline salt **159** (2.13 g, 9.17 mmol, 81%) was stored and handled in a glovebox, due to its hygroscopic nature.

IR (solid, ν_{max} / cm^{-1}) 3154, 1626, 1586, 1225, 1147, 1025; **^{1}H NMR** (500 MHz, DMSO-d_6) δ_H 14.13 (1H, bs, N*H*), 9.02 (1H, s, H2), 7.68 (1H, t, $J = 1.6$ Hz, H4), 7.66 (1H, t, $J = 1.6$ Hz, H5), 3.86 (3H, s, Me); **^{13}C NMR** (125 MHz, DMSO-d_6) δ_C 135.8, 120.8 (q, $^1J_{CF} = 322$ Hz), 123.2, 119.8, 35.5.

Data consistent with literature values.[239]

7.2.5 Tris(tetrabutylammonium) hydrogen pyrophosphate, 160



160

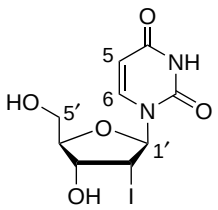
Disodium pyrophosphate (1.11 g, 5.00 mmol, 1.0 equiv.) was dissolved in deionised H_2O (20 mL). The solution was passed through a pre-washed column of Dowex 50wx-200 (acid form) resin (ca. 20 mL), and the resin was eluted with deionised H_2O (5×20 mL) until the pH of the eluent reached 7. The eluent was collected directly into a round-bottom flask containing a solution of $(Bu_4N)OH$ (0.2 M *aq.*, 25.0 mL, 5.00 mmol, 1.0 equiv.) at 0 °C. The solution was adjusted to pH 7 with a solution of $(Bu_4N)OH$ (1.0 M *aq.*, 5.0 mL). The solvent was removed *in vacuo*, and the residue was lyophilised overnight. Pyrophosphate salt **160** was isolated as a white solid (3.79 g, 4.20 mmol, 84%). Due to its hygroscopic nature, the salt was handled in a glovebox.

^{1}H NMR (400 MHz, D_2O) δ_H 3.17–3.13 (8H, m, $4 \times NCH_2CH_2$), 1.64–1.57 (8H, m, $4 \times NCH_2CH_2$), 1.32 (8H, tq, $J = 7.4$, 7.4 Hz, CH_2CH_3), 0.90 (12H, t, $J = 7.4$ Hz, CH_2CH_3); **^{13}C NMR** (100 MHz, D_2O) δ_C 58.7, 23.8, 19.8, 13.5; **^{31}P NMR** (162 MHz, D_2O) δ_P −8.12.

Data consistent with literature values.[240]

7.3 Synthesis of 2′-ethynyl-2′-deoxyuridine derivatives

7.3.1 2′-Iodo-2′-deoxyuridine, 53



53

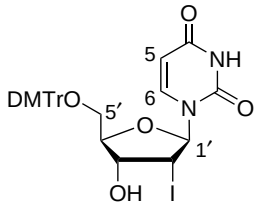
In a round bottom flask equipped with a stirrer bar and reflux condenser, 2,2′-*O*-cyclouridine (2.00 g, 8.84 mmol, 1.0 equiv.), NaI (1.99 g, 13.3 mmol, 1.5 equiv.) and *p*-toluenesulfonic

acid monohydrate (2.53 g, 13.3 mmol, 1.5 equiv.) were suspended in acetone (88 mL) and stirred at 50 °C for 5.5 h. After cooling to room temperature, the solids were removed by vacuum filtration and washed with acetone. The filtrate was concentrated and the resulting residue redissolved in acetone (15 mL). The solution was treated with $Na_2S_2O_3$ (*aq.* sat., 15 mL) until the colour turned pale yellow. The phases were separated, the aqueous phase washed with acetone (2×10 mL) and the combined organic phases were concentrated. The remaining residue was purified by column chromatography (methanol / CH_2Cl_2 (2 : 8)) to give iodonucleoside **53** as a white foam (3.13 g, 8.84 mmol, quant.).

$\mathbf{R}_f$ 0.26 (methanol / CH_2Cl_2 (1 : 9)); **IR** (solid, ν_{max} / cm^{-1}) 3369, 3220, 1671, 1462, 1274, 1087, 1046, 812; **^{1}H NMR** (400 MHz, DMSO-d_6) δ_H 11.41 (1H, s, N*H*), 7.85 (1H, d, $J = 8.1$ Hz, H6), 6.20 (1H, d, $J = 7.7$ Hz, H1′), 5.69 (1H, dd, $J = 8.1, 2.1$ Hz, H5), 4.48 (1H, dd, $J = 7.7, 5.0$ Hz, H2′), 3.97–3.93 (1H, m, H4′), 3.85–3.81 (1H, m, H3′), 3.64–3.53 (2H, m, H5′); **^{13}C NMR** (100 MHz, DMSO-d_6) δ_C 163.0, 150.7, 139.8, 102.4, 89.2, 85.7, 70.3, 60.8, 32.4.

Data consistent with literature values.[241]

7.3.2 5′-*O*-(4,4′-Dimethoxytrityl)-2′-iodo-2′-deoxyuridine, 54



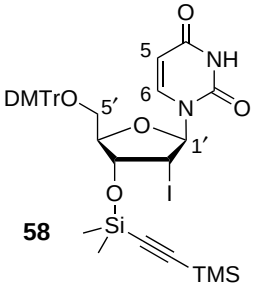
54

4,4′-Dimethoxytrityl chloride (2.30 g, 6.78 mmol, 1.2 equiv.) and alcohol **53** (2.00 g, 5.65 mmol, 1.0 equiv.) were dissolved in dry pyridine (23 mL) and stirred under N_2 at room temperature for 18.5 h. The reaction mixture was quenched with methanol (3 mL) and the solvent was removed by co-evaporation with toluene (2×15 mL) at 30 °C. The residue was dissolved in CH_2Cl_2 (50 mL) and washed with $NaHCO_3$ (5% *aq.*, 2×50 mL) and brine (30 mL) before drying over Na_2SO_4. The solvent was removed *in vacuo* and the

residue purified by column chromatography (ethyl acetate / petroleum ether (6 : 4)) to give protected iodonucleoside **54** as a yellow foam (3.25 g, 4.59 mmol, 88%).

$\mathbf{R_f}$ 0.23 (methanol / CH_2Cl_2 (1 : 19)); **m.p.** 83–85 °C (decomp.); **IR** (solid, ν_{max} / cm^{-1}) 3057, 1682, 1508, 1460, 1250, 1176, 1095, 1032, 828; **^{1}H NMR** (400 MHz, $CDCl_3$) δ_H 8.94 (1H, bs, N*H*), 7.75 (1H, d, $J = 8.2$ Hz, H6), 7.35–7.11 (9H, m, Ar), 6.83–6.77 (4H, m, Ar), 6.37 (1H, d, $J = 6.0$ Hz, H1′), 5.33 (1H, d, $J = 8.2$ Hz, H5), 4.49 (1H, t, $J = 5.5$ Hz, H2′), 4.23–4.17 (1H, m, H4′), 3.93 (1H, t, $J = 4.6$ Hz, H3′), 3.76 (6H, s, ArOCH_3), 3.57–3.42 (2H, m, H5′); **^{13}C NMR** (100 MHz, $CDCl_3$) δ_C 163.0, 158.9, 150.3, 144.2, 139.5, 135.1, 135.0, 130.2, 129.3, 128.3, 128.2, 127.4, 113.5, 113.3, 102.9, 90.5, 87.6, 83.8, 71.2, 62.5, 55.4, 33.9; **HRMS** (ES+) calc. for $C_{30}H_{29}IN_2NaO_7$ $[M + Na]^+$ 679.0912, found 679.0882; $\mathbf{[\alpha]_D^{20}}$ +15.4 ($c = 1.0$, $CHCl_3$).

7.3.3 5′-*O*-(4,4′-Dimethoxytrityl)-3′-*O*-(dimethyl((trimethylsilyl)ethynyl)silane)-2′-iodo-2′-deoxyuridine, 58

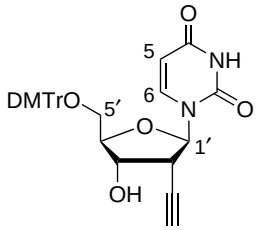


58

Methyl iodide (0.74 mL, 11.9 mmol, 4.0 equiv.) was added dropwise to a solution of aminosilane **57** (1.66 mL, 5.94 mmol, 2.0 equiv.) in dry CH_2Cl_2 (15 mL) under N_2. After stirring for 1 h, the mixture was cannulated into a solution of alcohol **54** (1.95 g, 2.97 mmol, 1.0 equiv.), imidazole (506 mg, 7.43 mmol, 2.5 equiv.) and DMAP (73 mg, 0.594 mmol, 0.2 equiv.) in dry CH_2Cl_2 under N_2. The mixture was stirred at room temperature for 1 h 20 min. The solvent was removed *in vacuo* and the residue redissolved in ethyl acetate (100 mL), washed with brine (3×50 mL) and dried (Na_2SO_4). The solvent was removed *in vacuo* and the residue purified by column chromatography (ethyl acetate / petroleum ether (45 : 55 to 1 : 0)) to give siloxane **58** as a white foam (2.32 g, 2.86 mmol, 96%).

R_f 0.32 (ethyl acetate / petroleum ether (3 : 7)); **m.p.** 71–75 °C; **IR** (thin film, ν_{max} / cm^{-1}) 3178, 3061, 2360, 1693, 1509, 1253, 834; **^{1}H NMR** (400 MHz, $CDCl_3$) δ_H 8.82 (1H, bs, N*H*), 7.76 (1H, d, $J = 8.2$ Hz, H6), 7.33–7.12 (9H, m, Ar), 6.80–6.73 (4H, m, Ar), 6.32 (1H, d, $J = 5.8$ Hz, H1′), 5.25 (1H, dd, $J = 8.2$, 2.2 Hz, H5), 4.40 (1H, t, $J = 5.4$ Hz, H2′), 4.19–4.14 (1H, m, H4′), 3.99 (1H, t, $J = 4.6$ Hz, H3′), 3.71 (6H, s, ArOCH_3), 3.46 (1H, dd, $J =$ 11.0, 2.7 Hz, H5′), 3.38 (1H, dd, $J = 11.1$, 2.1 Hz, H5′), 0.26 (3H, s, $Si(CH_3)_2$), 0.12 (3H, s, $Si(CH_3)_2$), 0.00 (9H, s, $Si(CH_3)_3$); **^{13}C NMR** (100 MHz, $CDCl_3$) δ_C 163.1, 158.9, 150.3, 144.2, 139.6, 135.2, 135.0, 130.3, 128.3, 128.2, 127.4, 116.5, 113.5, 109.8, 102.7, 91.1, 87.5, 84.6, 72.1, 62.1, 55.4, 31.8, 0.6, 0.5, –0.3; **HRMS** (ES+) calc. for $C_{37}H_{43}IN_2NaO_7Si_2$ $[M + Na]^+$ 833.1546, found 833.1570; **Anal.** (%) calc. for $C_{37}H_{43}IN_2O_7Si_2$: C, 54.81; H, 5.35; N, 3.45. Found: C, 54.71; H, 5.27; N, 3.51; **$[\alpha]_D^{20}$** +291 ($c = 0.10$, $CHCl_3$).

7.3.4 5′-*O*-(4,4′-Dimethoxytrityl)-2′-ethynyl-2′-deoxyuridine, 65

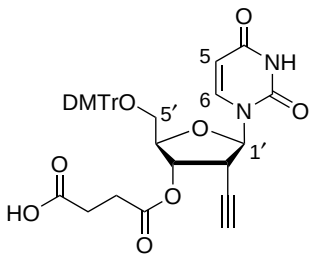


65

Siloxane **58** (2.32 g, 2.86 mmol, 1.0 equiv.) was dissolved in benzene (29 mL) in a pre-dried flask. The flask was flushed with N_2 and sealed. 2,6-Lutidine (34 µL, 0.29 mmol, 0.1 equiv.) was added to the reaction mixture, followed by dropwise addition of BEt_3 (1.0 M in hexanes, 286 µL, 0.286 mmol, 0.1 equiv.). After stirring at room temperature for 30 min, a solution of TBAF (1.0 M in THF, 7.2 mL, 2.5 equiv.) was added. After stirring for 20 min, the solvent was removed *in vacuo*. The remaining residue was redissolved in ethyl acetate (100 mL) and washed with $NaHCO_3$ (5% *aq.*, 3×50 mL). After drying over Na_2SO_4 the solvent was removed *in vacuo*, and the residue purified by column chromatography (ethyl acetate / petroleum ether (65 : 35)) to give 2′-ethynyl-2′-deoxyuridine derivative **65** as a white foam (1.56 g, 2.81 mmol, 98%).

R_f 0.37 (ethyl acetate / petroleum ether (7 : 3)); **m.p.** 100–102 °C; **IR** (thin film, ν_{max} / cm^{-1}) 3435, 3282, 3061, 2360, 1687, 1509, 1251, 1032, 828; **^{1}H NMR** (400 MHz, $CDCl_3$) δ_H 8.78 (1H, bs, N*H*), 7.72 (1H, d, $J = 8.2$ Hz, H6), 7.39–7.21 (9H, m, Ar), 6.89–6.82 (4H, m, Ar), 6.33 (1H, d, $J = 7.7$ Hz, H1′), 5.41 (1H, d, $J = 8.2$ Hz, H5), 4.52–4.45 (1H, m, H3′), 4.21–4.16 (1H, m, H4′), 3.80 (6H, s, ArOCH_3), 3.47 (2H, dq, $J = 10.8$, 2.6 Hz, H5′), 3.38–3.31 (1H, m, H2′), 2.45 (1H, d, $J = 2.4$ Hz, CC*H*); **^{13}C NMR** (100 MHz, $CDCl_3$) δ_C 162.9, 158.9, 150.4, 144.3, 139.8, 135.3, 135.1, 130.2, 130.2, 128.2, 128.2, 127.4, 113.5, 103.0, 87.5, 87.3, 84.8, 76.5, 72.8, 63.3, 55.4, 43.5; **HRMS** (ES+) calc. for $C_{32}H_{30}N_2NaO_7$ $[M+Na]^+$ 577.1945, found 577.1940; **Anal.** (%) calc. for $C_{32}H_{30}N_2O_7$: C, 69.30; H, 5.45; N, 5.05. Found: C, 69.02; H, 5.60; N, 5.09; **$[\alpha]_D^{20}$** +8.7 ($c = 1.0$, $CHCl_3$).

7.3.5 5′-*O*-(4,4′-Dimethoxytrityl)-2′-ethynyl-2′-deoxyuridine-3′-succinate, 67

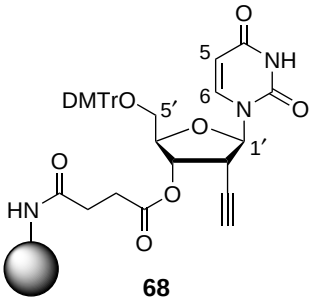


67

Alcohol **65** (150 mg, 0.270 mmol, 1.0 equiv.) and DMAP (3 mg, 0.027 mmol, 0.1 equiv.) were dissolved in dry CH_2Cl_2 (5.5 mL) under N_2. DIPEA (108 µL, 0.621 mmol, 2.3 equiv.) was added, then succinic anhydride (54 mg, 0.540 mmol, 2.0 equiv.). The reaction mixture was stirred at room temperature for 18 h before being diluted with CH_2Cl_2 (10 mL). The mixture was washed with aqueous citric acid (5% w/v, 2×10 mL) and the organic phase was poured into a solution of $NaHCO_3$ (*aq.* sat., 10 mL). Under vigorous stirring the mixture was acidified to pH 3 with HCl (1 M). The mixture was allowed to settle and the phases were separated. The aqueous phase was extracted with CH_2Cl_2 (3×20 mL) and the combined organic phases were dried over Na_2SO_4. The solvent was removed *in vacuo* and the residue was purified by column chromatography (methanol / CH_2Cl_2 (1 : 19 to 1 : 9)) to give succinate **67** as a white foam (170 mg, 0.260 mmol, 96%).

R_f 0.26 (methanol / CH_2Cl_2 (1 : 19)); **m.p.** 88 °C (decomp.); **IR** (thin film, ν_{max} / cm^{-1}) 3277, 3004, 1696, 1510, 1251, 1177, 753; **^{1}H NMR** (400 MHz, $CDCl_3$) δ_H 9.91 (1H, bs, N*H*), 7.63 (1H, d, $J = 8.2$ Hz, H6), 7.34–7.16 (9H, m, Ar), 6.86–6.77 (4H, m, Ar), 6.30 (1H, d, $J = 8.3$ Hz, H1′), 5.49 (1H, dd, $J = 5.6$, 1.8 Hz, H3′), 5.35 (1H, d, $J = 8.1$ Hz, H5), 4.15 (1H, d, $J = 2.0$ Hz, H4′), 3.76 (6H, s, ArOCH_3), 3.50–3.37 (3H, m, H2′, H5′), 2.80–2.60 (4H, m, CH_2CH_2), 2.32 (1H, d, $J = 2.3$ Hz, CC*H*); **^{13}C NMR** (100 MHz, $CDCl_3$) δ_C 176.8, 171.3, 163.8, 158.9, 158.9, 150.8, 144.1, 139.8, 135.1, 135.0, 130.3, 130.2, 128.3, 128.2, 127.4, 113.5, 103.2, 87.7, 87.3, 87.3, 75.5, 74.5, 74.4, 63.6, 55.4, 40.8, 29.1, 28.8; **HRMS** (ES+) calc. for $C_{36}H_{34}N_2NaO_{10}$ $[M+Na]^+$ 677.2111, found 677.2090; **$[\alpha]_D^{20}$** +14.8 ($c = 1.0$, $CHCl_3$).

7.3.6 3′-Succinyl resin bound 5′-*O*-(4,4′-dimethoxytrityl)-2′-ethynyl-2′-deoxyuridine, 68

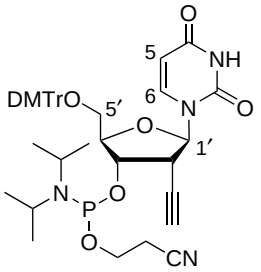


68

Amino-SynBase CPG resin (Link Technologies Ltd., 69 μmol/g, 2.0 g, 0.138 mmol, 1.0 equiv.) was divided equally between two Ar-purged solid-phase reaction tubes fitted with a frit, stopcock and screwcap. Each batch of resin was swelled with dry pyridine (5 mL) for 15 min, after which the tubes were drained. To each tube was added half of a solution of succinate **67** (362 mg, 0.552 mmol, 4.0 equiv.), anhydrous 1-hydroxybenzotriazole (299 mg, 2.21 mmol, 16 equiv.) and *N,N*′-diisopropylcarbodiimide (342 μL, 2.21 mmol, 16 equiv.) in dry pyridine (10 mL). After flushing with Ar, the tubes were sealed and agitated overnight. The reaction was followed by standard DMTr assay: a few mg of resin was removed from the tube and washed with pyridine (3×1 mL), CH_2Cl_2 (3×1 mL) and diethyl ether (3×1 mL) and air-dried. Ca. 1 mg of resin was accurately weighed (m_{resin}) into a small vial

and shaken with trichloroacetic acid (3% in CH_2Cl_2, 1.0 mL/mg resin), and the solution was filtered. The UV absorbance at 504 nm (A_{504}) of a 1 : 5 dilution of the filtrate in trichloroacetic acid (3% in CH_2Cl_2) was measured, and the resin loading L (µmol/g) was calculated according to the formula $L = \frac{5 \times A_{504}}{0.078 \times m_{resin}}$.[164] After 20 h, the resin loading was 42 µmol/g (∼60% conversion). Pentachlorophenol (34 mg) was added to each tube, and the tubes were flushed with Ar. After agitation for another 1 h, the reaction mixture was drained from the tubes. Each tube was washed with pyridine (3×5 mL), CH_2Cl_2 (3×5 mL) and diethyl ether (3×5 mL) and dried under Ar flow. The resin was treated with piperidine (10% in dry THF, 10 mL) for 1 min, and the resin was quickly washed with dry DMF (3×5 mL), CH_2Cl_2 (3×5 mL) and diethyl ether (3×5 mL). Each batch of resin was capped by agitation for 1 h with a 1 : 1 mixture (total 10 mL) of Cap Mix A (10% acetic anhydride, 10% pyridine, 80% THF) and Cap B (16% *N*-methylimidazole in THF). Each batch of resin was washed with THF (3×5 mL), CH_2Cl_2 (3×5 mL) and diethyl ether (3×5 mL), and dried under high vacuum overnight. Using the standard DMTr assay, the resin loading L of resin-bound uridine derivative **68** was determined as 37 µmol/g.

7.3.7 5′-*O*-(4,4′-Dimethoxytrityl)-2′-ethynyl-2′-deoxyuridine-3′-(2-cyanoethyl-*N,N*-diisopropyl)-phosphoramidite, 70



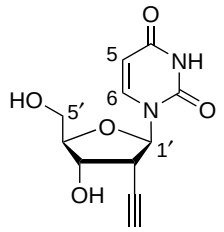
70

2-Cyanoethyl *N,N,N′,N′*-tetraisopropylphosphordiamidite **69** (0.35 mL, 1.08 mmol, 2.0 equiv.) was added to a solution of nucleoside **65** (300 mg, 0.541 mmol, 1.0 equiv.) in dry acetonitrile (5.5 mL) under Ar. *N*-Methylimidazolium triflate **159** (189 mg, 0.812 mmol, 1.5 equiv.) was added and the reaction mixture was stirred for 2 h at room temperature. The mixture was diluted with CH_2Cl_2 (50 mL) and washed with $NaHCO_3$ (*aq.* sat., 2×50 mL).

The aqueous washings were back-extracted with CH_2Cl_2 (50 mL). The combined organic phases were dried over Na_2SO_4 and the solvent was removed *in vacuo*. The crude product was purified by column chromatography (ethyl acetate / petroleum ether (4 : 6)) to afford phosphoramidite **70** (1.3 : 1 mixture of diastereomers A (major) and B (minor)) as a white foam (408 mg, 0.541 mmol, quant.).

R_f 0.40, 0.32 (ethyl acetate / petroleum ether (6 : 4)); **m.p.** 101–105 °C; **IR** (solid, ν_{max} / cm^{-1}) 3283, 3060, 2967, 2252, 1692, 1509, 1251, 1031; **^{1}H NMR** (400 MHz, $CDCl_3$) δ_H 8.96 (1H, bs, N*H*), 7.74–7.70 (1H, m, H6), 7.38–7.24 (9H, m, Ar), 6.86–6.83 (4H, m, Ar), 6.34–6.28 (1H, 2 × d, $J = 7.3, 7.3$ Hz, H1′), 5.41–5.36 (1H, 2 × d, $J = 8.2, 8.2$ Hz, H5), 4.65–4.56 (1H, m, H3′), 4.31–4.28 (1H, m, $H4'_B$), 4.23–4.19 (1H, m, $H4'_A$), 4.03–3.87 (1H, m, CH_2CN), 3.80–3.79 (6H, 2 × s, ArOCH_3), 3.73–3.34 (6H, m, H2′, H5′, CH_2CN, 2 × $(CH_3)_2$C*H*), 2.65 (1H, t, $J = 6.3$ Hz, (POCH_2)$_A$), 2.42 (1H, t, $J = 6.3$ Hz, (POCH_2)$_B$), 2.31 (1H, d, $J = 2.3$ Hz, CCH_A), 2.25 (1H, d, $J = 2.3$ Hz, CCH_B), 1.26–1.05 (12H, m, (CH_3)$_2$CH); **^{13}C NMR** (100 MHz, $CDCl_3$) δ_C 163.1, 158.9, 150.5, 150.4, 144.3, 144.1, 139.7, 139.7, 135.3, 135.2, 135.2, 135.0, 130.3, 130.2, 128.3, 128.2, 128.2, 128.1, 127.3, 117.7, 117.4, 113.5, 113.4, 102.9, 87.8, 87.8, 87.4, 87.3, 85.0 (d, $^3J_{CP} = 1.9$ Hz), 84.7 (d, $^3J_{CP} = 3.4$ Hz), 77.0, 76.6, 75.1, 74.8, 74.4 (d, $^2J_{CP} = 15.0$ Hz), 73.0 (d, $^2J_{CP} = 17.7$ Hz), 62.9, 62.8, 59.3 (d, $^3J_{CP} = 16.5$ Hz), 58.0 (d, $^3J_{CP} = 19.4$ Hz), 55.4, 43.4 (d, $^2J_{CP} = 12.3$ Hz), 43.4 (d, $^2J_{CP} = 12.4$ Hz), 42.6 (d, $^3J_{CP} = 3.0$ Hz), 42.2 (d, $^3J_{CP} = 4.9$ Hz), 24.8, 24.7, 24.7, 24.7, 24.6, 24.6, 24.6, 20.6 (d, $^2J_{CP} = 6.1$ Hz), 20.3 (d, $^2J_{CP} = 7.0$ Hz); **^{31}P NMR** (162 MHz, $CDCl_3$) δ_P 149.8, 149.5; **HRMS** (ES+) calc. for $C_{41}H_{48}O_8N_4P$ $[M+H]^+$ 755.32043, found 755.32007; $[\alpha]_D^{20} = +54$ ($c = 0.22$, $CHCl_3$).

7.3.8 2′-Ethynyl-2′-deoxyuridine, 48

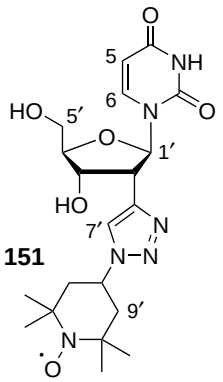


48

Dimethoxytrityl 2′-ethynyl-2′-deoxyuridine **65** (100 mg, 0.180 mmol, 1.0 equiv.) was dissolved in CH_2Cl_2 (2 mL) and the solution was cooled to 0 °C. Trifluoroacetic acid (30 µL, 0.360 mmol, 2.2 equiv.) was added dropwise and the reaction was stirred for 15 min. After quenching with methanol (1 mL), the solvent was removed *in vacuo* and the residue dried under high vacuum. The residue was redissolved in methanol (20 mL) and washed with heptane (3 × 20 mL). The methanol phase was concentrated *in vacuo*, and the residue was purified by column chromatography (methanol / CH_2Cl_2 (1 : 9)) to afford diol **48** as a white solid (43 mg, 0.170 mmol, 95%).

R_f 0.16 (methanol / CH_2Cl_2 (1 : 9)); **m.p.** 70–75 °C; **IR** (thin film, ν_{max} / cm^{-1}) 3378, 3272, 1667, 1464, 1195, 1092; **^{1}H NMR** (400 MHz, CD_3OD) δ_H 7.90 (1H, d, $J = 8.1$ Hz, H6), 6.20 (1H, d, $J = 8.4$ Hz, H1′), 5.70 (1H, d, $J = 8.1$ Hz, H5), 4.30 (1H, dd, $J = 5.3, 2.2$ Hz, H3′), 4.00 (1H, q, $J = 2.8$ Hz, H4′), 3.70 (2H, dd, $J = 10.4, 3.1$ Hz, H5′), 3.29–3.25 (1H, m, H2′), 2.58 (1H, d, $J = 2.5$ Hz, CC*H*); **^{13}C NMR** (100 MHz, CD_3OD) δ_C 165.9, 152.4, 142.2, 103.4, 88.9, 88.2, 77.7, 75.5, 73.6, 62.9, 43.3; **HRMS** (FI+) calc. for $C_{11}H_{12}N_2O_5$ $[M]^+$ 252.0746, found 252.0742; **$[\alpha]_D^{20}$** $= -33$ ($c = 1.0$, $CHCl_3$).

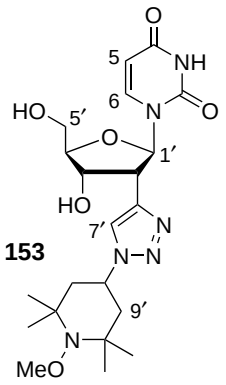
7.3.9 2′-(1-(2,2,6,6-Tetramethyl-1-oxylpiperidin-4-yl)-1,2,3-triazol-4-yl)-2′-deoxyuridine, 151



To a degassed 1 : 1 mixture of acetonitrile and H_2O (0.2 mL) was added CuI (1.0 mg, 0.005 mmol, 0.13 equiv.) and tris(3-hydroxypropyltriazolylmethyl)amine (**149**, 2.2 mg, 0.005 mmol, 0.13 equiv.). The mixture was added to a solution of nucleoside **48** (10 mg, 0.040 mmol, 1.0 equiv.) and spin label **40** (9.5 mg, 0.048 mmol, 1.2 equiv.) in degassed acetonitrile/H_2O (1 : 1, 0.2 mL) and stirred under Ar for 6 h. The solvent was removed *in vacuo*, and the residue purified by column chromatography (methanol / CH_2Cl_2 (5 : 95 to 1 : 9)) to yield triazole **151** as a pale orange solid (16 mg, 0.036 mmol, 90%). Prior to NMR analysis, radical **151** was reduced *in situ* to the corresponding hydroxylamine by stirring with excess hydrazine monohydrochloride and K_2CO_3 in the NMR solvent, followed by direct filtration into the NMR tube.

$\mathbf{R}_f$ 0.17 (methanol / CH_2Cl_2 (1 : 9)); **m.p.** 213–216 °C; **IR** (solid, ν_{max} / cm^{-1}) 3374, 1703, 1635, 1461, 1386, 1089, 1014; **^{1}H NMR** (500 MHz, DMSO-d_6) δ_H 8.01 (1H, d, $J = 8.2$ Hz, H6), 7.99 (1H, s, H7′), 6.26 (1H, d, $J = 9.4$ Hz, H1′), 5.69 (1H, d, $J = 8.1$ Hz, H5), 4.87 (1H, dt, $J = 17.2, 4.8$ Hz, H8′), 4.29 (1H, dd, $J = 5.0, 0.9$ Hz, H3′), 4.03–4.00 (1H, m, H4′), 3.73 (1H, dd, $J = 9.4, 5.1$ Hz, H2′), 3.66–3.60 (2H, m, H5′), 1.95–1.83 (4H, m, H9′), 1.24–1.11 (12H, m, 4× C*H*$_3$); **^{13}C NMR** (125 MHz, DMSO-d_6) δ_C 163.0, 150.7, 140.6, 140.1, 122.4, 102.4, 87.5, 86.7, 72.3, 61.6, 58.0, 52.0, 45.9, 45.0, 32.5, 19.4; **HRMS** (ES+) calc. for $C_{20}H_{30}O_6N_6$ $[M+H]^+$ 450.22213, found 450.22073; $[\alpha]_D^{20} = -79.5$ ($c = 1.0$, $CHCl_3$).

7.3.10 2′-(1-(2,2,6,6-Tetramethyl-1-methoxypiperidin-4-yl)-1,2,3-triazol-4-yl)-2′-deoxyuridine, 153



$FeSO_4 \cdot nH_2O$ (88% w/w, 222 mg, 1.15 mmol, 2.5 equiv.) was added to a solution of spin label **40** (91 mg, 0.461 mmol, 1.0 equiv.) in DMSO (2.5 mL). H_2O_2 (50% *aq.*, 0.15 mL, 2.30 mmol, 5.0 equiv.) was added dropwise over 15 min, and the solution was stirred at room temperature. Fresh H_2O_2 was carefully added after 4 h (0.3 mL), 6 h (0.3 mL) and 22 h (0.5 mL). After 24 h, the reaction mixture was diluted with H_2O (20 mL) and extracted with diethyl ether (3×20 mL). The combined organic extracts were dried (Na_2SO_4) and filtered through a silica plug. The filtrate was concentrated and dried at ∼300 mbar to give crude 2,2,6,6-tetramethyl-4-azido-1-methoxypiperidine (**152**) as an opaque oil (78 mg, 78% w/w, ∼0.287 mmol, ∼62%).

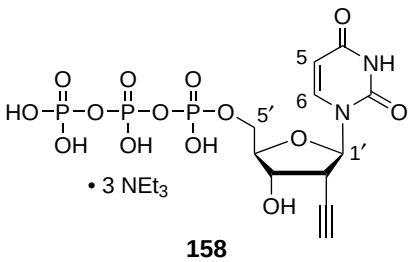
Nucleoside derivative **65** (133 mg, 0.239 mmol, 1.0 equiv.), crude **152** (78% w/w, 78 mg, ∼0.287 mmol, ∼1.2 equiv.) and ligand **150** (12.7 mg, 0.024 mmol, 10 mol%) were dissolved in dry acetonitrile (3 mL) under N_2. CuI (4.6 mg, 0.024 mmol, 10 mol%) was added, and the reaction was stirred for 2 h before being diluted with ethyl acetate (40 mL). The mixture was washed with a solution of disodium EDTA (0.25 M, pH 7, 3×20 mL), dried (Na_2SO_4), and concentrated *in vacuo*. The residue was purified by column chromatography (methanol / CH_2Cl_2 (4 : 96)) to give impure DMTr-protected triazolyl nucleoside as a white foam (160 mg, ∼0.209 mmol, ∼87%). The compound was not characterised due to the presence of multiple rotamers in the ^{1}H NMR spectrum.

The DMTr-protected triazolyl nucleoside (160 mg, ∼0.209 mmol, 1.0 equiv.) was

dissolved in CH_2Cl_2 (2 mL) and cooled to 0 °C. Trifluoroacetic acid (72 µL, 0.920 mmol, 4.4 equiv.) was added dropwise, and the reaction was stirred at 0 °C for 1 h. After quenching with methanol (1 mL), the solvent was removed *in vacuo*. The residue was redissolved in methanol (20 mL) and washed with heptane (3 × 10 mL). The methanol phase was concentrated *in vacuo*, and the residue was purified by column chromatography (methanol / CH_2Cl_2 (8 : 92 to 1 : 9)) to afford 2′-triazolyl nucleoside **153** as a white solid (76 mg, 0.164 mmol, 78%).

$\mathbf{R}_f$ 0.19 (methanol / CH_2Cl_2 (1 : 9)); **m.p.** 222–227 °C; **IR** (solid, ν_{max} / cm^{-1}) 3407, 2923, 1682, 1467, 1283, 1097, 1034; **^{1}H NMR** (500 MHz, DMSO-d_6) δ_H 11.24 (1H, bs, N*H*), 8.00–7.98 (2H, m, H6, H7′), 6.27 (1H, d, $J = 9.4$ Hz, H1′), 5.70 (1H, d, $J = 8.0$ Hz, H5), 5.46 (1H, d, $J = 4.9$ Hz, 3′-O*H*), 5.19 (1H, t, $J = 5.1$ Hz, 5′-O*H*), 4.92–4.85 (1H, m, H8′), 4.28 (1H, td, $J = 5.0, 1.0$ Hz, H3′), 4.01 (1H, td, $J = 3.6, 1.0$ Hz, H4′), 3.74 (1H, dd, $J = 9.4, 5.0$ Hz, H2′), 3.67–3.60 (2H, m, H5′), 3.58 (3H, s, OCH_3), 1.97–1.88 (4H, m, H9′), 1.20 (6H, s, 2 × CH_3), 1.18 (6H, s, 2 × CH_3); **^{13}C NMR** (125 MHz, DMSO-d_6) δ_C 162.9, 150.7, 140.5, 140.0, 122.4, 102.4, 87.4, 86.7, 72.3, 65.1, 61.7, 59.5, 51.6, 45.8, 44.9, 44.8, 32.5, 20.0; **HRMS** (ES+) calc. for $C_{21}H_{33}O_6N_6$ $[M+H]^+$ 465.24561, found 465.24524; $[\alpha]_D^{20} = -73.8$ ($c = 0.5$, CH_3OH).

7.3.11 Tris(triethylammonium) 2′-ethynyl-2′-deoxyuridine 5′-triphosphate, 158



158

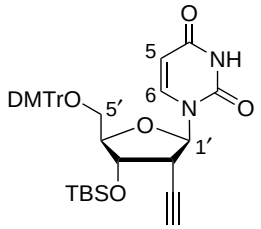
Nucleoside **48** (100 mg, 0.397 mmol, 1.0 equiv.) and proton sponge (128 mg, 0.596 mmol, 1.5 equiv.) were dried over KOH under high vacuum overnight, and dissolved in dry trimethyl phosphate (2 mL). The soluton was cooled to −15 °C. Phosphorus oxychloride (44 µL, 0.476 mmol, 1.2 equiv.) was added dropwise, and the reaction was stirred at

−15 °C for 1 h. A solution of tris(tetrabutylammonium) hydrogen pyrophosphate (**160**, 1.8 g, 1.99 mmol, 5.0 equiv.) in dry DMF (1.8 mL) and tributylamine (0.44 mL) was added, and the reaction was stirred for 3.5 h while allowed to slowly reach room temperature. The reaction was quenched with triethylammonium bicarbonate buffer (TEAB, 1.0 M, pH 7.5, 4 mL), and the solvent was removed *in vacuo*. The sirupy residue was redissolved in H_2O (3 mL) and NaCl (3 M, 300 µL), and precipitated by addition of ethanol (9 mL) and storing at −20 °C overnight. After centrifugation (9500 RPM, 20 min, 4 °C) the pellet was collected, and the supernatant was concentrated *in vacuo* and resubmitted to the precipitation procedure two times (2.5 mL H_2O, 250 µL NaCl (3 M), 7.5 mL ethanol). The collected pellets were redissolved in H_2O and purified by RP-HPLC (Phenomenex Gemini-NX 10 µm C18 110A AXIA column, 250 × 21.2 mm; buffer A: 0.1 M TEAB (pH 7.5), buffer B: 40% MeCN in 0.1 M TEAB (pH 7.5); 0–20% buffer B, monitoring at 280 nm) in portions of ∼100 OD_{260}. The collected fractions of triphosphate **158** were lyophilised separately, redissolved in 1000 µL H_2O and quantified by OD_{260} ($\varepsilon_{260} = 9.66\ mM^{-1}cm^{-1}$);[242] total yield: 735.8 OD_{260}, 76.2 µmol, 19%. Triphosphate **158** was aliqoted into vials, lyophilised, and stored at −20 °C.

^{1}H NMR (500 MHz, D_2O) δ_H 7.93 (1H, d, $J = 8.1$ Hz, H6), 6.28 (1H, d, $J = 8.4$ Hz, H1′), 6.00 (1H, d, $J = 8.1$ Hz, H5), 4.62 (1H, dd, $J = 5.5, 2.0$ Hz, H3′), 4.33–4.31 (1H, m, H4′), 4.26–4.18 (2H, m, H5′), 3.50–3.47 (1H, m, H2′), 3.20 (18H, q, $J = 7.3$ Hz, 9 × $NC\mathit{H}_2CH_3$), 2.65 (1H, d, $J = 2.3$ Hz, C$C\mathit{H}$), 1.28 (27H, t, $J = 7.3$ Hz, 9 × $NCH_2C\mathit{H}_3$); **^{13}C NMR** (125 MHz, D_2O) δ_C 167.4, 153.2, 142.6, 104.5, 88.6, 86.3 (d, $^3J_{CP} = 9.2$ Hz), 77.8, 76.4, 73.0, 66.6 (d, $^2J_{CP} = 5.4$ Hz), 47.9, 42.8, 9.5; **^{31}P NMR** (162 MHz, D_2O) δ_P −10.3 (1P, m), −11.4 (1P, d, $^2J_{PP} = 19.7$ Hz), −23.0 (1P, m); **HRMS** (ES−) calc. for $C_{22}H_{29}O_{28}N_4P_6$ $[2M-H]^-$ 982.9399, found 982.9876.

7.4 Synthesis of 2′-ethynyl-2′-deoxycytidine derivatives

7.4.1 5′-*O*-(4,4′-Dimethoxytrityl)-3′-*O*-*tert*-butyldimethylsilyl-2′-ethynyl-2′-deoxyuridine, 71

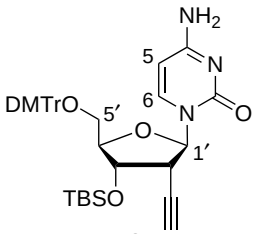


71

To a solution of alcohol **65** (100 mg, 0.180 mmol, 1.0 equiv.) in dry DMF (1 mL) was added imidazole (74 mg, 1.08 mmol, 6.0 equiv.) and then TBSCl (163 mg, 1.08 mmol, 6.0 equiv.). The reaction mixture was stirred at room temperature under N_2 for 24 h, before being quenched with $NaHCO_3$ (5% *aq.*, 20 mL). The mixture was diluted with ethyl acetate (20 mL) and separated. The organic phase was washed with $NaHCO_3$ (*aq.* sat., 2×20 mL) and brine (20 mL) and dried over Na_2SO_4. The solvent was removed *in vacuo*, and the residue purified by column chromatography (ethyl acetate / petroleum ether (4 : 6)) to give silyl ether **71** as a white foam (108 mg, 0.161 mmol, 89%).

$\mathbf{R}_f$ 0.39 (ethyl acetate / petroleum ether (1 : 1)); **m.p.** 89–92 °C; **IR** (solid, ν_{max} / cm^{-1}) 1690, 1608, 1509, 1250, 1032, 829; **^{1}H NMR** (400 MHz, $CDCl_3$) δ_H 9.52 (1H, bs, N*H*), 7.77 (1H, d, $J = 8.2$ Hz, H6), 7.39–7.21 (9H, m, Ar), 6.85 (4H, d, $J = 8.8$ Hz, Ar), 6.29 (1H, d, $J = 7.3$ Hz, H1′), 5.47 (1H, dd, $J = 8.1, 1.8$ Hz, H5), 4.36 (1H, dd, $J = 5.4, 2.9$ Hz, H3′), 4.07 (1H, q, $J = 2.8$ Hz, H4′), 3.79 (6H, s, ArOCH_3), 3.51 (1H, dd, $J = 11.0, 2.9$ Hz, H5′), 3.34 (1H, dd, $J = 10.9, 2.5$ Hz, H5′), 3.20–3.16 (1H, m, H2′), 2.24 (1H, d, $J =$ 2.4 Hz, CC*H*), 0.85 (9H, s, *t*-Bu), 0.10 (3H, s, SiCH_3), 0.01 (3H, s, SiCH_3); **^{13}C NMR** (100 MHz, $CDCl_3$) δ_C 163.4, 158.8, 150.5, 144.2, 139.9, 135.2, 135.1, 130.1, 128.1, 127.3, 113.4, 102.9, 87.9, 87.3, 86.2, 77.1, 74.7, 73.3, 62.7, 55.3, 43.1, 25.8, 18.2, −4.5, −4.8; **HRMS** (ES+) calc. for $C_{38}H_{44}O_7N_2NaSi$ $[M+Na]^+$ 691.28100, found 691.27844; $[\alpha]_D^{20} = +5.9$ ($c = 1.0$, $CHCl_3$).

7.4.2 5′-*O*-(4,4′-Dimethoxytrityl)-3′-*O*-*tert*-butyldimethylsilyl-2′-ethynyl-2′-deoxycytidine, 72



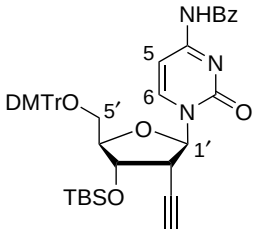
72

To a suspension of 1,2,4-triazole (1.90 g, 27.5 mmol, 18.0 equiv.) in dry acetonitrile (12 mL) was added $POCl_3$ (0.57 mL, 6.12 mmol, 4.0 equiv.) dropwise at 0 °C under Ar. After stirring for 5 min, triethylamine (3.8 mL, 28 mmol, 18 equiv.) was added dropwise and the mixture was stirred for another 30 min at 0 °C. A solution of uridine derivative **71** (1.02 g, 1.53 mmol, 1.0 equiv.) in dry acetonitrile (4 mL) was added slowly by cannula. The reaction mixture was stirred for 10 min at 0 °C and then 3 h at room temperature. After concentrating to one third of the volume, the reaction mixture was diluted with ethyl acetate (100 mL) and washed with H_2O (2×100 mL) and brine (20 mL). The combined aqueous phases were back-extracted with ethyl acetate (2×50 mL). The combined organic phases were dried (Na_2SO_4) and the solvent was removed *in vacuo*. The residue was redissolved in dioxane (30 mL) and NH_3 (25% *aq.*, 10 mL) was added. The mixture was stirred at room temperature for 3 h. The solvent was removed *in vacuo*, and the residue purified by column chromatography (methanol / CH_2Cl_2 (7 : 93)) to yield cytidine derivative **72** as a white foam (980 mg, 1.47 mmol, 96%).

$\mathbf{R}_f$ 0.36 (methanol / CH_2Cl_2 (8 : 92)); **m.p.** 129–131 °C; **IR** (solid, ν_{max} / cm^{-1}) 3292, 1645, 1608, 1508, 1220, 1031, 830; **^{1}H NMR** (400 MHz, $CDCl_3$) δ_H 8.17 (2H, s, NH_2), 7.93 (1H, d, $J = 7.5$ Hz, H6), 7.41–7.21 (9H, m, Ar), 6.85–6.83 (4H, m, Ar), 6.27 (1H, d, $J = 5.0$ Hz, H1′), 5.48 (1H, d, $J = 7.4$ Hz, H5), 4.36 (1H, t, $J = 5.6$ Hz, H3′), 4.10 (1H, dt, $J = 5.1, 2.6$ Hz, H4′), 3.79 (6H, s, ArOCH_3), 3.57 (1H, dd, $J = 10.9, 2.7$ Hz, H5′), 3.30 (1H, dd, $J = 10.9, 2.6$ Hz, H5′), 3.20–3.16 (1H, m, H2′), 2.20 (1H, d, $J = 2.5$ Hz, CC*H*), 0.81 (9H, s, *t*-Bu), 0.06 (3H, s, SiCH_3), −0.05 (3H, s, SiCH_3); **^{13}C NMR** (100

MHz, $CDCl_3$) δ_C 165.9, 158.8, 156.0, 144.3, 141.0, 135.4, 135.4, 130.2, 130.2, 128.3, 128.1, 127.2, 113.4, 113.3, 95.1, 89.1, 87.0, 84.8, 78.2, 74.4, 71.6, 61.9, 55.4, 43.5, 25.7, 18.2, −4.5, −4.9; **HRMS** (ES+) calc. for $C_{38}H_{45}O_6N_3SiNa$ $[M+Na]^+$ 690.29698, found 690.29517; $[\alpha]_D^{20} = +8.7$ ($c = 1.0$, $CHCl_3$).

7.4.3 4-*N*-Benzoyl-5′-*O*-(4,4′-dimethoxytrityl)-3′-*O*-*tert*-butyldimethylsilyl-2′-ethynyl-2′-deoxycytidine, 73



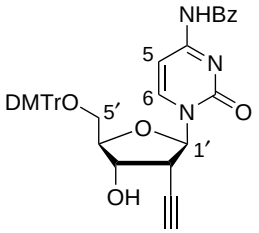
73

To a solution of amine **72** (980 mg, 1.47 mmol, 1.0 equiv.) in dry pyridine (15 mL) under N_2 was added benzoyl chloride (256 µL, 2.21 mmol, 1.5 equiv.). The solution was stirred at room temperature for 10 h before being diluted with H_2O (100 mL). The mixture was extracted with CH_2Cl_2 (3×50 mL) and the combined organic extracts were dried (Na_2SO_4). The solvent was removed *in vacuo*, and residual pyridine was removed by co-evaporation with toluene (3×5 mL). The residue was dried under high vacuum, then purified by column chromatography (ethyl acetate / petroleum ether (6 : 4)) to afford benzamide **73** as a white foam (926 mg, 1.20 mmol, 82%).

$\mathbf{R}_f$ 0.29 (ethyl acetate / petroleum ether (6 : 4)); **m.p.** 107–113 °C; **IR** (thin film, ν_{max} / cm^{-1}) 2930, 1697, 1509, 1484, 1253, 1073; **^{1}H NMR** (400 MHz, $CDCl_3$) δ_H 8.75 (1H, bs, N*H*), 8.39 (1H, d, $J = 7.0$ Hz, H6), 7.90 (2H, d, $J = 7.5$ Hz, Bz), 7.60 (1H, t, $J = 7.4$ Hz, Bz), 7.50 (2H, t, $J = 7.6$ Hz, Bz), 7.40 (2H, d, $J = 7.4$ Hz, Ar), 7.35–7.24 (8H, m, H5, Ar), 6.88 (4H, d, $J = 8.8$ Hz, Ar), 6.32 (1H, d, $J = 4.6$ Hz, H1′), 4.40 (1H, t, $J = 5.7$ Hz, H3′), 4.19–4.16 (1H, m, H4′), 3.82 (6H, s, ArOCH_3), 3.65 (1H, dd, $J = 11.0$, 2.6 Hz, H5′), 3.39 (1H, dd, $J = 11.0$, 2.4 Hz, H5′), 3.28–3.25 (1H, m, H2′), 2.27 (1H, d, $J = 2.4$ Hz, CC*H*), 0.83 (9H, s, *t*-Bu), 0.08 (3H, s, SiCH_3), −0.03 (3H, s, SiCH_3); **^{13}C NMR** (100 MHz, $CDCl_3$) δ_C 162.3, 158.9, 144.7, 144.0, 135.4, 135.3, 133.2, 130.2, 130.2, 129.1,

128.4, 128.2, 127.7, 127.4, 113.5, 89.7, 87.3, 85.2, 77.7, 74.8, 71.3, 61.7, 55.4, 43.9, 25.7, 18.2, −4.5, −4.9; **HRMS** (ES+) calc. for $C_{45}H_{50}N_3O_7Si$ $[M+H]^+$ 772.34125, found 772.34259; $[\alpha]_D^{25} = +12.0$ ($c = 1.0$, $CHCl_3$).

7.4.4 4-*N*-Benzoyl-5′-*O*-(4,4′-dimethoxytrityl)-2′-ethynyl-2′-deoxycytidine, 74

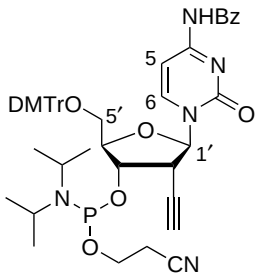


74

To a solution of silyl ether **73** (926 mg, 1.20 mmol, 1.0 equiv.) in THF (12 mL) was added a solution of TBAF (1 M in THF, 1.80 mL, 1.80 mmol, 1.5 equiv.) dropwise. The solution was stirred at room temperature for 2.5 h, and then diluted with brine (10 mL). The phases were separated, and the aqueous phase was extracted with CH_2Cl_2 (3×40 mL). The combined organic phases were dried (Na_2SO_4) and the solvent was removed *in vacuo*. The residue was purified by column chromatography (methanol / CH_2Cl_2 (3 : 97 to 5 : 95)) to afford alcohol **74** as a yellow foam (789 mg, 1.20 mmol, quant.).

$\mathbf{R}_f$ 0.32 (methanol / CH_2Cl_2 (5 : 95)); **m.p.** 120–126 °C; **IR** (thin film, ν_{max} / cm^{-1}) 3288, 2931, 1699, 1660, 1510, 1484, 1252, 1033; **^{1}H NMR** (400 MHz, $CDCl_3$) δ_H 8.83 (1H, bs, N*H*), 8.30 (1H, d, $J = 7.4$ Hz, H6), 7.88 (2H, d, $J = 7.6$ Hz, Bz), 7.58 (1H, t, $J = 7.3$ Hz, Bz), 7.48 (2H, t, $J = 7.6$ Hz, Bz), 7.41 (2H, d, $J = 7.6$ Hz, Ar), 7.34–7.24 (8H, m, H5, Ar), 6.87 (4H, d, $J = 8.7$ Hz, Ar), 6.32 (1H, d, $J = 4.6$ Hz, H1′), 4.52 (1H, t, $J = 5.7$ Hz, H3′), 4.24–4.21 (1H, m, H4′), 3.80 (6H, s, ArOC*H*$_3$), 3.58 (1H, dd, $J = 10.8$, 2.3 Hz, H5′), 3.51 (1H, dd, $J = 11.1$, 2.5 Hz, H5′), 3.47–3.43 (1H, m, H2′), 2.43 (1H, d, $J = 2.1$ Hz, CC*H*); **^{13}C NMR** (100 MHz, $CDCl_3$) δ_C 162.5, 158.9, 144.5, 144.2, 135.6, 135.4, 133.2, 130.2, 130.2, 129.1, 128.3, 128.2, 127.8, 127.3, 113.5, 89.1, 87.4, 84.4, 77.0, 76.5, 70.6, 62.2, 55.3, 44.2; **HRMS** (ES+) calc. for $C_{39}H_{36}N_3O_7$ $[M+H]^+$ 658.25478, found 658.25519; $[\alpha]_D^{25} = +23.9$ ($c = 1.0$, $CHCl_3$).

7.4.5 4-*N*-Benzoyl-5′-*O*-(4,4′-dimethoxytrityl)-2′-ethynyl-2′-deoxycytidine-3′-(2-cyanoethyl-*N*,*N*-diisopropyl)-phosphoramidite, 75



75

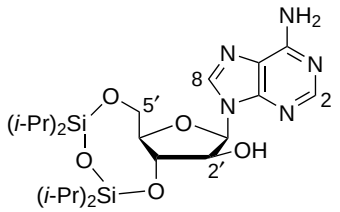
2-Cyanoethyl *N*,*N*,*N*′,*N*′-tetraisopropylphosphordiamidite **69** (174 µL, 0.548 mmol, 2.0 equiv.) was added to a solution of alcohol **74** (180 mg, 0.274 mmol, 1.0 equiv.) in dry acetonitrile (2.7 mL) under Ar. *N*-Methylimidazolium triflate **159** (95 mg, 0.411 mmol, 1.5 equiv.) was added and the reaction mixture was stirred for 2 h at room temperature. The mixture was diluted with CH_2Cl_2 (20 mL) and washed with $NaHCO_3$ (*aq.* sat., 2×20 mL). The aqueous washings were back-extracted with CH_2Cl_2 (20 mL). The combined organic phases were dried over Na_2SO_4 and the solvent was removed *in vacuo*. The crude product was purified by column chromatography (ethyl acetate / petroleum ether (7 : 3)) to afford phosphoramidite **75** (1 : 1.2 mixture of diastereomers A (minor) and B (major)) as a white foam (213 mg, 0.248 mmol, 91%).

$\mathbf{R_f}$ 0.35, 0.26 (ethyl acetate / petroleum ether (7 : 3)); **m.p.** 90–94 °C; **IR** (thin film, ν_{max} / cm^{-1}) 2967, 2252, 1666, 1482, 1250, 1031, 729; **^{1}H NMR** (400 MHz, $CDCl_3$) δ_H 8.35 (1H, d, $J = 7.3$ Hz, $H6_A$), 8.31 (1H, d, $J = 7.4$ Hz, $H6_B$), 7.89 (2H, d, $J = 7.5$ Hz, Bz), 7.60 (1H, t, $J = 7.4$ Hz, Bz), 7.50 (2H, t, $J = 7.6$ Hz, Bz), 7.43–7.39 (2H, m, H5, Ar), 7.36–7.25 (8H, m, Ar), 6.90–6.85 (4H, m, Ar), 6.34 (1H, d, $J = 4.4$ Hz, $H1'_B$), 6.31 (1H, d, $J = 4.6$ Hz, $H1'_A$), 4.64 (1H, dt, $J = 10.3$, 5.9 Hz, $H3'_A$), 4.60 (1H, dt, $J = 10.3$, 5.8 Hz, $H3'_B$), 4.36–4.33 (1H, m, $H4'_A$), 4.31–4.29 (1H, m, $H4'_B$), 4.00–3.77 (2H, m, $(CH_2CN)_B$), 3.82 (6H, s, $(ArOCH_3)_A$), 3.81 (6H, s, $(ArOCH_3)_B$), 3.72–3.54 (6H, m, H5′, $2\times CH(CH_3)_2$, $(CH_2CN)_A$), 3.53–3.44 (2H, m, H2′, H5′), 2.63 (2H, t, $J = 6.4$ Hz, $(POCH_2)_B$), 2.39 (2H, t, $J = 6.3$ Hz, $(POCH_2)_A$), 2.33 (1H, d, $J = 2.5$ Hz, CCH_B), 2.29 (1H, d, $J = 2.5$ Hz,

CCH_A), 1.31–1.16 (21H, m, 4×(CHCH_3)$_A$, 3×(CHCH_3)$_B$), 1.04 (3H, d, $J = 6.8$ Hz, (CHCH_3)$_B$); **^{13}C NMR** (100 MHz, $CDCl_3$) δ_C 162.3, 158.8, 144.1, 144.0, 135.4, 135.3, 135.2, 135.1, 133.2, 130.3, 130.3, 130.2, 130.2, 129.0, 128.4, 128.3, 128.1, 127.7, 127.3, 117.7, 117.5, 113.4, 89.5, 87.3, 87.2, 84.1 (d, $^3J_{CP} = 3.4$ Hz), 83.8 (d, $^3J_{CP} = 4.9$ Hz), 77.8, 74.9, 74.9, 72.0 (d, $^2J_{CP} = 15.1$ Hz), 71.3 (d, $^2J_{CP} = 15.2$ Hz), 61.7, 61.5, 60.4, 58.8 (d, $^3J_{CP} = 17.6$ Hz), 58.1 (d, $^3J_{CP} = 19.6$ Hz), 57.9, 55.3, 55.3, 53.5, 43.4 (d, $^2J_{CP} = 6.1$ Hz), 43.3 (d, $^2J_{CP} = 5.9$ Hz), 42.7 (d, $^3J_{CP} = 3.7$ Hz), 24.7, 24.7, 24.7, 24.6, 24.6, 24.6, 20.5 (d, $^2J_{CP} = 6.6$ Hz), 20.3 (d, $^2J_{CP} = 7.1$ Hz); **^{31}P NMR** (162 MHz, $CDCl_3$) δ_P 150.4, 150.3; **HRMS** (ES+) calc. for $C_{48}H_{52}O_8N_5NaP$ $[M+Na]^+$ 880.34457, found 880.34399; $[\alpha]_D^{25} = +42.8$ ($c = 1.0$, $CHCl_3$).

7.5 Synthesis of 2′-ethynyl-2′-deoxyadenosine derivatives

7.5.1 3′,5′-*O*-(Tetraisopropyldisiloxyl)-arabinoadenosine, 77



77

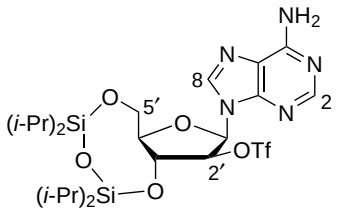
To a solution of 9-β-D-arabinofuranosyladenine **76** (500 mg, 1.87 mmol, 1.0 equiv.) and imidazole (484 mg, 7.11 mmol, 3.8 equiv.) in dry DMF (6 mL) was added 1,3-dichloro-1,1,3,3-tetraisopropyldisiloxane (659 µL, 2.06 mmol, 1.1 equiv.) dropwise. The reaction mixture was stirred at room temperature for 3 h before being quenched with ice-water (5 mL). The mixture was extracted with CH_2Cl_2 (3×40 mL). The solvent was removed *in vacuo* and the residue purified by column chromatography (methanol / CH_2Cl_2 (1 : 19)) to give disiloxane **77** as a white foam (707 mg, 1.39 mmol, 74%).

$\mathbf{R}_f$ 0.33 (methanol / CH_2Cl_2 (1 : 19)); **IR** (solid, ν_{max} / cm^{-1}) 3349, 3165, 1656, 1599, 1465, 1031, 696; **^{1}H NMR** (400 MHz, $CDCl_3$) δ_H 8.13 (1H, s, H2), 8.10 (1H, s, H8), 6.38 (2H, bs, NH_2), 6.20 (1H, d, $J = 6.0$ Hz, H1′), 5.74 (1H, bs, O*H*), 4.67–4.60 (1H, m, H3′),

4.60–4.53 (1H, m, H2′), 4.06–4.00 (2H, m, H5′), 3.87–3.80 (1H, m, H4′), 1.14–0.92 (28H, m, 4× *i*-Pr); **^{13}C NMR** (100 MHz, $CDCl_3$) δ_C 155.7, 152.6, 149.5, 140.2, 119.6, 84.0, 81.4, 76.7, 74.7, 61.6, 17.6, 17.5, 17.5, 17.2, 17.1, 17.0, 13.6, 13.2, 13.0, 12.5.

Data consistent with literature values.[169]

7.5.2 3′,5′-*O*-(Tetraisopropyldisiloxyl)-2′-*O*-triflylarabinoadenosine, 78



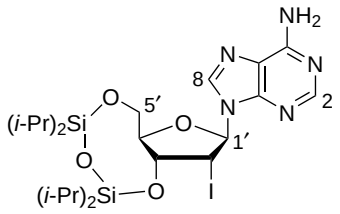
78

Alcohol **77** (1.00 g, 1.96 mmol, 1.0 equiv.) and DMAP (264 mg, 2.16 mmol, 1.1 equiv.) were dissolved in dry CH_2Cl_2 under N_2. Triethylamine (300 µL, 2.16 mmol, 1.1 equiv.) was added and the reaction mixture was cooled to 0 °C. Triflyl chloride (310 µL, 2.94 mmol, 1.5 equiv.) was added dropwise, and the solution was stirred at room temperature for 1.5 h. The reaction was quenched with ice-water (20 mL) and the phases were separated. The aqueous phase was extracted with CH_2Cl_2 (3 × 20 mL) and the combined organic phases were dried over Na_2SO_4. The solvent was removed *in vacuo* and the residue purified by column chromatography (methanol / CH_2Cl_2 (1 : 19)) to give triflate **78** as a white foam (1.15 mg, 1.79 mmol, 91%).

R_f 0.25 (methanol / CH_2Cl_2 (1 : 19)); **IR** (solid, ν_{max} / cm^{-1}) 3326, 3170, 1648, 1598, 1424, 1141, 1037, 884; **^{1}H NMR** (500 MHz, $CDCl_3$) δ_H 8.32 (1H, s, H2), 7.92 (1H, s, H8), 6.39 (1H, d, $J = 6.0$ Hz, H1′), 5.83 (1H, bs, NH_2), 5.47 (1H, t, $J = 6.3$ Hz, H2′), 5.39 (1H, t, $J = 6.9$ Hz, H3′), 4.22 (1H, dd, $J = 12.3, 6.1$ Hz, H5′), 4.08 (1H, dd, $J = 12.3, 3.3$ Hz, H5′), 3.98–3.92 (1H, m, H4′), 1.26–0.88 (28H, m, 4×*i*-Pr); **^{13}C NMR** (125 MHz, $CDCl_3$) δ_C 155.7, 153.4, 149.8, 139.7, 120.0, 118.3 (q, $^1J_{CF} = 320$ Hz), 88.6, 81.3, 80.9, 74.5, 62.2, 17.6, 17.5, 17.4, 17.4, 17.2, 17.2, 17.0, 16.9, 16.9, 16.9, 13.4, 13.2, 13.1, 12.7.

Data consistent with literature values.[169]

7.5.3 3′,5′-*O*-(Tetraisopropyldisiloxyl)-2′-iodo-2′-deoxyadenosine, 79



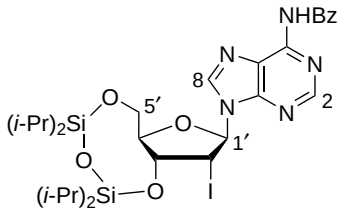
79

Triflate **78** (1.108 g, 1.73 mmol, 1.0 equiv.) and LiI (996 mg, 7.44 mmol, 4.3 equiv.) were dissolved in dry DMF (17 mL) under N_2 and stirred at 40 °C for 26 h. The reaction was quenched with ice-water (10 mL) and the mixture was extracted with CH_2Cl_2 (3×30 mL). The combined organic phases were washed with $Na_2S_2O_3$ (*aq.* sat., 10 mL) until the colour faded. The aqueous washing was diluted with H_2O (10 mL) and back-extracted with CH_2Cl_2 (3×10 mL). The combined organic layers were dried over Na_2SO_4. The solvent was removed *in vacuo* and the residue dried under high vacuum at 40 °C to remove residual DMF, before purification by column chromatography (methanol / CH_2Cl_2 (1 : 19)) to give iododeoxynucleoside **79** as a white foam (912 mg, 1.61 mmol, 93%).

$\mathbf{R}_f$ 0.41 (methanol / CH_2Cl_2 (1 : 19)); **IR** (solid, ν_{max} / cm^{-1}) 3328, 3178, 2360, 2341, 1671, 1648, 1465, 991; **^{1}H NMR** (400 MHz, $CDCl_3$) δ_H 8.30 (1H, s, H2), 8.04 (1H, s, H8), 6.54 (1H, d, $J = 2.1$ Hz, H1′), 6.35 (2H, bs, NH_2), 5.00 (1H, dd, $J = 5.7, 2.2$ Hz, H2′), 4.22–4.11 (3H, m, H3′, H5′), 4.06–3.99 (1H, m, H4′), 1.12–0.93 (28H, m, 4×*i*-Pr); **^{13}C NMR** (100 MHz, $CDCl_3$) δ_C 155.9, 153.3, 149.1, 138.9, 120.4, 92.2, 84.1, 68.5, 60.8, 34.3, 17.5, 17.4, 17.4, 17.4, 17.2, 17.1, 17.1, 17.1.

Data consistent with literature values.[169]

7.5.4 6-*N*-Benzoyl-3′,5′-*O*-(tetraisopropyldisiloxyl)-2′-iodo-2′-deoxyadenosine, 80

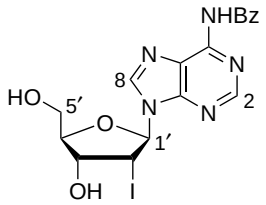


80

Amine **79** (600 mg, 0.969 mmol, 1.0 equiv.) was dissolved in dry pyridine (10 mL) under N_2. Benzoyl chloride (340 µL, 2.91 mmol, 3.0 equiv.) was added dropwise, and the mixture was stirred at room temperature for 4 h 15 min. A solution of NH_3 (25% *aq.*, 3 mL) was added dropwise and the reaction mixture was stirred for 10 min. The solution was diluted with $NaHCO_3$ (*aq.* sat., 20 mL) and extracted with CH_2Cl_2 (3×50 mL). The combined organic layers were dried over Na_2SO_4 and the solvent was removed *in vacuo*. Residual pyridine was removed by co-evaporation with toluene (3×5 mL). The residue was purified by column chromatography (ethyl acetate / petroleum ether (1 : 1)) to give benzamide **80** as a white foam (508 mg, 0.702 mmol, 72%).

$\mathbf{R}_f$ 0.39 (ethyl acetate / petroleum ether (1 : 1)); **m.p.** 79–84 °C; **IR** (solid, ν_{max} / cm^{-1}) 3328, 3178, 2360, 2341, 1671, 1648, 1465, 991; **^{1}H NMR** (400 MHz, $CDCl_3$) δ_H 9.41 (1H, s, N*H*), 8.70 (1H, s, H2), 8.21 (1H, s, H8), 7.97 (2H, d, $J = 7.4$ Hz, Bz), 7.53 (1H, t, $J = 7.6$ Hz, Bz), 7.44 (2H, t, $J = 7.6$ Hz, Bz), 6.59 (1H, d, $J = 2.1$ Hz, H1′), 5.00 (1H, dd, $J = 5.8, 2.0$ Hz, H2′), 4.22–4.09 (3H, m, H3′, H4′, H5′), 4.06–3.97 (1H, m, H5′), 1.13–0.91 (28H, m, 4×*i*-Pr); **^{13}C NMR** (100 MHz, $CDCl_3$) δ_C 164.9, 152.8, 150.9, 149.8, 141.4, 133.6, 132.7, 128.8, 127.9, 123.8, 92.2, 84.1, 68.4, 60.6, 33.8, 17.5, 17.3, 17.3, 17.3, 17.2, 17.0, 17.0, 17.0, 13.3, 13.0, 12.8, 12.7; **HRMS** (ES+) calc. for $C_{29}H_{42}IN_5NaO_5Si_2$ $[M+Na]^+$ 746.1667, found 746.1661; $\mathbf{[\alpha]_D^{20}}$ −68.9 ($c = 1.0$, $CHCl_3$).

7.5.5 6-*N*-Benzoyl-2′-iodo-2′-deoxyadenosine, 81

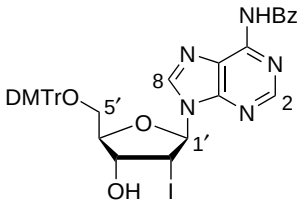


81

To a solution of disiloxane **80** (343 mg, 0.474 mmol, 1.0 equiv.) in THF (5 mL) was added a solution of TBAF (1.0 M in THF, 1.2 mL, 1.2 mmol, 2.5 equiv.). The reaction mixture was stirred for 30 min before methanol (1 mL) and then silica gel (ca. 1 g) were added. The solvent was carefully removed *in vacuo* until the silica gel was free-flowing. The silica gel was dry-loaded onto a short column and the mixture was purified by column chromatography (methanol / CH_2Cl_2 (4 : 96 to 5 : 95)). Diol **81** was obtained as a white foam (229 mg, 0.474 mmol, quant.).

$\mathbf{R}_f$ 0.14 (methanol / CH_2Cl_2 (5 : 95)); **m.p.** 116–120 °C; **IR** (solid, ν_{max} / cm^{-1}) 3274, 2929, 1697, 1611, 1582, 1455, 1089; **^{1}H NMR** (400 MHz, $CDCl_3$) δ_H 9.32 (1H, s, N*H*), 8.76 (1H, s, H2), 8.08 (1H, s, H8), 8.02 (2H, d, $J = 7.6$ Hz, Bz), 7.61 (1H, t, $J = 7.3$ Hz, Bz), 7.52 (2H, t, $J = 7.6$ Hz, Bz), 6.20 (1H, d, $J = 9.3$ Hz, H1′), 6.09–6.06 (1H, m, 5′-O*H*), 5.22 (1H, dd, $J = 9.3, 4.3$ Hz, H2′), 4.50 (1H, d, $J = 4.2$ Hz, H3′), 4.45–4.43 (1H, m, H4′), 3.99 (1H, d, $J = 13.0$ Hz, H5′), 3.79 (1H, t, $J = 11.9$ Hz, H5′), 3.72 (1H, bs, 3′-O*H*); **^{13}C NMR** (100 MHz, $CDCl_3$) δ_C 164.8, 152.4, 150.6, 150.5, 143.2, 133.5, 133.2, 129.1, 128.1, 124.6, 94.0, 87.5, 73.7, 63.2, 32.2; **HRMS** (ES+) calc. for $C_{17}H_{16}IN_5NaO_4$ $[M+Na]^+$ 504.0139, found 504.0145; $\mathbf{[\alpha]_D^{20}}$ −13.6 ($c = 1.0$, $CHCl_3$).

7.5.6 6-*N*-Benzoyl-5′-*O*-(4,4′-dimethoxytrityl)-2′-iodo-2′-deoxyadenosine, 82

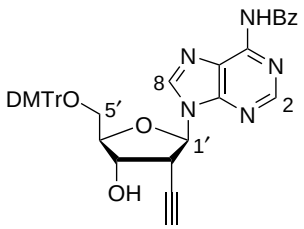


82

A solution of alcohol **81** (288 mg, 0.474 mmol, 1.0 equiv.) in dry pyridine (3 mL) was added to 4,4′-dimethoxytrityl chloride (193 mg, 0.569 mmol, 1.2 equiv.) under N_2. The reaction mixture was stirred at room temperature for 15 h before being diluted with CH_2Cl_2 (20 mL). The mixture was washed with $NaHCO_3$ (5% *aq.*, 2×20 mL), H_2O (20 mL) and brine (5 mL) and dried over Na_2SO_4. The solvent was removed *in vacuo*. Residual pyridine was removed by co-evaporation with toluene (2×10 mL) at 30 °C. The residue was purified by column chromatography (methanol / CH_2Cl_2 (3 : 97 to 4 : 96)) to afford protected 2′-iodo-2′-deoxyadenosine derivative **82** as a white foam (355 mg, 0.453 mmol, 96%).

$\mathbf{R}_f$ 0.61 (ethyl acetate); **m.p.** 108–112 °C; **IR** (thin film, ν_{max} / cm^{-1}) 3315, 3003, 1704, 1610, 1509, 1250, 754; **^{1}H NMR** (400 MHz, $CDCl_3$) δ_H 9.13 (1H, s, N*H*), 8.64 (1H, s, H2), 8.09 (1H, s, H8), 7.97 (2H, d, $J = 7.4$ Hz, Bz), 7.56 (1H, t, $J = 7.4$ Hz, Bz), 7.47 (2H, t, $J = 7.5$ Hz, Bz), 7.38–7.36 (2H, m, Ar), 7.30–7.14 (7H, m, Ar), 6.77–6.75 (4H, m, Ar), 6.37 (1H, d, $J = 8.0$ Hz, H1′), 5.38 (1H, dd, $J = 7.9, 4.6$ Hz, H2′), 4.36–4.31 (1H, m, H4′), 4.30–4.25 (1H, m, H3′), 3.73 (6H, s, ArOCH_3), 3.49 (1H, dd, $J = 10.6, 4.4$ Hz, H5′), 3.37 (1H, dd, $J = 10.6, 4.1$ Hz, H5′), 3.33 (1H, bs, O*H*); **^{13}C NMR** (100 MHz, $CDCl_3$) δ_C 164.8, 158.7, 152.9, 151.8, 149.7, 144.5, 142.2, 135.6, 135.6, 133.7, 133.0, 130.1, 130.1, 129.0, 128.2, 128.1, 128.0, 127.1, 123.6, 113.3, 91.0, 86.9, 84.2, 72.6, 63.4, 55.4, 31.4; **HRMS** (ES+) calc. for $C_{38}H_{34}IN_5NaO_6$ $[M+Na]^+$ 806.1451, found 806.1436; $[\alpha]_D^{20}$ −22.2 ($c = 1.0$, $CHCl_3$).

7.5.7 6-*N*-Benzoyl-5′-*O*-(4,4′-dimethoxytrityl)-2′-ethynyl-2′-deoxyadenosine, 84



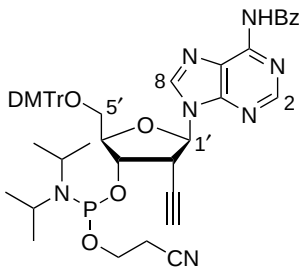
84

Aminosilane **57** (340 µL, 1.22 mmol, 2.0 equiv.) was dissolved in dry CH_2Cl_2 (3 mL) under Ar. Methyl iodide (150 µL, 2.44 mmol, 4.0 equiv.) was added dropwise. The solution was stirred for 1 h at room temperature before being cannulated into a solution of alcohol **82** (479 mg, 0.611 mmol, 1.0 equiv.), imidazole (104 mg, 1.53 mmol, 2.5 equiv.) and DMAP (15 mg, 0.122 mmol, 0.2 equiv.) in dry CH_2Cl_2 (3 mL) under Ar. The reaction mixture was stirred for 2 h at room temperature. The solvent was removed *in vacuo*, and the remaining residue redissolved in ethyl acetate (50 mL). The solution was washed with H_2O (3×20 mL) and brine (20 mL) and dried over Na_2SO_4. The solvent was removed *in vacuo*, and the residual white foam was dried under high vacuum.

The crude material was dissolved in dry benzene (6.1 mL). The reaction vessel was flushed with N_2 and then sealed. 2,6-Lutidine (7.1 µL, 0.061 mmol, 0.1 equiv.) was added, before a solution of BEt_3 (1.0 M in hexane, 61 µL, 0.061 mmol, 0.1 equiv.) was added dropwise. The reaction mixture was stirred at room temperature and monitored by TLC analysis. Reinitiation of the reaction by addition of 2,6-lutidine (14.2 µL, 0.122 mmol, 0.2 equiv.) and BEt_3 (1.0 M in hexane, 122 µL, 0.122 mmol, 0.2 equiv.) was necessary after 40 min, 2.5 h and 3.5 h. After 4.5 h a solution of TBAF (1.0 M in THF, 1.53 mL, 1.53 mmol, 2.5 equiv.) was added and the solution was stirred for another hour. The solvent was removed *in vacuo*, and the remaining residue redissolved in ethyl acetate (50 mL) and washed with $NaHCO_3$ (5% *aq.*, 3×50 mL). After drying over Na_2SO_4 the solvent was removed *in vacuo*, and the residue was purified by column chromatography (ethyl acetate / petroleum ether (75 : 25 to 1 : 0)). Alkyne **84** was isolated as a white foam (211 mg, 0.310 mmol, 51%).

R_f 0.38 (methanol / CH_2Cl_2 (5 : 95)); **m.p.** 160–165 °C; **IR** (solid, ν_{max} / cm^{-1}) 3281, 2931, 1703, 1608, 1581, 1508, 1247, 1029, 704; **^{1}H NMR** (400 MHz, $CDCl_3$) δ_H 9.10 (1H, bs, N*H*), 8.68 (1H, s, H2), 8.16 (1H, s, H8), 8.02 (2H, d, $J = 7.3$ Hz, Bz), 7.60 (1H, t, $J = 7.4$ Hz, Bz), 7.51 (2H, t, $J = 7.5$ Hz, Bz), 7.41 (2H, d, $J = 7.1$ Hz, Ar), 7.33–7.18 (7H, m, Ar), 6.82–6.78 (4H, m, Ar), 6.31 (1H, d, $J = 8.5$ Hz, H1′), 4.61–4.57 (1H, m, H3′), 4.32 (1H, td, $J = 4.1, 1.5$ Hz, H4′), 4.28–4.20 (1H, m, H2′), 3.77 (6H, s, ArOCH_3), 3.49 (1H, dd, $J = 10.5, 4.4$ Hz, H5′), 3.36 (1H, dd, $J = 10.5, 4.1$ Hz, H5′), 2.97 (1H, d, $J = 2.4$ Hz, O*H*), 2.30 (1H, d, $J = 2.4$ Hz, CC*H*); **^{13}C NMR** (100 MHz, $CDCl_3$) δ_C 164.7, 158.7, 152.9, 152.1, 149.7, 144.5, 142.1, 135.7, 135.7, 133.7, 132.9, 130.1, 130.1, 129.0, 128.2, 128.1, 128.0, 127.1, 123.7, 113.3, 87.8, 86.8, 85.5, 76.4, 76.1, 73.4, 63.5, 55.4, 42.2; **HRMS** (ES+) calc. for $C_{40}H_{35}N_5NaO_6$ $[M+Na]^+$ 704.2480, found 704.2476; $[\alpha]_D^{20} = -28.1$ ($c = 1.0$, $CHCl_3$).

7.5.8 6-*N*-Benzoyl-5′-*O*-(4,4′-dimethoxytrityl)-2′-ethynyl-2′-deoxyadenosine-3′-(2-cyanoethyl-*N*,*N*-diisopropyl)phosphoramidite, 92



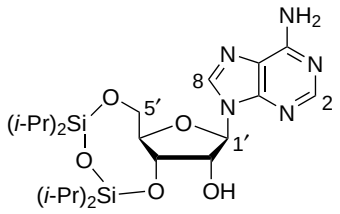
92

Alcohol **84** (190 mg, 0.279 mmol, 1.0 equiv.) was dried by co-evaporation with dry pyridine (3×3 mL) and dry CH_2Cl_2 (3×3 mL) in a pre-dried flask and dried under high vacuum. A pre-dried and Ar-flushed stirrer bar and activated molecular sieves (4 Å) was added, and the flask was evacuated and purged with Ar three times. Dry CH_2Cl_2 (2 mL) and dry DIPEA (250 µL, 1.40 mmol, 5.0 equiv.) were added to the flask. Over stirring, 2-cyanoethyl *N*,*N*-diisopropylchlorophosphoramidite (**93**, 187 µL, 0.873 mmol, 3.0 equiv.) was added dropwise over several minutes. The reaction mixture was stirred for 1 h until TLC analysis

showed complete conversion. The reaction mixture was transferred to dry CH_2Cl_2 (20 mL) under Ar, and washed with an Ar-purged solution of KCl (*aq.* sat., 10 mL). The solution was dried (Na_2SO_4) under Ar, and the solvent was removed *in vacuo*. The residue was dried under high vacuum, and purified by column chromatography (ethyl acetate / petroleum ether (75 : 25)) under an Ar blanket to give phosphoramidite **92** (1.6 : 1 mixture of diastereomers A (major) and B (minor)) as a white foam (238 mg, 0.270 mmol, 97%).

$\mathbf{R_f}$ 0.47, 0.39 (ethyl acetate / petroleum ether (75 : 25)); **m.p.** 90–95 °C; **IR** (solid, ν_{max} / cm^{-1}) 2967, 2251, 1703, 1608, 1581, 1455, 1248, 1028, 909, 728; **^{1}H NMR** (400 MHz, $CDCl_3$) δ_H 9.18 (1H, bs, N*H*), 6.65–6.64 (1H, 2 × s, H2), 8.18–8.17 (1H, 2 × s, H8), 7.99 (2H, d, $J = 7.5$ Hz, Bz), 7.55 (1H, t, $J = 7.3$ Hz, Bz), 7.49–7.40 (4H, m, Ar, Bz), 7.33–7.17 (7H, m, Ar), 6.82–6.78 (4H, m, Ar), 6.33 (1H, d, $J = 8.2$ Hz, $H1'_A$), 6.27 (1H, d, $J = 8.5$ Hz, $H1'_B$), 4.76–4.68 (1H, m, H3′), 4.46–4.44 (1H, m, $H4'_B$), 4.40–4.37 (1H, m, $H4'_A$), 4.33–4.28 (1H, m, H2′), 4.04–3.87 (2H, m, $(POCH_2)_A$), 3.76–3.75 (6H, 2 × s, $ArOCH_3$), 3.74–3.47 (5H, m, H5′, 2× $CH(CH_3)_2$, $(POCH_2)_B$), 3.36–3.33 (1H, m, H5′), 2.63 (2H, t, $J = 6.4$ Hz, $(CH_2CN)_A$), 2.39 (2H, t, $J = 6.4$ Hz, $(CH_2CN)_B$), 2.24 (1H, d, $J = 2.3$ Hz, CCH_A), 2.16 (1H, d, $J = 2.3$ Hz, CCH_B), 1.30–1.19 (18H, m, 2× $(CHCH_3)_A$, 4× $(CHCH_3)_B$), 1.09 (6H, d, $J = 6.8$ Hz, 2× $(CHCH_3)_A$); **^{13}C NMR** (100 MHz, $CDCl_3$) δ_C 164.7, 158.6, 152.7, 152.1, 152.0, 149.7, 144.5, 144.4, 142.1, 135.7, 135.6, 135.5, 133.7, 132.8, 130.1, 130.1, 128.8, 128.2, 128.2, 127.9, 127.9, 127.0, 123.9, 117.6, 117.4, 113.2, 88.2, 88.1, 86.8, 86.7, 85.9, 85.5 (d, $^3J_{CP} = 3.0$ Hz), 77.1, 76.7, 75.3 (d, $^2J_{CP} = 15.5$ Hz), 75.0, 74.6, 73.9 (d, $^2J_{CP} = 18.3$ Hz), 63.3, 63.1, 59.3 (d, $^2J_{CP} = 16.8$ Hz), 58.0 (d, $^2J_{CP} = 19.6$ Hz), 55.2, 43.4 (d, $^2J_{CP} = 12.8$ Hz), 43.3 (d, $^2J_{CP} = 12.4$ Hz), 41.0 (d, $^3J_{CP} = 3.4$ Hz), 40.8 (d, $^3J_{CP} = 5.3$ Hz), 24.8, 24.7, 24.7, 24.6, 24.6, 24.5, 24.5, 20.5 (d, $^3J_{CP} = 6.2$ Hz), 20.2 (d, $^3J_{CP} = 7.2$ Hz); **^{31}P NMR** (162 MHz, $CDCl_3$) δ_P 150.6, 149.9; **HRMS** (ES+) calc. for $C_{49}H_{53}N_7O_7P$ $[M+H]^+$ 882.37386, found 882.37299.

7.5.9 3′,5′-*O*-(Tetraisopropyldisiloxyl)-adenosine, 95



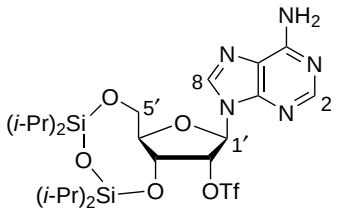
95

Adenosine (**94**, 1.00 g, 3.74 mmol, 1.0 equiv.) was dissolved in dry pyridine (20 mL) under N_2 and 1,3-dichloro-1,1,3,3-tetraisopropyldisiloxane (1.44 mL, 4.49 mmol, 1.2 equiv.) was added dropwise over stirring. The reaction was stirred under N_2 for 28 h, and quenched with ice-water (10 mL). The mixture was extracted with CH_2Cl_2 (3×50 mL) and the organic extracts were dried over Na_2SO_4. The solvent was removed *in vacuo*, and residual pyridine was removed by co-evaporation with toluene (2×20 mL). The crude product was purified by column chromatography (methanol / CH_2Cl_2 (3 : 97 to 4 : 96)) to give disiloxane **95** as a white foam (1.665 g, 3.27 mmol, 87%).

$\mathbf{R}_f$ 0.44 (methanol / CH_2Cl_2 (1 : 9)); **IR** (solid, ν_{max} / cm^{-1}) 3326, 3158, 2944, 2867, 1643, 1599, 1465, 1035, 649; **^{1}H NMR** (400 MHz, $CDCl_3$) δ_H 8.27 (1H, s, H2), 8.00 (1H, s, H8), 6.15 (2H, bs, NH_2), 6.00 (1H, d, $J = 0.8$ Hz, H1′), 5.02 (1H, dd, $J = 8.0$, 5.3 Hz, H3′), 4.57 (1H, d, $J = 5.3$ Hz, H2′), 4.18–4.10 (2H, m, H4′, H5′), 4.07–4.00 (1H, m, H5′), 3.95 (1H, bs, O*H*), 1.14–0.95 (28H, m, 4× *i*-Pr); **^{13}C NMR** (100 MHz, $CDCl_3$) δ_C 155.8, 153.1, 149.2, 139.5, 120.5, 89.9, 82.2, 75.2, 70.7, 61.7, 17.6, 17.5, 17.5, 17.4, 17.2, 17.1, 17.1, 17.0, 13.4, 13.2, 12.9, 12.7.

Data consistent with literature values.[243]

7.5.10 3′,5′-*O*-(Tetraisopropyldisiloxyl)-2′-*O*-triflyladenosine, 96



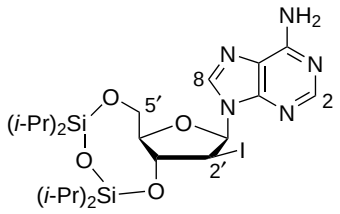
96

Alcohol **95** (500 mg, 0.981 mmol, 1.0 equiv.) and DMAP (132 mg, 1.08 mmol, 1.1 equiv.) were dissolved in dry CH_2Cl_2 (10 mL) under N_2. Triethylamine (150 µL, 1.08 mmol, 1.1 equiv.) was added and the reaction mixture was cooled to 0 °C. Trifluoromethanesulfonyl chloride (156 µL, 1.47 mmol, 1.5 equiv.) was added dropwise, the cooling bath was removed and the reaction mixture was stirred for 5 h at room temperature. The reaction was quenched with ice-water (10 mL) and the biphasic mixture was separated. The aqueous phase was extracted with CH_2Cl_2 (3×20 mL) and the combined organic layers were dried over Na_2SO_4. The solvent was removed *in vacuo*, and the crude residue was purified by column chromatography (methanol / CH_2Cl_2 (4 : 96)) to afford triflate **96** as a white foam (559 mg, 0.871 mmol, 89%).

$\mathbf{R}_f$ 0.44 (methanol / CH_2Cl_2 (1 : 9)); **IR** (solid, ν_{max} / cm^{-1}) 3287, 3135, 2947, 1691, 1637, 1610, 1423, 1207; **^{1}H NMR** (400 MHz, $CDCl_3$) δ_H 8.26 (1H, s, H2), 7.96 (1H, s, H8), 6.10 (1H, s, H1′), 5.82–5.81 (3H, m, NH_2, H2′), 5.30 (1H, dd, $J = 9.2, 4.8$ Hz, H3′), 4.18 (1H, dd, $J = 13.2, 1.8$ Hz, H5′), 4.09 (1H, dt, $J = 9.3, 2.2$ Hz, H4′), 4.04 (1H, dd, $J = 13.2, 2.7$ Hz, H5′), 1.15–0.99 (28H, m, 4× *i*-Pr); **^{13}C NMR** (100 MHz, $CDCl_3$) δ_C 155.7, 153.5, 149.2, 139.4, 120.4, 118.7 (q, $^1J_{CF} = 309$ Hz), 88.5, 87.1, 81.6, 68.3, 59.7, 17.5, 17.4, 17.4, 16.9, 16.9, 16.8, 13.3, 13.0, 12.9, 12.9.

Data consistent with literature values.[244]

7.5.11 3′,5′-*O*-(Tetraisopropyldisiloxyl)-2′-iodo-2′-deoxyarabinoadenosine, 97



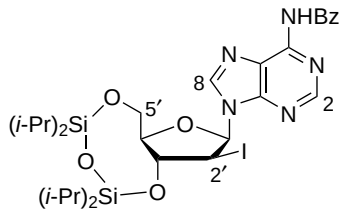
97

Triflate **96** (515 mg, 0.802 mmol, 1.0 equiv.) and LiI (430 mg, 3.21 mmol, 4.0 equiv.) were dissolved in dry DMF (4 mL) under N_2 and stirred at 40 °C for 20 h. The reaction was quenched with ice-water (10 mL) and the resulting mixture was extracted with CH_2Cl_2 (3×20 mL). The combined organic extracts were washed with $Na_2S_2O_3$ (*aq.* sat., 2 mL) until they turned colourless. The aqueous layer was diluted with H_2O (10 mL) and back-extracted with CH_2Cl_2 (2×20 mL). The total combined organic phases were dried over Na_2SO_4. The solvent was removed *in vacuo* and the residue was dried under high vacuum at 40 °C to remove residual DMF. The crude product was purified by column chromatography (methanol / CH_2Cl_2 (5 : 95)) to give iodide **97** as a light yellow foam (343 mg, 0.554 mmol, 69%).

$\mathbf{R}_f$ 0.52 (methanol / CH_2Cl_2 (1 : 9)); **IR** (solid, ν_{max} / cm^{-1}) 3319, 3158, 2944, 1644, 1596, 1465, 1033, 693; **^{1}H NMR** (400 MHz, $CDCl_3$) δ_H 8.35 (1H, s, H2), 8.11 (1H, s, H8), 6.28 (1H, d, $J = 6.7$ Hz, H1′), 5.99 (1H, bs, NH_2), 4.96 (1H, dd, $J = 9.0, 8.1$ Hz, H3′), 4.72 (1H, dd, $J = 9.3, 6.7$ Hz, H2′), 4.24 (1H, dd, $J = 12.9, 3.5$ Hz, H5′), 4.09 (1H, dd, $J = 12.9, 3.1$ Hz, H5′), 3.87 (1H, dd, $J = 7.6, 3.4$ Hz, H4′), 1.20–0.99 (28H, m, 4× *i*-Pr); **^{13}C NMR** (100 MHz, $CDCl_3$) δ_C 155.7, 153.2, 149.9, 138.6, 119.8, 84.3, 84.0, 77.0, 61.3, 30.8, 17.6, 17.5, 17.5, 17.4, 17.3, 17.2, 17.1, 14.0, 13.2, 13.0, 12.6.

Data consistent with literature values.[244]

7.5.12 4-*N*-Benzoyl-3′,5′-*O*-(tetraisopropyldisiloxyl)-2′-iodo-2′-deoxyarabino-adenosine, 98

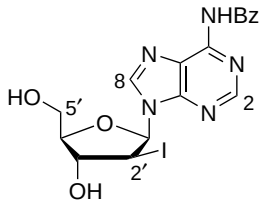


98

Iodide **97** (220 mg, 0.355 mmol, 1.0 equiv.) was dissolved in dry pyridine (2 mL) under N_2. The solution was cooled to 0 °C, and benzoyl chloride (124 µL, 1.07 mmol, 3.0 equiv.) was added dropwise. The reaction mixture was stirred at room temperature for 29 h, before NH_3 (25% *aq.*, 1 mL) was added. The reaction was stirred for another 10 min, before being diluted with $NaHCO_3$ (*aq.* sat., 15 mL). The mixture was extracted with CH_2Cl_2 (3×20 mL) and the combined extracts were dried over Na_2SO_4. The solvent was removed *in vacuo*, and residual pyridine was removed by co-evaporation with toluene (3×5 mL). The crude product was purified by column chromatography (ethyl acetate / petroleum ether (45 : 55 to 1 : 1)) to give amide **98** as a white foam (260 mg, 0.359 mmol, quant.).

$\mathbf{R}_f$ 0.36 (ethyl acetate / petroleum ether (6 : 4)); **m.p.** 94–97 °C; **IR** (solid, ν_{max} / cm^{-1}) 2945, 1701, 1610, 1581, 1455, 1034, 701; **^{1}H NMR** (400 MHz, $CDCl_3$) δ_H 9.36 (1H, s, N*H*), 8.77 (1H, s, H2), 8.26 (1H, s, H8), 7.99 (2H, d, $J = 7.2$ Hz, Bz), 7.55 (1H, t, $J = 7.4$ Hz, Bz), 7.46 (2H, t, $J = 7.5$ Hz, Bz), 6.34 (1H, d, $J = 6.8$ Hz, H1′), 4.99–4.94 (1H, m, H3′), 4.73 (1H, dd, $J = 9.6, 6.8$ Hz, H2′), 4.23 (1H, dd, $J = 12.9, 3.7$ Hz, H5′), 4.07 (1H, dd, $J = 12.8, 3.0$ Hz, H5′), 3.88 (1H, t, $J = 11.9$ Hz, H4′), 1.15–1.02 (28H, m, 4× *i*-Pr); **^{13}C NMR** (100 MHz, $CDCl_3$) δ_C 168.4, 152.8, 151.6, 149.8, 141.0, 133.8, 132.7, 128.9, 127.9, 123.1, 84.3, 84.2, 77.0, 61.2, 30.5, 17.5, 17.5, 17.4, 17.3, 17.2, 17.1, 17.1, 13.9, 13.1, 12.9, 12.5; **HRMS** (ES+) calc. for $C_{29}H_{43}O_5N_5ISi_2$ $[M+H]^+$ 724.18419, found 724.18182; $[\alpha]_D^{20} = -51$ ($c = 1.1$, $CHCl_3$).

7.5.13 4-*N*-Benzoyl-2′-iodo-2′-deoxyarabinoadenosine, 99

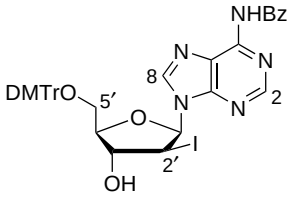


99

Acetic acid (18.5 µL, 0.318 mmol, 2.5 equiv.) was added to a solution of disiloxane **98** (100 mg, 0.127 mmol, 1.0 equiv.) in THF (1.3 mL). A solution of TBAF (1.0 M in THF, 0.32 mL, 0.32 mmol, 2.5 equiv.) was added and the reaction mixture was stirred at room temperature for 20 min. Silica gel (1 g) was added and the solvent was carefully removed *in vacuo* until the silica gel was free-flowing. The residue was purified by column chromatography with dry loading (methanol / CH_2Cl_2 (8 : 92)) to give diol **99** as a white solid (54 mg, 0.112 mmol, 88%).

R_f 0.19 (methanol / CH_2Cl_2 (1 : 9)); **m.p.** 95–99 °C; **IR** (thin film, ν_{max} / cm^{-1}) 3332, 1700, 1644, 1612, 1582, 1457, 1071; **^{1}H NMR** (400 MHz, CD_3OD) δ_H 8.77 (1H, s, H2), 8.71 (1H, s, H8), 8.08 (2H, d, $J = 7.3$ Hz, Bz), 7.65 (1H, t, $J = 6.8$ Hz, Bz), 7.55 (2H, t, $J = 7.6$ Hz, Bz), 6.48 (1H, d, $J = 5.9$ Hz, H1′), 4.84–4.77 (2H, m, H2′, H3′), 4.03–3.89 (3H, m, H4′, H5′); **^{13}C NMR** (100 MHz, CD_3OD) δ_C 168.1, 153.2, 153.1, 151.2, 143.9, 134.9, 133.9, 129.8, 129.4, 124.7, 86.5, 86.2, 77.2, 61.3, 32.3; **HRMS** (ES+) calc. for $C_{17}H_{17}O_4N_5I$ $[M+H]^+$ 482.03116, found 482.03197; **$[\alpha]_D^{20}$** $= -22$ ($c = 0.37$, CH_3OH).

7.5.14 6-*N*-Benzoyl-5′-*O*-(4,4′-dimethoxytrityl)-2′-iodo-2′-deoxyarabinoadenosine, 100



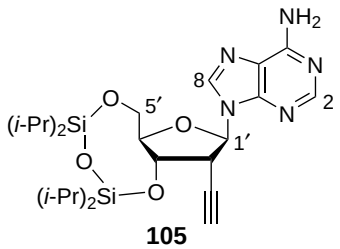
100

To a solution of nucleoside **99** (64 mg, 0.112 mmol, 1.0 equiv.) in dry DMF (1.2 mL) under

Ar was added 2,6-lutidine (16 µL, 0.134 mmol, 1.2 equiv.) and 4,4′-dimethoxytrityl chloride (45 mg, 0.134 mmol, 1.2 equiv.). The reaction mixture was stirred for 49 h, before being quenched with H_2O (10 mL). The mixture was extracted with CH_2Cl_2 (3×20 mL), and the combined extracts were concentrated *in vacuo*. The residue was dried under high vacuum, and purified by column chromatography (ethyl acetate / petroleum ether (7 : 3 to 1 : 0)) to afford protected nucleoside **100** as a white foam (50 mg, 0.064 mmol, 57%). The product was very unstable, and decomposed before full characterisation could be performed.

$\mathbf{R}_f$ 0.06 (ethyl acetate / petroleum ether (6 : 4)); **^{1}H NMR** (400 MHz, $CDCl_3$) δ_H 9.26 (1H, bs, N*H*), 8.74 (1H, s, H2), 8.28 (1H, s, H8), 8.02 (2H, d, $J = 7.3$ Hz, Bz), 7.60 (1H, t, $J = 7.4$ Hz, Bz), 7.51 (2H, t, $J = 7.5$ Hz, Bz), 7.44 (2H, d, $J = 7.2$ Hz, Ar), 7.36–7.16 (7H, m, Ar), 6.83–6.80 (4H, m, Ar), 6.26 (1H, d, $J = 6.1$ Hz, H1′), 4.95–4.90 (1H, m, H3′), 4.73 (1H, t, $J = 6.5$ Hz, H2′), 4.13–4.06 (1H, m, H4′), 3.77 (6H, s, ArOCH_3), 3.65 (1H, dd, $J = 10.4$, 5.4 Hz, H5′), 3.60 (1H, dd, $J = 10.3$, 4.4 Hz, H5′), 2.15 (1H, bs, O*H*); **^{13}C NMR** (100 MHz, $CDCl_3$) δ_C 164.9, 158.7, 158.7, 152.9, 147.4, 144.4, 141.2, 139.6, 135.7, 135.6, 133.7, 133.0, 130.2, 129.3, 129.0, 128.3, 128.1, 128.0, 128.0, 127.9, 127.2, 127.2, 113.4, 113.4, 113.3, 86.9, 85.0, 83.8, 78.7, 63.3, 55.4, 31.9; **HRMS** (ES+) calc. for $C_{38}H_{35}O_6N_5I$ $[M+H]^+$ 784.16265, found 784.16113.

7.5.15 3′,5′-*O*-(Tetraisopropyldisiloxyl)-2′-ethynyl-2′-deoxyadenosine, 105



105

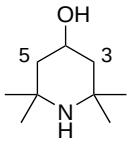
Trimethylsilylacetylene (70 µL, 0.468 mmol, 3.0 equiv.) and CuI (6 mg, 0.031 mmol, 20 mol%) were suspended in dry THF (1 mL) under Ar. The suspension was cooled to −78 °C and *n*-BuLi (2.5 M in hexane, 0.2 mL, 0.5 mmol, 3.2 equiv.) was added dropwise. After stirring for 10 min, a solution of triflate **78** (100 mg, 0.156 mmol, 1.0 equiv.) in dry THF (1 mL) was added dropwise. The reaction mixture was stirred at −78 °C for

30 min, and the cooling bath was allowed to slowly reach room temperature. After stirring at room temperature for 7 h, K_2CO_3 in methanol (10% w/v, 1 mL) was added and the reaction mixture was stirred vigorously for 45 min. H_2O (10 mL) was added and the mixture was extracted with CH_2Cl_2 (3×20 mL). The combined extracts were dried over Na_2SO_4 and the solvent was removed *in vacuo*. The crude product was purified by column chromatography (methanol / CH_2Cl_2 (9 : 191 to 5 : 95)) to give alkyne **105** as a white foam (24 mg, 0.046 mmol, 29%).

$\mathbf{R_f}$ 0.52 (methanol / CH_2Cl_2 (1 : 9)); **m.p.** 108–111 °C; **IR** (solid, ν_{max} / cm^{-1}) 3293, 3161, 2946, 2034, 1648, 1600, 1465, 1056; **^{1}H NMR** (500 MHz, $CDCl_3$) δ_H 8.35 (1H, s, H2), 8.06 (1H, s, H8), 6.22 (1H, s, H1′), 5.68 (2H, bs, NH_2), 4.43–4.40 (2H, m, H3′, H4′), 4.18 (1H, d, $J = 2.6$ Hz, H2′), 3.98 (1H, dd, $J = 10.8, 4.6$ Hz, H5′), 3.93 (1H, dd, $J = 10.8, 6.6$ Hz, H5′), 2.38 (1H, s, CCH), 1.04–0.94 (28H, m, 4 × *i*-Pr); **^{13}C NMR** (125 MHz, $CDCl_3$) δ_C 155.6, 153.3, 149.7, 139.4, 120.1, 94.1, 86.4, 84.1, 81.2, 62.6, 59.3, 58.5, 17.3, 17.2, 17.1, 17.1, 17.1, 17.1, 13.9, 12.9, 12.7; **HRMS** (ES+) calc. for $C_{24}H_{40}O_4N_5Si_2$ $[M+H]^+$ 518.26133, found 518.25995; $\mathbf{[\alpha]_D^{20}} = +46$ ($c = 0.07$, $CHCl_3$).

7.6 Synthesis of spin labels

7.6.1 4-Hydroxy-2,2,6,6-tetramethylpiperidine, 112



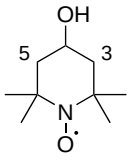
112

To a solution of 2,2,6,6-tetramethylpiperidone (1.00 g, 6.44 mmol, 1.0 equiv.) in ethanol (4 mL) was carefully added $NaBH_4$ (122 mg, 3.22 mmol, 0.5 equiv.). The reaction mixture was stirred at room temperature for 6 h, and brine (10 mL) was added. The mixture was extracted with ethyl acetate (3×50 mL), and the combined organic phases were dried (K_2CO_3). The solvent was removed *in vacuo* and alcohol **112** was obtained as a white solid (879 mg, 5.59 mmol, 87%) with no further purification necessary.

IR (solid, ν_{max} / cm^{-1}) 3253, 3148, 2927, 1362, 1231, 1057, 857, 758; **^{1}H NMR** (400 MHz, $CDCl_3$) δ_H 4.01 (1H, tt, $J = 17.1, 4.1$ Hz, H4), 1.89 (2H, dd, $J = 12.5, 4.1$ Hz, H3, H5), 1.15 (6H, s, 2 × CH_3), 1.11 (6H, s, 2 × CH_3), 0.97 (2H, t, $J = 11.6$ Hz, H3, H5); **^{13}C NMR** (100 MHz, $CDCl_3$) δ_C 64.8, 51.8, 48.3, 35.1, 28.8.

Data consistent with literature values.[194]

7.6.2 4-Hydroxy-2,2,6,6-tetramethylpiperidine-1-oxyl, 7



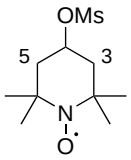
7

To a solution of aminoalcohol **112** (1.11 g, 7.06 mmol, 1.0 equiv.) in degassed methanol (14 mL) under N_2 was added $Na_2WO_4{\cdot}2\,H_2O$ (350 mg, 1.06 mmol, 15 mol%). A solution of H_2O_2 (30% *aq.*, 4.3 mL, 42.4 mmol, 6 equiv.) was added dropwise and the reaction mixture was stirred at room temperature for 50 h. After diluting with brine (10 mL), the mixture was extracted with ethyl acetate (3 × 30 mL). The combined organic extracts were dried over Na_2SO_4 and the solvent was removed *in vacuo*. The residue was purified by column chromatography (ethyl acetate / petroleum ether (4 : 6)) to give nitroxyl **7** as an orange solid (1.19 g, 6.91 mmol, 98%). Prior to NMR analysis, radical **7** was reduced *in situ* to the corresponding hydroxylamine by addition of phenylhydrazine directly to the NMR tube.

$\mathbf{R}_f$ 0.22 (ethyl acetate / petroleum ether (1 : 1)); **IR** (thin film, ν_{max} / cm^{-1}) 3407, 1472, 1376, 1174, 1161, 1066; **^{1}H NMR** (400 MHz, $CDCl_3$) δ_H 3.89 (1H, tt, $J = 11.4, 4.3$ Hz, H4), 1.82–1.77 (2H, m, H3, H5), 1.43 (2H, t, $J = 11.9$ Hz, H3, H5), 1.14 (6H, s, 2 × CH_3), 1.07 (6H, s, 2 × CH_3); **^{13}C NMR** (100 MHz, $CDCl_3$) δ_C 63.1, 47.5, 31.6, 20.6.

Data consistent with literature values.[245]

7.6.3 4-Methanesulfonyloxy-2,2,6,6-tetramethylpiperidine-1-oxyl, 113



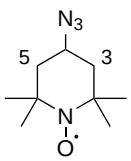
113

To a solution of alcohol **7** (200 mg, 1.16 mmol, 1.0 equiv.) in dry pyridine (2.3 mL) under N_2 was added methanesulfonyl chloride (0.18 mL, 2.32 mmol, 2.0 equiv.) at 0 °C. The reaction mixture was warmed slowly to room temperature and stirred for 3 h. The reaction was quenched with $NaHCO_3$ (*aq.* sat., 5 mL) at 0 °C. The mixture was diluted with H_2O (10 mL) and extracted with $CHCl_3$ (3×20 mL). The combined organic extracts were washed with $NaHCO_3$ (*aq.* sat., 20 mL) and H_2O (20 mL) and dried over Na_2SO_4. The solvent was removed *in vacuo* and the residue was dried under high vacuum. The mesylate **113** was isolated as an orange-red solid (278 mg, 1.11 mmol, 96%) with no further purification necessary. Prior to NMR analysis, radical **113** was reduced *in situ* to the corresponding hydroxylamine by addition of phenylhydrazine directly to the NMR tube.

$\mathbf{R}_f$ 0.44 (ethyl acetate / petroleum ether (1 : 1)); **IR** (thin film, ν_{max} / cm^{-1}) 2981, 1468, 1348, 1171, 934, 871, 829; **^{1}H NMR** (400 MHz, $CDCl_3$) δ_H 4.83 (1H, tt, $J = 11.3, 4.5$ Hz, H4), 2.90 (3H, s, OSO_2CH_3), 1.99–1.95 (2H, m, H3, H5), 1.77–1.66 (2H, m, H3, H5), 1.14 (6H, s, $2 \times CH_3$), 1.11 (6H, s, $2 \times CH_3$); **^{13}C NMR** (100 MHz, $CDCl_3$) δ_C 74.9, 59.9, 44.9, 39.0, 31.8, 20.6.

Data consistent with literature values.[246]

7.6.4 4-Azido-2,2,6,6-tetramethylpiperidine-1-oxyl, 40



40

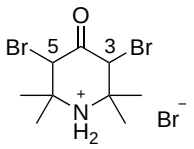
Mesylate **113** (100 mg, 0.400 mmol, 1.0 equiv.) and NaN_3 (156 mg, 2.40 mmol, 6.0 equiv.)

were dissolved in dry DMF (1 mL) under N_2. The reaction was heated at 80 °C for 26 h, before being quenched with ice-water (10 mL). The mixture was extracted with diethyl ether (3 × 20 mL) and the combined organic extracts were washed with brine (10 mL) and dried over Na_2SO_4. The solvent was removed *in vacuo*, and the residue was purified by column chromatography (diethyl ether / petroleum ether (7 : 93)) to afford azide **40** as an orange-red solid (54 mg, 0.274 mmol, 69%). Prior to NMR analysis, radical **40** was reduced *in situ* to the corresponding hydroxylamine by addition of phenylhydrazine directly to the NMR tube.

$\mathbf{R}_f$ 0.19 (diethyl ether / petroleum ether (1 : 9)); **IR** (solid, ν_{max} / cm^{-1}) 2940, 2088, 1466, 1234, 1174, 902; **^{1}H NMR** (400 MHz, $CDCl_3$) δ_H 3.52 (1H, tt, $J = 12.0, 4.0$ Hz, H4), 1.81–1.77 (2H, m, H3, H5), 1.55 (2H, t, $J = 12.3$ Hz, H3, H5), 1.18 (6H, s, 2 × CH_3), 1.10 (6H, s, 2 × CH_3); **^{13}C NMR** (100 MHz, $CDCl_3$) δ_C 60.5, 52.5, 43.7, 31.6, 20.3.

Data consistent with literature values.[247]

7.6.5 3,5-Dibromo-2,2,6,6-tetramethylpiperidinium bromide, 115



115

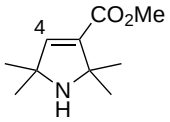
To a solution of 2,2,6,6-tetramethylpiperidone (1.00 g, 6.44 mmol, 1.0 equiv.) in acetic acid (2.5 mL) was slowly added a solution of Br_2 (2.06 g, 12.9 mL, 2.0 equiv.) in acetic acid (2.5 mL). The reaction mixture was stirred at room temperature for 16 h. The precipitate was collected by filtration and washed with acetic acid (10 mL) and then diethyl ether (3 × 15 mL) and dried under high vacuum. The hydrobromide salt **115** (1 : 1.3 mixture of diastereomers A (minor) and B (major)) was isolated as white crystals with no further purification necessary (2.19 g, 5.55 mmol, 86%).

IR (solid, ν_{max} / cm^{-1}) 2969, 2891, 2694, 1750, 1559, 1543, 1386, 1254, 639; **^{1}H NMR** (400 MHz, DMSO-d_6) δ_H 9.70 (4H, bs, 2 × NH_2), 5.56 (2H, s, $H3_A$, $H5_A$), 5.45 (2H, s, $H3_B$, $H5_B$), 1.74 (6H, s, 2 × (CH_3)$_A$), 1.65 (6H, s, 2 × (CH_3)$_B$), 1.54 (6H, s, 2 × (CH_3)$_B$),

1.37 (6H, s, $2 \times (CH_3)_A$); **^{13}C NMR** (100 MHz, DMSO-d_6) δ_C 191.2, 188.6, 64.4, 62.0, 60.0, 56.0, 27.5, 26.6, 24.9, 21.9.

Data consistent with literature values.[185,186]

7.6.6 Methyl 2,2,5,5-tetramethyl-2,5-dihydropyrrole-3-carboxylate, 116



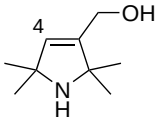
116

A solution of fresh NaOMe was prepared by careful addition of small pieces of Na (175 mg, 7.62 mmol, 3.0 equiv.) to dry methanol (3 mL) under N_2 at 0 °C. After stirring for 30 min at room temperature, hydrobromide salt **115** was slowly added at 0 °C. The reaction was stirred at room temperature for 3 h. The solvent was removed *in vacuo*, and the residue redissolved in diethyl ether (50 mL) and washed with $NaHCO_3$ (5% *aq.*, 50 mL). The aqueous washing was back-extracted with diethyl ether (2×20 mL). The combined organic extracts were dried over Na_2SO_4 and the solvent was removed *in vacuo*. The methyl ester **116** was isolated as a pale brown oil with no further purification necessary (415 mg, 2.26 mmol, 89%).

R_f 0.39 (diethyl ether / petroleum ether (6 : 4)); **IR** (thin film, ν_{max} / cm^{-1}) 2965, 1716, 1634, 1436, 1253, 1060, 771; **^{1}H NMR** (400 MHz, $CDCl_3$) δ_H 6.60 (1H, s, H4), 3.71 (1H, s, OCH_3), 1.91 (1H, bs, N*H*), 1.38 (6H, s, $2 \times$ CH_3), 1.25 (6H, s, $2 \times$ CH_3); **^{13}C NMR** (100 MHz, $CDCl_3$) δ_C 164.6, 149.2, 139.1, 66.0, 63.5, 51.4, 30.0, 29.9.

Data consistent with literature values.[185]

7.6.7 3-(Hydroxymethyl)-2,2,5,5-tetramethyl-2,5-dihydropyrrole, 117



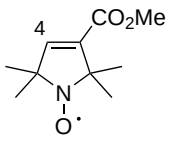
117

A solution of methyl ester **116** (400 mg, 2.18 mmol, 1.0 equiv.) in dry THF (10 mL) under

Ar was cooled to −78°C. A solution of DIBAL (1 M in hexanes, 4.8 mL, 4.80 mmol, 2.2 equiv.) was added dropwise, and the reaction mixture was stirred while slowly warming up to room temperature over 3 h. The reaction was quenched with acetone (1 mL), and sodium potassium tartrate (*aq.* sat., 10 mL) was added. After vigorous stirring, the mixture was diluted with NaOH (1 M, 10 mL) and ethyl acetate (20 mL). The mixture was separated and the aqueous phase extracted with ethyl acetate (3 × 20 mL). The combined organic phases were dried (Na_2SO_4) and the solvent was removed *in vacuo*. The amino alcohol **117** was obtained as white crystals (231 mg, 1.49 mmol, 68%) without any further purification. **IR** (thin film, ν_{max} / cm^{-1}) 3200, 2963, 1463, 1363, 1195, 1030, 732; **^{1}H NMR** (400 MHz, $CDCl_3$) δ_H 5.43 (1H, s, H4), 4.04 (2H, d, $J = 1.4$ Hz, CH_2OH), 1.15 (6H, s, 2 × CH_3), 1.13 (6H, s, 2 × CH_3); **^{13}C NMR** (100 MHz, $CDCl_3$) δ_C 147.2, 130.9, 65.8, 63.3, 57.8, 30.5, 29.6.

Data consistent with literature values.[248]

7.6.8 Methyl 2,2,5,5-tetramethyl-2,5-dihydropyrrole-3-carboxylate-1-oxyl, 119



119

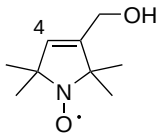
Amine **116** (50 mg, 0.273 mmol, 1.0 equiv.) was dissolved in dry diethyl ether (1 mL) under N_2. A solution of *m*-CPBA (77% w/w, 123 mg, 0.546 mmol, 2.0 equiv.) in dry diethyl ether (1 mL) was added dropwise at 0 °C, and the reaction mixture was stirred at room temperature for 1.5 h. The reaction mixture was diluted with Na_2CO_3 (10% *aq.*, 10 mL) and the mixture was extracted with diethyl ether (3 × 20 mL). The combined organic phases were dried (Na_2SO_4) and the solvent was removed *in vacuo*. The nitroxyl radical **119** was obtained as a yellow solid (54 mg, 0.272 mmol, quant.) with no further purification necessary. Prior to NMR analysis, radical **119** was reduced *in situ* to the corresponding hydroxylamine by addition of phenylhydrazine directly to the NMR tube.

R_f 0.36 (ethyl acetate / petroleum ether (2 : 8)); **IR** (thin film, ν_{max} / cm^{-1}) 1713, 1627,

1439, 1352, 1289, 1257, 1195; **^{1}H NMR** (400 MHz, $CDCl_3$) δ_H 6.48 (1H, s, H4), 3.65 (3H, s, OC*H*$_3$), 1.35–1.19 (12H, m, 4 × C*H*$_3$); **^{13}C NMR** (100 MHz, $CDCl_3$) δ_C 164.0, 145.8, 136.4, 70.2, 68.2, 51.4, 24.9, 24.6.

Data consistent with literature values.[249]

7.6.9 3-(Hydroxymethyl)-2,2,5,5-tetramethyl-2,5-dihydropyrrole-1-oxyl, 118



118

By oxidation of amine 117

Aminoalcohol **117** (230 mg, 1.48 mmol, 1.0 equiv.) was dissolved in degassed methanol (3 mL) under N_2. $Na_2WO_4{\cdot}2H_2O$ (73 mg, 0.222 mmol, 15 mol%) was added, followed by dropwise addition of H_2O_2 (30% *aq.*, 1.0 mL, 7.9 mmol, 5.3 equiv.). The reaction was stirred for 43 h, before being diluted with brine (10 mL) and extracted with ethyl acetate (3 × 20 mL). The combined extracts were dried (Na_2SO_4) and the solvent was removed *in vacuo*. The residue was purified by column chromatography (ethyl acetate / petroleum ether (4 : 6)) to afford nitroxyl radical **118** as a yellow solid (81 mg, 0.476 mmol, 32%).

By reduction of ester 119

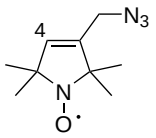
Methyl ester **119** (300 mg, 1.51 mmol, 1.0 equiv.) was dissolved in dry THF (3 mL) under N_2 and cooled to −78 °C. A solution of DIBAL (1 M in hexanes, 3.78 mL, 3.78 mmol, 2.5 equiv.) was added dropwise, and the mixture was allowed to warm slowly to −50 °C over stirring. When TLC analysis showed complete conversion (total 4.5 h), the reaction was quenched by the addition of NaOH (2 M, 2 mL), warmed to room temperature and diluted with NaOH (2 M, 10 mL), brine (10 mL) and ethyl acetate (20 mL). The solids were removed by filtration, and the mixture was separated. The aqueous phase was extracted with ethyl acetate (3 × 20 mL). The combined organic extracts were dried over Na_2SO_4 and the solvent was removed *in vacuo*. The residue was purified by column chromatography (ethyl

acetate / petroleum ether (1 : 1)) to give alcohol **118** as a yellow solid (246 mg, 1.45 mmol, 96%). Prior to NMR analysis, radical **118** was reduced *in situ* to the corresponding hydroxylamine by addition of phenylhydrazine directly to the NMR tube.

$\mathbf{R}_f$ 0.26 (ethyl acetate / petroleum ether (1 : 1)); **IR** (thin film, ν_{max} / cm^{-1}) 3351, 1458, 1374, 1160, 1112, 1033, 829; **^{1}H NMR** (400 MHz, $CDCl_3$) δ_H 5.48–5.40 (1H, m, H4), 4.17–4.08 (2H, m, CH_2OH), 1.35–1.12 (12H, m, 4 × CH_3); **^{13}C NMR** (100 MHz, $CDCl_3$) δ_C 144.4, 128.8, 70.0, 67.9, 59.4, 25.6, 24.7.

Data consistent with literature values.[250]

7.6.10 3-(Azidomethyl)-2,2,5,5-tetramethyl-2,5-dihydropyrrole-1-oxyl, 106



106

Alcohol **118** (480 mg, 2.82 mmol, 1.0 equiv.) was dissolved in dry CH_2Cl_2 under N_2. After cooling to 0 °C, triethylamine (430 µL, 3.10 mmol, 1.1 equiv.) and then methanesulfonyl chloride (240 µL, 3.10 mmol, 1.1 equiv.) were added dropwise. The reaction was stirred at room temperature for 3 h, before being diluted with CH_2Cl_2 (50 mL). The solution was washed with $NaHCO_3$ (5% *aq.*, 30 mL) and H_2O (30 mL) and dried (Na_2SO_4). The solvent was removed *in vacuo* to afford pure 3-(mesyloxymethyl)-2,2,5,5-tetramethyl-2,5-dihydropyrrole-1-oxyl (668 mg, ∼2.69 mmol) as yellow crystals.

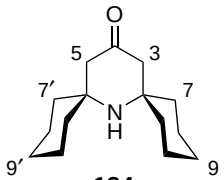
The material was immediately dissolved in dry DMF (5 mL) under N_2 and NaN_3 (345 mg, 5.30 mmol, 2.0 equiv.) was added. The reaction was stirred at room temperature for 1 h, before being diluted with ethyl acetate (50 mL) and brine (20 mL). The phases were separated, and the aqueous layer extracted with ethyl acetate (2 × 20 mL). The combined organic layers were dried (Na_2SO_4) and the solvent was removed *in vacuo*. The residue was purified by column chromatography (diethyl ether / petroleum ether (3 : 7)) to give azide **106** as a yellow oil (507 mg, 2.60 mmol, 93% over two steps). Prior to NMR analysis, radical **106** was reduced *in situ* to the corresponding hydroxylamine by addition

of phenylhydrazine directly to the NMR tube.

R_f 0.32 (diethyl ether / petroleum ether (4 : 6)); **IR** (thin film, ν_{max} / cm^{-1}) 2976, 2096, 1467, 1358, 1282, 1161, 843; **^{1}H NMR** (400 MHz, $CDCl_3$) δ_H 5.50 (1H, s, H4), 3.66 (2H, s, CH_2N$_3$), 1.17 (12H, s, 4 × CH_3); **^{13}C NMR** (100 MHz, $CDCl_3$) δ_C 138.5, 133.3, 70.2, 68.1, 48.1, 26.0, 24.7.

Data consistent with literature values.[184]

7.6.11 2,6-Bis(spirocyclohexyl)-4-piperidone, 124



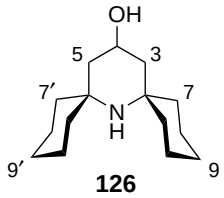
124

2,2,6,6-Tetramethylpiperidone (6.55 g, 42.2 mmol, 1.0 equiv.), NH_4Cl (11.3 g, 211 mmol, 5.0 equiv.) and cyclohexanone (13.2 mL, 127 mmol, 3.0 equiv.) were dissolved in dry DMSO (28 mL) under N_2. Triton B (40% in methanol, 8.44 mL) was added dropwise over stirring, and the reaction mixture was stirred at 50 °C for 43 h. H_2O (50 mL) was added and the mixture was stirred for a further 30 min. The solution was acidified with HCl (conc., 2 mL) and extracted with diethyl ether (2 × 100 mL). The ether washings were discarded, and the aqueous DMSO solution was adjusted to pH > 9 with NaOH (6 M). The mixture was extracted with ethyl acetate (3 × 150 mL) and the combined extracts were dried over Na_2SO_4. The solvent was removed *in vacuo* and the residue purified by column chromatography (ethyl acetate / petroleum ether (2 : 8)). Subsequent recrystallisation (ethanol) provided **124** as white crystals (6.25 g, 25.4 mmol, 60%).

R_f 0.38 (ethyl acetate / petroleum ether (3 : 7)); **IR** (solid, ν_{max} / cm^{-1}) 2933, 2856, 1694, 1441, 721; **^{1}H NMR** (400 MHz, $CDCl_3$) δ_H 2.28 (4H, s, H3, H5), 1.67–1.29 (20H, m, H7–11), 1.07 (1H, bs, N*H*); **^{13}C NMR** (100 MHz, $CDCl_3$) δ_C 211.6, 57.0, 52.5, 40.9, 25.8, 22.5.

Data consistent with literature values.[193]

7.6.12 4-Hydroxy-2,6-bis(spirocyclohexyl)piperidine, 126

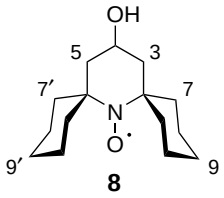


126

Ketone **124** (600 mg, 2.55 mmol, 1.0 equiv.) was dissolved in ethanol (5 mL). $NaBH_4$ (97 mg, 2.55 mmol, 1.0 equiv.) was added carefully at 0 °C over stirring. The reaction mixture was stirred at room temperature for 7 h, before being saturated with NaCl. The mixture was extracted with diethyl ether (3×50 mL) and the combined organic layers were dried over K_2CO_3. After filtering through celite the solvent was removed *in vacuo* to afford aminoalcohol **126** as light brown crystals (644 mg, 2.55 mmol, quant.).

$\mathbf{R}_f$ 0.14 (ethyl acetate / petroleum ether (3 : 7)); **m.p.** 74–77 °C; **IR** (solid, ν_{max} / cm^{-1}) 3293, 2924, 2850, 1443, 1027, 1012, 680; **^{1}H NMR** (400 MHz, $CDCl_3$) δ_H 3.94 (1H, tt, $J = 11.4$, 4.1 Hz, H4), 2.13 (2H, dd, $J = 12.3$, 3.9 Hz, H3, H5), 1.87 (1H, bs, O*H*), 1.68–1.26 (20H, m, H7–11), 0.86 (2H, t, $J = 11.9$ Hz, H3, H5), 0.65 (1H, bs, N*H*); **^{13}C NMR** (100 MHz, $CDCl_3$) δ_C 64.2, 53.5, 46.0, 43.8, 37.8, 26.3, 22.9, 22.3; **HRMS** (ES+) calc. for $C_{15}H_{28}NO$ $[M+H]^+$ 238.2165, found 238.2169.

7.6.13 4-Hydroxy-2,6-bis(spirocyclohexyl)piperidine-1-oxyl, 8



8

Oxidation by H_2O_2

Triton B (40% w/v in methanol, 2.85 mL, 3.0 equiv.) was added to a solution of amine **126** (539 mg, 2.27 mmol, 1.0 equiv.) in ethanol (8.5 mL) and the mixture was degassed by the freeze-pump-thaw method. Under an atmosphere of N_2, $Na_2WO_4{\cdot}2H_2O$ (376 mg, 1.14 mmol, 0.5 equiv.) was added. H_2O_2 (30% *aq.*, 6.95 mL, 68.0 mmol, 30 equiv.) was

added dropwise, and the mixture was stirred for 48 h under a balloon of N_2. Additional H_2O_2 (30% *aq.*, 6.95 mL, 68.0 mmol, 30 equiv.) and ethanol (6 mL) was added, and the reaction was stirred for a further 16 h. The mixture was diluted with H_2O (50 mL) and extracted with CH_2Cl_2 (3×50 mL). The combined organic phases were dried (Na_2SO_4) and the solvent was removed *in vacuo*. The residue was purified by column chromatography (ethyl acetate / CH_2Cl_2 (15 : 85)) to yield nitroxyl radical **8** (476 mg, 1.89 mmol, 83%) as an orange solid.

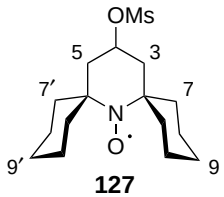
Oxidation by *m*-CPBA

Amine **126** (605 mg, 2.55 mmol, 1.0 equiv.) was dissolved in dry CH_2Cl_2 (10 mL) under N_2 and the solution was cooled to 0 °C. A solution of *m*-CPBA (77% w/w, 1.15 g, 5.10 mmol, 2.0 equiv.) in dry CH_2Cl_2 (7 mL) was added dropwise, and the reaction mixture was stirred at room temperature for 2 h. The mixture was washed with Na_2CO_3 (10% *aq.*, 15 mL), and the aqueous phase was back-extracted with CH_2Cl_2 (3×20 mL). The combined organic phases were dried (Na_2SO_4) and the solvent was removed *in vacuo*. The residue was purified by column chromatography (ethyl acetate / CH_2Cl_2 (10 : 90 to 15 : 85)) to afford nitroxyl radical **8** (421 mg, 1.67 mmol, 65%) as an orange solid. Prior to NMR analysis, radical **8** was reduced *in situ* to the corresponding hydroxylamine by addition of phenylhydrazine directly to the NMR tube.

$\mathbf{R}_f$ 0.42 (ethyl acetate / CH_2Cl_2 (15 : 85)); **IR** (solid, ν_{max} / cm^{-1}) 3398, 2928, 2858, 1451, 1100, 1031, 721; **^{1}H NMR** (400 MHz, DMSO-d_6) δ_H 4.40 (1H, d, $J = 4.4$ Hz, O*H*), 3.66–3.57 (1H, m, H4), 2.24 (2H, d, $J = 9.8$ Hz, H3, H5), 1.92–0.94 (20H, m, H7–11), 0.87 (2H, t, $J = 11.8$ Hz, H3, H5); **^{13}C NMR** (100 MHz, DMSO-d_6) δ_C 61.1, 60.7, 41.4, 39.1, 28.3, 25.6, 23.1, 22.7.

Data consistent with literature values.[25]

7.6.14 4-Methanesulfonyloxy-2,6-bis(spirocyclohexyl)piperidine-1-oxyl, 127



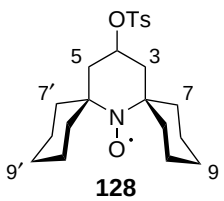
127

Alcohol **8** (421 mg, 1.41 mmol, 1.0 equiv.) was dissolved in dry CH_2Cl_2 (14 mL) under N_2. Triethylamine (216 µL, 1.55 mmol, 1.1 equiv.) was added, followed by dropwise addition of methanesulfonyl chloride (120 µL, 1.55 mmol, 1.1 equiv.). The reaction mixture was stirred for 2 h at room temperature, before being diluted with CH_2Cl_2 (50 mL). The solution was washed with $NaHCO_3$ (5% *aq.*, 20 mL) and H_2O (20 mL), and dried (Na_2SO_4). The solvent was removed *in vacuo*, and the residue was purified by column chromatography (ethyl acetate / petroleum ether (2 : 8)) to give mesylate **127** (454 mg, 1.37 mmol, 97%) as an orange solid. Prior to NMR analysis, radical **127** was reduced *in situ* to the corresponding hydroxylamine by addition of phenylhydrazine directly to the NMR tube.

R_f 0.25 (ethyl acetate / petroleum ether (2 : 8)); **m.p.** 122–125 °C; **IR** (thin film, ν_{max} / cm^{-1}) 2930, 2861, 1352, 1177, 932, 908; **^{1}H NMR** (400 MHz, $CDCl_3$) δ_H 4.80–4.74 (1H, m, H4), 2.96 (3H, s, SO_2CH_3), 2.64–2.47 (2H, m, H3, H5), 1.94–0.96 (22H, m, H3, H5, H7–11); **^{13}C NMR** (100 MHz, $CDCl_3$) δ_C 74.7, 64.9, 38.9, 38.0, 37.9, 28.9, 25.3, 23.1, 22.6; **HRMS** (EI+) calc. for $C_{16}H_{28}NO_4S$ $[M]^+$ 330.1739, found 330.1739.

Data consistent with literature values.[250]

7.6.15 4-*p*-Toluylsulfonyloxy-2,6-bis(spirocyclohexyl)piperidine-1-oxyl, 128



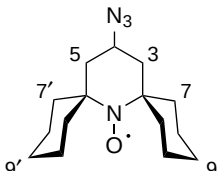
128

To a solution of alcohol **8** (50 mg, 0.198 mmol, 1.0 equiv.) in dry CH_2Cl_2 under N_2 was added triethylamine (68 µL, 0.476 mmol, 2.4 equiv.) and DMAP (2.5 mg, 0.020 mmol,

0.1 equiv.), then 4-toluenesulfonyl chloride (46 mg, 0.238 mmol, 1.2 equiv.). The reaction mixture was stirred at room temperature for 22 h, before being diluted with CH_2Cl_2 (10 mL) and washed with H_2O (3 × 10 mL). The organic phase was dried (Na_2SO_4) and the solvent was removed *in vacuo*. The residue was purified by column chromatography (ethyl acetate / petroleum ether (15 : 85)) to afford tosylate **128** as orange crystals (69 mg, 0.170 mmol, 86%). Prior to NMR analysis, radical **128** was reduced *in situ* to the corresponding hydroxylamine by addition of phenylhydrazine directly to the NMR tube.

$\mathbf{R_f}$ 0.30 (ethyl acetate / petroleum ether (2 : 8)); **m.p.** 97–99 °C; **IR** (solid, ν_{max} / cm^{-1}) 2926, 2870, 1453, 1362, 1177, 949, 871; **^{1}H NMR** (400 MHz, $CDCl_3$) δ_H 7.82 (2H, d, $J = 8.2$ Hz, Ar), 7.36 (2H, d, $J = 8.0$ Hz, Ar), 4.66 (1H, tt, $J = 11.1, 4.1$ Hz, H4), 2.45 (3H, s, ArC*H*$_3$), 2.38–2.32 (2H, m, H3, H5), 1.98–1.88 (4H, m, H7, H11, H7′, H11′), 1.65–1.46 (12H, m, H3, H5, H7–H11), 1.29–0.99 (6H, m, H8–10, H8′–10′); **^{13}C NMR** (100 MHz, $CDCl_3$) δ_C 145.0, 134.5, 130.0, 127.9, 74.8, 65.0, 37.4, 29.1, 25.3, 22.9, 22.6, 21.7; **HRMS** (ES+) calc. for $C_{22}H_{32}NO_4NaS$ $[M+Na]^+$ 429.19443, found 429.19421.

7.6.16 4-Azido-2,6-bis(spirocyclohexyl)piperidine-1-oxyl, 107

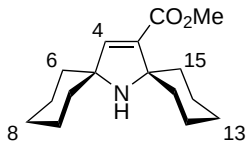


107

Mesylate **127** (454 mg, 1.37 mmol, 1.0 equiv.) was dissolved in dry DMSO (10 mL) under Ar. NaN_3 (339 mg, 5.21 mmol, 3.8 equiv.) was added, and the reaction mixture was stirred at 80 °C for 2 h. After cooling to room temperature, brine (40 mL) was added. The mixture was extracted with diethyl ether (3 × 50 mL) and the combined organic phases were dried (Na_2SO_4). The solvent was removed *in vacuo*, and the residue was purified by column chromatography (diethyl ether / petroleum ether (0 : 1 to 1 : 9)) to give azide **107** as a red solid (246 mg, 0.888 mmol, 65%). Prior to NMR analysis, radical **107** was reduced *in situ* to the corresponding hydroxylamine by addition of phenylhydrazine directly to the NMR tube.

$\mathbf{R}_f$ 0.28 (diethyl ether / petroleum ether (1 : 9)); **m.p.** 132–135 °C; **IR** (solid, ν_{max} / cm^{-1}) 2926, 2862, 2085, 1453, 1255, 905; **^{1}H NMR** (400 MHz, $CDCl_3$) δ_H 3.49 (1H, tt, J = 12.2, 3.9 Hz, H4), 2.44–2.40 (2H, m, H3, H5), 2.04–1.92 (4H, m, H7, H11, H7′, H11′), 1.70–1.23 (16H, m, H3, H5, H7–11), 1.10 (2H, qt, J = 13.0, 3.9 Hz, H8–10, H8′–10′); **^{13}C NMR** (100 MHz, $CDCl_3$) δ_C 63.6, 52.3, 38.7, 37.2, 28.5, 25.6, 23.3, 22.8; **HRMS** (EI+) calc. for $C_{15}H_{25}N_4O$ $[M]^+$ 277.2028, found 277.2030.

7.6.17 Methyl 2,5-bis(spirocyclohexyl)-2,5-dihydropyrrole-3-carboxylate, 131



131

Piperidone **124** (500 mg, 2.12 mmol, 1.0 equiv.) was dissolved in glacial acetic acid (1.1 mL). Over stirring, a solution of Br_2 (1.40 g, 8.48 mmol, 4.0 equiv.) in glacial acetic acid (1 mL) was added dropwise. The reaction mixture was diluted with glacial acetic acid (2 mL) and stirred at room temperature. After 95 h, LRMS monitoring indicated complete conversion. The reaction mixture was diluted with diethyl ether (5 mL) and the suspended solids were allowed to settle. The supernatant was removed, and the washing procedure was repeated five times. The remaining finely powdered, yellow solid was dried under high vacuum.

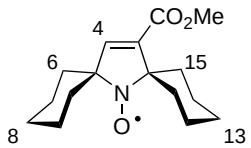
A fresh solution of NaOMe was prepared by carefully dissolving Na (292 mg, 12.7 mmol, 6.0 equiv.) in dry methanol (4.3 mL) under N_2. At 0 °C and over stirring, the dried hydrobromide salt was added to the NaOMe solution. The reaction mixture was stirred at room temperature for 4 h, before the solvent was removed *in vacuo*. The residue was redissolved in ethyl acetate (50 mL). After washing with H_2O (2 × 20 mL), the organic phase was dried (Na_2SO_4) and the solvent was removed *in vacuo*. The residue was purified by column chromatography (diethyl ether / petroleum ether (0 : 100 to 15 : 85)) to afford methyl ester **131** as a pale yellow oil (294 mg, 1.12 mmol, 53%).

$\mathbf{R}_f$ 0.28 (diethyl ether / petroleum ether (1 : 9)); **IR** (thin film, ν_{max} / cm^{-1}) 2925, 2853,

1717, 1631, 1449, 1435, 1190; **^{1}H NMR** (400 MHz, $CDCl_3$) δ_H 6.81 (1H, s, H4), 3.70 (3H, s, OC*H*$_3$), 2.05 (2H, td, J = 12.7, 5.2 Hz, H15), 1.65–1.10 (18H, m, H6–14); **^{13}C NMR** (100 MHz, $CDCl_3$) δ_C 164.9, 147.9, 139.4, 67.7, 66.4, 51.2, 40.0, 37.6, 25.6, 25.3, 23.3, 22.5.

Data consistent with literature values.[251]

7.6.18 Methyl 2,5-bis(spirocyclohexyl)-2,5-dihydropyrrole-3-carboxylate-1-oxyl, 132



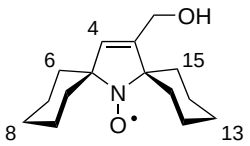
132

A solution of amine **131** (530 mg, 2.01 mmol, 1.0 equiv.) in dry CH_2Cl_2 (5 mL) under N_2 was cooled to 0 °C, and a solution of *m*-CPBA (77% w/w, 901 mg, 4.02 mmol, 2.0 equiv.) in dry CH_2Cl_2 (5 mL) was added dropwise. The reaction was stirred at room temperature for 8 h, before being washed with Na_2CO_3 (10% *aq.*, 30 mL). The aqueous phase was extracted with CH_2Cl_2 (3 × 20 mL) and the combined organic phases were dried (Na_2SO_4). The solvent was removed *in vacuo*, and the residue was purified by column chromatography (diethyl ether / petroleum ether (1 : 9)) to yield nitroxyl radical **132** as orange crystals (464 mg, 1.67 mmol, 83%). Prior to NMR analysis, radical **132** was reduced *in situ* to the corresponding hydroxylamine by addition of phenylhydrazine directly to the NMR tube.

R$_f$ 0.29 (diethyl ether / petroleum ether (1 : 9)); **IR** (solid, ν_{max} / cm^{-1}) 2929, 1714, 1627, 1444, 1305, 1249; **^{1}H NMR** (400 MHz, $CDCl_3$) δ_H 6.97 (1H, s, H4), 3.74 (3H, s, OC*H*$_3$), 2.21–1.10 (20H, m, H6–15); **^{13}C NMR** (100 MHz, $CDCl_3$) δ_C 164.4, 144.1, 136.9, 72.9, 72.7, 51.2, 35.1, 34.3, 25.5, 24.8, 23.7, 22.9.

Data consistent with literature values.[251]

7.6.19 3-(Hydroxymethyl)-2,5-bis(spirocyclohexyl)-2,5-dihydropyrrole-1-oxyl, 133



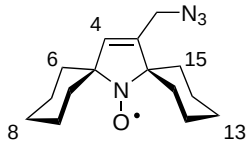
133

A solution of ester **132** (195 mg, 0.700 mmol, 1.0 equiv.) in dry THF (2.5 mL) under Ar was cooled to −78 °C. A solution of DIBAL (1 M in hexane, 1.75 mL, 1.75 mmol, 2.5 equiv.) was added dropwise, and the reaction mixture was stirred while slowly warming up to −50 °C. After being maintained between −50 °C and −45 °C for 1 h 15 min, the reaction was quenched with NaOH (2 M, 1 mL), and allowed to reach room temperature. After diluting with ethyl acetate (20 mL) and NaOH (2 M, 10 mL), the mixture was filtered through a cotton plug to remove the precipitate. Brine (10 mL) was added, the mixture was separated and the aqueous phase extracted with ethyl acetate (3 × 20 mL). The combined organic phases were dried (Na_2SO_4) and the solvent was removed *in vacuo*. After purification by column chromatography (ethyl acetate / petroleum ether (3 : 7)) alcohol **133** was obtained as an orange solid (159 mg, 0.635 mmol, 91%). Prior to NMR analysis, radical **133** was reduced *in situ* to the corresponding hydroxylamine by addition of phenylhydrazine directly to the NMR tube.

$\mathbf{R}_f$ 0.31 (ethyl acetate / petroleum ether (3 : 7)); **IR** (thin film, ν_{max} / cm^{-1}) 3331, 2927, 1621, 1581, 1447, 1284, 1111, 1069; **^{1}H NMR** (400 MHz, $CDCl_3$) δ_H 6.00 (1H, s, H4), 4.27 (2H, s, CH_2OH), 1.99–1.13 (20H, m, H6–15); **^{13}C NMR** (100 MHz, $CDCl_3$) δ_C 146.6, 125.9, 72.4, 71.6, 60.4, 35.4, 34.3, 25.7, 24.9, 24.0, 23.5.

Data consistent with literature values.[252]

7.6.20 3-(Azidomethyl)-2,5bis(spirocyclohexyl)-2,5-dihydropyrrole-1-oxyl, 108



108

Alcohol **133** (211 mg, 0.843 mmol, 1.0 equiv.) was dissolved in dry CH_2Cl_2 (8.5 mL) under N_2 and cooled to 0 °C. Triethylamine (177 µL, 1.27 mmol, 1.5 equiv.) was added, followed by dropwise addition of methanesulfonyl chloride (98 µL, 1.27 mmol, 1.5 equiv.). The reaction was stirred at room temperature for 5.5 h, before being diluted with CH_2Cl_2 (40 mL). After washing with $NaHCO_3$ (5% *aq.*, 20 mL) and H_2O (20 mL), the organic phase was dried (Na_2SO_4). The solvent was removed *in vacuo*, and the residue was dried under high vacuum.

The freshly prepared mesylate was dissolved in dry DMF (1.7 mL) under N_2 and NaN_3 (110 mg, 1.69 mmol, 2.0 equiv.) was added. The reaction was stirred at room temperature for 30 min, before being diluted with ethyl acetate (40 mL) and H_2O (20 mL). The phases were separated, and the aqueous layer extracted with ethyl acetate (2×20 mL). The combined organic layers were dried (Na_2SO_4) and the solvent was removed *in vacuo*. The residue was purified by column chromatography (diethyl ether / petroleum ether (1 : 9)) to give azide **108** as a yellow solid (214 mg, 0.777 mmol, 92%). Prior to NMR analysis, radical **108** was reduced *in situ* to the corresponding hydroxylamine by addition of phenylhydrazine.

$\mathbf{R}_f$ 0.25 (diethyl ether / petroleum ether (1 : 9)); **m.p.** 72–74 °C; **IR** (solid, ν_{max} / cm^{-1}) 2930, 2853, 2085, 1433, 1259, 905; **^{1}H NMR** (400 MHz, $CDCl_3$) δ_H 6.03 (1H, s, H4), 3.88 (2H, s, CH_2N$_3$), 1.97–1.15 (20H, m, H6–15); **^{13}C NMR** (100 MHz, $CDCl_3$) δ_C 139.9, 131.1, 71.7, 71.4, 49.5, 35.7, 34.3, 25.7, 24.9, 24.0, 23.3; **HRMS** (ES+) calc. for $C_{15}H_{23}N_4ONa$ $[M+Na]^+$ 298.17641, found 298.17648.

7.7 DNA synthesis, characterisation and spin labelling

Standard DNA phosphoramidites, solid supports (controlled pore glass, CPG) and additional reagents were purchased from Link Technologies, Glen Research and Applied Biosystems. NAP Sephadex gel filtration columns were purchased from GE Healthcare and used according to the manufacturer's instructions. All oligonucleotides were synthesised on an Applied Biosystems 394 automated DNA/RNA synthesiser using a standard 1.0 µmol phosphoramidite cycle of acid-catalysed detritylation, coupling, capping, and iodine oxidation. Stepwise coupling efficiencies and overall yields were determined by automated trityl cation conductivity monitoring and were in all cases $> 98.0\%$. All β-(cyanoethyl)phosphoramidite monomers were dissolved in anhydrous acetonitrile to a concentration of 0.1 M immediately prior to use. The coupling time for dA, dG, dC, and dT monomers was 60 s, and the coupling time for the modified phosphoramidites was extended to 600 s. Cleavage of the oligonucleotides from the solid support and subsequent deprotection was achieved by exposure to concentrated aqueous ammonia solution for 1 h at room temperature, followed by heating in a sealed tube for 5 h at 55 °C.

The oligonucleotides were purified by reversed-phase HPLC on a Gilson system using a Luna 10 µm C8 100 Å pore Phenomenex column (10×250 mm) with a gradient of acetonitrile in ammonium acetate over 20 min at a flow rate of 4 mL min^{-1}. Ammonium acetate buffers (buffer A: 0.1 M ammonium acetate, pH 7.3; buffer B: 0.1 M ammonium acetate, pH 7.3, with 50% acetonitrile) were used (0% to 35% buffer B over 20 min). Elution was monitored by UV absorption at 298 nm. After HPLC purification, all oligonucleotides were desalted and quantified by measuring the OD_{260} on a Cary 50 Bio UV-VIS spectrometer. The oligonucleotides were characterised by LC-HRMS on a Waters Acquity UPLC system coupled to a Bruker micrOTOF II focus ESI-TOF MS instrument in ESI− mode. Data were processed using MaxEnt.

7.7.1 General procedures for spin labelling of oligonucleotides

Reactions were performed on single stranded 16-mer oligodeoxynucleotides with a 2′-ethynyl modification, on scales ranging from 50 to 100 nmol. Desalting was performed on illustra NAP-10 columns (GE Healthcare Life Sciences). 'Click'-labelled oligonucleotides were purified by RP-HPLC using the instrument mentioned above, with a gradient of acetonitrile in triethylammonium acetate (TEAA; buffer A: 0.1 M TEAA, pH 7.3; buffer B: 0.1 M TEAA, pH 7.3, with 50% acetonitrile) or triethylammonium bicarbonate (TEAB; buffer A: 0.1 M TEAB, pH 7.5; buffer B: 0.1 M TEAB, pH 7.5, with 50% acetonitrile) over 20 min at a flow rate of 4 mL min^{-1}, gradient as specified below. Elution was monitored by UV absorption at 285–295 nm, depending on scale. Oligonucleotides purified with TEAA were subsequently desalted. After purification, all oligonucleotides were characterised by mass spectrometry and processed as mentioned above.

Spin labelling with 40 (6-Me)

A freshly made solution of CuI (50 mM in degassed acetonitrile, 20.0 µL, 1.00 µmol, 10 equiv.) was mixed with a solution of THPTA (**149**, 0.25 M in ultrapure H_2O, 4.0 µL, 1.00 µmol, 10 equiv.) and a solution of **40** (0.5 M in degassed acetonitrile, 20.0 µL, 10.0 µmol, 100 equiv.). The mixture was added to a solution of oligodeoxynucleotide (100 nmol) in ultrapure H_2O (36.0 µL) under Ar. The reaction mixture was vortexed, and left to react for 3 h at room temperature. After diluting to a total volume of 1000 µL with ultrapure H_2O, the mixture was desalted and purified by RP-HPLC (3.5–35% buffer B).

Spin labelling with 106 (5-Me)

A freshly made solution of CuI (50 mM in degassed acetonitrile, 20.0 µL, 1.00 µmol, 10 equiv.) was mixed with a solution of THPTA (**149**, 0.25 M in ultrapure H_2O, 4.0 µL, 1.00 µmol, 10 equiv.) and a solution of **106** (0.5 M in degassed acetonitrile, 20.0 µL, 10.0 µmol, 100 equiv.). The mixture was added to a solution of oligodeoxynucleotide (100 nmol) in ultrapure H_2O (26.0 µL) under Ar. The reaction mixture was vortexed, and left to react for 3 h at room temperature. After diluting to a total volume of 1000 µL with

ultrapure H_2O, the mixture was desalted and purified by RP-HPLC (3.5–35% buffer B).

Spin labelling with 107 (6-Sp)

A freshly made solution of CuI (125 mM in degassed acetonitrile, 8.0 µL, 1.00 µmol, 10 equiv.) was mixed with a solution of THPTA (**149**, 0.25 M in ultrapure H_2O, 4.0 µL, 1.00 µmol, 10 equiv.) and a solution of **107** (56 mM in degassed DMF, 179 µL, 10.0 µmol, 100 equiv.). The mixture was added to a solution of oligodeoxynucleotide (100 nmol) in ultrapure H_2O (86.0 µL) under Ar. The reaction mixture was vortexed and adjusted to homogeneity with H_2O or acetonitrile, sonicated, and left to react for 6 h at room temperature with regular vortexing and sonication. After diluting to a total volume of 1000 µL with ultrapure H_2O, the mixture was desalted and purified by RP-HPLC (3.5–55% buffer B).

Spin labelling with 108 (5-Sp)

A freshly made solution of CuI (50 mM in degassed acetonitrile, 20.0 µL, 1.00 µmol, 10 equiv.) was mixed with a solution of THPTA (**149**, 0.25 M in ultrapure H_2O, 4.0 µL, 1.00 µmol, 10 equiv.) and a solution of **108** (0.5 M in degassed acetonitrile, 20.0 µL, 10.0 µmol, 100 equiv.). The mixture was added to a solution of oligodeoxynucleotide (100 nmol) in ultrapure H_2O (26.0 µL) under Ar. The reaction mixture was vortexed, adjusted to homogeneity with H_2O or acetonitrile, sonicated, and left to react for 4 h at room temperature with regular vortexing and sonication. After diluting to a total volume of 1000 µL with ultrapure H_2O, the mixture was desalted and purified by RP-HPLC (3.5–45% buffer B).

Spin labelling with 134 (In-Me)

A freshly made solution of CuI (50 mM in degassed acetonitrile, 20.0 µL, 1.00 µmol, 10 equiv.) was mixed with a solution of THPTA (**149**, 0.25 M in ultrapure H_2O, 4.0 µL, 1.00 µmol, 10 equiv.) and a solution of **134** (0.5 M in degassed acetonitrile, 20.0 µL, 10.0 µmol, 100 equiv.). The mixture was added to a solution of oligodeoxynucleotide (100 nmol) in ultrapure H_2O (26.0 µL) under Ar. The reaction mixture was vortexed,

adjusted to homogeneity with H_2O or acetonitrile, sonicated, and left to react for 4 h at room temperature with regular vortexing and sonication. After diluting to a total volume of 1000 µL with ultrapure H_2O, the mixture was desalted and purified by RP-HPLC (3.5–45% buffer B).

Spin labelling with 135 (In-Et)

A freshly made solution of CuI (50 mM in degassed acetonitrile, 14.0 µL, 700 nmol, 10 equiv.) was mixed with a solution of THPTA (**149**, 0.25 M in ultrapure H_2O, 2.8 µL, 700 nmol, 10 equiv.) and a solution of **135** (0.5 M in degassed acetonitrile, 14.0 µL, 7.0 µmol, 100 equiv.). The mixture was added to a solution of oligodeoxynucleotide (70 nmol) in ultrapure H_2O (30.0 µL) under Ar. The reaction mixture was vortexed, adjusted to homogeneity with H_2O or acetonitrile, sonicated, and left to react for 4 h at room temperature with regular vortexing and sonication. After diluting to a total volume of 1000 µL with ultrapure H_2O, the mixture was desalted and purified by RP-HPLC (3.5–45% buffer B).

7.7.2 UV denaturation studies

All UV melting measurements were performed on a Varian Cary 4000 UV-VIS spectrophotometer with a Cary temperature controller, using the Cary Win UV Thermal software. Samples were analysed in 1 mL cuvettes (Hellma synthetic quartz 'precision cell QG'; 1 cm path length) and were made to 3 µM oligonucleotide concentration (total volume = 1.0 mL) in phosphate buffer (NaH_2PO_4, 10 mM, pH 7.3) with 200 mM NaCl. The samples were initially denatured by heating to 85 °C at 10 °C min^{-1}, then cooled to 20 °C at 1 °C min^{-1} and maintained at 20 °C for 2 min before heating to 85 °C at 1 °C min^{-1}. UV absorption at 260 nm was recorded at 0.5 °C intervals. The melting temperature (T_m^{260}) values were obtained from the 1st derivatives of the melting curves using the Cary Win UV Thermal application software. 16 successive melting curves were measured and averaged, except for measurements performed by Rachel Porter,[198] which are the average of 6 melting curves.

References

1. Schiemann, O.; Prisner, T. F. *Q. Rev. Biophys.* **2007**, *40*, 1–53.
2. Reginsson, G. W.; Schiemann, O. *Biochem. J.* **2011**, *434*, 353–363.
3. Nguyen, P.; Qin, P. Z. *Wiley Interdiscip. Rev.: RNA* **2012**, *3*, 62–72.
4. Shelke, S. A.; Sigurdsson, S. T. *Eur. J. Org. Chem.* **2012**, 2291–2301.
5. Ward, R.; Schiemann, O. *Struct. Bond.* **2014**, *152*, 249–281.
6. Shelke, S. A.; Sigurdsson, S. T. *Struct. Bond.* **2014**, *152*, 121–162.
7. Endeward, B.; Marko, A.; Denysenkov, V. P.; Sigurdsson, S. T.; Prisner, T. F. *Methods Enzymol.* **2015**, *564*, 403–425.
8. Saha, S.; Jagtap, A. P.; Sigurdsson, S. T. *Methods Enzymol.* **2015**, *563*, 397–414.
9. Eaton, G. R.; Eaton, S. S.; Barr, D. P.; Weber, R. T. *Quantitative EPR: A Practitioners Guide*, 1st ed.; Springer: Vienna, 2010.
10. Gerson, F.; Huber, W. *Electron spin resonance spectroscopy of organic radicals*, 1st ed.; Wiley-VHC: Weinheim, 2003.
11. Banham, J. E.; Baker, C. M.; Ceola, S.; Daye, I. J.; Grant, G. H.; Groenen, E. J. J.; Rodgers, C. T.; Jeschke, G.; Timmel, C. R. *J. Magn. Reson.* **2008**, *191*, 202–218.
12. Schweiger, A.; Jeschke, G. *Principles of Pulse Electron Paramagnetic Resonance*, 1st ed.; Oxford University Press: New York, 2001.
13. Engels, J. W.; Grünewald, C.; Wicke, L. In *Chemical Biology of Nucleic Acids*; Erdmann, V. A., Markievicz, W. T., Barciszewski, J., Eds.; RNA Technologies; Springer: Berlin Heidelberg, 2014; pp 385–407.
14. Yulikov, M. In *Electron Paramagnetic Resonance*; Gilbert, B. C., Chechik, V., Murphy, D. M., Eds.; Specialist Periodical Reports; Royal Society of Chemistry: Cambridge, 2014; Vol. 24; pp 1–31.
15. Fielding, A.; Concilio, M.; Heaven, G.; Hollas, M. *Molecules* **2014**, *19*, 16998–17025.
16. Ching, H. Y. V.; Mascali, F. C.; Bertrand, H. C.; Bruch, E. M.; Demay-Drouhard, P.; Rasia, R. M.; Policar, C.; Tabares, L. C.; Un, S. *J. Phys. Chem. Lett.* **2016**, *7*, 1072–1076.
17. Shevelev, G. Y.; Krumkacheva, O. A.; Lomzov, A. A.; Kuzhelev, A. A.; Rogozhnikova, O. Y.; Trukhin, D. V.; Troitskaya, T. I.; Tormyshev, V. M.; Fedin, M. V.; Pyshnyi, D. V.; Bagryanskaya, E. G. *J. Am. Chem. Soc.* **2014**, *136*, 9874–9877.

18. Shevelev, G. Y.; Krumkacheva, O. A.; Lomzov, A. A.; Kuzhelev, A. A.; Trukhin, D. V.; Rogozhnikova, O. Y.; Tormyshev, V. M.; Pyshnyi, D. V.; Fedin, M. V.; Bagryanskaya, E. G. *J. Phys. Chem. B* **2015**, *119*, 13641–13648.

19. Yang, Z.; Bridges, M. D.; López, C. J.; Rogozhnikova, O. Y.; Trukhin, D. V.; Brooks, E. K.; Tormyshev, V.; Halpern, H. J.; Hubbell, W. L. *J. Magn. Reson.* **2016**, *269*, 50–54.

20. Rozantsev, E. G. *Free Nitroxyl Radicals*, 1st ed.; Springer: New York, 1970.

21. Morris, S.; Sosnovsky, G.; Hui, B.; Huber, C.; Rao, N.; Swartz, H. *J. Pharm. Sci.* **1991**, *80*, 149–152.

22. Yamasaki, T.; Mito, F.; Ito, Y.; Pandian, S.; Kinoshita, Y.; Nakano, K.; Murugesan, R.; Sakai, K.; Utsumi, H.; Yamada, K.-I. *J. Org. Chem.* **2011**, *76*, 435–440.

23. Couet, W. R.; Brasch, R. C.; Sosnovsky, C.; Lukszo, J.; Prakash, I.; Gnewech, C. T.; Tozer, T. N. *Tetrahedron* **1985**, *41*, 1165–1172.

24. Belkin, S.; Mehlhorn, R. J.; Hideg, K.; Hankovsky, O.; Packer, L. *Arch. Biochem. Biophys.* **1987**, *256*, 232–243.

25. Paletta, J. T.; Pink, M.; Foley, B.; Rajca, S.; Rajca, A. *Org. Lett.* **2012**, *14*, 5322–5325.

26. Kirilyuk, I. A.; Bobko, A. A.; Semenov, S. V.; Komarov, D. A.; Irtegova, I. G.; Grigor'ev, I. A.; Bagryanskaya, E. *J. Org. Chem.* **2015**, *80*, 9118–9125.

27. Jagtap, A. P.; Krstić, I.; Kunjir, N. C.; Hänsel, R.; Prisner, T. F.; Sigurdsson, S. T. *Free Radical Res.* **2015**, *49*, 78–85.

28. Saha, S.; Jagtap, A. P.; Sigurdsson, S. T. *Chem. Commun.* **2015**, *51*, 13142–13145.

29. Dzuba, S. A.; Maryasov, A. G.; Salikhov, K. M.; Tsvetkov, Y. D. *J. Magn. Reson.* **1984**, *58*, 95–117.

30. Zecevic, A.; Eaton, G. R.; Eaton, S. S.; Lindgren, M. *Mol. Phys.* **1998**, *95*, 1255–1263.

31. Kathirvelu, V.; Smith, C.; Parks, C.; Mannan, M. A.; Miura, Y.; Takeshita, K.; Eaton, S. S.; Eaton, G. R. *Chem. Commun.* **2009**, 454–456.

32. Rajca, A.; Kathirvelu, V.; Roy, S. K.; Pink, M.; Rajca, S.; Sarkar, S.; Eaton, S. S.; Eaton, G. R. *Chem. Eur. J.* **2010**, *16*, 5778–5782.

33. Babaylova, E. S.; Ivanov, A. V.; Malygin, A. A.; Vorobjeva, M. A.; Venyaminova, A. G.; Polienko, Y. F.; Kirilyuk, I. A.; Krumkacheva, O. A.; Fedin, M. V.; Karpova, G. G.; Bagryanskaya, E. G. *Org. Biomol. Chem.* **2014**, *12*, 3129–3136.

34. Babaylova, E. S.; Malygin, A. A.; Lomzov, A. A.; Pyshnyi, D. V.; Yulikov, M.; Jeschke, G.; Krumkacheva, O. A.; Fedin, M. V.; Karpova, G. G.; Bagryanskaya, E. G. *Nucleic Acids Res.* [Online early access]. DOI: 10.1093/nar/gkw516. Published online: 6th June, 2016.

35. Kuzhelev, A. A.; Strizhakov, R. K.; Krumkacheva, O. A.; Polienko, Y. F.; Morozov, D. A.; Shevelev, G. Y.; Pyshnyi, D. V.; Kirilyuk, I. A.; Fedin, M. V.; Bagryanskaya, E. G. *J. Magn. Reson.* **2016**, *266*, 1–7.

36. Watson, J. D.; Crick, F. H. C. *Nature* **1953**, *171*, 737–738.

37. Wilkins, M. H. F.; Stokes, A. R.; Wilson, H. R. *Nature* **1953**, *171*, 738–740.

38. Franklin, R. E.; Gosling, G. R. *Nature* **1953**, *171*, 740–741.

39. Fedor, M. J.; Williamson, J. R. *Nat. Rev. Mol. Cell Biol.* **2005**, *6*, 399–412.

40. Baum, D. A.; Silverman, K. *Cell. Mol. Life Sci.* **2008**, *65*, 2156–2174.

41. Hollenstein, M. *Molecules* **2015**, *20*, 20777–20804.

42. Serganov, A.; Patel, D. J. *Nat. Rev. Genet.* **2007**, *8*, 776–790.

43. Song, K.-M.; Lee, S.; Ban, C. *Seonsors* **2012**, *12*, 612–631.

44. Keefe, A. D.; Pai, S.; Ellington, A. *Nat. Rev. Drug Discovery* **2010**, *9*, 537–550.

45. Mayer, G. *Angew. Chem. Int. Ed.* **2009**, *48*, 2672–2689.

46. Bunka, D. H. J.; Stockley, P. G. *Nat. Rev. Microbiol.* **2006**, *4*, 588–596.

47. Cheah, M. T.; Wachter, A.; Sudarsan, N.; Breaker, R. R. *Nature* **2007**, *447*, 497–501.

48. Batey, R. T. *Curr. Opin. Struct. Biol.* **2006**, *16*, 299–306.

49. Tucker, B. J.; Breaker, R. R. *Curr. Opin. Struct. Biol.* **2005**, *15*, 342–348.

50. Fire, A.; Xu, S.; Montgomery, M. K.; Kostas, S. A.; Driver, S. E.; Mello, C. C. *Nature* **1998**, *391*, 806–811.

51. Nelson, D. L.; Cox, M. M. *Lehninger Principles of Biochemistry*, 5th ed.; W. H. Freeman and Co.: New York, 2008.

52. Sullenger, B. A.; Nair, S. *Science* **2016**, *352*, 1417–1420.

53. Dorsett, Y.; Tuschl, T. *Nat. Rev. Drug Discovery* **2004**, *3*, 318–329.

54. Schübeler, D. *Nature* **2015**, *517*, 321–326.

55. Altona, C.; Sundaralingam, M. *J. Am. Chem. Soc.* **1972**, *94*, 8205–8212.

56. Plavec, J.; Tong, W.; Chattopadhyaya, J. *J. Am. Chem. Soc.* **1993**, *115*, 9734–9746.

57. Plavec, J.; Thibaudeau, C.; Chattopadhyaya, J. *J. Am. Chem. Soc.* **1994**, *116*, 6558–6560.

58. de Leeuw, H. M. P.; Haasnoot, C. A. G.; Altona, C. *Isr. J. Chem.* **1980**, *20*, 108–126.

59. Neidle, S. *Nucleic Acid Structure and Recognition*, 1st ed.; Oxford University Press: Oxford, 2002.

60. Altona, C.; Sundaralingam, M. *J. Am. Chem. Soc.* **1973**, *95*, 2333–2344.

61. Thibaudeau, C.; Plavec, J.; Chattopadhyaya, J. *J. Org. Chem.* **1996**, *61*, 266–286.

62. Harvey, S. C.; Prabhakaran, M. *J. Am. Chem. Soc.* **1986**, *108*, 6128–6136.

63. Mak, C. H. *J. Phys. Chem. B* **2016**, *120*, 6010–6020.

64. Yakovchuk, P.; Protozanova, E.; Frank-Kamenetskii, M. D. *Nucleic Acids Res.* **2006**, *34*, 564–574.

65. Bochman, M. L.; Paeschke, K.; Zakian, V. A. *Nat. Rev. Genet.* **2012**, *13*, 770–780.

66. Laing, C.; Schlick, T. *Curr. Opin. Struct. Biol.* **2011**, *21*, 306–318.

67. Shi, H.; Moore, P. B. *RNA* **2000**, *6*, 1091–1105.

68. Cruse, W. B. T.; Saludjan, P.; Biala, E.; Strazewski, P.; Prangé, T.; Kennard, O. *Proc. Natl. Acad. Sci. U.S.A.* **1994**, *91*, 4160–4164.

69. Flinders, J.; Dieckmann, T. *Prog. Nucl. Magn. Reson. Spectrosc.* **2006**, *48*, 137–159.

70. Duss, O.; Yulikov, M.; Jeschke, G.; Allain, F. H.-T. *Nat. Commun.* **2014**, *5*, 3669.

71. Duss, O.; Michel, E.; Yulikov, M.; Scubert, M.; Jeschke, G.; Allain, F. H.-T. *Nature* **2014**, *509*, 588–592.

72. Cekan, P.; Smith, A. L.; Barhate, N.; Robinson, B. H.; Sigurdsson, S. T. *Nucleic Acids Res.* **2008**, *36*, 5946–5954.

73. Osiecki, J. H.; Ullman, E. F. *J. Am. Chem. Soc.* **1968**, *90*, 1078–1079.

74. Rozantsev, E. G.; Sholle, V. D. *Synthesis* **1971**, 190–202.

75. Gannett, P. M.; Darian, E.; Powell, J.; Johnson, E. M.; Mundoma, C.; Greenbaum, N. L.; Ramsey, C. M.; Dalal, N. S.; Budil, D. E. *Nucleic Acids Res.* **2002**, *30*, 5328–5337.

76. Piton, N.; Mu, Y.; Stock, G.; Prisner, T. F.; Schiemann, O.; Engels, J. W. *Nucleic Acids Res.* **2007**, *35*, 3128–3143.

77. Abakumov, G. A.; Tikhonov, V. D. *Bull. Acad. Sci. USSR, Div. Chem. Sci. (Engl. Transl.)* **1969**, *18*, 724–727.

78. Tikhonov, I. V.; Sen', V. D.; Borodin, L. I.; Pliss, E. M.; Golubev, V. A.; Rusakov, A. I. *J. Phys. Org. Chem.* **2014**, *27*, 114–120.

79. Spaltenstein, A.; Robinson, B. H.; Hopkins, P. B. *J. Am. Chem. Soc.* **1988**, *110*, 1299–1301.

80. Spaltenstein, A.; Robinson, B. H.; Hopkins, P. B. *Biochemistry* **1989**, *28*, 9484–9495.

81. Spaltenstein, A.; Robinson, B. H.; Hopkins, P. B. *J. Am. Chem. Soc.* **1989**, *111*, 2303–2305.

82. Gannett, P. M.; Powell, J. H.; Johnson, E. M.; Darian, E.; Dalal, N. S.; Norton, M. L.; Budil, D. E. *Tetrahedron Lett.* **2002**, *43*, 1931–1933.

83. Singh, V.; Azarkh, M.; Exner, T. E.; Hartig, J. S.; Drescher, M. *Angew. Chem. Int. Ed.* **2009**, *48*, 9728–9730.

84. Azarkh, M.; Singh, V.; Okle, O.; Dietrich, D. R.; Hartig, J. S.; Drescher, M. *ChemPhysChem* **2012**, *13*, 1444–1447.

85. Azarkh, M.; Singh, V.; Okle, O.; Seemann, I. T.; Dietrich, D. R.; Hartig, J. S.; Drescher, M. *Nat. Protoc.* **2013**, *8*, 131–147.

86. Fischhaber, P. L.; Reese, A. W.; Nguyen, T.; Kirchner, J. J.; Hustedt, E. J.; Robinson, B. H.; Hopkins, P. B. *Nucleosides Nucleotides* **1997**, *16*, 365–377.

87. Bannwarth, W.; Schmidt, D. *Bioorg. Med. Chem. Lett.* **1994**, *4*, 977–980.

88. Giordano, C.; Fratini, F.; Attanasio, D.; Cellai, L. *Synthesis* **2001**, 565–572.

89. Cekan, P.; Sigurdsson, S. T. *J. Am. Chem. Soc.* **2009**, *131*, 18054–18056.

90. Miller, T. R.; Alley, S. C.; Reese, A. W.; Solomon, M. S.; McCallister, W. V.; Mailer, C.; Robinson, B. H.; Hopkins, P. B. *J. Am. Chem. Soc.* **1995**, *117*, 9377–9378.

91. Okonogi, T.; Reese, A.; Alley, S.; Hopkins, P.; Robinson, B. *Biophys. J.* **1999**, *77*, 3256–3276.

92. Okonogi, T.; Alley, S.; Reese, A.; Hopkins, P.; Robinson, B. *Biophys. J.* **2000**, *78*, 2560–2571.

93. Okonogi, T.; Alley, S.; Reese, A.; Hopkins, P.; Robinson, B. *Biophys. J.* **2002**, *83*, 3446–3459.

94. Barhate, N.; Cekan, P.; Massey, A. P.; Sigurdsson, S. T. *Angew. Chem. Int. Ed.* **2007**, *46*, 2655–2658.

95. Cekan, P.; Jonsson, E. O.; Sigurdsson, S. T. *Nucleic Acids Res.* **2009**, *37*, 3990–3995.

96. Schiemann, O.; Cekan, P.; Margraf, D.; Prisner, T. F.; Sigurdsson, S. T. *Angew. Chem. Int. Ed.* **2009**, *48*, 3292–3295.

97. Marko, A.; Margraf, D.; Cekan, P.; Sigurdsson, S. T.; Schiemann, O.; Prisner, T. F. *Phys. Rev. E* **2010**, *81*, 021911.

98. Edwards, T. E.; Cekan, P.; Reginsson, G. W.; Shelke, S. A.; Ferre-D'Amare, A. R.; Schiemann, O.; Sigurdsson, S. T. *Nucleic Acids Res.* **2011**, *39*, 4419–4426.

99. Marko, A.; Denysenkov, V.; Margraf, D.; Cekan, P.; Schiemann, O.; Sigurdsson, S. T.; Prisner, T. F. *J. Am. Chem. Soc.* **2011**, *133*, 13375–13379.

100. Cekan, P.; Sigurdsson, S. T. *Biochem. Biophys. Res. Commun.* **2012**, *420*, 656–661.

101. Höbartner, C.; Sicoli, G.; Wachowius, F.; Gophane, D. B.; Sigurdsson, S. T. *J. Org. Chem.* **2012**, *77*, 7749–7754.

102. Grytz, C. M.; Marko, A.; Cekan, P.; Sigurdsson, S. T.; Prisner, T. F. *Phys. Chem. Chem. Phys.* **2016**, *18*, 2993–3002.

103. Ramos, A.; Varani, G. *J. Am. Chem. Soc.* **1998**, *120*, 10992–10993.

104. Borbat, P. P.; Davis, J. H.; Butcher, S. E.; Freed, J. H. *J. Am. Chem. Soc.* **2004**, *126*, 7746–7747.

105. Leulliot, N.; Quevillon-Cheruel, S.; Graille, M.; van Tilbeurgh, H.; Leeper, T. C.; Godin, K. S.; Edwards, T. E.; Sigurdsson, S. T.; Rozenkrants, N.; Nagel, R. J.; Ares, M.; Varani, G. *EMBO J.* **2004**, *23*, 2468–2477.

106. Okamoto, A.; Inasaki, T.; Saito, I. *Bioorg. Med. Chem. Lett.* **2004**, *14*, 3415–3418.

107. Sicoli, G.; Mathis, G.; Delalande, O.; Boulard, Y.; Gasparutto, D.; Gambarelli, S. *Angew. Chem. Int. Ed.* **2008**, *47*, 735–737.

108. Sicoli, G.; Mathis, G.; Aci-Sèche, S.; Saint-Pierre, C.; Boulard, Y.; Gasparutto, D.; Gambarelli, S. *Nucleic Acids Res.* **2009**, *37*, 3165–76.

109. Sicoli, G.; Wachowius, F.; Bennati, M.; Höbartner, C. *Angew. Chem. Int. Ed.* **2010**, *49*, 6443–6447.

110. Halbmair, K.; Seikowski, J.; Tkach, I.; Höbartner, C.; Sezer, D.; Bennati, M. *Chem. Sci.* **2016**, *17*, 3172–3180.

111. Schiemann, O.; Piton, N.; Mu, Y.; Stock, G.; Engels, J. W.; Prisner, T. F. *J. Am. Chem. Soc.* **2004**, *126*, 5722–5729.

112. Piton, N.; Schiemann, O.; Mu, Y.; Stock, G.; Prisner, T.; Engels, J. W. *Nucleosides, Nucleotides Nucleic Acids* **2005**, *24*, 771–775.

113. Schiemann, O.; Piton, N.; Plackmeyer, J.; Bode, B. E.; Prisner, T. F.; Engels, J. W. *Nat. Protoc.* **2007**, *2*, 904–923.

114. Krstić, I.; Frolow, O.; Sezer, D.; Endeward, B.; Weigand, J. E.; Suess, B.; Engels, J. W.; Prisner, T. F. *J. Am. Chem. Soc.* **2010**, *132*, 1454–1455.

115. Krstić, I.; Hänsel, R.; Romainczyk, O.; Engels, J. W.; Dötsch, V.; Prisner, T. F. *Angew. Chem. Int. Ed.* **2011**, *50*, 5070–5074.

116. Romainczyk, O.; Endeward, B.; Prisner, T. F.; Engels, J. W. *Mol. BioSyst.* **2011**, *7*, 1050–1052.

117. Jakobsen, U.; Shelke, S. A.; Vogel, S.; Sigurdsson, S. T. *J. Am. Chem. Soc.* **2010**, *132*, 10424–10428.

118. Ding, P.; Wunnicke, D.; Steinhoff, H. J.; Seela, F. *Chem. Eur. J.* **2010**, *16*, 14385–14396.

119. Flaender, M.; Sicoli, G.; Aci-Seche, S.; Reignier, T.; Maurel, V.; Saint-Pierre, C.; Boulard, Y.; Gambarelli, S.; Gasparutto, D. *ChemBioChem* **2011**, *12*, 2560–3.

120. Makino, K.; Murakami, A.; Nagahara, S.; Nakatsuji, Y.; Takeuchi, T. *Free Radical Res. Commun.* **1989**, *6*, 311–316.

121. Nagahara, S.; Murakami, A.; Makino, K. *Nucleosides Nucleotides* **1992**, *11*, 889–901.

122. Murakami, A.; Mukae, M.; Nagahara, S.; Konishi, Y.; Ide, H.; Makino, K. *Free Radical Res. Commun.* **1993**, *19*, s117–s128.

123. Fidanza, J.; McLaughlin, L. W. *J. Am. Chem. Soc.* **1989**, *111*, 9117–9119.

124. Fidanza, J. A.; Ozaki, H.; McLaughlin, L. W. *J. Am. Chem. Soc.* **1992**, *114*, 5509–5517.

125. Xi, X.; Sun, Y.; Karim, C. B.; Grigoryants, V. M.; Scholes, C. P. *Biochemistry* **2008**, *47*, 10099–10110.

126. Shepherd, N. E.; Gamsjaeger, R.; Vandevenne, M.; Cubeddu, L.; Mackay, J. P. *Tetrahedron* **2015**, *71*, 813–819.

127. Qin, P. Z.; Butcher, S. E.; Feigon, J.; Hubbell, W. L. *Biochemistry* **2001**, *40*, 6929–6936.

128. Cai, Q.; Kusnetzow, A. K.; Hubbell, W. L.; Haworth, I. S.; Gacho, G. P. C.; Van Eps, N.; Hideg, K.; Chambers, E. J.; Qin, P. Z. *Nucleic Acids Res.* **2006**, *34*, 4722–4730.

129. Cai, Q.; Kusnetzow, A. K.; Hideg, K.; Price, E. A.; Haworth, I. S.; Qin, P. Z. *Biophys. J.* **2007**, *93*, 2110–2117.

130. Grant, G. P. G.; Qin, P. Z. *Nucleic Acids Res.* **2007**, *35*, e77.

131. Qin, P. Z.; Haworth, I. S.; Cai, Q.; Kusnetzow, A. K.; Grant, G. P. G.; Price, E. A.; Sowa, G. Z.; Popova, A.; Herreros, B.; He, H. *Nat. Protoc.* **2007**, *2*, 2354–2365.

132. Grant, G. P. G.; Popova, A.; Qin, P. Z. *Biochem. Biophys. Res. Commun.* **2008**, *371*, 451–455.

133. Grant, G. P. G.; Boyd, N.; Herschlag, D.; Qin, P. Z. *J. Am. Chem. Soc.* **2009**, *131*, 3136–3137.

134. Popova, A. M.; Kálai, T.; Hideg, K.; Qin, P. Z. *Biochemistry* **2009**, *48*, 8540–8550.

135. Macosko, J.; Pio, M.; Tinoco, I.; Shin, Y.-K. *RNA* **1999**, *5*, 1158–1166.

136. Popova, A. M.; Qin, P. Z. *Biophys. J.* **2010**, *99*, 2180–2189.

137. Gish, G.; Eckstein, F. *Science* **1988**, *240*, 1520–1522.

138. Edwards, T. E.; Okonogi, T. M.; Robinson, B. H.; Sigurdsson, S. T. *J. Am. Chem. Soc.* **2001**, *123*, 1527–8.

139. Edwards, T. E.; Sigurdsson, S. T. *Biochemistry* **2002**, *41*, 14843–14847.

140. Edwards, T. E.; Okonogi, T. M.; Sigurdsson, S. T. *Chem. Biol.* **2002**, *9*, 699–706.

141. Edwards, T. E.; Sigurdsson, S. T. *Biochem. Biophys. Res. Commun.* **2003**, *303*, 721–725.

142. Schiemann, O.; Weber, A.; Edwards, T. E.; Prisner, T. F.; Sigurdsson, S. T. *J. Am. Chem. Soc.* **2003**, *125*, 3434–3435.

143. Edwards, T. E.; Sigurdsson, S. T. *Biochemistry* **2005**, *44*, 12870–12878.

144. Edwards, T. E.; Robinson, B. H.; Sigurdsson, S. T. *Chem. Biol.* **2005**, *12*, 329–337.

145. Kim, N.-K.; Murali, A.; DeRose, V. J. *J. Am. Chem. Soc.* **2005**, *127*, 14134–14135.

146. Edwards, T. E.; Sigurdsson, S. T. *Nat. Protoc.* **2007**, *2*, 1954–1962.

147. Ward, R.; Keeble, D. J.; El-Mkami, H.; Norman, D. G. *ChemBioChem* **2007**, *8*, 1957–1964.

148. Kim, N.-K.; Bowman, M. K.; DeRose, V. J. *J. Am. Chem. Soc.* **2010**, *132*, 8882–8884.

149. Wunnicke, D.; Strohbach, D.; Weigand, J. E.; Appel, B.; Feresin, E.; Suess, B.; Müller, S.; Steinhoff, H.-J. *RNA* **2011**, *17*, 182–188.

150. Helmling, C.; Bessi, I.; Wacker, A.; Schnorr, K. A.; Jonker, H. R. A.; Richter, C.; Wagner, D.; Kreibich, M.; Schwalbe, H. *ACS Chem. Biol.* **2014**, *9*, 1330–1339.

151. Kim, N.-K.; Murali, A.; DeRose, V. J. *Chem. Biol.* **2004**, *11*, 939–948.

152. Büttner, L.; Javadi-Zarnaghi, F.; Höbartner, C. *J. Am. Chem. Soc.* **2014**, *136*, 8131–8137.

153. Flaender, M.; Sicoli, G.; Fontecave, T.; Mathis, G.; Saint-Pierre, C.; Boulard, Y.; Gambarelli, S.; Gasparutto, D. *Nucleic Acids Symp. Ser.* **2008**, 147–148.

154. Wildsmith, E. *Synthesis of Spin Labelled Oligonucleotides as Biological Probes*; Part II Thesis; University College, University of Oxford, 2011.

155. Aigner, M.; Hartl, M.; Fauster, K.; Steger, J.; Bister, K.; Micura, R. *ChemBioChem* **2011**, *12*, 47–51.

156. Fauster, K.; Hartl, M.; Santner, T.; Aigner, M.; Kreutz, C.; Bister, K.; Ennifar, E.; Micura, R. *ACS Chem. Biol.* **2012**, *7*, 581–589.

157. Sukeda, M.; Ichikawa, S.; Matsuda, A.; Shuto, S. *Angew. Chem. Int. Ed.* **2002**, *41*, 4748–4750.

158. Sukeda, M.; Ichikawa, S.; Matsuda, A.; Shuto, S. *J. Org. Chem.* **2003**, *68*, 3465–3475.

159. Peña, J. *Summer Project: Synthesis of C2′-Alkynyl Oligonucleotides for EPR Spectroscopy*; Department of Chemistry, University of Oxford, 2012.

160. Sheng, J.; Hassan, A. E. A.; Huang, Z. *J. Org. Chem.* **2008**, *73*, 3725–3729.

161. Yamamoto, Y.; Shimizu, H.; Matui, C.; Chinda, M. *Main Group Chem.* **1996**, *1*, 409–414.

162. Hamada, Y.; Yamamoto, Y.; Hideaki, S. *J. Organomet. Chem.* **1996**, *510*, 1–6.

163. Ohshita, J.; Iwata, A.; Kanetani, F.; Kunai, A.; Yamamoto, Y.; Matui, C. *J. Org. Chem.* **1999**, *64*, 8024–8026.

164. Pon, R. T. In *Methods in Molecular Biology 20: Protocols for Oligonucleotides and Analogs*; Agrawal, S., Ed.; Humana Press: Totowa, New Jersey, USA, 1993; p 467.

165. Barone, A. D.; Tang, J.-Y.; Caruthers, M. H. *Nucleic Acids Res.* **1984**, *12*, 4051–4061.

166. Sanghvi, Y. S.; Guo, Z.; Pfundheller, H. M.; Converso, A. *Org. Process Res. Dev.* **2000**, *4*, 175–181.

167. Xie, C.; Staszak, M. A.; Quatroche, J. T.; Sturgill, C. D.; Khau, V. V.; Martinelli, M. J. *Org. Process Res. Dev.* **2005**, *9*, 730–737.

168. Divakar, K. J.; Reese, C. B. *J. Chem. Soc. Perkin Trans. 1* **1982**, 1171–1176.

169. Gruen, M.; Becker, C.; Beste, A.; Siethoff, C.; Scheidig, A. J.; Goody, R. S. *Nucleosides Nucleotides* **1999**, *18*, 137–151.

170. Corey, E. J.; Venkateswarlu, A. *J. Am. Chem. Soc.* **1972**, *94*, 6190–6191.

171. Davies, D. B.; Danyluk, S. S. *Biochemistry* **1974**, *13*, 4417–4434.

172. Curran, D. P.; McFadden, T. R. *J. Am. Chem. Soc.* **2016**, *138*, 7741–7752.

173. Lindahl, T. *Nature* **1993**, *362*, 709–715.

174. Mengel, R.; Wiedner, H. *Chem. Ber.* **1976**, *109*, 1395–1406.

175. Gimisis, T.; Ialongo, G.; Chatgilialoglu, C. *Tetrahedron* **1998**, *54*, 573–592.

176. Altenhoff, G.; Würtz, S.; Glorius, F. *Tetrahedron Lett.* **2006**, *47*, 2925–2928.

177. Hatakeyama, T.; Okada, Y.; Yoshimoto, Y.; Nakamura, M. *Angew. Chem. Int. Ed.* **2011**, *50*, 10973–10976.

178. Thaler, T.; Guo, L. N.; Mayer, P.; Knochel, P. *Angew. Chem. Int. Ed.* **2011**, *50*, 2174–2177.

179. Yi, J.; Lu, X.; Sun, Y. Y.; Xiao, B.; Liu, L. *Angew. Chem. Int. Ed.* **2013**, *52*, 12409–12413.

180. Cheung, C. W.; Ren, P.; Hu, X. *Org. Lett.* **2014**, *16*, 2566–2569.

181. DeAngelis, A.; Colacot, T. J. In *New Trends in Cross-Coupling: Theory and Applications*; Colacot, T. J., Ed.; RSC Catalysis Series; The Royal Society of Chemistry: Cambridge, 2015; pp 20–90.

182. Liu, H.-J.; Shia, K.-S.; Shang, X.; Zhu, B.-Y. *Tetrahedron* **1999**, *55*, 3803–3830.

183. Miura, Y.; Nakamura, N.; Taniguchi, I. *Macromolecules* **2001**, *34*, 447–455.

184. Hankovszky, O. H.; Hideg, K.; Lex, L. *Synthesis* **1981**, 147–149.

185. Hatano, B.; Araya, H.; Yoshimura, Y.; Sato, H.; Ito, T.; Ogata, T.; Kijima, T. *Heterocycles* **2010**, *81*, 349–356.

186. Alcock, N. W.; Golding, B. T.; Ioannou, P. V.; Sawyer, J. F. *Tetrahedron* **1977**, *33*, 2969–2980.

187. Toda, T.; Mori, E.; Murayama, K. *Bull. Chem. Soc. Jpn.* **1972**, *45*, 1904–1908.

188. Cella, J. A.; Kelley, J. A.; Kenehan, E. F. *J. Org. Chem.* **1975**, *40*, 1860–1862.

189. Ganem, B. *J. Org. Chem.* **1975**, *40*, 1998–2000.

190. Powell, J. H.; Johnson, E. M.; Gannett, P. M. *Molecules* **2000**, *5*, 1244–1250.

191. Sár, C. P.; Jekö, J.; Hideg, K. *Synthesis* **1998**, 1497–1500.

192. Meyer, V.; Swanson, M.; Clouston, L.; Boratyński, P.; Stein, R.; Mchaourab, H.; Rajca, A.; Eaton, S.; Eaton, G. *Biophys. J.* **2015**, *108*, 1213–1219.

193. Sakai, K.; Yamada, K.-I.; Yamasaki, T.; Kinoshita, Y.; Mito, F.; Utsumi, H. *Tetrahedron* **2010**, *66*, 2311–2315.

194. Kelemen, P.; Lugtenburg, J.; Klumperman, B. *J. Org. Chem.* **2003**, *68*, 7322–7328.

195. Sen', V. D.; Golubev, V. A.; Efremova, N. N. *Bull. Acad. Sci. USSR, Div. Chem. Sci. (Engl. Transl.)* **1982**, *31*, 53–63.

196. Gophane, D. B.; Sigurdsson, S. T. *Chem. Commun.* **2013**, *49*, 999–1001.

197. Gophane, D. B.; Endeward, B.; Prisner, T. F.; Sigurdsson, S. T. *Chem. Eur. J.* **2014**, *20*, 15913–15919.

198. Porter, R. *The synthesis of novel spin labels and alkynyl phosphoramidites for spin labelling of DNA*; Part II Thesis; Somerville College, University of Oxford, 2015.

199. Haugland, M. M.; El-Sagheer, A. H.; Porter, R. J.; Peña, J.; Brown, T.; Anderson, E. A.; Lovett, J. E. *J. Am. Chem. Soc.* **2016**, *138*, 9069–9072.

200. Rostovtsev, V. V.; Grenn, L. G.; Fokin, V. V.; Sharpless, K. B. *Angew. Chem. Int. Ed.* **2002**, *41*, 2596–2599.

201. Tornøe, C. W.; Christensen, C.; Meldal, M. *J. Org. Chem.* **2002**, *67*, 3057–3064.

202. Meldal, M.; Tornøe, C. W. *Chem. Rev.* **2008**, *108*, 2952–3015.

203. El-Sagheer, A. H.; Brown, T. *Chem. Soc. Rev.* **2010**, *39*, 1388–1405.

204. Besanceney-Webler, C.; Jiang, H.; Zheng, T.; Feng, L.; del Amo, D. S.; Wang, W.; Klivansky, L. M.; Marlow, F. L.; Liu, Y.; Wu, P. *Angew. Chem. Int. Ed.* **2011**, *50*, 8051–8056.

205. Hong, V.; Presolski, S. I.; Ma, C.; Finn, M. G. *Angew. Chem. Int. Ed.* **2009**, *48*, 9879–9883.

206. Kennedy, D. C.; McKay, C. S.; Legault, M. C. B.; Danielson, D. C.; Blake, J. A.; Pegoraro, A. F.; Stolow, A.; Mester, Z.; Pezacki, J. P. *J. Am. Chem. Soc.* **2011**, *133*, 17993–18001.

207. Cooke, M. S.; Evans, M. D.; Dizdaroglu, M.; Lunec, J. *FASEB J.* **2003**, *17*, 1195–1214.

208. Weber, R. T. *Xenon User's Guide*, 3rd ed.; Bruker BioSpin Corporation: Billerica, MA, USA, 2011.

209. Mergny, J.-L.; Lacroix, L. *Oligonucleotides* **2003**, *13*, 515–537.

210. Richards, R. G.; Sowers, L. C.; Laszlo, J.; Sedwick, W. D. *Adv. Enzyme Regul.* **1984**, *22*, 157–185.

211. Chandler, D. *Nature* **2005**, *437*.

212. Kypr, J.; Kejnovska, I.; Renciuk, D.; Vorlickova, M. *Nucleic Acids Res.* **2009**, *37*, 1713–1725.

213. Gray, D. M.; Ratliff, R. L.; Vaughan, M. R. *Methods Enzymol.* **1992**, *211*, 389–406.

214. Steeley, H. T., Jr.; Gray, D. M.; Ratliff, R. L. *Nucleic Acids Res.* **1986**, *14*, 10071–10090.

215. Sabahi, A.; Guidry, J.; Inamati, G. B.; Manoharan, M.; Wittung-Stafshede, P. *Nucleic Acids Res.* **2001**, *29*, 2163–2170.

216. Pallan, P. S.; Greene, E. M.; Jicman, P. A.; Pandey, R. K.; Manoharan, M.; Rozners, E.; Egli, M. *Nucleic Acids Res.* **2011**, *39*, 3482–3495.

217. Williams, A. A.; Darwanto, A.; Theruvathu, J. A.; Burdzy, A.; Neidigh, J. W.; Sowers, L. C. *Biochemistry* **2009**, *48*, 11994–12004.

218. Chalmers, B. A.; Morris, J. C.; Fairfull-Smith, K. E.; Grainger, R. S.; Bottle, S. E. *Chem. Commun.* **2013**, *49*, 10382–4.

219. Altona, C.; Ippel, J. H.; Westra Hoekzema, A. J. A.; Erkelens, C.; Groesbeek, M.; Donders, L. A. *Magn. Reson. Chem.* **1989**, *27*, 564–576.

220. Hendrickx, P. M. S.; Martins, J. C. *Chem. Cent. J.* **2008**, *2*, 20.

221. de Leeuw, F. A. A. M.; van Kampen, P. N.; Altona, C. *J. Mol. Struct.* **1984**, *125*, 67–88.

222. Donders, L. A.; de Leeuw, F. A. A. M.; Altona, C. *Magn. Reson. Chem.* **1989**, *27*, 556–563.

223. Altona, C.; Francke, R.; de Haan, R.; Ippel, J. H.; Daalmans, G. J.; Westra Hoekzema, A. J. A.; van Wijk, J. *Magn. Reson. Chem.* **1994**, *32*, 670–678.

224. Kosuri, S.; Church, G. M. *Nat. Methods* **2014**, *11*, 499–507.

225. LeProust, E. M.; Peck, B. J.; Spirin, K.; McCuen, H. B.; Moore, B.; Namsaraev, E.; Caruthers, M. H. *Nucleic Acids Res.* **2010**, *38*, 2522–2540.

226. El-Sagheer, A. H.; Brown, T. *Proc. Natl. Acad. Sci. U.S.A.* **2010**, *107*, 15329–15334.

227. Padilla, R.; Sousa, R. *Nucleic Acids Res.* **2002**, *30*, e138.

228. Obeid, S.; Yulikov, M.; Jeschke, G.; Marx, A. *Angew. Chem. Int. Ed.* **2008**, *47*, 6782–6785.

229. Winz, M.-L.; Samanta, A.; Benzinger, D.; Jäschke, A. *Nucleic Acids Res.* **2012**, *40*, e78.

230. Liu, Y.; Holmstrom, E.; Zhang, J.; Yu, P.; Wang, J.; Dyba, M. A.; Chen, D.; Ying, J.; Lockett, S.; Nesbitt, D. J.; Ferré-D'Amaré, A. R.; Sousa, R.; Stagno, J. R.; Wang, Y.-X. *Nature* **2015**, *522*, 368–372.

231. Lauridsen, L. H.; Rothnagel, J. A.; Veedu, R. N. *ChemBioChem* **2012**, *13*, 19–25.

232. Caton-Williams, J.; Lin, L.; Smith, M.; Huang, Z. *Chem. Commun.* **2011**, *47*, 8142–8144.

233. Kovács, T.; Ötvös, L. *Tetrahedron Lett.* **1988**, *29*, 4525–4528.

234. Burgess, K.; Cook, D. *Chem. Rev.* **2000**, *100*, 2047–2059.

235. Hollenstein, M. *Molecules* **2012**, *17*, 13569–13591.

236. Beignet, J.; Jervis, P. J.; Cox, L. R. *J. Org. Chem.* **2008**, *73*, 5462–5475.

237. Xi, Z.; Rong, J.; Chattopadhyaya, J. *Tetrahedron* **1994**, *50*, 5255–5272.

238. Ji, Y.-H.; Bannwarth, W.; Luu, B. *Tetrahedron* **1990**, *46*, 487–502.

239. Jeong, Y.; Kom, D.-Y.; Choi, Y.; Ryu, J.-S. *Org. Biomol. Chem.* **2011**, *9*, 374–378.

240. Koohang, A.; Bailey, J. L.; Coates, R. M.; Erickson, H. K.; Owen, D.; Poulter, C. D. *J. Org. Chem.* **2010**, *75*, 4769–4777.

241. Sukeda, M.; Shuto, S.; Sugimoto, I.; Ichikawa, S.; Matsuda, A. *J. Org. Chem.* **2000**, *65*, 8988–8996.

242. Cavaluzzi, M. J. *Nucleic Acids Res.* **2004**, *32*, 13e.

243. Zhong, M.; Strobel, S. A. *J. Org. Chem.* **2008**, *73*, 603–611.

244. Fukukawa, K.; Uedao, T.; Hirano, T. *Chem. Pharm. Bull.* **1983**, *31*, 1582–1592.

245. Zhu, J.; Wang, P.-C.; Ming, L. *Synth. Commun.* **2013**, *43*, 1871–1881.

246. Mannini, M.; Cicchi, S.; Berti, D.; Caneschi, A.; Brandi, A.; Lascialfari, L.; Sorace, L. *ChemPlusChem* **2013**, *78*, 149–156.

247. Braslau, R.; Rivera, F.; Lilie, E.; Cottman, M. *J. Org. Chem.* **2013**, *78*, 238–245.

248. Krishna, M. C.; DeGraff, W.; Hankovszky, O. H.; Sár, C. P.; Kálai, T.; Jekő, J.; Russo, A.; Mitchell, J. B.; Hideg, K. *J. Med. Chem.* **1998**, *41*, 3477–3492.

249. Rozantzev, E. G.; Krinitzkaya, L. A. *Tetrahedron* **1965**, *21*, 491–499.

250. Schmidt, M. J.; Borbas, J.; Drescher, M.; Summerer, D. *J. Am. Chem. Soc.* **2014**, *136*, 1238–1241.

251. Wang, Y.; Paletta, J. T.; Berg, K.; Reinhart, E.; Rajca, S.; Rajca, A. *Org. Lett.* **2014**, *16*, 5298–5300.

252. Kirilyuk, I. A.; Polienko, Y. F.; Krumkacheva, O. A.; Strizhakov, R. K.; Gatilov, Y. V.; Grigor'ev, I. A.; Bagryanskaya, E. G. *J. Org. Chem.* **2012**, *77*, 8016–27.